Development of a novel model of optic neuritis to assess neuroprotective and repair strategies in multiple sclerosis

Lidster, Katie

Development of a novel model of optic neuritis to assess neuroprotective and repair strategies in multiple sclerosis

Katie Lidster

Queen Mary University of London

Submitted for the degree of Doctor of Philosophy (PhD)

Abstract

Multiple sclerosis (MS) is a putative autoimmune disease of the central nervous system (CNS), which often affects the optic nerve pathway. Optic neuritis (ON) is a clinical feature of MS that can cause loss of vision due to conduction block and demyelination. Visual function may not recover due to axonal loss in the optic nerve and subsequent loss of retinal ganglion cells (RGC) in the retina. The visual system is the most accessible and best studied part of the CNS and provides an ideal target to monitor the efficacy of strategies aimed at neuroprotection and repair.

A C57BL/6 mouse expressing a T cell receptor (TCR) transgene specific for 35-55 residues of myelin oligodendrocyte glycoprotein (MOG), which develops ON spontaneously (approximately 5%) was characterised and an immunising protocol developed with a combination of immune adjuvants (*Pertussis* toxin, MOG-specific Z12 monoclonal antibody) to give a high incidence of disease. ON is associated with extensive axonal loss in the optic nerve and RGC loss in the retina. These animals were crossed with C57BL/6.*Thy1* CFP mice, which express cyan fluorescent protein (CFP) under control of a *Thy1* promoter that limits expression of CFP to the RGC in the eye. The resultant MOG^{TCR}x*Thy1*CFP mice develop ON leading to neuronal loss that can be monitored longitudinally in "real-time" in the living animal using techniques that correlate with studies undertaken in humans (visually evoked potentials, scanning laser ophthalmoscopy and optical coherence tomography). These techniques were used in the MOG^{TCR}x*Thy1*CFP to study neuroprotective and repair therapies for their potential in human trials.

This novel model of optic neuritis will be invaluable for the study of neuroprotective and repair strategies in autoimmune diseases and offers a refinement of previous models of MS, such as "classical" EAE.

Contents

List of Figures

List of Tables

Abbreviations

AMPA	α-amino-3-hydroxy-5-methil-4-isoxazol-propionic acid
ANOVA	Analysis of variance
ART	Average real time
BBB	Blood brain barrier
bCSLO	Blue light confocal scanning laser ophthalmoscope
CB1	Cannabinoid receptor type 1
CBZ	Carbamazepine
CFA	Complete Freund's adjuvant
CFM1604	Novel sodium channel blocker
CFP	Cyan fluorescent protein
CNS	Central nervous system
CSF	Cerebral spinal fluid
cSLO	Confocal scanning laser ophthalmoscope
C_t	Cycle threshold
DMSO	Dimethyl sulfoxide
dB	Decibels
EAE	Experimental autoimmune encephalomyelitis
EBV	Epstein-Barr virus
eCFP	Enhanced cyan fluorescent protein
EDSS	Expanded disability status scale
Epo	Erythropoietin
FITC	Fluorescein isothiocyanate
GA	Glatiramer acetate
GCL	Ganglion cell layer
GFP	Green fluorescent protein
HLA	Human leucocyte antigen
I	Inferior
i.p.	Intraperitoneal
IFNβ	Interferon-β
IGF-1	Insulin growth factor-1
IR	Infra red
LGN	Lateral geniculate nucleus
mAb	Monoclonal antibody
MAG	Myelin associated glycoprotein
MBP	Myelin basic protein
MHC	Major histocompatibility complex
MOG	Myelin oligodendrocyte glycoprotein
MOG^{TCR}	Myelin oligodendrocyte specific T-cell receptor
MOG^{TCR}x*Thy1*CFP	Myelin oligodendrocyte specific T-cell receptor x *Thy1* cyan fluorescent protein transgenic mouse
MRI	Magnetic resonance imaging
MS	Multiple sclerosis
N	Nasal
Na_v	Voltage gated sodium channel
NI	Nasal inferior

NC3Rs	National Centre for the Replacement, Refinement and Reduction of Animals
NMDA	N-Methyl-D-aspartate
NO	Nitric oxide
NS	Nasal superior
OCT	Optical coherence tomography
OD	Oculus dextrus
OKN	Optokinetic
ON	Optic neuritis
ONTT	Optic neuritis treatment trial
OPC	Oligodendrocyte precursor cell
OS	Oculus sinister
OXC	Oxcarbazepine
PBS	Phosphate buffered saline
PCR	Polymerase chain reaction
PE	Phycoerythrin
PFA	Paraformaldehyde
PLP	Proteolipid protein
PML	Progressive multifocal leukoencephalopathy
PNS	Peripheral nervous system
PPMS	Primary progressive multiple sclerosis
PTX	*Bordetella pertussis* toxin
qPCR	Quantitative PCR
RFP	Red fluorescent protein
RGC	Retinal ganglion cell
RNFL	Retinal nerve fibre layer
RPS29	Ribosomal protein S29
RRMS	Relapsing remitting multiple sclerosis
s.c.	Subcutaneous
S1P	Sphingosine-1-phosphate
SC	Superior colliculus
SD-OCT	Spectral-domain OCT
SEM	Standard error of mean
siRNA	Small interfering ribonucleic acid
SPMS	Secondary progressive multiple sclerosis
T	Temporal
TCR	T cell receptor
Tcrd	T-cell receptor delta chain
Th1	T helper 1
Th17	T helper 17
Th2	T helper -2
*Thy1*CFP	*Thy1* cyan fluorescent protein transgene
TI	Temporal inferior
TMEV	Theiler's murine encephalomyelitis virus
TNFα	Tumour necrosis factor α
TS	Temporal superior
UHR-OCT	Ultrahigh-resolution OCT

VEP	Visual evoked potential

Acknowledgements

I would like to acknowledge the following people for their support throughout my PhD studies. I am sincerely thankful to my supervisors Prof. David Baker, Prof. Gavin Giovannoni and Dr. Samuel Jackson and for their continuous guidance and support. In particular, I would like to express my sincere gratitude to Prof. David Baker for his expertise, mentoring, and patience throughout my PhD studies.

I would like to thank Dr. Mark Baker (Queen Mary University of London) for his assistance with electrophysiology and his expertise and direction. Thanks to the researchers at the Institute of Ophthalmology, UCL; Prof. Peter Munro for his help with electron microscopy, Prof. Pete Coffey for his guidance and loan of the optokinetic drum and Dr. Peter Lund von Leithner for his expertise on ophthalmic devices. Thanks to Dr. Dave Selwood (The Wolfson Institute for Biomedical Research, UCL) for providing CFM1604. Thanks to Dr. Zubair Ahmed (School of Clinical and Experimental Medicine, University of Birmingham) and Quark Pharmaceuticals Inc (USA) for providing the caspase-2 siRNA.

It has been a pleasure to work with everyone in the Neuroimmunology Research Group (Blizard Institute, Queen Mary University of London) who are a friendly and enthusiastic team to work with. In particular I would like to thank Sarah Al-Izki for her help in the lab, encouragement through stressed times and for her tremendous support over the past few years.

I would like to thank my husband, Aidan for his constant love and support and his patience and understanding throughout my PhD. I would also like to thank my parents who I will be forever grateful for their constant source of love and encouragement throughout my education.

This PhD project would not have been possible without funding from the Medical Research Council, Barts and The London Charitable Fund, Multiple Sclerosis Society, National Multiple Sclerosis Society and in particular the National Centre for the Replacement, Refinement and Reduction for the funding to advance the project by purchase of the Heidelberg Spectralis machine.

Chapter 1

Introduction

1.1 Multiple sclerosis

Multiple sclerosis (MS) is a chronic inflammatory neurodegenerative disease of the central nervous system (CNS), which due to its high prevalence is the most common disabling disease in young adults (Noseworthy *et al.*, 2000). The first definitive clinicopathological account of MS as a disease was by Jean-Martin Charcot in 1868 (McDonald, 1993) who described MS as a neurological condition with the presence of *'la sclérose en plaques'* in the brain and spinal cord following autopsy. MS presents as a series of attacks of potentially autoimmune-mediated inflammation leading to demyelination and neuronal damage and consequently neurological disability. Globally, MS affects approximately 2.5 million people with a mean onset age of 30 years and a variable disease course and outcome (McQualter & Bernard, 2007). It is estimated that there are 100,000 people in the UK with MS and a MS Register is currently being setup to gain a more accurate estimate (MS Society).

There is no known single causative element in MS and it is plausible that there are several interacting factors (Weiner, 2004). Disease susceptibility is associated with environmental (Ebers, 2008), genetic (Sawcer, 2008) and gender factors (Orton *et al.*, 2006). Environmental factors studied for their association with disease prevalence include infections, diet, trauma, pollution, climate, chemical exposures, vitamin D and occupational hazards (Hauser & Oksenberg, 2006). Evidence suggesting that environmental triggers are causative factors comes from migration and epidemiological studies (Gale & Martyn, 1995). The most researched and plausible causative factors in MS are infectious agents, such as Epstein-Barr virus (EBV), Human Herpesvirus type 6, Human endogenous retrovirus and *Chlamydia pneumonia* (Hauser & Oksenberg, 2006; Marrie, 2004).

Currently, EBV is being intensively investigated as one of the primary infectious agents associated with a moderately increased risk of MS (Pohl, 2009). EBV is a member of the gamma-herpes virus family, which is present in 90% of adults in all populations (Straus *et al.*, 1993). EBV infection in

children is usually asymptomatic, however in young adults EBV infection can cause infectious mononucleosis due to an increase in circulating cytotoxic T lymphocytes and inflammatory cytokines (Kutok & Wang, 2006). A link between infectious mononucleosis and MS was initially proposed from epidemiological evidence showing a similarity in terms of age, distribution and ethnicity (Warner & Carp, 1981). Large population studies show EBV infection leads to an increase in susceptibility to MS (Ramagopalan *et al.*, 2009b), (Levin *et al.*, 2010). However, in paediatric MS the rate of EBV infection is 83-99% (Alotaibi *et al.*, 2004; Banwell *et al.*, 2007); therefore suggesting that EBV infection is associated with the risk of developing MS but not a requisition for the development of MS. Additional evidence for a link between EBV and MS comes from studies which show increased levels of EBV antibody titre in MS patients compared to controls (Bray *et al.*, 1983). EBV infected B cells were present in ectopic meningeal follicles of MS patients (Serafini *et al.*, 2007), suggesting EBV infected B cells infiltrate the brain and elicit damage leading to the initiation of MS. However, these results have not been reproduced (Peferoen *et al.*, 2009 ; Willis *et al.*, 2009) and the role of EBV in the pathogenesis of MS remains to be clarified due to the difficulty in ascertaining the presence of viral infections in the brain. There is therefore compelling evidence to show a link between MS and EBV infection, although the underlying mechanisms are unclear and future studies will reveal if EBV is a leading causative element in MS.

Epidemiological studies have identified clusters of MS cases, which indicate a genetic component of disease susceptibility independent of geographical location and familial aggregation of MS (Riise, 1997). Population studies have shown an increased risk of disease in family members of affected individuals compared to the general population (Ebers *et al.*, 1995; Sadovnick *et al.*, 1996). Monozygotic twins have a greater concordance (~30%) than dizygotic twins (~6.5%); these values are relatively low therefore indicating other factors influencing disease susceptibility (Sadovnick *et al.*, 1993). There is a link between MS and genes of the major histocompatibility complex (MHC), which plays an important role in the immune system and autoimmunity (Lincoln *et al.*, 2005). The human leucocyte antigen (HLA) class II region, a subset of MHC genes, is associated with disease susceptibility (Oksenberg & Barcellos, 2005). In particular the *DRB1*1501* allele and its associated serotype *DR2* have been found to have a dose effect on MS susceptibility (Barcellos *et al.*, 2003). More recently, genome-wide association studies have been conducted to reveal SNPs, which are associated with MS (Kemppinen *et al.*, 2011). From these studies 16 putative loci have been identified with immunological or neurological functions, including IL7 receptor (Lundmark *et al.*, 2007), CD58 (De Jager *et al.*, 2009) and IL2 receptor (Alcina *et al.*, 2009).

A collaborative genome-wide association study of 9,792 MS patients confirmed previously suggested genetic associations and revealed a further 29 new susceptible loci involved in the pathogenesis of MS (Sawcer *et al.*, 2011).

Gender factors also play an important role in disease susceptibility. Population based studies show a bias towards females (2:1), due to an unidentified sex specific susceptibility factor (Orton *et al.*, 2006). The gender bias appears to be increasing and is speculated to be caused by environmental and lifestyle factors (Debouverie *et al.*, 2007; Noonan *et al.*, 2002).

The prevalence of MS varies around the world; as a general rule the prevalence increases with increasing latitude from the equator (Kurtzke, 1991). The highest prevalence of MS occurs in North America, Northern Europe, Southern Australia and New Zealand (Kurtzke, 1975). The geographical variation in MS incidences has been correlated to UV exposure and its resultant effect on vitamin D synthesis (Handunnetthi & Ramagopalan, 2010). There is an increasing interest in the positive role of vitamin D in MS; based on experimental (Cantorna *et al.*, 1996) and epidemiological evidence (Pierrot-Deseilligny, 2009). The benefits of vitamin D are thought to be mediated by its effects on the immune system (Mora *et al.*, 2008), although vitamin D is neuroprotective in neuronal cultures (Wang *et al.*, 2001). Vitamin D is an immunoregulatory agent, which modulates T cell activation and regulates class II HLA and CD4 antigen expression (Rigby *et al.*, 1990). Vitamin D controls HLA gene expression by a direct interaction with a functional vitamin D response element in the promoter region of *HLA-DRB1*, which is preserved in the MS associated *DRB1*1501* allele (Ramagopalan *et al.*, 2009a). These results provide a mechanism which links genetic and environmental factors of MS susceptibility.

Migration studies have also indicated a link between environmental factors and the risk of developing MS. Migration of individuals as adults from areas of low MS risk to high MS risk (UK) retained their low risk of MS from their country of origin (Visscher *et al.*, 1977). In contrast migration as a child from a low risk to a high risk area increases your risk of developing MS.

1.1.1 Clinical

In the majority of people with MS the disease course is characterized by episodes of relapse and remission of paralysis, which after a variable period of time enters the secondary progressive

phase. A minority of people (~10-15%) have a progressive course from the onset and are referred to as having primary progressive MS (PPMS). Based on the clinical course, several subtypes of disease have been defined (Keegan & Noseworthy, 2002). MS is clinically diagnosed according to the 'McDonald Criteria', which required one to demonstrate dissemination of disease in both time and space using both clinical and MRI criteria (McDonald *et al.*, 2001). The diagnostic criteria also incorporate abnormal cerebral spinal fluid (CSF) and evoked potentials (Polman *et al.*, 2006).

In 80% of clinical definite MS cases, patients with active disease have a relapsing-remitting form of MS (RRMS), categorised by intermittent attacks followed by periods of remission (Noseworthy *et al.*, 2000). Due to accumulation of CNS damage, the disease usually progresses and deteriorates to become secondary progressive disease (SPMS). In 10-15% of clinically definite MS cases, patients present with a PPMS with no signs of remission from onset (Miller & Leary, 2007). There is also a subgroup of patients that have 'benign' MS, which shows little or no progression in disease severity. The true frequency of benign cases is unknown due to its unclear definition, current literature suggests 6-64% of MS cases are benign (Ramsaransing & De Keyser, 2006). Furthermore, the clinical implications of benign MS are variable and some patients will show clinical deterioration many years after diagnosis (Pittock *et al.*, 2004).

Neurological symptoms present in MS vary depending on the specific CNS pathways involved. Common initial symptoms include weakness of limbs, sensory disturbance, optic neuritis (ON), diplopia and ataxia (Hauser & Oksenberg, 2006). As the disease progresses, patients may suffer from vertigo, fatigue and bowel and bladder disturbance (Hauser & Oksenberg, 2006). Patients may also suffer from cognitive deficits and depression. Although MS is typically not life threatening, mortality is slightly higher in MS patients due to long-term disability and complications associated with disease (Ragonese *et al.*, 2008); on average the life expectancy of someone with MS is reduced by 7 to 10 years.

1.1.2 **Pathophysiology**

The pathology of MS is complex and the sequence of events leading to initiation of disease remains to be established. Complexity arises due to the heterogeneous nature of the disease, which progresses in a dynamic and unpredictable manner (McFarland & Martin, 2007). MS appears to be an immune-mediated disease initiated by the activation of autoreactive T cells,

which leads to an inflammatory cascade and ultimately myelin destruction, axonal loss and neurological deficit (Figure 1.1) (Weiner, 2004).

MS is initiated by an unknown mechanism, which appears to activate auto-reactive T cells in the periphery and leads to a disruption of the blood brain barrier (BBB). Disruption of the BBB in MS has been demonstrated using histology (Broman, 1964) and clinically using gadolinium enhanced MRI (Alnemri *et al.*, 1996) which identifies active lesions in MS patients (Grossman *et al.*, 1986). Activated circulating T cells adhere to the endothelium by ligand-receptor interactions of adhesion molecules, such as very late activation antigen-4 (VLA-4/CD49d) with its ligand vascular cell adhesion molecule-1 (VCAM-1 CD106) on brain endothelium (Hemler, 1990). Upon binding, T cells penetrate the BBB using matrix metalloproteinases, matrix degrading enzymes expressed under inflammatory conditions capable of degrading tissue macromolecules (Kouwenhoven *et al.*, 2001). As a result, the BBB develops a lack of structural integrity, leading to a disruption and reorganisation of tight junctions and an influx of immune cells into the microenvironment of the CNS (Kirk *et al.*, 2003; Plumb *et al.*, 2002). Homeostatic regulation in the CNS is also maintained by P-glycoprotein and other ATP-binding cassette transporters, which keep hydrophobic molecules out of the brain (Schinkel *et al.*, 1994). During neuroinflammation, CD4+ T cells decrease the expression of P-glycoprotein on the BBB, therefore disturbing this balance, potentially aggravating disease (Kooij *et al.*, 2010).

In the CNS the autoimmune response is activated further and targeted towards putative oligodendrocytes and myelin components, such as alpha B-crystallin, myelin associated glycoprotein (MAG), myelin oligodendrocyte glycoprotein (MOG), proteolipid protein (PLP) and myelin basic protein (MBP) (Sospedra & Martin, 2005). This leads to chronic inflammation in the CNS, which amplifies the response of pro-inflammatory molecule release, such as cytokines, chemokines, adhesion molecules and matrix degrading enzymes (Hjelmström *et al.*, 1998). This environment results in further BBB permeability and leucocyte trafficking and results in amplification of disease severity. The complex cascade of events in MS ultimately leads to demyelination and accumulative axonal loss, contributing towards neurological disturbances (Neumann, 2003). Remyelination occurs spontaneously in response to a demyelinating attack in MS (Gensert & Goldman, 1997).

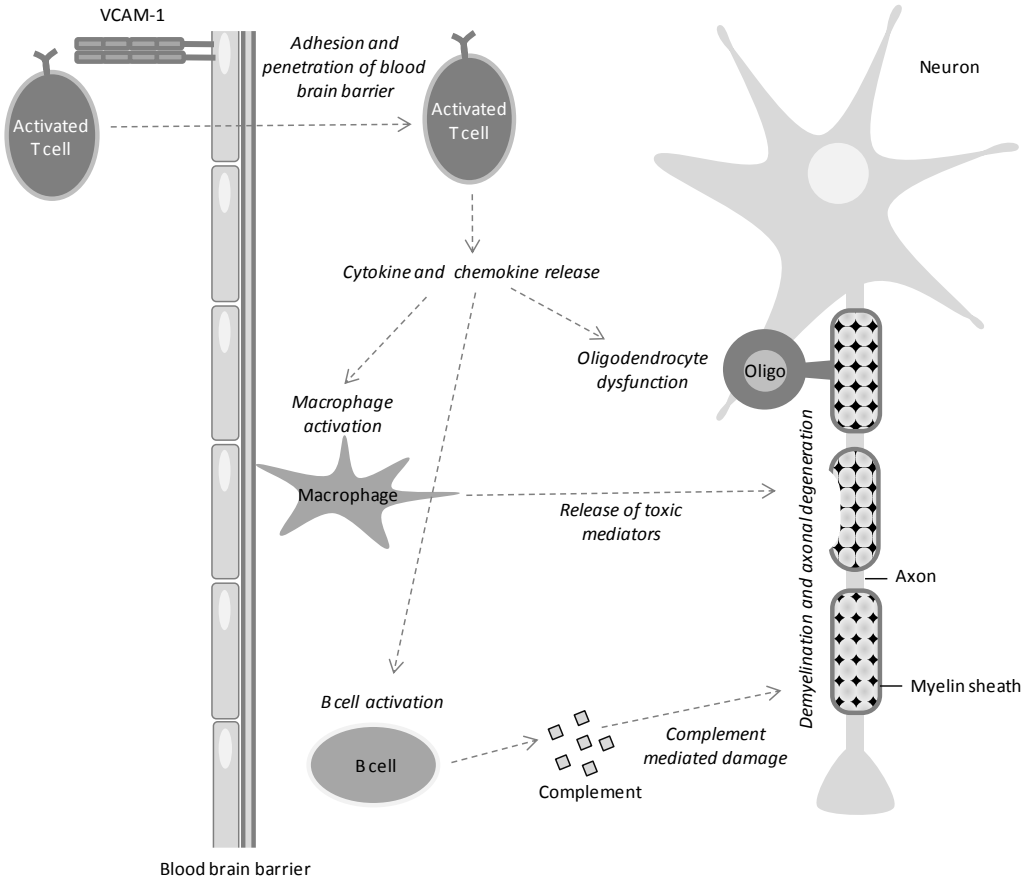

Figure 1.1 ***Demyelination and neurodegeneration in MS****. Activated T cells cross the BBB and by expression of VCAM-1 on brain endothelium. Inside the CNS, activated T cells release pro-inflammatory cytokines and chemokines leading to recruitment and activation of inflammatory cells (macrophages, CD8+ cytotoxic T cells and B cells), which mediate oligodendrocyte dysfunction resulting in demyelination and axonal degeneration.*

The major histopathalogical hallmark of MS is the demyelinated plaque or lesion. Lesions can be found in the optic nerves, periventricular white matter, brain stem, cerebellum and spinal cord (Noseworthy *et al.*, 2000). The lesion is characterized by a loss of myelin and oligodendrocytes, axonal damage, hypertophic astrocytes and macrophages (Frohman *et al.*, 2006). Variations in the structure and immunology of plaques verify the complex pathogenic nature and heterogeneity of disease progression. Lesions can be characterized and defined into pathological subtypes by the degree of myelin loss, geography and extension of lesions, pattern of oligodendrocyte destruction and complement activation (Lucchinetti *et al.*, 2000). There are predominately two main types of lesions in an MS brain; the active lesion and the chronic lesion. An active lesion can be defined by an indistinct margin, perivascular infiltration, loss of myelin and oligodendrocytes and myelin laden macrophages. A method used to classify lesions was proposed to identify heterogeneity between patients with four distinct groups (Patterns I, II, III and IV) (Table 1.1) (Lassmann *et al.*, 2001).

Pattern of demyelination	Pathology
Pattern I	Demyelination due to T cell and macrophage infiltration.
Pattern II	Demyelination due to antibody and complement deposition.
Pattern III	Demyelination due to oligodendrocyte dysfunction and apoptosis.
Pattern IV	Primary oligodendrocyte degeneration through DNA fragmentation with secondary demyelination.

Table 1.1 ***Different patterns of demyelination in multiple sclerosis****. Description of the pathology of Patterns I, II, III and IV and the heterogeneity of immunopathological process in MS.*

Chronic lesions contain sharp edges, perivascular cuffs, increased recruitment of oligodendrocytes and some signs of remyelination. The centre of a chronic lesion contains naked axons surrounded by scarring astrocytes with no oligodendrocyte support.

Demyelination in MS is thought to be caused by autoimmunity to CNS myelin components and a repeated activation of an inflammatory cascade, which attacks oligodendrocytes and myelin (McQualter & Bernard, 2007). The traditional view is that demyelination is the key event in MS, which results in neurological deficits. Demyelination results in reduced axonal support, redistributed ion channel density and reduced neuronal excitability leading to conduction block (McDonald, 1969 #412) and axonal loss (Kornek, 2000 #1511). As a result of demyelination, axons become exposed to damage from proteases, inflammatory cytokines, nitric oxide, free radicals and glutamate (Bjartmar *et al.*, 2003). However, it is debatable whether demyelination is a prerequisite to axonal injury and long term neurological disability. Demyelination is thought to be mediated by mediators of both the adaptive (T cells and B cells) and the innate immune system (macrophages, NK cells, γ/σ T cells) (Pouly & Antel, 1999).

Activated T cells can indirectly damage the CNS by the production of proinflammatory products which activate endogenous microglia and infiltrating macrophages (Jack *et al.*, 2005). Although more emphasis has been given to research on the role of CD4+ T cells, CD8+ T cells are also implicated in the pathogenesis of MS and are associated with pathological lesions (Traugott *et al.*, 1983). It is speculated that CD4+ T cells initiate the formation of MS lesions and CD8+ T cells amplify the damage to axons and play a regulatory role (McFarland & Martin, 2007).

1.1.3 Current treatments

Current therapies are aimed at modulating the immune response. Anti-inflammatory and immunosuppressive therapies can provide beneficial effects on relapse rate and symptoms in early disease, but do not appear to impact on disease progression (Confavreux & Vukusic, 2004). There is an urgent need for remyelination and neuroprotective strategies as well as targeted immunomodulatory therapies.

Initially, immunosuppressive therapies were used to treat MS based on the assumption that MS is an autoimmune disease (Whitaker, 1994). Corticosteroids are currently used to treat relapses and modulate the duration of relapse in MS patients by suppressing crucial elements of the immune system and vascular permeability (Tischner & Reichardt, 2007). However, many of these treatments produce systemic adverse effects and are only partially effective in reducing disease severity (Thrower, 2009).

Immunomodulatory drugs were later developed and used to control relapses of MS; the most successful therapies include interferon-β-1b (IFNβ) (Betaferon™, Bayer) and IFN-β-1a (Avonex™, Biogen Idec; Rebif™, MerckSerono), glatiramer acetate (Copaxone™, Teva Pharmaceuticals) and more recently natalizumab (Tysabri™, Biogen Idec) (Kieseier *et al.*, 2008), fingolimod (Gilenya®, Novartis) (Kappos *et al.*, 2010) and cladribine (Movectro™, Merck Serono) (Giovannoni *et al.*, 2010). IFNβ has been proven to decrease the frequency of clinical relapses (Paty *et al.*, 1993) and slow disease progression in some studies (Rudick *et al.*, 1997). This may shift the immune response by altering cytokine production to promote anti-inflammatory conditions over pro-inflammatory conditions (Neuhaus *et al.*, 2007). Glatiramer acetate (GA) is a widely prescribed immunomodulatory drug for RRMS. GA is a synthetic analogue of MBP, initially developed as a research tool to induce experimental autoimmune encephalomyelitis (EAE) but it was discovered to inhibit the development of EAE (Lisak *et al.*, 1983). A successful pilot study of GA (Bornstein *et al.*, 1987) followed by a large scale clinical trial (Johnson *et al.*, 2001) led to approval of GA for the treatment of RRMS. GA primarily affects T cell reactivity and acts as an altered peptide ligand to induce a cytokine shift to T-helper 2 (Th2) cells (Farina *et al.*, 2005). GA acts as a T cell receptor antagonist and binds with high affinity to MHC and prevents MBP binding to inhibit immune cell activation (Fridkis-Hareli *et al.*, 1999).

Natalizumab (Tysabri™) is the first highly targeted therapy for MS and represents a new era of immune specific therapy (Miller *et al.*, 2003). Natalizumab is a humanised monocolonal antibody (mAb) against α4β1-integrin, which is approved for use as a monotherapy for treatment of highly-active relapsing forms of MS. In the highly-active cohort it reduces relapse rates by over 80%. Natalizumab works by reducing the transmigration of lymphocytes into the CNS and also reduces T cell activation and contributes towards T cell apoptosis (Miller *et al.*, 2003). Natalizumab is the first of the next generation of MS drugs that can reduce the relapse by more than 50% (Hutchinson *et al.*, 2009). However, treatment with Natalizumab is associated with an increased risk of developing progressive multifocal leukoencephalopathy (PML) (Twyman & Berger, 2010). PML is caused by JC virus (JCV) infection, which leads to lysis of oligodendrocytes and widespread white matter demyelination. The relatively high incidence of PML cases in patients treated with Natalizumab has raised significant issues over the future of immunomodulatory treatments and our understanding of disease mechanisms.

Rituximab (Mabthera®/Rituxan®) is an anti-CD20 monoclonal antibody, which depletes CD20+ B lymphocytes involved in the pathogenesis of MS, originally developed for the treatment of non-Hodgkin's B cell lymphomas (Maloney *et al.*, 1994). Rituximab has been successful in clinical trials for RRMS (Bar-Or *et al.*, 2008; Hauser *et al.*, 2008) and PPMS (Hawker *et al.*, 2009) and results showed Rituximab slows disease progression and reduces the number of new lesions on MRI and the number of relapses.

Alemtuzumab (Campath™/Lemtrada™) is a human monoclonal antibody targeting CD52, a cell surface antigen expressed by T and B cells, which produces rapid and prolonged lymphopenia (Moreau *et al.*, 1996). A Phase II clinical trial in RRMS showed Alemtuzumab prolonged time to disability and improved clinical and MRI outcomes (Coles *et al.*, 2008). Phase III trial results reported Alemtuzumab reduced the frequency of relapses but did not prevent the progression to disability. This drug however can induce antibody mediated autoimmunity such as idiopathic thrombocytopenic purpura, Grave's disease and Goodpasture's syndrome (Treon *et al.*, 2011; Weetman, 2009).

Fingolimod, FTY720 (Gilenya™) is a sphingosine-1-phosphate (S1P) receptor agonist, which binds to S1P1 receptors on lymphocytes and affects receptor signalling to inhibit lymphocyte migration from secondary lymphatic organs to the periphery (Brinkmann *et al.*, 2004). *In vitro* studies show

that Fingolimod also has functional effects on oligodendrocyte precursor cells (OPC) and may contribute to the remyelinative process (Miron *et al.*, 2008). The latter has recently been challenged by others, which showed Fingolimod failed to promote remyelination *in vivo* (Hu *et al.*, 2011). In clinical trials, Fingolimod reduces the relapse rate, the risk of disability progression and improves MRI outcomes (Kappos *et al.*, 2010) and was shown to be more effective than IFNβ (Cohen *et al.*, 2010). Fingolimod has now been approved in Europe for use in patients with highly active RRMS. Side effects of Fingolimod include an increased risk of secondary tumours and opportunistic infections (Cohen & Chun, 2011). Fingolimod also has off-target effects on several systems in the body due to the wide variety of cellular mechanisms mediated by S1P (Spiegel & Milstien, 2003), resulting in adverse events such as transient bradycardia (Budde *et al.*, 2002).

Cladribine (2-chlorodeoxyadenosine) (Movectro™) is a purine nucleoside analogue resistant to degradation by adenosine deaminase (Carson *et al.*, 1983). Cladribine triphosphate, the activated form of cladribine, causes an accumulation of deoxynucleotides in lymphocytes and disrupts DNA synthesis and repair leading to T cell depletion (Brousil *et al.*, 2006). Phase III clinical trials of oral cladribine showed a statistically significant reduction in relapase rates (Giovannoni *et al.*, 2010). However, cladribine has recently been withdrawn from the market.

The increased efficacy of these new agents has been associated with potentially life threatening complications, which could be anticipated following marked immunosupression such as infections and the development of tumours (Hartung, 2009; Ismail *et al.*, 2008). Immunomodulatory drugs, such as Alemtuzumab, Cladribine, and bone marrow transplantation, significantly affect relapse rate but have a limited effect on disease progression and a new generation of drugs which enhance neuroprotection and neurorepair is required (Pilz *et al.*, 2008; Rice & Scolding, 2007). The ultimate goal in MS is to halt disease progression by focusing on treatment strategies beyond the immune system, which target axonal damage.

1.2 Axonal injury

Neurological disturbances in MS were originally thought to occur as a result of demyelination; however it was subsequently found that axonal injury plays a significant role in early disease pathogenesis (Bitsch *et al.*, 2000; Trapp *et al.*, 1998) and recent findings have shown that axonal loss is the major determinant of neurological disability (Bjartmar *et al.*, 2003). Progression to SPMS and permanent disability appears to occur when a threshold of axonal loss is reached and compensatory mechanisms are exhausted, such as reorganisation of functional pathways (Reddy *et al.*, 2000; Waxman, 1998). There is a matter of debate regarding the sequence of events and the proposition that demyelination is a perquisite to axonal injury, or whether the two events are independent of each other. The "axonal hypothesis" proposes that cumulative axonal loss results in irreversible neurological disability (Bjartmar *et al.*, 2003; Ferguson *et al.*, 1997).

1.2.1 Mechanisms of axonal injury

Axonal injury can be described as the transection of axons and the formation of axonal spheroids and end bulbs (Trapp *et al.*, 1998). Initially axonal loss was hypothesised to occur due to a loss of trophic support for axons following demyelination (Compston, 1996). Mechanisms of axonal injury are unclear, but axonal damage is mediated by a range of factors including inflammatory mediators (Ferguson *et al.*, 1997), NO (Smith *et al.*, 2001), CD8+ T cells (Babbe *et al.*, 2000), glutamate excitotoxicity (Pitt *et al.*, 2000b), mitochondrial dysfunction (Su *et al.*, 2009) and metabolic disturbances leading to toxic ion concentration within the nerve (Dutta *et al.*, 2006).

Studies have shown a correlation of expression between axonal injury and macrophages, microglia and CD8+ T lymphocytes, therefore suggesting axonal injury can be mediated by immune cells (Bitsch *et al.*, 2000). Immune cell mediated axonal injury has also been shown to be a common feature in EAE animal models (Dandekar *et al.*, 2001).

The prolonged activation of glutamate, the main excitatory CNS neurotransmitter, can contribute to axonal damage (Olney, 1969). During neuroinflammation, the levels of glutamate increase due to decreased capability of astrocytes to metabolise glutamate (Hardin-Pouzet *et al.*, 1997) and increased release from unmyelinated axons (Ziskin *et al.*, 2007). Increased availability of glutamate results in an overstimulation of NMDA (N-Methyl-D-aspartate)**,** AMPA (α-amino-3-hydroxy-5-methil-4-isoxazol-propionic acid) and kainite receptors, an influx of sodium and calcium, reversal

of sodium-calcium exchanger and ultimately leads to toxic calcium accumulation in the mitochondria (Matute *et al.*, 2002; Pitt *et al.*, 2000a; Smith *et al.*, 2001; Stout *et al.*, 1998).

Nitric oxide (NO) is a potent signalling molecule, which influences a variety of biological cell responses. The extent that NO contributes towards axonal damage in MS is not fully understood due to its complex biochemistry, production and interaction with its microenvironment. Studies have shown NO has both a beneficial and deleterious effect in MS (Smith & Lassmann, 2002). During inflammation, NO is released from activated inflammatory cells and exposed to axons, leading to axonal damage (Smith *et al.*, 2001a). Circumstantial evidence has been postulated that NO causes axonal damage by a variety of mechanisms inducing impairment of sodium channels (Ahern *et al.*, 2000), potassium and calcium channels (Kurenny *et al.*, 1994), depolarization of axons (Garthwaite *et al.*, 2002) and disruption of the sodium-potassium ATPase pump (Guzman *et al.*, 1995). It is clear that NO has a significant role in the pathogenesis of MS and axonal damage but the role is complex and unclear (Kapoor *et al.*, 1999). Oxidation of NO can produce the highly toxic epitope, peroxynitrite, which induces demyelination and axonal damage (Touil *et al.*, 2001). Peroxynitrite has been found in areas of demyelination and inflammation in MS patients (Cross *et al.*, 1998) and correlates with disease activity in EAE (van der Veen *et al.*, 1997).

In vitro studies suggested a major role for sodium channels in axonal injury (Stys *et al.*, 1992) and propose a sodium cascade. The initial stage in the cascade is energy failure of the Na^+K^+ATPase, which leads to depolarisation and loss of transmembrane gradient. This results in activation of $Na_v1.6$ channels, which stimulates an increase in intracellular calcium (Nikolaeva *et al.*, 2005) leading to activation of calcium dependant degenerative pathways (Stys *et al.*, 1992). This also leads to activation of calpain, a calcium dependant protease, which actively degrades myelin (Banik *et al.*, 1985). Demyelinated axons show an increased expression of sodium channels along the membrane and are more susceptible to injury (Craner *et al.*, 2004b).

1.2.2 Neuroprotective therapies

The impetus to study neuroprotection in MS came from studies in the late 1990's, which showed an increased frequency of axon degeneration in acute lesions (Ferguson *et al.*, 1997; Trapp *et al.*, 1998) and the presence of axonal damage in early stages of MS (Filippi *et al.*, 2003). Axonal damage was also found to correlate with functional disability and reinforce the need for neuroprotective therapies (Davie *et al.*, 1995; De Stefano *et al.*, 1998). Whilst immune suppression

therapies will be indirectly neuroprotective by virtue of preventing the immune cells from triggering damage, this is not sufficient to prevent disease progression due to a neurodegenerative microenvironment (Al-Izki *et al.*, 2011; Pilz *et al.*, 2008; Pryce *et al.*, 2005).

Neuroprotective therapies currently being studied include drugs which are currently approved for use in other indications, including glutamate antagonists (Gilgun-Sherki *et al.*, 2003), sodium, calcium and potassium channel blockers, cannabinoids (Pryce *et al.*, 2003) and erythropoietin (Li *et al.*, 2004b). Research has also identified modulators that prevent axonal loss (such as leukaemia-inhibitory factor, ciliary neurotrophic factor, erythropoietin and insulin-like growth factor), which could potentially be used as neuroprotective therapies but require further exploration before clinical application.

Sodium channel blockers, such as Carbamazepine, were initially used to treat trigeminal neuralgia, a positive symptom of MS (Espir & Millac, 1970). Tetrodotoxin (Craner *et al.*, 2004b), lidocaine (Craner *et al.*, 2004a), phenytoin and carbamazepine (Fern *et al.*, 1993) have been shown to prevent axonal injury in *in vitro* preparations of central myelinated axons. Sodium channel blockers have also shown to reduce axonal loss and have a protective effect in animal models of EAE (Bechtold *et al.*, 2004; Bechtold *et al.*, 2006; Lo *et al.*, 2002). However, flecanide reduced clinical disease severity in early stages of disease, which therefore suggests an immunomodulatory effect (Bechtold *et al.*, 2005). Sodium channels are present on macrophages and microglia in EAE and acute MS lesions, and therefore suggest a role in immune cell function (Black *et al.*, 2007b; Craner *et al.*, 2005).

The protective effects of voltage-gated calcium channel antagonists have been demonstrated *in vivo* to prevent calcium dependant axonal damage (Imaizumi *et al.*, 1999), reduced inflammation and ameliorate EAE (Brand-Schieber & Werner, 2004). An alternative method of inhibiting the effect of calcium is targeting calpain, a calcium-dependant protease, which degrades myelin and axonal elements (Hendriks *et al.*, 2005). Using a calpain-inhibitor (cycteic-leucyl-argininal), the levels of axonal damage were reduced in an chronic progressive model of EAE (Hassen *et al.*, 2008). However, there are currently no clinical trials investigating calcium channel blockers as a neuroprotective therapy in MS.

Several studies have shown the AMPA receptor antagonist NBQX (2,3-dihydroxy-6-nitro-7-sulfamoyl-benzo(F)quinoxaline) has neuroprotective effects in EAE models (Pitt *et al.*, 2000b;

Smith *et al.*, 2000). The effects of riluzole, a drug which inhibits glutamate release and modulates kainate and NMDA receptors, were investigated in a pilot study in PPMS and showed a favourable but not significant effect on axonal loss (Kalkers *et al.*, 2001). To investigate the full potential of glutamate antagonists, larger clinical trials are needed across a variety of MS subtypes.

Insulin growth factor-1 (IGF-1) has been shown to promote oligodendrocyte growth and maturation and has been proposed as a neuroprotective therapy (McMorris & McKinnon 1996). However, there are conflicting reports of the effect of IGF-1 in animal models of EAE; studies have either shown an improvement in clinical deficits (Liu *et al.*, 1997; Yao *et al.*, 1996) or have been limited to a transient effect (Cannella *et al.*, 2000). Erythropoietin (Epo) is a haematopoietic growth factor, which has also a candidate for neuroprotective therapy. Epo receptors are expressed throughout the CNS and activation has beneficial effects on neurological injury, including ischemia, trauma and epilepsy (Brines *et al.*, 2000; Buemi *et al.*, 2003). In animal models of EAE, Epo has both an anti-inflammatory and neuroprotective effect (Diem *et al.*, 2005; Li *et al.*, 2004a). Following on from beneficial experimental models, a pilot study in PPMS was carried out, initial results show a reduction in disability and an improvement in cognition (Ehrenreich *et al.*, 2007).

Cannabis is used by approximately 15% of MS patients to continually relieve symptoms such as sleep, pain and to improve mood (Clark *et al.*, 2004). Cannabinoids have also been shown *in vitro* to have an effect on several mechanisms of axonal injury, including inhibition of glutamate release and the resultant excitotoxic damage (Fujiwara & Egashira 2004). In addition, they can slow the neurodegenerative process: exogenous agonists for the CB1 (cannabinoids type 1) receptors offered significant neuroprotection in an animal model of EAE (Pryce *et al.*, 2003). The neuroprotective effects of tetrahydrocannabinol are currently being investigated in a clinical trial for people with PPMS (Cannabis Use in Progressive Inflammatory brain Disease, CUPID), based upon evidence indicating neuroprotective effects of cannabinoids (El-Remessy *et al.*, 2003; Hampson *et al.*, 1998; van der Stelt *et al.*, 2001)

1.3 Optic Neuritis

ON is an acute inflammatory condition affecting the afferent visual system which causes painful vision decline over several days. Acute ON is one of the most common causes of unilateral painful visual loss. The incidence of ON is 3-5/100,000 cases per year (Kaufman *et al.*, 2000). ON may either occur in isolation (clinically isolated syndrome) or in association with MS. A significant amount of information has been gathered from the ON Treatment Trial (ONTT), which assessed treatment with corticosteroids, visual function, and development of MS over a period of 15 years (Beck, 1988). The cause of ON is unclear and there are numerous conditions which may lead to the development of ON: MS, neuromyelitis optica (Devic's disease), viral infections (measles, mumps), mycoplasma, infectious mononucleosis, herpes zoster and intraocular inflammation (Burton *et al.*, 2010).

1.3.1 Clinical

The primary symptom of ON is loss of vision, which is due to inflammation and oedema (Youl, 1991 #1086), demyelination and axonal loss in the myelinated part of the optic nerve or chiasm. Presenting symptoms usually last approximately 7-10 days and include sub-acute visual loss, diminished central acuity, disturbed colour vision and afferent pupillary defects (Optic Neuritis Study, 1991). Approximately 90% of ON cases occur in association with periocular pain (Lee *et al.*, 2004). Misdiagnosis of ON commonly occurs as clinical symptoms overlap with other optic neuropathies: neuromyelitis optica (known as Devic's disease), anterior and posterior ischemic optic neuropathies and infective conditions (Shams & Plant, 2009).

The visual prognosis following acute optic neuritis is good, with approximately 80% of patients recovering within 2-3 weeks and stabilising within a year (Beck *et al.*, 2004). Results from the ONTT trial showed that one year following ON attack, 93% of patients had vision better than 20/40 and 69% patients had vision better than 20/20 (Optic Neuritis Study, 2008). Long term follow up of acute ON patients has shown that visual function recovers in the majority of patients (Hickman *et al.*, 2004).

1.3.2 Treatment

Treatment of ON is typically treated with corticosteroids, which also reduce the rate of development of MS (Beck *et al.*, 1993b). The ONNT assessed the benefits of corticosteroid

treatment on visual recovery (Optic Neuritis Study, 1991). The trial reported 92% of patients suffered from concomitant pain with eye movements with a varying degree of vision loss. A meta-analysis of clinical studies of corticosteroid treatment in ON concluded that corticosteroid treatment improves short term visual recovery but had no long term benefits (Brusaferri & Candelise, 2000). Corticosteroid treatment is associated with a range of side effects including insomnia, mood changes, stomach upset, hypertension, hyperglycaemia, acne and weight gain (Beck *et al.*, 1992). As there is no alternative treatment, the recommendation from the ONTT is 1g of intravenous methylprednisolone per day for three days for patients with who require fast recovery (Beck *et al.*, 1992).

1.3.3 Pathophysiology

The pathophysiology of ON closely reflects the pathophysiology of MS; all pathological features of MS present in the brain and spinal cord are recapitulated in the anterior visual system during ON, which can therefore be used as an insight into the pathophysiology of MS (Trapp *et al.*, 1998). The relationship between pathological features of ON and clinical deficits have been well documented using MRI and recording VEP (visual evoked potential) (Youl *et al.*, 1991). Inflammation can be present in any part of the afferent visual system, including the optic chiasm and optic tract. It is hypothesized that ON starts with a focal area of inflammation around venules in the optic nerve, which leads to increased permeability of the blood nerve barrier (Rizzo *et al.*, 2002). Peripheral memory T-lymphocytes, which cross the BBB and become activated ultimately lead to demyelination and axonal loss, leading to conduction block and impairment of vision.

1.3.4 Relationship between ON and MS

There is a significant relationship between MS and ON. Following an episode of ON, the risk of developing MS can be assessed by MRI and the presence of oligoclonal bands in the CSF. Approximately 50-70% of people presenting with ON will have white matter abnormalities in the brain or spinal cord, which can be detected by MRI (Beck *et al.*, 1993a; Dalton *et al.*, 2003; Jacobs *et al.*, 1991). Approximately 40% of MS patients experience ON as their first clinical demyelination event and 50-70% of patients with monosymptomatic ON have clinically silent MS lesions (Söderström, 2001). Results from the ONTT reported the risk of developing MS after acute ON is 38% after 10 years (The Optic Neuritis Study, 2003) and 50% after 15 years (The Optic Neuritis Study, 2008). The risk of children developing MS after acute ON is much lower and estimated at approximately 26% after 40 years (Lucchinetti *et al.*, 1997).

Post-mortem studies of MS patients show a high frequency of histological lesions in the visual pathway, despite no clinical signs of optic abnormalities (Toussaint *et al.*, 1983). Measurement of retinal nerve fibre layer (RNFL) thickness, in secondary progressive MS patients with no clinical history of ON, is significantly reduced compared to healthy controls (Henderson *et al.*, 2008). Therefore, it is clear that there is an important link between ON and MS. Early and accurate diagnosis of ON and MS is crucial due to the availability of disease modifying therapies, which can slow disease progress and relapse rate. Clinical studies of IFNβ in patients with acute ON reported a delayed conversion to clinically definite MS (Kappos *et al.*, 2006).

1.3.5 Imaging ON

A range of techniques are used to examine changes in structure and function of the afferent visual pathway in ON: visual evoked potential (VEP), MRI, magnetisation transfer imaging, magnetic resonance spectroscopy, diffusion tensor imaging, optical coherence tomography (Sinha *et al.*) and confocal scanning laser ophthalmoscopy (cSLO) (Kolappan *et al.*, 2009).

VEP measures the gross electrical potential from the visual cortex in response to a visual stimulus and can be used to quantify retinal nerve cell loss (Ridder & Nusinowitz, 2006). Prior to the development of MRI technology, optic nerve conduction was measured using VEP, which are capable of detecting subclinical optic nerve demyelination (Holder, 2004). Measurement of VEP has been proposed as an outcome measure for remyelinative therapies to quantify subclinical demyelination in MS patients (Niklas *et al.*, 2009). MS patients have an increased frequency of VEP abnormalities due to visual pathway disruption (Lester *et al.*, 2009). During ON, the VEP is characteristically delayed with preserved amplitude. Severe ON results in reduced amplitude due to temporary conduction block. The VEP may return to normal following resolution of ON (Youl *et al.*, 1991). However, measuring VEP has a limited clinical utility and is normally only used when there is a lack of other techniques available to accurately diagnose MS (Gronseth & Ashman, 2000), the exception being primary progressive MS, where it is very helpful in demonstrating dissemination in space (McDonald criteria).

MRI is routinely used to identify lesions in brain and spinal cord, however, the optic nerve is rather small and challenging to routinely study on MRI (Miller *et al.*, 1988). However, MRI can be used to determine variations in dimensions of intraorbital optic nerve and can therefore be used to

support diagnosis of ON. In approximately 90% of cases, ON can be detected by an increased signal in optic nerves using gadolinium enhanced MRI; gadolinium enhancement represents a breach in the integrity of the blood nerve barrier (Rizzo *et al.*, 2002). MRI is an important prognostic tool to identify white matter lesions and determine the risk of developing MS following an attack of ON (Barkhof *et al.*, 1997).

OCT is a relatively new technology, which is increasingly being used as an imaging outcome for MS clinical trials. OCT detects changes in RNFL thickness and macular volume using reflection patterns from infra-red light. Retinal imaging using OCT provides a correlate to underlying pathology of ON and can detect RNFL thinning due to axonal loss (Costello *et al.*, 2006; Fisher *et al.*, 2006; Frohman *et al.*, 2008b; Gordon-Lipkin *et al.*, 2007; Grazioli *et al.*, 2008; Henderson *et al.*, 2008; Sergott *et al.*, 2007; Trip *et al.*, 2005). The development of high-resolution spectral domain scanners has increased the sensitivity and reliability of OCT systems and led to the proposal that they should be used as a primary outcome measure for analysing the efficacy of neuroprotective agents by using the retina as a target organ for therapeutic studies (Barkhof *et al.*, 2009).

1.4 The visual system

As described in the previous section there is a clear relationship between ON and MS showing that the anterior visual pathway is frequently involved in the pathogenesis of MS (Diem *et al.*, 2003; Henderson *et al.*, 2008; Toussaint *et al.*, 1983). The visual pathway is an ideal model to develop neuroprotective therapies due to its ease of accessibility through the pupil opening and the development of novel technology to quantify changes in neuronal integrity, including OCT and cSLO (Frohman *et al.*, 2008a). Therefore to produce a novel animal model, which can be used as a correlate for human studies, the visual pathway can be used as a target for investigating neuroprotective therapies.

1.4.1 Structure of the eye

The eye is formed of three major layers (Berne & Levy, 2000); the outer layer, the middle layer and the inner layer. The outer layer is composed of a fibrous coat, which includes the transparent cornea, conjunctiva and opaque sclera. The middle layer is composed of the vascular coat, iris and choroid. The iris contains smooth muscles (pupillary dilator and sphincter muscles), which is used to control the size of the pupil and the amount of light entering the eye. The inner layer is composed of the retina, which converts the external environment into neural impulses that can be transmitted to the brain. The eye also contains a lens, which focuses light onto the retina.

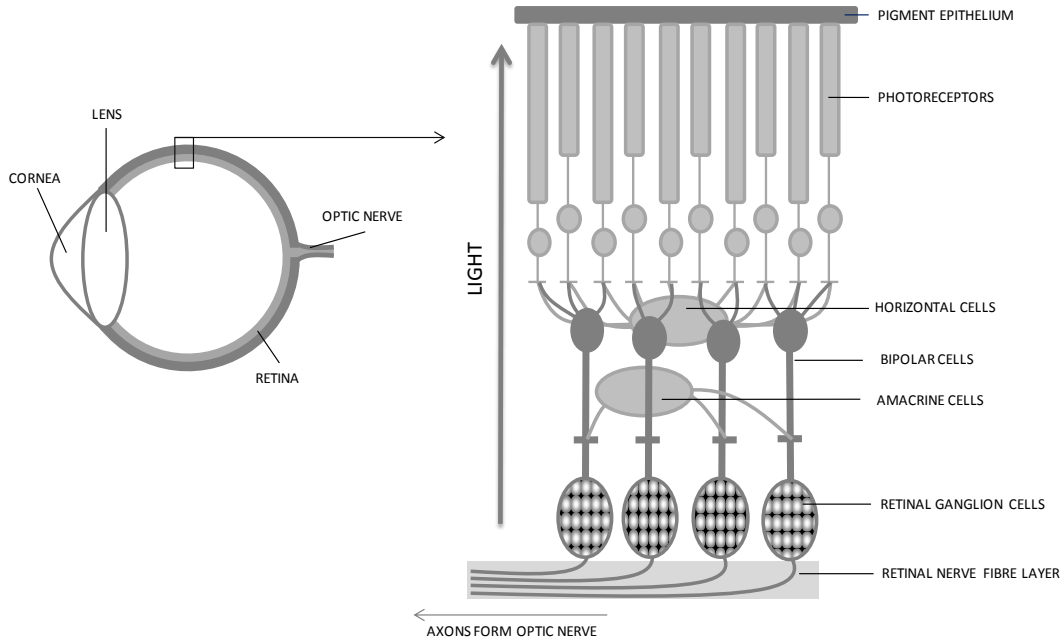

Figure 1.1 ***A schematic diagram of the cross sectional structure of the a) eye and b) retina.*** *The retinal nerve fibre layer (RNFL) contains axons from the retinal ganglion cells (RGC) that form the optic nerve.*

The retina consists of several layers of neuronal and non-neuronal components (Figure 1.). Photoreceptors transduce light energy into neural impulses. There are two types which are functionally distinct and heterogeneously distributed – the rods and the cones (Kawamura & Tachibanaki, 2008). Rods have a low threshold and are responsible for light sensitivity (scotopic vision). In contrast, cones require more light to become activated and are responsible for colour vision (photopic vision) (Conway, 2009). Information is transmitted from the photoreceptors to converge on bipolar cells and then ganglion cells (Snellman *et al.*, 2008). The retina also contains interneurones, consisting of horizontal cells and amacrine cells. Müller cells are the predominate glial cells in the retina, which synthesise and secrete signalling molecules which promote neuron viability, differentiation, synaptogenesis and neuroprotection (Bringmann *et al.*, 2006; de Melo Reis *et al.*, 2008). Ganglion cells can be divided into three groups according to their response to stimuli and receptive fields (X-, Y-, W-) (Hide-Aki, 1983) and are located at the interface of the retina and the vitreous humour.

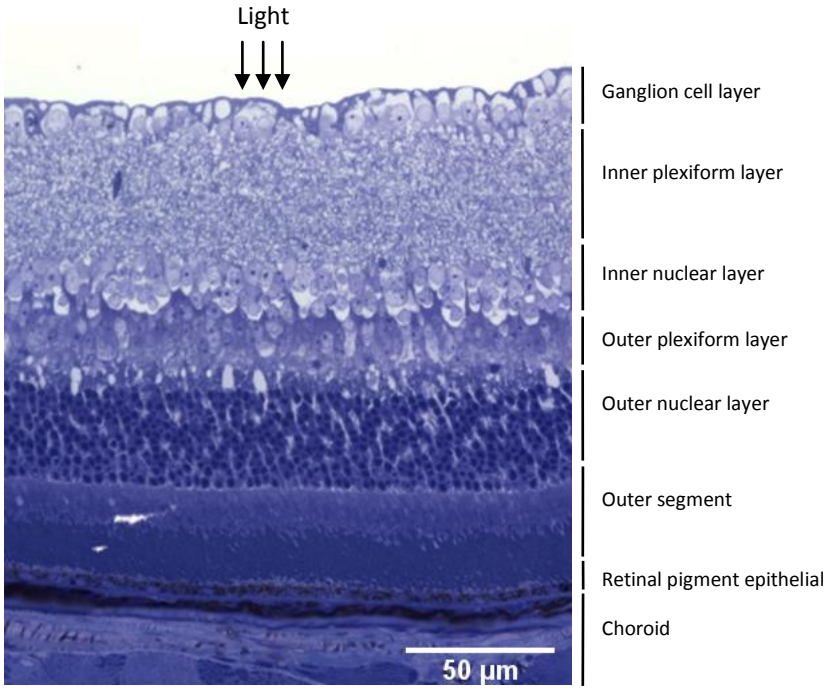

Figure 1.3 ***Layers of the retina****. Histological cross-section of retina taken from C57BL/6 mouse. Animals were perfused and tissue was fixed in Karnovsky's Fixative. Tissue was embedded in resin and semi-thin sections (0.7µm) were cut. 20x objective lens magnification*

Ganglion cell axons leave the retina to form the optic nerve (cranial nerve II), which becomes myelinated after passing out of the eye through the lamina cribrosa (Selhorst & Chen, 2009).

Axons from both eyes converge at the optic chiasm (Jeffery, 2001). There are three main pathways that transmit information along the optic nerve from the retina to the brain; reinogeniculocalcarine (visual processing), retinomesencephalic (pupillary light reflex) and retinohypothalamic (regulation of the circadian clock) (Frohman *et al.*, 2008a).

The optic tract synapses at the lateral geniculate nucleus (LGN) in the thalamus. The LGN consists of six layers; ipsilateral input (layers 2, 3 and 5) and contralateral input (layers 1, 4 and 6) (Sherman & V.A. Casagrande, 2005). The LGN also receives input from other areas, including visual cortex, brainstem nuclei and reticular nucleus of the thalamus. The LGN projects to the primary visual cortex of the occipital lobe in the cerebral cortex (Sincich & Horton, 2005).

1.4.2 The visual system as a model

The visual system is a valuable tool for studying neurodegeneration in the CNS due to its ease of accessibility and CNS characteristics (the presence of astrocytes, oligodendrocytes, microglia, BBB and neurons). Mice were initially disregarded as an ophthalmic research tool due to small eye size, experimental fragility and low acuity. Also, mice are not considered to be "visual animals" (Pinto & Enroth-Cugell, 2000) due to their nocturnal nature. However, advances in mouse genetics and breeding and the introduction of transgenic and knockout technology lead to the generation of mice replicating ocular diseases, such as retinitis pigmentosa (Humphries *et al.*, 1997), cataract formation (Runge *et al.*, 1992), retinal degeneration (Chang *et al.*, 1993) and glaucoma (John *et al.*, 1998). There are several differences between human and rodent eyes; the most noticeable being the size. Rodent eyes also lack a macula, a fovea and have a significantly larger lens.

The development of mouse models in ophthalmic research led to the demand for tests to evaluate the mouse visual system. Recent advances in live imaging allow the visual system to be studied in detail with accurate correlation of behaviour, function and pathophysiological changes in neurons over time. For a successful *in vivo* technique to evaluate the mouse visual system it must be rapid and reliable to allow a high number of mice to be screened. However, techniques developed to allow live imaging in rodent eyes have restricted resolution due to the optical quality of rodent eyes in comparison to human eyes. Rodent eyes have a smaller axial length, higher optical power and larger refractive error, which makes them problematic to image. Several techniques which have been used in humans are being translated for use in rodents, including OCT, cSLO and electrophysiology (discussed in detail in Chapter 5).

1.5 Animal models of MS and ON

There are several animal models, which recapitulate pathological and clinical aspects of MS and ON. Animal models have contributed significantly to our understanding of MS disease mechanisms and the development of new therapies. Each model mimics specific aspects of MS comprehensively and are important in differentiating key pathways in MS.

1.5.1"Classic" Experimental Autoimmune Encephalomyelitis

EAE is the most intensively used animal model for the study of demyelination and has contributed towards several developments in the field of MS research. The earliest reports of EAE came from studies in rhesus monkeys, which were injected with brain tissue from rabbits leading to the development of a neurological disease with pathological evidence of an inflammation and demyelination (Rivers & Schwentker, 1935; Rivers *et al.*, 1933). The addition of Freund's adjuvant, which amplified the production of antibodies against horse serum in guinea pigs (Freund & McDermott, 1942), was used to induce a rapid onset of encephalomyelitis after inoculation with brain material (Freund *et al.*, 1947; Morgan, 1947; Morrison, 1947). EAE was later documented for its resemblance to human demyelinating disease (Wolf *et al.*, 1947) and was later used expansively in research into the immunogenetic and histopathalogical basis of MS.

EAE is induced by injecting genetically susceptible animal strains with CNS myelin proteins (myelin basic protein, myelin oligodendrocyte glycoprotein, myelin-associated oligodendrocyte basic protein, proteolipid protein, myelin associated glycoprotein), glial proteins (glial fibrillary acidic protein, αβ-crystallin), neuronal proteins (neurofilament-L, neurofilament-M, β-synuclein, conatactin-2, neurofascin) or spinal cord homogenate emulsified with an adjuvant (Krishnamoorthy & Wekerle, 2009). EAE can also be induced by adoptive transfer of myelin reactive T cells (Mokhtarian *et al.*, 1984). The responsiveness of EAE depends on the nature of the autoantigen and the species of rodent, for example, C57BL/6 mice are highly responsive to MOG but not to MBP (Lando *et al.*, 1979; Mendel *et al.*, 1995). EAE is a versatile model which produces lesions in the CNS and sometimes in the visual pathway. For example, induction of EAE with MOG-derived encephalitogenic peptides results in a high incidence of ON in association with EAE (Shao *et al.*, 2004). Optic nerve lesions are normally associated with inflammation and demyelination in the brain and spinal cord (O'Neill *et al.*, 1998). EAE recapitulates many clinical, neuropathological and immunological features of MS and has aided the understanding of MS (Gold *et al.*, 2006). Clinically, EAE presents initially with tail atony followed by hind limb muscle tonicity and paralysis,

which can further develops to quadriplegia (Krishnamoorthy & Wekerle, 2009). The EAE model has many similarities with MS; genetic susceptibility, environmental triggers, white matter pathology, grey matter pathology, clinical presentation and clinical forms (Steinman & Zamvil, 2005).

The EAE model has contributed towards the successful development of approved drugs for the treatment of MS, such as GA (Arnon *et al.*, 1989) and Natalizumab (Yednock *et al.*, 1992). However, the EAE model has failed to predict clinical toxicity; for example, Linomide (quinoline 3-carboxamide) ameliorated EAE but failed clinical testing due to unacceptable levels of cardiotoxicity (Schwid & Trotter, 2000). The usefulness of EAE as a pre-screen for potential MS drugs is controversial due to its failure to predict clinical outcomes (Ransohoff, 2006). The EAE model is clearly valuable as a pre-clinical proof of concept tool, however, there is no guarantee results in EAE will be translated to humans (Steinman & Zamvil, 2005).

It has long been established that EAE is mediated by T helper type 1 cells (Th1), based on cytokine secretion and transcription factor expression. However, new evidence suggests EAE is mediated by T helper type 17 cells (Th17) (Batoulis *et al.*, 2010). Mice deficient in IL-23 cytokine are resistant to EAE (Cua *et al.*, 2003), therefore suggesting IL-23 is critical for EAE pathogenesis. The cytokine Il-23 is necessary for Th17 development and differentiation (McGeachy *et al.*, 2009). Both Th1 and Th17 cells are critical in the pathogenesis of EAE but the role of each subset of T cell helper cells remains a matter of debate (El-behi *et al.*, 2010) and are likely to play differing roles dependant on the antigen and strain combination used.

1.5.2 Virus-induced demyelination

Demyelinating disease can also be induced in animals by chronic viruses, including murine hepatitis virus and Semliki Forest virus (Dal Canto & Rabinowitz, 1982). The most reliable and frequently used model of demyelination is the TMEV (Theiler's murine encephalomyelitis virus) model, which induces the formation of demyelinating lesions following intracerebral infection (Brahic *et al.*, 2005; Theiler, 1937). TMEV induced demyelination presents with many similarities to MS and is used to understand the contribution of viruses to MS (Lipton & Dal Canto, 1979). The exact mechanism of demyelination by TMEV remains to be defined.

1.5.3 Toxin-induced demyelination

Another approach to initiating demyelination, is to use agents like cuprizone (a copper chelating agent) (Blakemore, 1973), ethidium bromide (Blakemore, 1982) or lysolecithin (activator of phospholipase A_2) (Blakemore, 1978) to induce the formation of focal areas of demyelination. These models have the advantage of producing lesions by microinjection at defined CNS regions. Toxin models are not immune mediated and are therefore used as a system to study demyelination rather than mimic disease (Blakemore & Franklin, 2008).

1.5.4 Animal models of ON

Attempts to develop and animal model of ON have been based on techniques described earlier; EAE (Shindler *et al.*, 2006) and virus-induced demyelination (Shindler *et al.*, 2008). EAE induced in mice can frequently affect the visual system and lead to optic neuritis. The first evidence of the development of optic neuritis in a mouse model of EAE was identified in SJL/J mice immunised with PLP, 17 days after immunisation, which showed histopathalogical evidence of cellular infiltration in optic nerve (Potter & Bigazzi, 1992). Immunisation of SJL/J mice with oligodendrocyte-specific protein (Sospedra & Martin, 2005) also induces EAE with ON (Kaushansky *et al.*, 2006). However, the occurrence of ON in mouse models is approximately 60-70% (Kezuka *et al.*, 2011).

The development of a novel model of optic neuritis would be highly advantageous compared to classical 'EAE' models currently being used and would allow study of new therapies in addition to offering a refinement and reduction of current methods (Table 1.2).

	Classical 'EAE' model	Novel model of optic neuritis	Advantages of new model
Disease induction	Severe – PTX , Freund's adjuvant and immunogen.	Moderate - PTX	Refinement
Time in procedure	Weeks/months	Weeks	Refinement
Disease fatality	High	Low	Refinement
Home Office procedure	Substantial	Moderate	Refinement
Clinical response	Sight disturbance, paralysis, weight loss, bladder problems, faecal incontinence, tremor/spasticity, sensory loss	Sight disturbance and occasional paralysis	Refinement
Outcome measures	Subjective non-parametric scale	Parametric	Reduction
Neuroprotection outcome measures	Histological – serial assessment not possible	Serial monitoring, instant readout, parametric	Reduction
Assessment of RGC	Not possible – need to use surgical injection of retrograde tracer	Use CFP expression in Thy1	Refinement

Table 1.2 ***Comparison of classical 'EAE' model and a novel model of optic neuritis (MOG^{TCR}xThy1CFP)****. Advantages of new model in accordance with the NC3Rs – reduction, refinement and replacement.*

1.6 Aims of project

The aim of the project is to develop and characterise a novel transgenic mouse model for the study of neuroprotection and repair strategies in autoimmune diseases.

The objectives of the project are;

1. To develop a transgenic mouse model that can be used to monitor inflammation, demyelination and neurodegeneration in the absence of clinical paralysis typically associated with “classical” EAE (Chapter 2).

2. To refine immunisation protocols to optimise the extent and timing of demyelination and axonal loss to produce a model with optimal disease that can be used in drug studies (Chapter 3).

3. To develop a non-invasive means to correlate visual dysfunction with optic nerve pathology and neurodegeneration using electrophysiology (Chapter 4).

4. To develop methods to measure RGC loss and provide an animal model correlate to concurrent human studies using ophthalmic microscopes (Chapter 5).

5. To test potential neuroprotective and repair therapies using the drug screening transgenic mouse model (Chapter 6).

By achieving these objectives, the transgenic mouse model can be used to identify potential new drug treatments and offers a refinement and reduction of existing animal models of autoimmune diseases in accordance with the cohort of 3Rs (reduction, refinement, replacement).

Chapter 2

Establishment of animal model

2.1 Introduction

An aim of the project was to develop an animal model of optic neuritis that can be used to study demyelination, remyelination and neuroprotection. In particular, the model is required to be a refinement over previous models of EAE which are associated with clinical paralysis. Several models were investigated for their potential as a novel model of optic neuritis.

2.1.1 Myelin-associated glycoprotein (MAG) knockout mice

The potential of the MAG knockout as a slow demyelinating model in the optic nerve was assessed in collaboration with Prof. P. Calabresi, MS Center, The John Hopkins University School of Medicine, Baltimor, USA.

2.1.1.1 Structure and function of MAG

MAG was first detected in CNS myelin extracted from the rat (Quarles *et al.*, 1973), which was subsequently followed by the discovery of MAG in periaxonal oligodendroglial membranes of CNS myelin sheaths (Sternberger *et al.*, 1979). MAG was also found to be located in the periphery in periaxonal Schwann cell membranes (Figlewicz *et al.*, 1982). The detailed structure of MAG was revealed from the predicted protein sequence following cloning of the rat MAG gene (Arquint *et al.*, 1987), which revealed a long extracellular domain, short transmembrane domain, intracellular carboxyl-terminal domain and the presence of Ig-like domains.

The role of MAG in myelination is poorly understood, however, the expression of MAG is observed early in myelination (Keita *et al.*, 2002; Owens & Bunge, 1989) suggesting a function during the initial oligodendrocyte processes. It was later discovered, that a high level of MAG expression continues in later stages of myelination (Päiväläinen & Heape, 2007) suggesting a function in the maintenance of myelinated axons.

2.1.1.2 MAG knockout mice

MAG knockout mice (MAG-/-) were initially created by disruption of exon 5 of the *Mag* gene and were used to investigate the function of this molecule and its role in myelination (Li *et al.*, 1994; Montag *et al.*, 1994). MAG-/- mice were later used to test the hypothesis that removal of MAG would transfer the CNS from an inhibitory environment to one that will promote neurite growth (Ng *et al.*, 1996). MAG-/- mice exhibit hypomyelination and an increased number of unmyelinated axons compared to controls (Bartsch *et al.*, 1997), which confirms the hypothesis that MAG is involved in early stages of myelination. Several other abnormalities are present in the CNS in MAG-/- mice, including reduced length of oligodendrocyte periaxonal cytoplasmic collar, myelin sheaths containing cytoplasmic loops and axons surrounded by more than one myelin sheath. In the peripheral nervous system (PNS), MAG-/- mice show evidence of demyelination with the formation of onion bulbs (Fruttiger *et al.*, 1995) and late axonal loss is observed in the CNS and PNS (Nguyen *et al.*, 2009; Pan *et al.*, 2005; Yin *et al.*, 1998). From these results it was hypothesised that MAG may play an important protective role and contributes towards axonal stabilisation and survival following injury (Nguyen *et al.*, 2009). The phenotype of MAG-/- mice is mild and it is therefore speculated that there are compensatory mechanisms occurring to contribute to the lack of the molecule.

2.1.2 T-cell receptor transgenic mice

The search for a spontaneous animal model of EAE led to the generation of T-cell receptor (TCR) transgenic models, which display a T cell repertoire directed towards specific myelin autoantigens. TCR transgenic mice are valuable research tools for elucidating immune system mechanisms. They have been used to study the pathogenesis of autoimmune diseases such as MS, type 1 diabetes, rheumatoid arthritis (Lafaille, 2004) and have been crucial to understanding the behaviour of autoimmune T cells against self antigens (Davto *et al.*, 1990).

2.1.2.1 The T-cell receptor structure

The TCR is a cell surface disulphide-linked heterodimer composed of two chains of α and β or γ and δ with a variable (V) region and constant (C) region (Chothia *et al.*, 1988; Yanagi *et al.*, 1984). The TCR is polymorphic and has a diverse amino acid variability in the V region, which interacts with antigens (Nobuhara *et al.*, 1989). T-cells in the immune system recognise foreign antigens linked to the MHC complex by the TCR, as demonstrated by gene transfer experiments (Dembic *et al.*, 1986; Saito *et al.*, 1987). The ligand is usually a peptide attached to the surface of an antigen-

presenting cell with a class I or II MHC molecule. TCR α and β chains are members of immunoglobulin superfamily. The mouse α gene family is located on chromosome 14 (Kranz *et al.*, 1985) and is composed of 100 variable (Vα), 50 joining (Jα) and a single constant (Cα) gene segments. Mouse β family is located on chromosome 6 in mice (Caccia *et al.*, 1984) and is composed of 21 variable (Vβ), 2 diversity (Dβ), 12 functional Jβ and two Cβ gene segments (Lai *et al.*, 1987). Gene segments are arranged in the thymus during T cell differentiation.

2.1.2.2 Generation of T-cell receptor constructs

Genetic transfection of α- and β- genes is sufficient to transmit functional MHC specificity from the donor T cell to the recipient T-cell (Dembic *et al.*, 1986; Saito *et al.*, 1987). This technique opened new avenues of research to allow *in vivo* manipulation of T-cell receptor specificity, leading to a greater understanding of interactions, genetic regulations and development of T-cells. TCR constructs were originally constructed with large fragments of genomic DNA and heterologous promoter fragments such as MHC class I (Pircher *et al.*, 1989) and CD2 (Mamalaki *et al.*, 1993), which resulted in abnormal timing and expression of TCR genes. Cassette vectors were developed with short segments of α and β regions driven by natural TCR regulatory elements (Kouskoff *et al.*, 1995). DNA segments originated from fragments of DNA from a T-cell clone used to produce HY-specific TCR mice (Blüthmann *et al.*, 1988; Uematsu *et al.*, 1988).

2.1.2.3 Generation of T-cell receptor transgenic mice

The first TCR transgenic mouse created contained a TCR which recognised the male H-Y antigen in the context of class I, H-2D^{d} molecule (Kisielow *et al.*, 1988; Teh *et al.*, 1988). As a model of MS, EAE is commonly used as a disease model, which replicates many pathological elements of MS. In EAE, the main CNS antigens reactive to autoimmune T cells are MBP, PLP and MOG. Therefore, a MBP-specific TCR transgenic mouse was created to study the spontaneous induction and pathology in autoimmune diseases (Goverman *et al.*, 1993). MBP-specific TCR mice housed in a pathogen free environment did not develop spontaneous EAE. However, a proportion of mice housed in an environment with pathogens developed spontaneous EAE. It was later reported that a MBP-specific TCR transgenic mouse crossed with a RAG-/- (recombination activating gene knockout) mouse had been created, which removed expression of TCR encoded by endogenous genes (Lafaille *et al.*, 1994). These mice developed T cells that all expressed the MBP-specific TCR transgene and as a result 100% of mice developed spontaneous EAE.

PLP-specific TCR mice were generated using an encephalitogenic (5B6) and non-encephalitogneic PLP-specific T-cell clone (4E3) (Waldner *et al.*, 2000). These mice behave in a similar manner to MBP-specific TCR mice, although PLP-specific TCR mice develop a higher incidence of spontaneous EAE. The higher incidence of EAE was hypothesised to be due to a more effective allelic exclusion of endogenous TCR genes, which are needed for regulatory T cells to prevent spontaneous EAE.

2.1.2.4 Structure and function of MOG

MOG is located on the surface of myelin sheaths and is therefore the leading candidates as the primary target autoantigen in the pathophysiology of MS (Iglesias *et al.*, 2001). MOG was identified as a target antigen in a guinea pig model of EAE (Lebar *et al.*, 1986a), which lead to the development of MOG induced models of EAE with evidence of demyelination caused by MOG-specific auto-antibodies (Adelmann *et al.*, 1995). The demyelinating nature of MOG is attributed to its localisation within CNS myelin exposed on the outermost surface of myelin (Brunner *et al.*, 1989). Cloning of MOG identified the protein as a member of the immunoglobulin superfamily (Gardinier *et al.*, 1992).

2.1.2.5 MOG-specific T-cell receptor transgenic mice

MOG-specific TCR transgenic mice were generated from the "2D2" clone, which expressed a TCR combination of Vα3.2 and Vβ11 (clone picked due to the availability of specific antibodies to detect the TCR) (Bettelli *et al.*, 2003). Plasmids containing linearised TCR were injected into pronuclei of fertilised C57BL/6 oocytes and transgenic founder mice were bred with C57BL/6 mice (Kouskoff *et al.*, 1995). The MOG-specific TCR (MOG^{TCR}) transgenic mice develop spontaneous or induced ON, in the absence of clinical or histological EAE, with evidence of loss of retinal ganglion cell (RGC) and demyelination in the optic nerve (Guan *et al.*, 2006). The predisposition of mice to develop ON can be explained by the higher levels of MOG present in optic nerve compared to spinal cord and brain (Bettelli *et al.*, 2003). The MOG^{TCR} can be used as an experimental model to study ON in isolation and to gain a greater understanding of autoimmune diseases.

2.1.3 Fluorescent transgenic mice

The identification of the complimentary DNA encoding the green fluorescent protein (GFP) from jellyfish (*Aequorea victoria*) was a major advancement for monitoring gene expression and protein localisation (Chalfie *et al.*, 1994). GFP is a versatile protein that requires no exogenous cofactors to

be expressed and can be fused with proteins to allow cell specific fluorescence (Kain *et al.*, 1995). GFP can also be mutated to produce spectral variants; cyan fluorescent protein (CFP), red fluorescent protein (RFP) and yellow fluorescent protein, (YFP) (Yang *et al.*, 1998). GFP and its variants have been used extensively in neuroscience and have significantly aided studies in neuronal development and plasticity (Dynes *et al.*, 1998; Knobel *et al.*, 1999; Murray *et al.*, 1998; Rodriguez *et al.*, 1999; Zito *et al.*, 1999).

Thy-1 is a glycoprotein expressed on thymocytes, peripheral T cells and neurons throughout the CNS (Haeryfar & Hoskin, 2004). Of particular interest, *Thy1* can be used as a RGC specific marker (Barnstable & Dräger, 1984). Neuronal specific expression of *Thy1* can be generated by altering its genomic composition; deletion of the third intron in mouse *Thy-1* genes eliminates non-neuronal expression (Vidal *et al.*, 1990). Therefore, the *Thy1* gene can be used to selectively express fluorescent proteins in neuronal cells and facilitate the study of neuronal structure, function and development. Several transgenic lines have been generated, which have variations in expression due to differences in integration site and copy number of the construct (Feng *et al.*, 2000) (Table 2.1). Each transgenic line can be used to study a specific neuronal subset of interest, for example, the CFP-23 strain can be used to study RGC due to its high expression in the retina.

The most widely used method to label RGC is by retrograde-labeling using a stereotactic injection of a fluorescent tracer into the superior colliculus (SC). Approximately 98% of RGC project to the SC (Forrester & Peters, 1967) therefore this method allows almost all RGC to be labeled. However, this method has very invasive and is a severe procedure, which requires expose of the brain. Also, the dye is only available for a short time dye and is phagocytosed by microglia, which can cause problems when analyzing data (Kanamori *et al.*, 2010). Therefore, the *Thy1*CFP model offers an advantage over previous methods as the RGC are labeled endogenously through the expression of the transgene.In order to study disease progress in real time, the MOG-specific TCR mice will be crossbred with *Thy1*CFP line CFP-23mice with fluorescent RGC. This will produce a mouse model that develops optic neuritis, with the potential to quantitatively monitor disease progress longitudinally by measuring RGC population expressing CFP. The *Thy1*CFP model offers a quick and rapid approach to quantifying RGC loss, which is essential for an efficient model system.

Transgenic Line	Motor Axon	Retina		SCG		DRG	Cortex	Cerebellum		
		RGC	INL	Pre	Post			Mossy	Purk	Molec
YFP-12	All	Many	A	None	None	Many	5,6	All	Many	Few
YFP-16	All	All	A+B	All	Few	All	2-6	All	None	Few
YFP-21	All	All	A	All	Many	All	2-6	All	All	None
YFP-A	Many	Many	A	Many	None	Many	2-6	All	Many	Few
YFP-C	All	All	A+B+M	All	Few	All	2-6	All	None	None
YFP-D	All	All	A	All	None	All	2-6	All	None	Few
YFP-F	All	Many	A	Many	None	All	2-6	All	Few	Few
YFP-G	All	Many	A	All	Few	All	2-6	All	None	None
YFP-H	Few	Few	None	Few	Few	Many	5	Many	None	None
GFP-F	All	All	A+B+M	All	None	All	2-6	All	Many	Few
GFP-G	All	All	A+B+M	All	Few	All	2-6	All	Many	Few
GFP-H	All	Many	None	All	None	Many	2-6	Many	None	None
GFP-I	All	Few	None	All	None	All	6	All	Many	None
GFP-J	All	All	A+BM	All	None	All	2-6	All	Many	None
GFP-M	Few	Few	None	None	None	Many	Few	Many	None	None
GFP-O	All	Few	None	None	None	All	2-6	All	Many	None
GFP-S	Few	Few	None	None	None	None	Few	Few	None	None
CFP-4	All	Many	None	None	Few	Many	5,6	All	Many	None
CFP-11	All	Many	None	Few	Few	Many	2-6	All	Few	Few
CFP-23	All	All	A	None	None	Many	2-6	All	None	None
CFP-D	All	Few	None	None	None	All	5,6	All	None	None
CFP-F	All	Many	None	All	None	All	2-6	All	None	Few
CFP-H	All	Many	None	None	None	Many	2-6	Many	None	None
CFP-I	All	All	None	None	None	All	2-6	All	None	None
CFP-S	Few	None	None	None	None	Few	Few	Few	None	None

Table 2.1 ***Patterns of transgene expression in Thy1-XFP lines of transgenic mice expressing fluorescent protein under the control of the Thy1 promoter.*** *A number of transgenic mice were produced that contain a transgene for a fluorescent protein under the control of the Thy1 promoter (Reproduced from Feng et al., 2000). Tissue sections were prepared and cryostat sections were visualised using fluorescence microscopy to analyse the fluorescence profile of expression in the CNS. A, amacrine cells; B, bipolar cells; DRG, dorsal root ganglion (lumbar ganglia were examined); INL, inner nuclear layer of the retina; Mossy, mossy fibres in internal granule layer of the cerebellum; Purk, cerebellar Purkinje cells; Molec, interneurons of the cerebellar molecular layer; RGC, retinal ganglion cells; SCG, superior cervical ganglion.*

2.2 Materials and methods

2.2.1 Animals

2.2.1.1 GFP expressing mice

GFP expressing mice eyes (C57BL/6-Tg(UBC-GFP)30Scha/J) (Schaefer *et al.*, 2001) were supplied by Kunihiko Takahashi, William Harvey Institute, Barts and the London School of Medicine and Dentistry, London, UK.

2.2.1.2 MAG knockout mice

MAG knockout mice (Yin *et al.*, 1998) were supplied by Peter Calabresi, John Hopkins Hospital, Baltimore, USA.

2.2.1.3 MOG^{TCR} transgenic mice

The novel TCR (T cell receptor) transgenic mouse specific for MOG 35-55 (myelin oligodendrocyte glycoprotein) peptide on a C57BL/6 mouse background (Bettelli *et al.*, 2003) were supplied by Dr. Steven Anderton, University of Edinburgh with permission from Vijay Kuchroo, Harvard University, Cambridge, Massachusetts, USA. Mating pairs were setup and a breeding stock established. Experiments were performed according to UK Animals (Scientific Procedures) Act 1986.

2.2.1.4 Thy1-CFP transgenic mice

Transgenic mice expressing enhanced CFP protein under control of the *Thy1* promoter, named B6.Cg-Tg(*Thy1*-CFP)23Jrs/J (Stock number 003710) were developed by (Feng *et al.*, 2000) and were obtained from the Jackson Laboratory, Bar Harbor, Maine, USA. Mating pairs were setup and a breeding stock established.

2.2.2 Genotyping and Phenotyping

2.2.2.1 MOG^{TCR} transgenic mice

Blood samples were taken from mice and analysed by flow cytometry. A 20-50µl sample of heparinised blood was stained with a 1:50 dilution of anti-mouse Vβ11 TCR fluorescein isothiocyanate (FITC) conjugated antibody (Invitrogen, Paisley, UK) and anti-mouse CD4 phycoerythrin (PE) conjugated antibody (Invitrogen, Paisley, UK) in 5% normal mouse serum in phosphate buffered saline (PBS). Cells were incubated with the antibodies for 30 minutes at 4°C and contaminating red blood cells were then lysed by addition of 500µl of 1:10 dilution FACS Lysis Buffer (Becton Dickinson, Oxford, UK). Samples were vortexed and incubated for a minimum of 10 minutes at room temperature. Samples were analysed by flow cytometry (Becton Dickinson, Oxford, UK). Positive animals were selected for the expression of Vβ11 TCR in the majority of CD4 T cell population.

2.2.2.2 Thy1-CFP transgenic mice

Thy1-CFP transgenic mice were genotyped using polymerase chain reaction (PCR). Tissue samples were removed from the ear of animals and digested over night at 60°C with 487.5µl Nucleon™ reagent B (400mM TRIS, 60mM EDTA, 15mM NaCl) and 12.5µl (20mg/ml) proteinase K (Invitrogen, Paisley, UK). The samples were deproteinised in 187.5µl 6M sodium perchlorate (Sigma-Aldrich, Poole, Dorset, UK), vortexed and placed in 60°C for 30 minutes. Following the addition of 750µl chloroform, samples were shaken for 10 minutes and centrifuged for 2 minutes at 18,000xg. The aqueous layer was removed and mixed with 1000µl ethanol to precipitate the DNA. Samples were inverted and spun for 1 minute at 12,000xg. The supernatant was removed and the pellet of DNA was dried at 60°C for 10 minutes. Samples were resuspended in 200µl of distilled H_2O (dH_2O).

Primers sequences for the target transgene and a Wildtype control were obtained from Jackson Laboratory, Bar Harbor, Maine, USA (Table 2.2). The PCR volume was 50µl and run on specific cycling conditions (Table 2.3, Table 2.4).

Transgene primers (from Thy1 and CFP sequence)	**Sequence**
*Thy1*F1 EYFPR1	TCTGAGTGGCAAAGGACCTTAGG CCGTCGCCGATGGGGGTGTT
Control primers (from T cell receptor delta chain sequence)	**Sequence**
Wildtype forward Wildtype reverse	AAATGTTGCTTGTCTGGTG GTCAGTCGAGTGCACAGTTT

Table 2.2 ***PCR primers and probes****. Oligonucleotide sequence of transgene primers and control primers (Sigma-Aldrich Ltd, Poole, Dorset, UK)*

Initial concentration reaction components	**Final concentration reaction components**	**Volume (µl)**
H_2O	H_2O	15.5
10 x PE Buffer II (Invitrogen, Paisley, UK) (Tris HCl [pH8.3], 50mM KCl)	10 x PE Buffer II (Tris HCl [pH8.3], 50mM KCl)	5
50mM $MgCl_2$ (Invitrogen, Paisley, UK)	2mM $MgCl_2$	2
2.5mM dNTP (Invitrogen, Paisley, UK)	0.2mM dNTP	5
5M Betaine (Sigma-Aldrich Ltd, Poole, Dorset, UK)	0.7M Betaine	7
20µM*Thy1* primer (Sigma-Aldrich Ltd, Poole, Dorset, UK)	1µM*Thy1* primer	2.5
20µM ECFPR1 primer (Sigma-Aldrich Ltd, Poole, Dorset, UK)	1µM ECFPR1 primer	2.5
20µM Wt forward primer (Sigma-Aldrich Ltd, Poole, Dorset, UK)	1µM Wt forward primer	2.5
20µM Wt reverse primer (Sigma-Aldrich Ltd, Poole, Dorset, UK)	1µM Wt reverse primer	2.5
1.25U/µl Taq Polymerase (Invitrogen, Paisley, UK)	0.0125U/µl Taq Polymerase	0.5
DNA sample	DNA sample	5
Total volume		**50.00µl/reaction**

Table 2.3 PCR components for master mix. Initial concentrations, final concentrations and volume of components required for PCR master mix to produce a final concentration of 50µl per reaction.

Step	Temperature	Time	Notes
1	94°C	90 seconds	
2	94°C	30 seconds	
3	60°C	60 seconds	
4	72°C	60 seconds	Repeat steps 2-4 for 35 cycles
5	72°C	120 seconds	
6	10°C	-	

Table 2.4 ***Cycling conditions for PCR.*** *Temperature and time of each step involved in PCR amplification, including repeated steps at step 4.*

The PCR products were analysed using gel electrophoresis. For each sample, 5µl was loaded with 3µl bromophenol blue loading buffer and 5µl distilled water (dH_2O). Samples were run on a 1% agarose gel (20ml Tris/Borate/EDTA (TBE) buffer (Sigma-Aldrich Ltd, Poole, UK), 2g agarose (Fisher BioReagents, Loughborough, UK), 10µl Safeview (NBS Biologicals, Huntingdon, Cambridgeshire, UK) and 180ml TBE. A 50bp ladder (Invitrogen, Paisley, UK) was used as a reference. Gels were imaged on a luminescent imaging system (UVIdoc).

Alternatively, *Thy1*CFP mice were phenotyped using a fluorescent microscope. Animals were placed under a fluorescence microscope on the FITC channel for approximately 5 seconds. Positive animals were confirmed by the presence of fluorescent RGC producing a pupil that appeared green.

2.2.2.3 Genotyping homozygous mice

To refine time and costs of the breeding process, the aim was to produce a homozygous breeding colony, which would therefore minimise the need for genotyping or phentoyping every new offspring. Initially, a homozygous transgenic mouse was identified by breeding with a Wildtype mouse and analysing the genetics of the offspring (ie. 100% offspring positive for transgene shows a homozygous parent). However, this technique was time consuming and uneconomical so a quantitative PCR method was developed to determine homozygous mice.

To design primers and probes needed for quantitative PCR, the oligonucleotide sequence of the transgene needs to be known to allow a sequence to be targeted appropriately. The CFP sequence was identified using NCBI Nucleotide library to locate the oligonucleotide sequence for CFP.

Although primers for the MOG^{TCR} transgene were known and were accessible from Jackson Laboratory (Bar Harbor, Maine, USA), the full oligonucleotide sequence of the transgene has not been published. The 675bp MOG^{TCR} transgene was therefore sequenced from PCR products using Sanger sequence technology based at The Genome Centre, William Harvey Research Institute, Queen Mary University of London.

Quantitative PCR was carried out as a duplex reaction with a reference gene to compare expression with the target gene. Ribosomal protein S29 (RPS29) was used as an endogenous control as it is expressed at a constant level (Svingen *et al.*, 2009). Primer 3 software **(**Whitehead Institute for Biomedical Research, Cambridge, MA, USA) was used to design oligonucleotide primers and probes based upon enhanced CFP (eCFP), MOG^{TCR} and RPS29 sequence (Table 2.5). The target gene probes were made with the fluorescent dye FAM attached to the 5' end and a fluorescent quencher TAMRA attached to the 3' end. The reference gene probes were made with HEX attached to the 5' end to allow distinction between target and reference gene.

Target gene (eCFP)	**Sequence**
eCFP Forward primer	GCCTACATACCTCGCTCTGC
eCFP Reverse primer	CAACCCGGTAAGACACGACT
eCFP Probe	[FAM]-ATCCTGTTACCAGTGGCTGC-[TAM]
MOG^{TCR} Forward primer	ACCCAGTGGTTCAAGGAGTG
MOG^{TCR} Reverse primer	CTTGGTTCCCTGTCCAAAGA
MOG^{TCR} Probe	[FAM]- AGCGACTGGGCTGTGTACTT -[TAM]
Reference gene (RPS29)	**Sequence**
RPS29 Forward primer	ACGGTCTGATCCGCAAATAC
RPS29 Reverse primer	CATTCAAGGTCGCTTAGTCCA
RPS29 Probe	[HEX]-TACGCGAAGGACATAGGCTT-[TAM]

Table 2.5 ***PCR primers and probes****. Oligonucleotide sequence of Target gene (eCFP) primers and probe and Reference gene (RPS29) primers and probe (Sigma-Aldrich Ltd, Poole, Dorset, UK).*

Tissue samples were removed from the ear of animals, digested and DNA extracted as described previously and a duplex quantitative PCR reaction was carried out to quantify the number of transgenes in each animal. Quantitative PCR was carried out in triplicates in 96-well reaction plates with the Applied Biosystems 7500 Real-Time PCR system (Applied Biosystems, Warrington, Cheshire, UK). The PCR volume was 20µl including TaqMan® Gene Expression Master Mix, eCFP forward and reverse primers and probe, RPS29 forward and reverse primers and probe (Table 2.6) and run on specific cycling conditions (Table 2.7).

Initial concentration reaction components	**Final concentration reaction components**	**Volume (µl)**
TaqMan® Gene Expression Master Mix (2x) (Applied Biosystems, Warrington, Cheshire, UK)	TaqMan® Gene Expression Master Mix (1x) (Applied Biosystems, Warrington, Cheshire, UK)	10
100µM *CFP* or MOG^{TCR} Forward Primer (Sigma-Aldrich Ltd, Poole, Dorset, UK)	1µM *CFP* Forward primer	0.2
100µM *CFP or* MOG^{TCR} Reverse primer (Sigma-Aldrich Ltd, Poole, Dorset, UK)	1µM *CFP* Reverse primer	0.2
100µM *RSP29 F*orward primer (Sigma-Aldrich Ltd, Poole, Dorset, UK)	1µM *RSP29* Forward primer	0.2
100µM *RSP29 Reverse* primer (Sigma-Aldrich Ltd, Poole, Dorset, UK)	1µM *RSP29* Reverse primer	0.2
100µM *CFP* or MOG^{TCR} probe (Sigma-Aldrich Ltd, Poole, Dorset, UK)	500nM *CFP* Reverse probe	0.1
100µM *RSP29* probe (Sigma-Aldrich Ltd, Poole, Dorset, UK)	500nM *RSP29* Reverse probe	0.1
DNA sample	DNA sample	5
H_2O	H_2O	4
Total volume		**20µl/reaction**

Table 2.6 ***PCR components for master mix****. Initial concentrations, final concentrations and volume of components required for PCR master mix to produce a final concentration of 50µl per reaction.*

	Temperature	Time	Step	Notes
1	95°C	10 minutes	Initial denaturation	Repeat steps 2-4 for 40 cycles
2	95°C	45 seconds	Denaturation	
3	60°C	45 seconds	Annealing	
4	72°C	120 seconds	Extension	

Table 2.7 ***Cycling conditions for PCR.*** *Temperature and time of each step involved in PCR amplification, including repeated steps 2-4.*

Data was collected on 7500 System Sequence Detection Software (Applied Biosystems, Warrington, Cheshire, UK) and cycle threshold (C_t) values were analysed by using a manual baseline of 0.2. Results were exported in .csv format and analysed using CopyCaller™ software (Applied Biosystems, Warrington, Cheshire, UK).

2.2.3 Histological techniques

2.2.3.1 Primary Fixation

Karnovsky's Fixative was freshly prepared for use as a primary fixative for tissue used in epoxy resin sectioning for confocal and electron microscopy. The fixative was composed of paraformaldehyde (PFA) (Sigma-Aldrich Ltd, Poole, Dorset, UK), glutaraldehyde (Agar Scientific Ltd, Stansted, Essex, UK) and 400ml 0.2M sodium cacodylate buffer (Agar Scientific Ltd, Stansted, Essex, UK).

(1) 10% PFA was made by adding 10g PFA (Sigma-Aldrich Ltd, Poole, Dorset, UK) to 100ml distilled water and mixed on an electric hotplate with stirrer to 60-70°C in a fume hood (without boiling). After approximately 15 minutes the solution turns from milky to opalescent. To clarify the solution, 2-5 drops of 1M sodium hydroxide were added. The pH was adjusted 7.2 using HCl or NaOH. The solution was left to cool and filtered.

(2) 0.2M sodium cacodylate was prepared by adding 21.4g sodium cacodylate (Agar Scientific Ltd, Stansted, Essex, UK) to 500ml distilled water.

(3) 100ml of 10% PFA (1) (Sigma-Aldrich Ltd, Poole, Dorset, UK) was added to 120ml 25% glutaraldehyde (Agar Scientific Ltd, Stansted, Essex, UK) and 400ml sodium cacodylate (2)

(Agar Scientific Ltd, Stansted, Essex, UK). The solution was made up to 1 litre with distilled water and the pH was adjusted to 7.2.

Cardiac perfusion with approximately 20ml PBS followed by 20ml Karnovsky's fixative was performed. Samples were preserved in Karnovsky's fixative at 4°C.

2.2.3.2 Secondary Fixation

Following primary fixation, optic nerves and eyes were rinsed in 0.1M sodium cacodylate buffer (Agar Scientific Ltd, Stansted, Essex, UK) for three changes of 10 minute cycles. Secondary fixation and impregnation of a contrast agent was achieved using 1% aqueous (w/v) osmium tetroxide. Tissue samples were left in secondary fixative for 2 hours with agitation.

2.2.3.3 Dehydration

Following secondary fixation, tissue samples were rinsed with distilled water and passed through a series of ascending alcohols, each for 10 minutes at 50%, 70%, 90% and 100% ethanol (three times).

2.2.3.4 Infiltration of samples with resin

Samples were passed through two 15 minute changes of 100% propylene oxide (Agar Scientific Ltd, Stansted, Essex, UK) followed by an overnight immersion in 1:1 mixture of propylene oxide and resin with agitation. Resin was prepared by adding 20ml araldite CY212 resin to 25ml Dodecenyl Succinic Anhydride (DDSA) (Agar Scientific Ltd, Stansted, Essex, UK)and 0.8ml DMP30 (tri-dimethylamnomethyl phenol) (Agar Scientific Ltd, Stansted, Essex, UK). The following day, samples were removed and placed in 100% resin. After 3-6 hours samples were transferred into moulds with full resin and placed in the oven overnight at 60°C to polymerise. Resin blocks were trimmed with a fine-toothed hacksaw and roughly cut with a glass knife. Semi-thin sections were cut at 0.7µm thickness using a 6mm Histo diamond knife (Leica Microsystems Ltd, Milton Keynes, UK) on an Ultra Microtome (Leica Microsystems Ltd, Milton Keynes, UK) and placed on microscope slides (RA. Lamb, Eastbourne, UK). Ultra-thin sections were cut between 80-90nm with an Ultradiamond knife (Leica Microsystems Ltd, Milton Keynes, UK) on an Ultra Microtome (Leica Microsystems Ltd, Milton Keynes, UK) and placed on copper grids.

2.2.3.5 Staining of resin sections

Semi-thin sections were allowed to dry for several minutes on a hotplate and were stained with 1-2 drops of 1% toluidine blue for 10-20 seconds and rinsed with distilled water. Slides were left to dry then mounted in DPX (dibutyl-phthalate-xylene) (Merck, Leicester, UK) and coverslipped (RA. Lamb, Eastbourne, UK).

Ultra-thin sections were stained with a drop of Reynold's Lead Citrate. Reynold's Lead Citrate was prepared by dissolving 1.33g lead nitrate and 2.67g sodium citrate in 20ml distilled water and agitated for 30 minutes. 8ml of 0.1M NaOH was added and volume adjusted to 50ml with distilled water. To stain samples, drops of lead citrate are placed on a square of parafilm in a petri dish. Several sodium hydroxide pellets were added to the petri dish, moistened with distilled water and left for 2 minutes to absorb the CO_2 from the dish. Copper grids with samples were inverted on droplets of lead citrate in the petri dish for approximately 2 minutes. Grids were quickly rinsed in distilled water and dried by blotting on clean filter paper.

2.2.4 Microscopy

Samples were viewed on a Nikon Eclipse 80i microscope and images analysed with Stereo Investigator 7.35.1. Axons were counted by drawing a contour around the optic nerve and using a fractionator probe to create 10 counting frames (80µm x 80µm). RGCs were counted along 3 contour lines drawn along the edge of the RNFL. Further analysis was carried out with a Zeiss S10LSM confocal microscope and JEOL1010 transmission electron microscope.

2.2.4.1 Tissue sections

The brain, spleen, spinal cord and eyes were studied from *Thy1*CFP transgenic animals. Animals were perfused with 4% PFA and tissue was placed in 4% PFA overnight. Tissue was cryoprotected with 15% sucrose, followed by 30% sucrose until samples were submerged. Tissue was embedded in O.C.T. embedding compound (VWR, Lutterworth, Leicestershire, UK) and immersed in cold isopentane (VWR, Lutterworth, Leicestershire, UK) cooled with dry ice until frozen. Sections of 40µm thickness were cut on a cryostat and coverslipped with anti-fade glycerol (CitiFluor Ltd, London, UK).

2.2.5 Retinal flatmounts

Eyes were dissected from mice and immersed in 2% PFA (Sigma, Poole, Dorset, UK) in PBS (pH7.4) overnight. The retinae were dissected and the cornea, sclera, lens, hyaloid vasculature and connective tissue were removed in 2x normal strength PBS. Four radial incisions were cut around the retinae, which allowed it to lie flat (Figure 2.1). Flatmounts were mounted onto slides and cover slipped with anti-fade glycerol (CitiFluor Ltd, London, UK). The retinal flatmounts were imaged by fluorescent microscopy and RGC density was calculated by counting CFP expressing RGC using a fractionator probe.

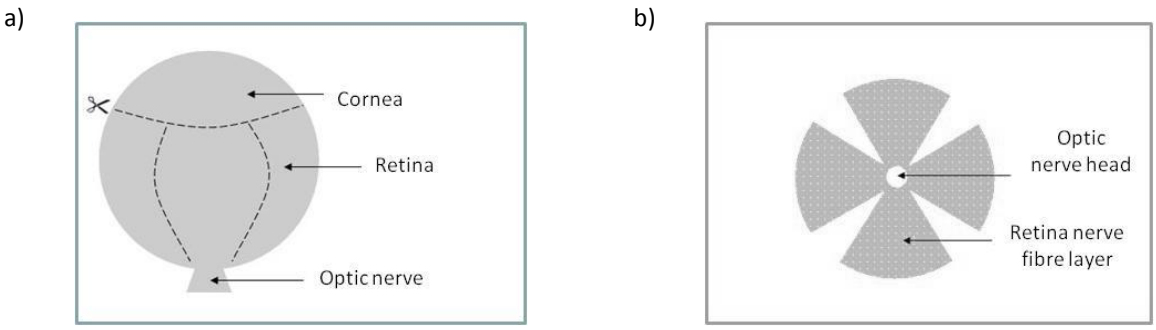

Figure 2.1 ***Retinal flatmount dissection to create a retinal flatmount to expose RGC and allow quantification****. a) Cornea is dissected and lens removed from eye. Four radial incisions made in the retina to create a Maltese cross shape. b) The retina was flattened and mounted on a microscope slide and cover slipped with ant-fade glycerol.*

2.2.6 *In vivo* imaging

The retina from *Thy1*CFP animals was imaged *in vivo* under a fluorescent microscope. To study the RGC cells in detail, mice were anaesthetised with Euthatal (a terminal anaesthetic) and pupils were dilated with Mydriacyl® 1% (active ingredient tropicamide, Alcon, Hemel Hempstead, Hertfordshire, UK) and drops of Viscotears® (active ingredient carbomer, polyacylic acid, Novartis, Basel, Switzerland) were dropped onto the eye as a substitute for tear fluid and a coverslip was used to achieve optimal resolution.

2.2.7 Statistical analysis

Statistical analysis was performed in SigmaStat 3.1. Results were presented as mean values ± standard error of mean. Differences between two groups were analysed by Students t-test following normality tests. Differences between multiple groups were analysed by one way analysis of variance (ANOVA) tests. Correlations were analysed using the Pearson product correlation. Results were considered significantly different if the probability level $P<0.05$ (*), $P<0.01$(**) or $P<0.001$(***) was reached between groups.

2.3 Results

2.3.1 MAG knockout mice

MAG knockout mice were investigated for their potential as a model of demyelination and axonal loss. MAG knockout mice were sacrificed at 2.5 months (n=5) and 7 months (n=5). Optic nerve tissue and retinae were embedded in resin, sectioned and stained with toluidine blue. Density of axons and RGC were calculated using stereology software to count 15 random squares. The retina was analysed and density of RGC quantified (Figure 2.2). The average RGC density at 2.5 and 7.5 months was 63.6±0.002 and 63.5±0.005 respectively, with no significant difference (p=0.975). Optic nerves were analysed and density of myelinated axons were quantified (Figure 2.3). The average axonal density at 2.5 and 7.5 months was 184±12 and 181±16 respectively, with no significant difference (p=0.885).

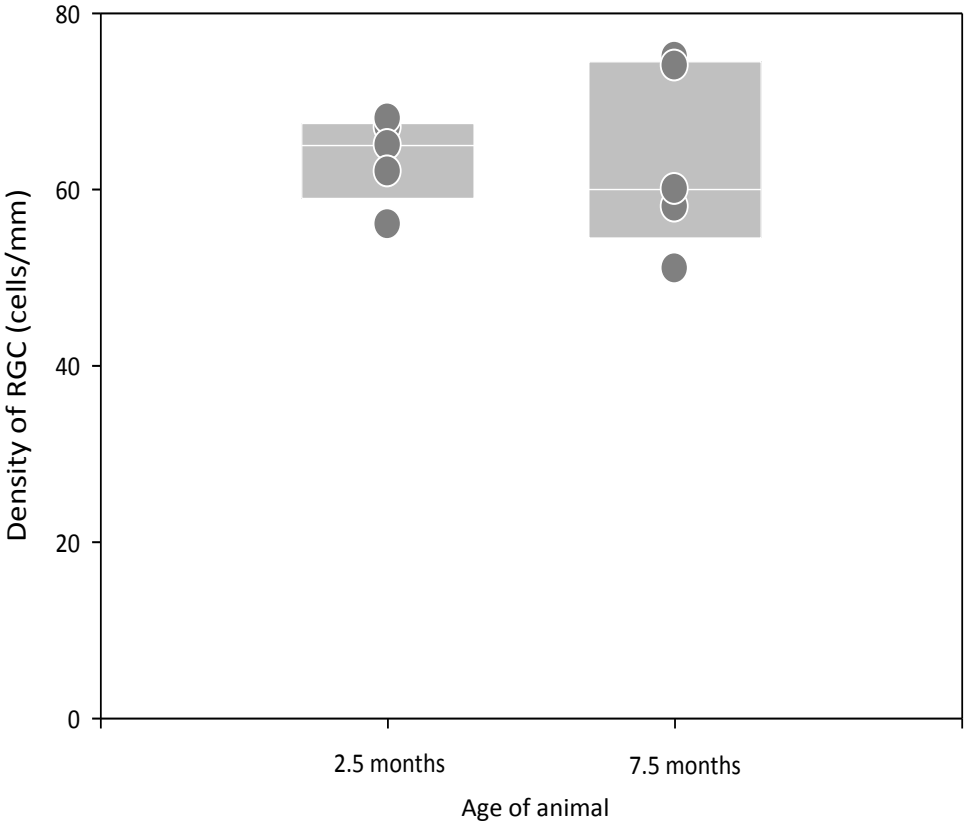

Figure 2.2 ***RGC counts from retina of MAG knockout animals at 2.5 and 7 months****. C57BL/6 MAG knockout were sacrificed at two different time points, 2.5 months (n=5) and 7 months (n=5). Retinae were embedded in resin, sectioned and stained with toluidine blue. Density of RGC was calculated using stereology software to count number of cells along retina perimeter. The results show individual values (circles) and boxes show mean and 25% and 75% percentiles.*

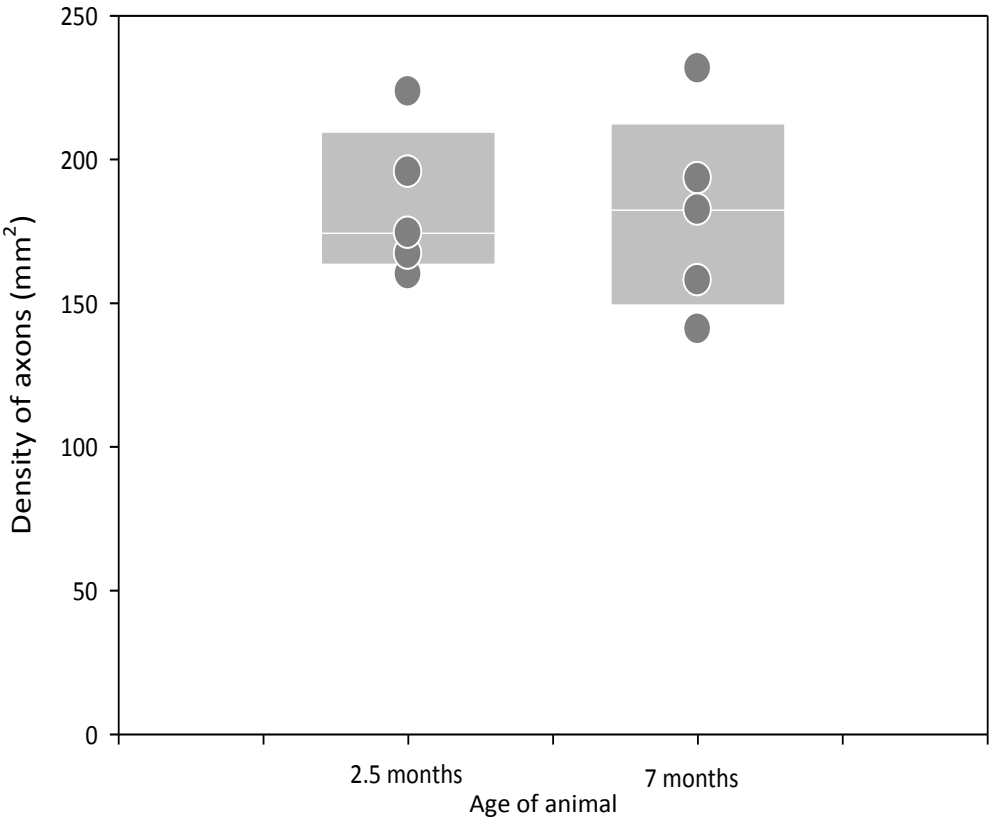

Figure 2.3 ***Axonal counts from optic nerves proximal to the optic nerve chiasm from MAG knockout animals at 2.5 and 7 months.*** *C57BL/6 MAG knockouts were sacrificed at two different time points, 2.5 months (n=5) and 7 months (n=5). Optic nerve tissue were embedded in resin, sectioned and stained with toluidine blue. Density of axons was calculated using stereology software to count 15 random squares. The results show individual values (circles) and boxes show mean and 25% and 75% percentiles.*

Between the ages of 2.5 and 7 months MAG knockout mice do not lose a significant amount of axons to be used as a model of disease. Previous studies suggest axonal degeneration occurs later in disease course (approx 18 months) (Yin *et al.*, 1998), which would make the MAG knockout mouse an unviable experimental model of disease.

2.3.2 MOG-TCR transgenic mice

2.3.2.1 Phenotyping MOG^{TCR} transgenic mice

A breeding stock of MOG^{TCR} mice cross-bred with *Thy1*-CFP mice was setup and genotyping protocols were developed. MOG-specific TCR animals were phenotyped using flow cytometer. Blood samples were stained with CD4-specific mAb conjugated with FITC and TCR Vβ11-specific mAb conjugated with PE. In normal samples, about 95% of stained cell population were TCR Vβ11 negative (Quadrant 1 and 3, Q1 and Q3) and about 5% of cells were Vβ11 positive (Quadrant 2, Q2). Samples were confirmed as positive MOG^{TCR} transgenic if the T cell population was largely positive for both CD4 and TCR Vβ11 expression (Figure 2.4). Positive MOG^{TCR} transgenic T cells also express TCRVα3.

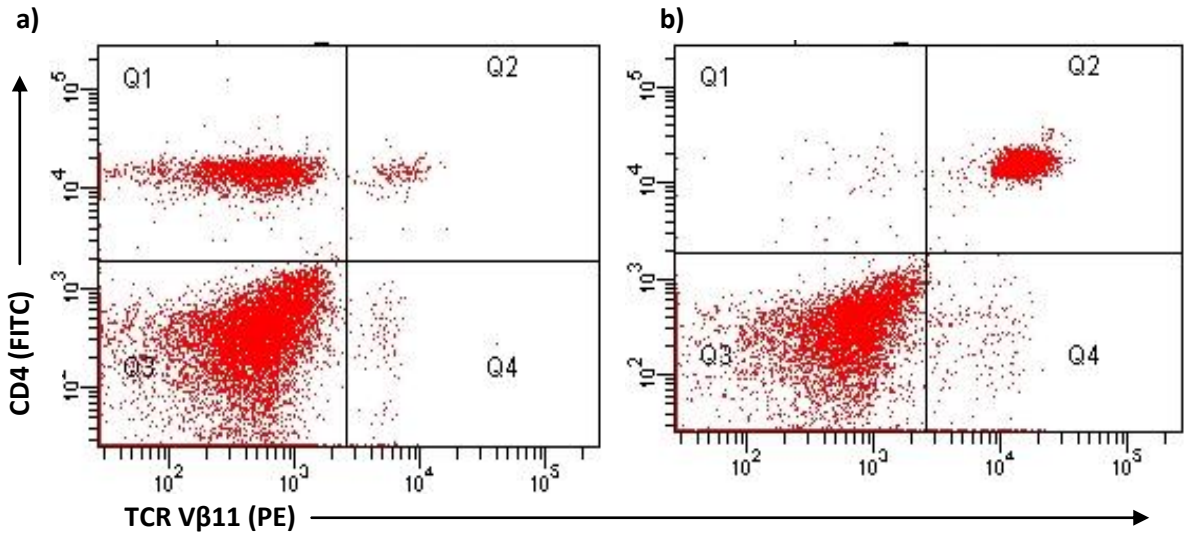

Figure 2.4 ***Immunophenotyping MOG-specific TCR transgenic mice.*** *Flow cytometry analysis of the T cell population specific for TCR expression in MOG^{TCR} mice to determine phenotype of animal. Peripheral blood cells from 4-6 week old MOG^{TCR} mice were obtained in heparinised tubes and stained with CD4 (FITC) and TCR Vβ11 (PE) specific antibodies for 30 minutes and red blood cells were lysed with lysis buffer. Samples were analysed by flow cytometry and events were gated to contain lymphoid cells based on forward and side scatter. a) An example of a negative sample which shows approximately 95% of CD4+ T cells were Vβ11 negative and 5% are TCR Vβ11 positive. b) An example of a positive sample which shows approximately 100% of CD4+ T cells are TCR Vβ11 positive.*

Approximately 5% of MOG^{TCR} animals develop spontaneous EAE from 8 weeks of age, consistent with previous reports (Bettelli *et al.*, 2003). These results were supported from observations made during routine care of MOG^{TCR} transgenic mice. The first signs of spontaneous EAE were typically a limp tail followed by partial and full hindlimb paralysis. Optic nerves and eyes from mice with spontaneous EAE were studied for signs of optic neuritis. The majority of animals that developed spontaneous EAE also had signs of optic neuritis. Any clinical signs were associated with the development of optic nerve involvement included eyelid swelling, tearing and reddening of the eye. Histological optic neuritis occurred at a higher frequency than clinical disease. ON was difficult to determine using macroscopic clinical signs due to the low number of animals that show clinical signs of ON. ON could only be confirmed by histological examination of optic nerve and retina. Optic nerve tissue from animals developing spontaneous neurological EAE was analysed for histological signs of ON using toluidine blue semi-thin stained sections (Figure 2.5, 2.7). Optic nerve tissue was also imaged using EM transmission microscopy to allow a more detailed analysis of pathology and allow identification of possible demyelinated fibres (Figure 2.6). Tissue was taken two weeks after spontaneous EAE developed or when the animal reached grade 5, a clinical endpoint due to the severity of disease. There is a loss in the integrity of axons in spontaneous ON optic nerves compared with normal optic nerves (Figure 2.).

a)

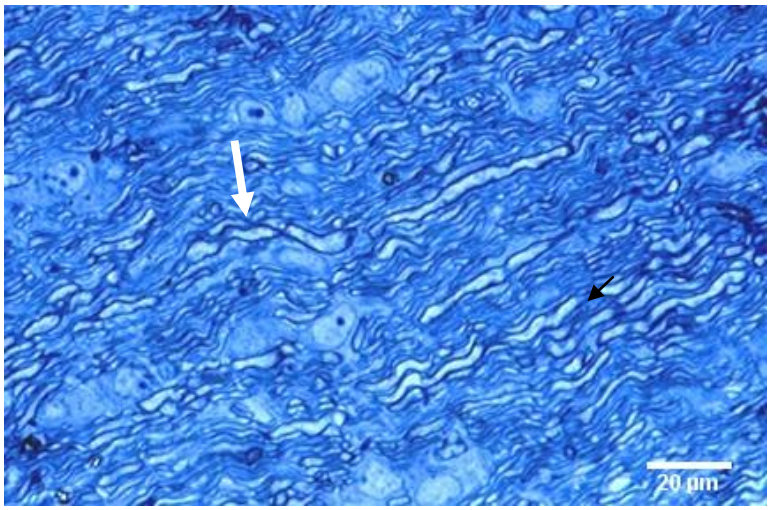

b)

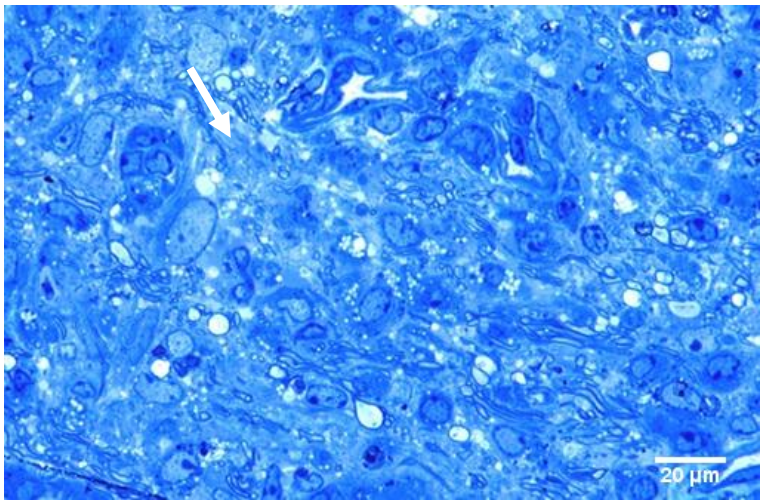

Figure 2.5 ***Longitudinal stained sections of optic nerves from wildtype and MOG^{TCR} mice****. Animals were perfused and tissue was fixed in Karnovsky's Fixative. Tissue was embedded in resin and 0.7µm thin sections were cut and stained with Toluidine blue. a) Tissue taken from wildtype C57BL/6 without ON, showed the appearance of normal myelinated fibres (arrows). b) Tissue taken from MOG^{TCR} mice with spontaneous ON, showed a relative absence of myelinated fibres and areas of axonal loss (arrows). Animals were sacrificed two weeks after developing spontaneous EAE.*

In optic nerve tissue from spontaneous ON, there appeared to be areas of axonal loss (Figure 2.5, Figure 2.6). There are a few demyelinated axons, which were difficult to identify. Well defined blood vessels appear in the optic nerve and do not appear to be compromised as shown by the lack of evidence of perivascular cuffing. There were distinct foamy macrophages containing myelin debris and swollen mitochondria could often be seen throughout the optic nerve. This could reflect pathology or this could be due to a fixation artefact.

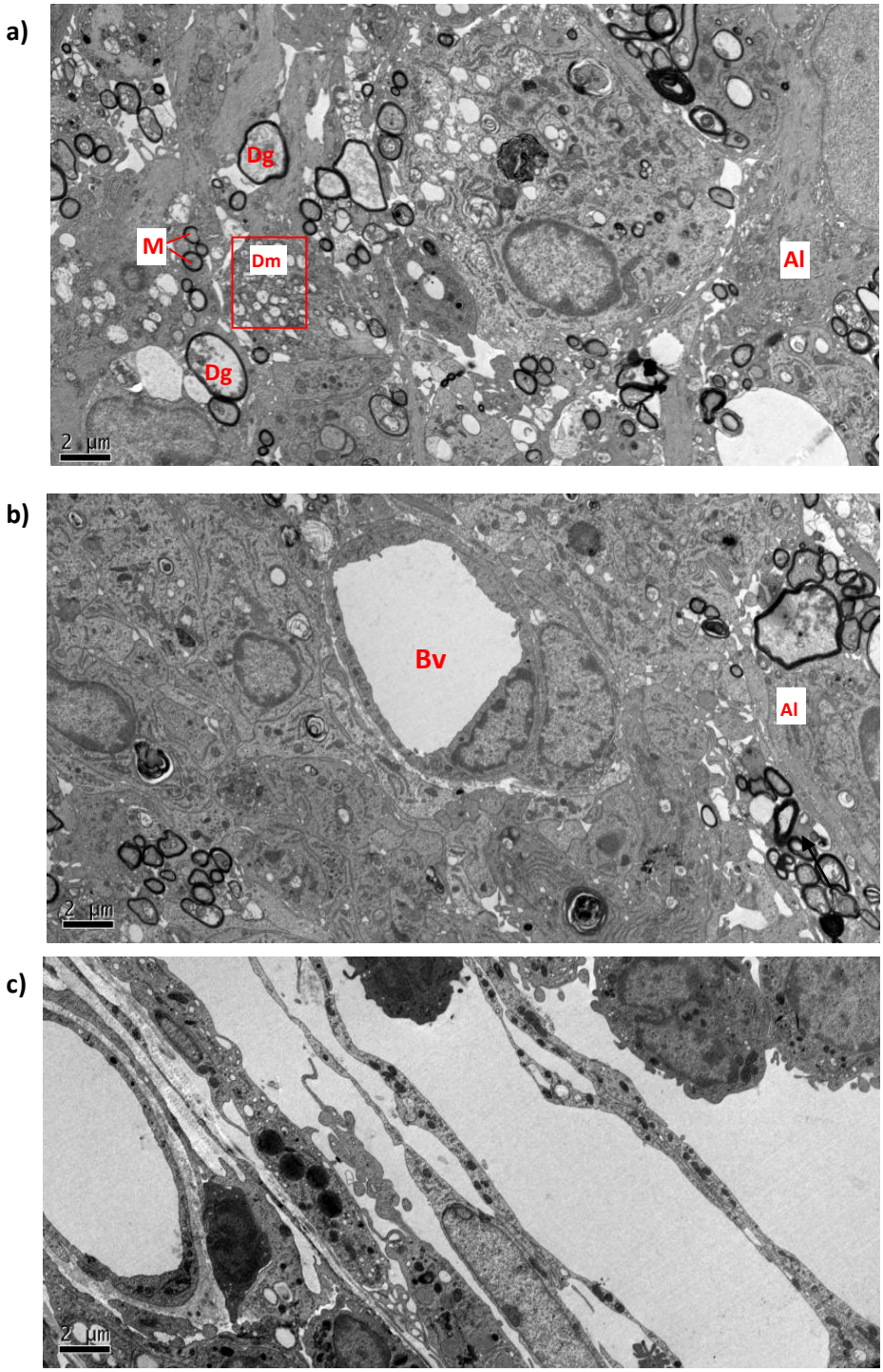

Figure 2.6 ***Cross section EM images from the optic nerve of MOG^{TCR} mice with spontaneous EAE.*** *MOG^{TCR} transgenic mice were perfused and tissue was fixed in Karnovsky's fixative. Tissue was embedded in resin and ultra-thin sections (90nm) were cut, tissue was stained with lead citrate and examined by transmission EM. Animals were sacrificed two weeks after developing spontaneous EAE. a) Cross section of optic nerve with myelinated axons (M) and histological signs of ON including degenerating axons (Dg) and demyelinated axons (Dm) and areas of axonal loss (AL). b) Cross section of optic nerve showing the presence of a blood vessel (Bv). c) Cross section of optic nerve showing the presence of inflammatory cells (arrows) surrounding the optic nerve sheath.*

There was evidence to suggest the integrity of the BBB had been compromised due to the inflammatory response and the presence of mononuclear leucocytes, which could be seen within the parenchyma, on surrounding blood vessels and on the surface of the optic nerve (Figure 2.7).

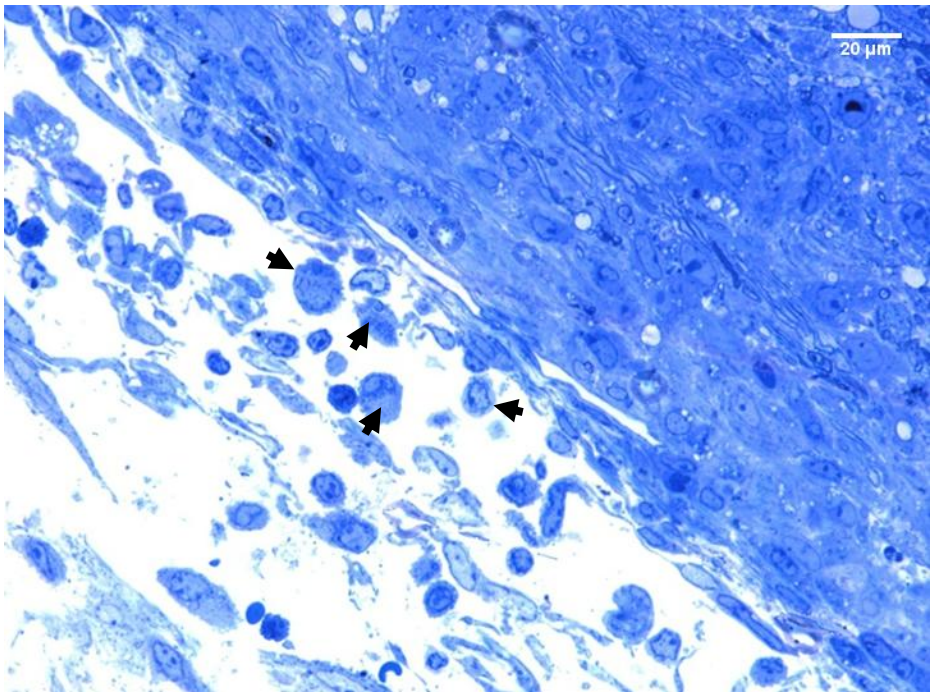

Figure 2.7 ***Longitudinal stained sections of optic nerves from MOG^{TCR} mice with spontaneous ON.*** *Longitudinal section showing meninges of optic nerve with cellular infiltration in spontaneous ON. MOG^{TCR} transgenic mice were perfused and tissue was fixed in Karnovsky's Fixative. Tissue was embedded in resin and semi-thin sections (0.7µm) were cut and stained with toluidine blue. Animals were sacrificed two weeks after developing spontaneous EAE. Infiltrating white blood cells could be detected (arrows) in areas surrounding the optic nerve.*

2.3.3 GFP expressing transgenic mice

To improve the MOG^{TCR} model and optimise its use as a drug screening model, a method needed to be developed, which would allow quick and reliable measurement of RGC loss without the need for surgical injection of tracer compounds or time consuming histology. The first approach was to examine the retinae of (C57BL/6-Tg(UBC-GFP)30Scha/J) mice which ubiquitously express GFP under the human ubiquitin C promoter as a potential method to quantify RGC by GFP selective expression in RGC (Inoue *et al.*, 2005). Retinal flatmounts were studied, however, RGC could not be identified in retinal flat mounts due to the high level of expression in surrounding tissue. Therefore, this would not be a useful method to quantify RGC loss and was not pursued as a model.

2.3.4 *Thy1*CFP transgenic mice

An alternative was to use *Thy1*CFP mice which selectively express CFP in RGC, allowing RGC to be easily quantified (Feng *et al*., 2006).

2.3.4.1 Phenotyping Thy1CFP transgenic mice

The potential to phenotype *Thy1*CFP mice using FACS was explored. Blood samples were analysed by FACS to identify CFP expression on peripheral T cells. The results were negative and T cells did not express CFP, probably due to the transgenic only expressing CFP on neuronal *Thy1* (negative data not shown). CFP expression was also absent from T cell areas in the spleen, as assessed by fluorescence and confocal microscopy, confirming negative FACS results.

Alternatively, *Thy1*-CFP mice were phenotyped by their CFP expressing retina, which can be visualised under a fluorescent microscope on the FITC channel (Figure 2.9). Positive phenotypes can be distinguished in normal eyes by the observation of cyan pupil under fluorescent light. It was easier to determine positive phenotypes when the pupil was dilated but this was not necessary and 3-4 week mice could be easily screened. This is a quick and rapid method to determine positive *Thy1*-CFP mice.

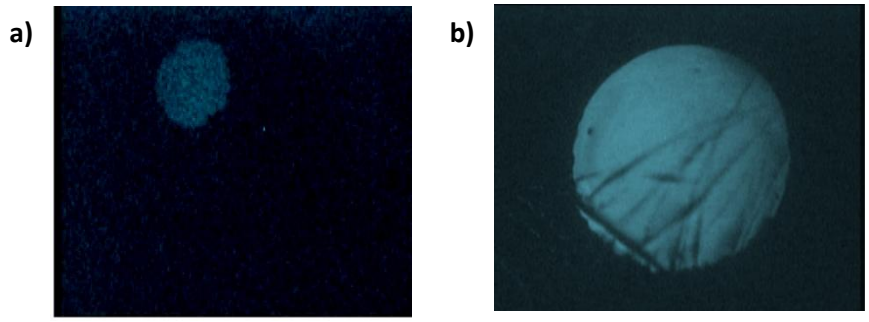

Figure 2.9 ***Phenotyping Thy1-CFP transgenic mice using fluorescent microscopy****. Fluorescence microscopy was used to visualise CFP expressing retina. MOG^{TCR} mice between the ages of 4-6 weeks were screened for the presence of CFP expressing RGC in the eye. Mice were held under a standard fluorescent microscope on a FITC channel for several seconds to observe CFP expression. a) Image taken of an undilated pupil showing very weak CFP fluorescence. b) CFP expression is clearer in an image taken of a pupil dilated with tropicamide, which allows visualisation of the whole retina. This quick technique removes the need for PCR genotyping to identify CFP expressing animals.*

2.3.4.2 Genotyping Thy1CFP transgenic mice

Thy1-CFP mice were genotyped using PCR analysis. Positive *Thy1*-CFP transgenic mice showed a 700bp band, which corresponded to the CFP gene (Figure 2.10). Positive control bands showed a 200bp product, which corresponded to Tcrd (T-cell receptor delta chain).

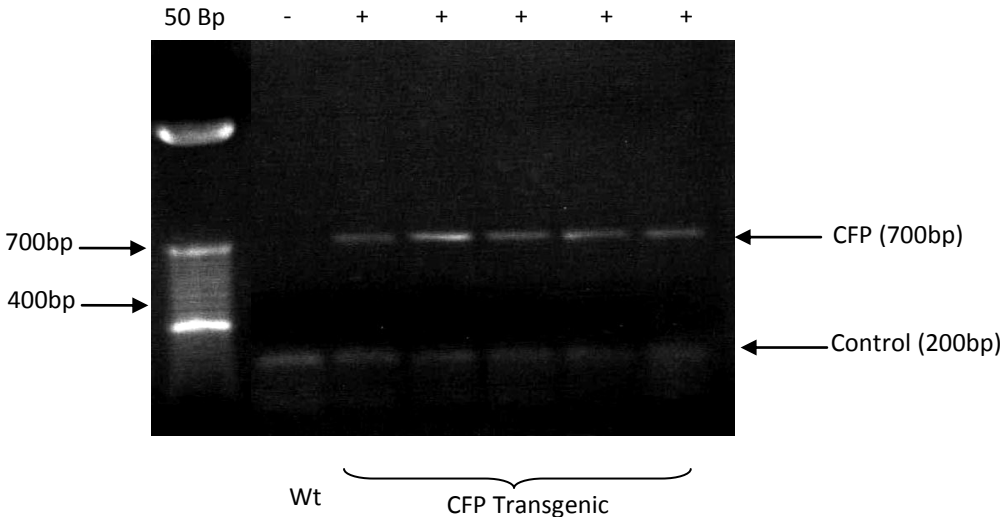

Figure 2.10 ***Genotyping Thy1-CFP transgenic mice by PCR.*** *DNA samples were prepared from 4-6 week old* MOG^{TCR} *mice and analysed by PCR using primers for specific CFP and Tcrd sequences. These were detected following agrose gel electrophoresis using a 2% agarose gel stained with quick view to detect DNA. Negative samples produced a single band at 200bp corresponding to Tcrd as a control for the integrity of DNA. Positive samples also produced a band at 700bp corresponding to CFP and a band at 200bp corresponding to Tcrd.*

Quantitative PCR (qPCR) was used to determine homozygous mice, which can be used in the breeding stock to produce a homozygous breeding colony. Tissue samples were taken from known heterozygous and homozygous *Thy1*CFP mice based upon the genotypes of their offspring and negative tissue samples were taken from Wildtype C57BL/6 mice. Quantitative PCR showed heterozygous samples with one copy of the transgene, homozygous samples with two or more copies of the gene and negative samples with no copies of the gene (Figure 2.11). Using qPCR allowed mice to be screened and only mice homozygous for the *Thy1*CFP gene were used as breeders to produce a homozygous mouse colony which would require no further genotyping or phenotyping.

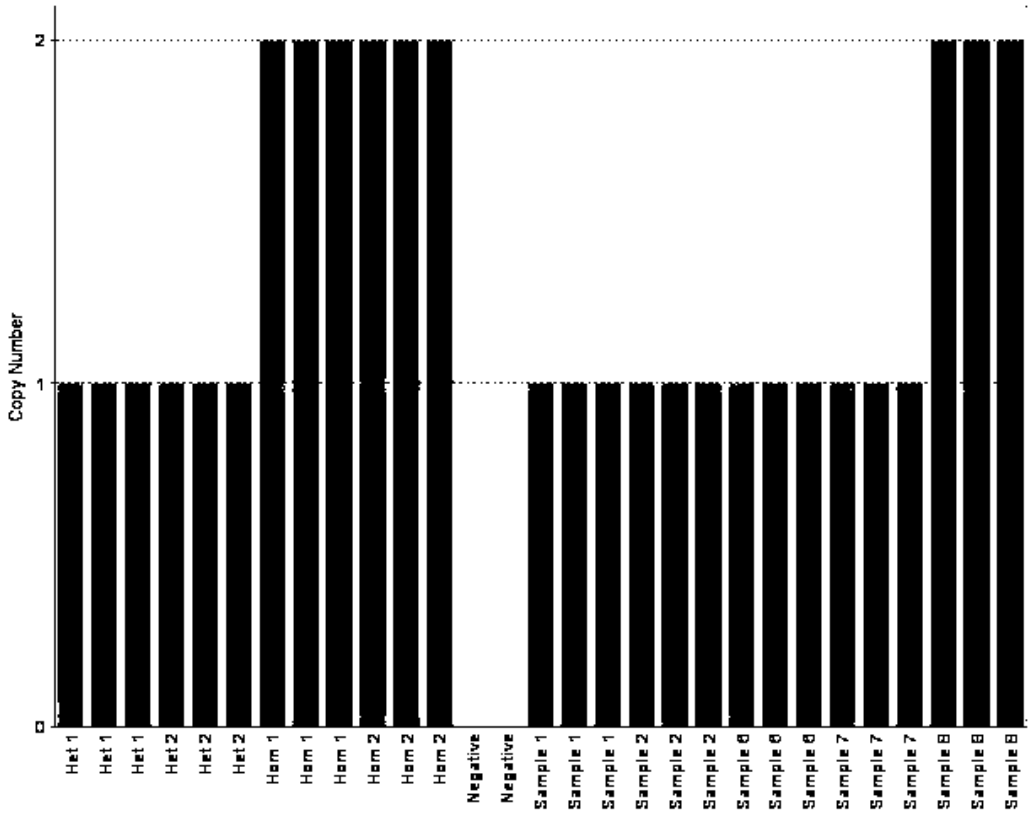

Figure 2.11 ***Predicted gene copy number in samples.*** *Results from qPCR were analysed using CopyCaller™ software. Ct values were used to determine predicted copy numbers of target CFP gene and calibrated against known heterozygous and homozygous samples. Hetrozygous samples (het), homozygous samples (hom). Results show samples 1, 2, 6, 7 were heterozygous and were not used in the breeding stock, sample 8 was homozygous and used in the breeding stock.*

2.3.4.2 Characterising Thy1-CFP transgenic mice

The retina of *Thy1*CFP transgenic mice can be visualised both *in vitro* and *in vivo* (Figure 2.12).The optic nerve head is clearly visible in both images and individual RGC can be easily identified. The cross section of retina shows the many layers of the retina; RGC are clearly expressing CFP in the RNFL (Figure 2.12a).

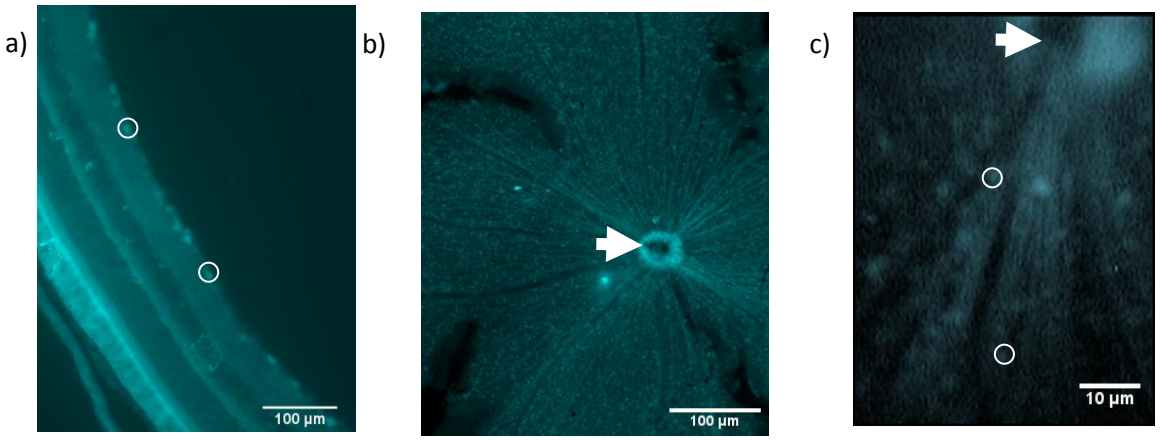

Figure 2.12 ***Fluorescent images from Thy1CFP transgenic mice.*** *a) Animals were perfused and tissue fixed in 4% PFA and cryoprotected. Frozen sections of the retina were cut at 40µm thickness. RGC (arrows) were visualised under fluorescence microscopy. b) Tissue was fixed in 4% PFA overnight and retina was dissected and flatmounted. RGC (circles) and the optic nerve head (arrow) were visible with fluorescence microscopy. c) Animals were held briefly (unanaesthetised) under a fluorescence microscope focused on the back of the retina. RGC (circles) and optic nerve head (arrow) are visible.*

Other areas of tissue were examined for CFP expression. CFP expression is found in *Thy1*CFP transgenic mice in the brain and spleen (Figure 2.13). These results support the findings according to (Feng et al., 2000); CFP expression is found in the cerebellum and cortex. The spleen was examined for CFP expression. There was some low-level expression of CFP but the white pulp typically failed to show expression suggesting lack of expression on T cells (Figure 2.13c).

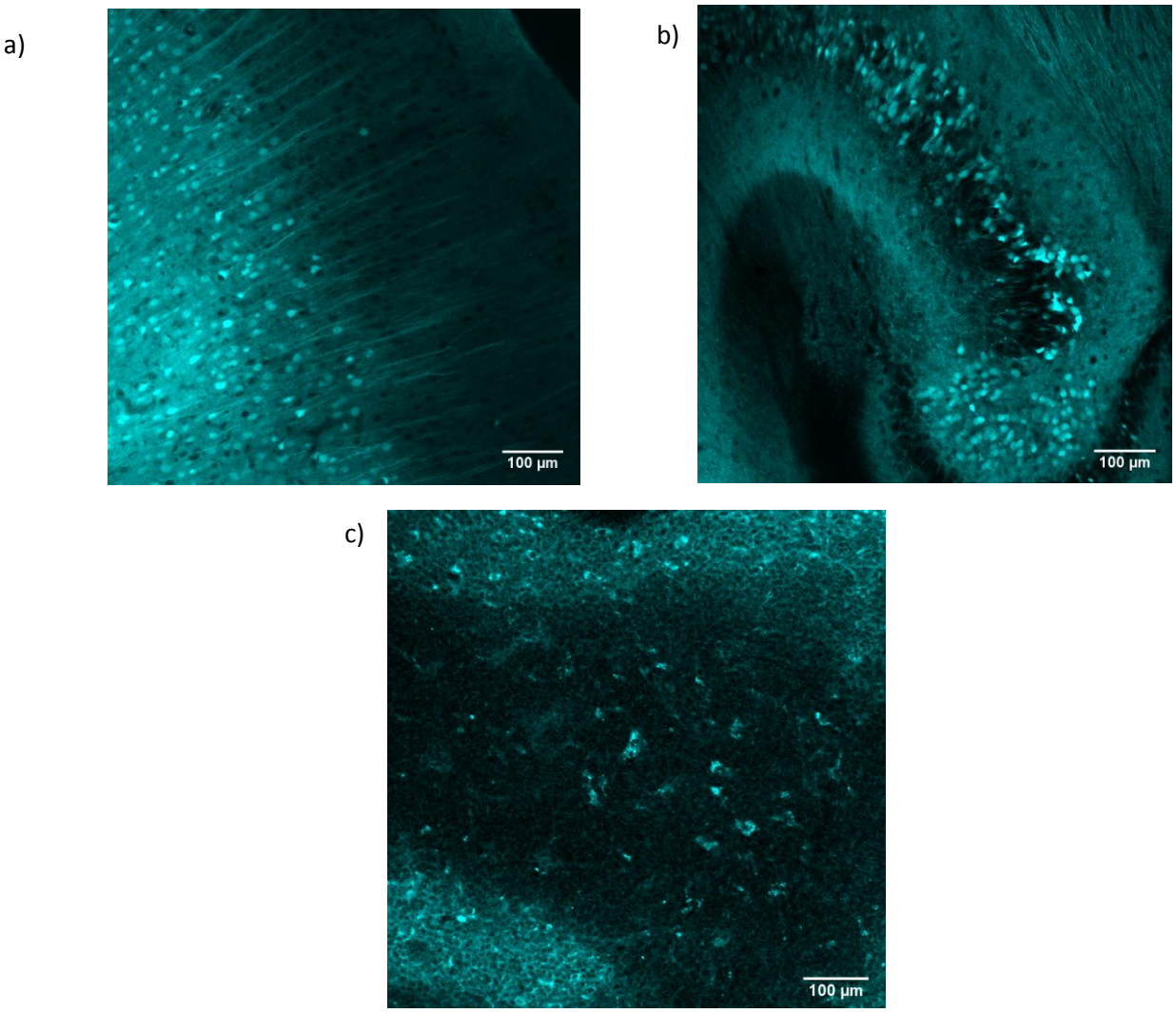

Figure 2.13 ***CFP expression in the brain and spleen of Thy1CFP transgenic mice****. Mice were perfused with 4% PFA and cryoprotected. Frozen sections of tissue were cut at 40µm thickness and visualised with fluorescence microscopy. CFP expression was detected in brain (a,b) and the spleen (c) in Thy1CFP transgenic mice.*

2.3.5 MOG^{TCR} x*Thy1*CFP transgenic mice

*Thy1*CFP transgenic mice were crossbred with MOG^{TCR} transgenic mice to create a double transgenic MOG^{TCR}x*Thy1*CFP mouse (Figure 2.14), which develops spontaneous and induced optic neuritis with CFP expressing RGC, such that optic nerve loss can be visualised in the retina. These mice can develop ON in the absence of paralytic experimental autoimmune encephalomyelitis (EAE) and RGC can be seen in the living eye. Therefore the model has potential advantages over standard EAE models.

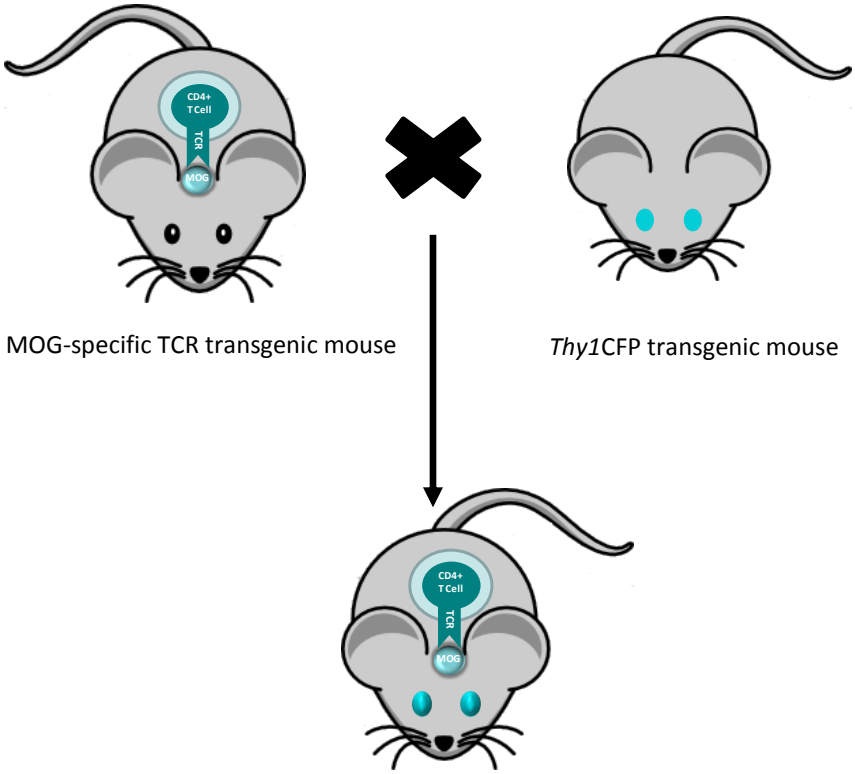

Figure 2.14 ***MOG-TCR crossed with Thy1CFP transgenic mouse.*** *MOG-specific TCR transgenic mice were bred with Thy1CFP transgenic mice to create a double transgenic MOG^{TCR}xThy1CFP mouse.*

2.3.6 Characterising RGC loss in MOG^{TCR} x *Thy1*CFP transgenic mice

To gain a better understanding of factors affecting the disease susceptibility and severity in MOG^{TCR}x*Thy1*CFP mice, the average density of RGC was investigated in different groups of mice to determine which mice should be selected for future experiments.

There is a clear role for gender factors influencing the susceptibility of MS. Gender difference has also been observed in EAE disease susceptibility (Reddy *et al.*, 2005; Sinha *et al.*, 2008). Therefore, the possibility of a gender difference in disease susceptibility in this strain of mice was investigated by looking at the differences in RGC density between male and female MOG^{TCR}x*Thy1*CFP mice (Figure 2.15). There was found to be no significant difference (P=0.197) between these two groups, therefore supporting the use of both male and female MOG^{TCR}x*Thy1*CFP mice in future experiments.

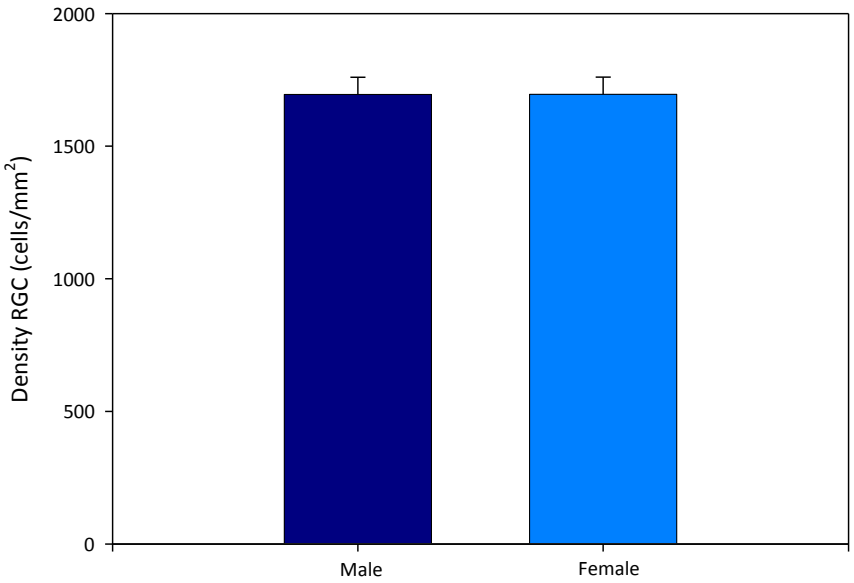

Figure 2.15 ***No difference in RGC loss between male and female MOG^{TCR}xThy1CFP mice.*** *Animals were immunised with 150ng PTX on Day 0 and Day 2. Animals were sacrificed 21 days post immunisation. Eyes were dissected immediately and placed in 4% PFA overnight. Eyes were flatmounted and mounted on slides. RGC were counted using stereology software to count 15 random 100µm x 100µm squares. The RGC density was compared between male (n=5) and female mice (n=8).*

The pathophysiology of ON can develop either bilaterally or unilaterally (Youl *et al.*, 1991). The pathogenesis of the disease in MOG^{TCR}x*Thy1*CFP mice was unknown and eyes from MOG^{TCR}x*Thy1*CFP mice were studied to analyse if disease is bilateral or unilateral (Figure 2.16). There was found to be a strong correlation between left and right eyes ($r=0.972$, $p<0.005$), therefore suggesting the development of ON in MOG^{TCR}x*Thy1*CFP typically occurs bilaterally.

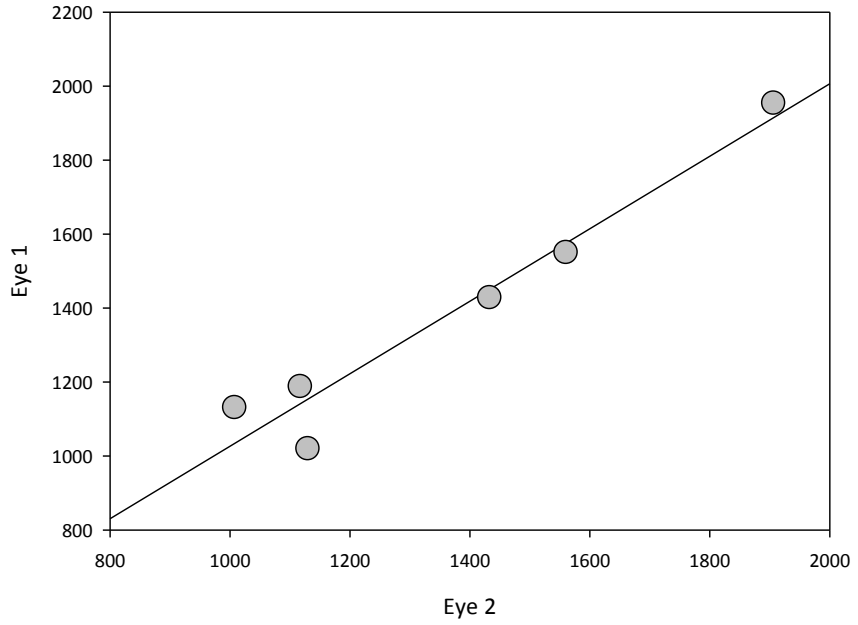

Figure 2.16 ***Correlation between RGC loss in both eyes of MOG^{TCR}xThy1CFP mice.*** *Animals were immunised with 150ng PTX on Day 0 and Day 2. Animals were sacrificed 21 days post immunisation. Eyes were dissected immediately and placed in 4% PFA overnight. Eyes were flatmounted and mounted on slides. RGC were counted using sterology software to count 15 random 100µm x 100µm squares. The RGC density was compared between left eyes (n=6) and right eyes (n=6).*

Previous analysis of MOG^{TCR} mice suggested EAE occurred as a continuum of the pathology seen in the optic nerve (Bettelli *et al.*, 2003). This reflects the pathology observed in humans, as ON is often the presenting symptom before MS occurs (The Optic Neuritis Study, 2008). The correlation between neurological EAE score and RGC density was examined (Figure 2.17). The results show that neurological EAE score was significantly correlated with RGC density (P=0.0176), correlation coefficient (r=-0.45), therefore suggesting a decreasing linear relationship, such that as the neurological EAE score increased, the RGC density decreased. The lack of significance in the correlation between EAE and RGC density could be due to lack of data of histological EAE, which is not clinically observed.

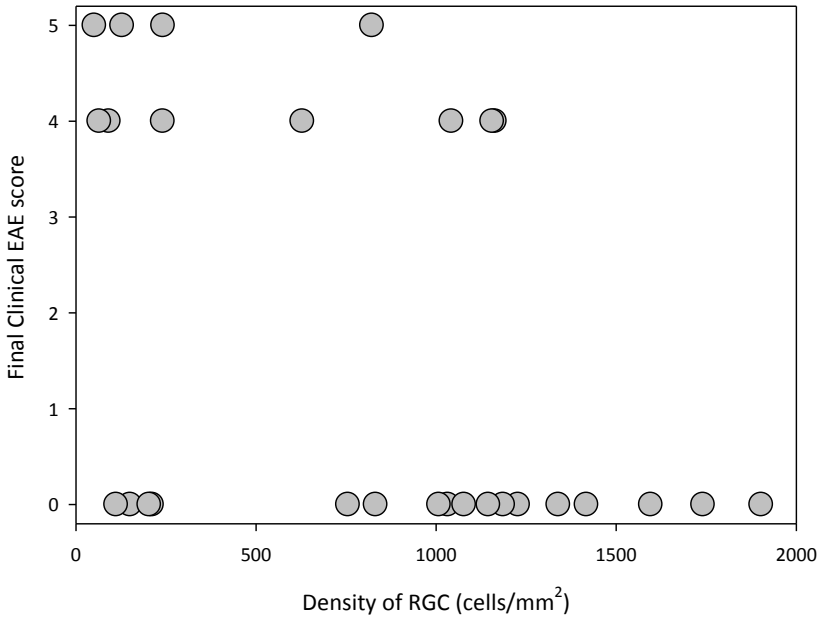

Figure 2.17 ***No correlation between neurological EAE score and RGC density in MOG^{TCR}xThy1CFP mice.*** *Animals were immunised with 150ng PTX on Day 0 and Day 2. Animals were sacrificed 21 days post immunisation. Eyes were dissected immediately and placed in 4% PFA overnight. Eyes were flatmounted and mounted on slides. RGC were counted using stereology software to count 15 random 100µm x 100µm squares. Animals were scored daily and final neurological EAE score recorded on Day 21.*

The correlation between weight of animal and RGC density was examined (Figure 2.18). The weight of the animal was not correlated with the density of RGC (P=0.832, r=0.018); therefore future experiments do not have to be selective for animal weight.

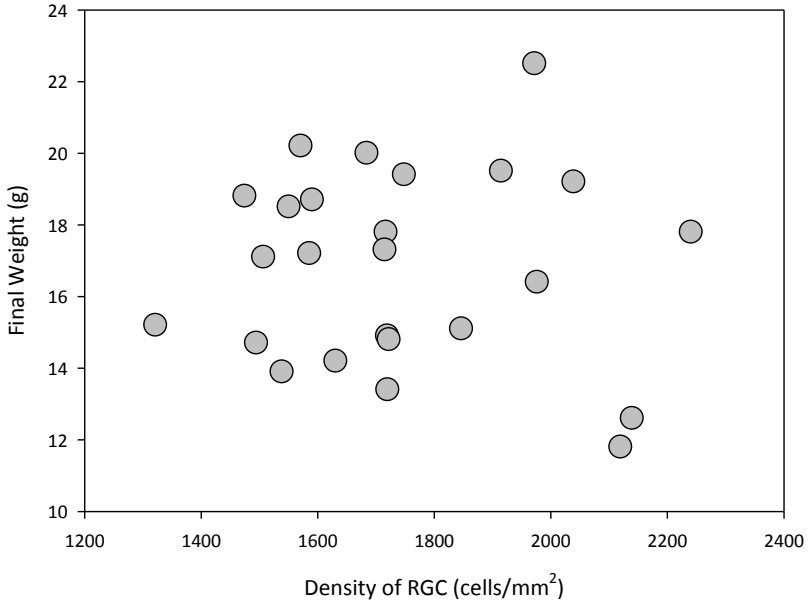

Figure 2.18 ***No correlation between weight and RGC density in MOG^{TCR}xThy1CFP mice.*** *Animals were immunised with 150ng PTX on Day 0 and Day 2. Animals were sacrificed 21 days post immunisation. Eyes were dissected immediately and placed in 4% PFA overnight. Eyes were flatmounted and mounted on slides. RGC were counted using stereology software to count 15 random 100µm x 100µm squares. Animals were weighed daily and final weight recorded on Day 21.*

From these results it can be concluded that the weight and sex of the mouse does not affect the density of RGC and all animals can be included in future experiments. The results also show that ON develops bilaterally and therefore taking results from a single eye will be representative of the pathology in both eyes. The relationship between neurological EAE score and RGC density appears to be ambiguous, however there is evidence to suggest a weak relationship between neurological EAE score and development of ON.

2.4 Discussion

Animal models are essential in scientific research to clarify disease mechanisms and to test novel therapeutic treatments. This chapter details the establishment of a novel animal model and its potential use as a model for demyelination, remyelination and neuroprotection.

Initial research into the pathology of disease of MAG transgenic mouse led to the conclusion that this would be an unsuitable model to use due to the slow degenerative process, which was not evident after 7 months and previous data which suggests this could be a very slow process (Pan *et al.*, 2005). This would therefore be a costly and time consuming experiment to run using this transgenic strain of mice. As an alternative, the MOG-specific TCR transgenic mouse was investigated as a potential animal model. Histological results from MOG-specific TCR provided evidence that would support the use of this model as a rapid model of axonal loss and possibly demyelination, although the evidence to suggest the model demyelinates is limited. As only 30% of mice develop ON, it would be necessary to develop an immunising protocol to achieve 100% disease occurrence (discussed in Chapter 3). Observations from MOG^{TCR} mice reveal that spontaneous ON developed at a higher rate than spontaneous EAE (Bettelli *et al.*, 2003); therefore implying that EAE pathologically follows ON. This could be attributable to differences in permeability of the BBB, variations in MOG expression and/or T cell infiltration in the optic nerve and spinal cord. Previous studies show MOG mRNA expression was significantly higher in the optic nerve compared to the brain and spinal cord and suggests that selective distribution as antigen is the cause of increased disease activity in the optic nerve (Bettelli *et al.*, 2003). This study may indicate that the pathology starts in the optic nerve and development to EAE is due to a continuum of disease pathology. This mechanism can be related to MS pathology in humans, which initially develops as ON in a significant number of cases. To confirm this hypothesis, further studies should address the kinetics by which activated MOG-specific T cells invade cross the BBB and invade the CNS.

The visual system offers a unique way to monitor axonal loss and changes in tissue architecture in the retina relating directly to pathophysiology in the optic nerve. In MS, the eye is a valuable biomarker and is regularly used to monitor changes in disease progression using OCT technology to measure changes in RNFL thickness (Frohman *et al.*, 2008b). Therefore animal models which offered the potential to monitor RGC expression were evaluated. The GFP expressing rat was not suitable as an animal model to detect RGC, although a transgenic rat model is a future avenue of

research, which could still be followed. Rat transgenic models are currently difficult and time consuming to create due to the unstable nature of their embryonic stem cells, which are isolated in mice and genetically modified before reintroducing into the embryo (Babinet *et al.*, 1989). Using a rat model instead of a mouse model would be beneficial due to the increased size of the eye, which would allow any changes in RGC to be easily studied at a higher resolution.

However, the *Thy1*CFP model offered selective expression of RGC, which allowed RGC to be rapidly quantified using retinal flatmounts and offered an advantage over the single transgenic MOG-specific TCR mouse which could only be evaluated with time consuming histology. By crossing MOG-specific TCR mice with *Thy1*CFP mice to produce the MOG^{TCR}x*Thy1*CFP transgenic mouse, a valuable mouse model to study neuroinflammation and nerve damage has been created and can be developed for use in the study of demyelination, neuroprotection and repair. The model offers many benefits for the study of autoimmune diseases; the optic nerve is an accessible CNS target that can be serially assessed by a range of techniques that are applicable to humans. The RGC are also an accessible neuronal target, which can be easily visualised to study neurodegeneration. One of the most valuable aspects of this model is the opportunity to study axonal degeneration via the RNFL. The RNFL is the only part of the CNS that allows direct visualisation of axons (Henderson *et al.*, 2008). A lesion in the optic nerve will result in retrograde degeneration leading to RGC loss and thinning of the RNFL. Previous evidence to support this comes from primate studies (Quigley *et al.*, 1977) and rat models of ON (Hobom *et al.*, 2004).

Compared to the EAE model, the MOG^{TCR}x*Thy1*CFP model would offer a beneficial refinement in accordance with the UK Home Office 3R's principle of reduction, replacement and refinement of research animals. The EAE induction protocol is considered to be a 'substantial' Home Office procedure and so the lack of paralysis leads to less distress to animal and reduced severity of animals in procedure. It also avoids the use of Freund's adjuvant which can cause morbidity to animals such as the development of granulomas and allodynia. It allows disease progress to be studied in animals without the necessity of paralysis and can be serially monitored without the need for sacrificing the animal for histological assessment, therefore reducing animal numbers used. Disease progress can be accurately determined by quantitatively measuring CFP-expressing RGC. Although the mice will lose vision, sight is a sense that is not of primary importance to rodents as they have evolved to be active in the dark and have poor visual acuity. Many laboratory strains of mice (e.g. SJL, CBA) have hereditary retinal dystrophy, which do not affect normal behaviour (Hafezi *et al.*, 2000).

In summary the MOG-specific TCR transgenic mice was successfully crossed with the *Thy1*CFP transgenic model to produce a novel model that expresses fluorescent RRC and develops ON, which will be invaluable for the study of neurodegeneration in autoimmune diseases. The MOG^{TCR}x*Thy1*CFP model will help understand the pathogenesis of demyelination and its relationship with axonal loss and will contribute towards the development of therapeutics and validation of targets for drug intervention.

Chapter 3

Development of immunising protocol

3.1 Introduction

Once the double transgenic mouse model MOG^{TCR}x*Thy1*CFP had been created (Chapter 2), research focused upon developing an immunisation protocol to induce disease. Approximately 30% of the MOG^{TCR} transgenic mice develop spontaneous ON with a wide range of time to onset (from 2.5 months to 5 months) (Bettelli *et al.,* 2003). The aim therefore was to develop a method of immunisation to ensure a significantly large proportion of mice develop ON with optimal disease activity that can be manipulated with anti-inflammatory, neuroprotective or remyelinative therapies.

3.1.1 Complete Freund's adjuvant

Adjuvants are administered in combination with antigens, which boost the T cell response leading to an increase in activated T cells and a more vigorous immune response to the antigen. One of the most widely used adjuvants in experimental models of autoimmune disease is Complete Freund's Adjuvant (CFA), which enhances antibody production and T cell response (Billiau & Matthys, 2001). CFA contains heat-killed mycobacteria (*Mycobacterium tuberculosis)* in an oil and water emulsion. Administering antigens in an oil and water emulsion prolongs the lifetime of the antigen and allows a slow release over a long period of time (Herbert, 1968). CFA has also been shown to promote dendritic cell maturation (Tsuji *et al.*, 2000), enhance phagocytosis (Pulendran *et al.*, 2001), cytokine induction (Tovey & Lallemand, 2010) and activation and proliferation of CD4+ lymphocytes (Dalton *et al.*, 2000). CFA was used in early EAE experiments and is used today as an immunological adjuvant (Freund *et al.*, 1947).

3.1.2 Pertussis Toxin

Bordetella pertussis toxin (PTX) is frequently used as an immunological adjuvant in animal models of autoimmune disease. The traditional belief is that PTX predisposes animals to autoimmunity by disrupting the BBB to allow passage of inflammatory mediators, which target the CNS (Linthicum & Frelinger, 1982). The permabilisation of the BBB was classically associated with an increased

sensitisation to the histamine sensitisation factor of PTX (Teuscher, 1985). However, PTX is mitogenic for lymphoid cells as evidenced by the enlargement of the spleen with the expansion of antigen specific T cell following injection with PTX (Ryan *et al.*, 1998). Accumulating evidence suggests PTX mediates its effects on the CNS by an alternate immunomodulatory mechanism in contrary to traditionally held belief, with effects on the blood-brain barrier being secondary. PTX has a range of effects and is associated with enhanced T cell differentiation, (Ryan *et al.*, 1998), increased cytokine responses, activation of Toll-like receptor 4 signalling (Kerfoot *et al.*, 2004; Racke *et al.*, 2005) and depletion of CD4+,CD25+,FoxP3 subpopulation of regulatory T cells (Cassan *et al.*, 2006; Chen *et al.*, 2006). The discovery of these further effects of PTX highlights the complex interplay between PTX and autoimmunity.

3.1.3 MOG and MOG-specific antibodies

Although myelin reactive T lymphocytes can trigger the development of EAE, myelin specific B lymphocytes can contribute to pathology through antigen presenting capacities and the production of demyelinating autoantibodies (Pollinger *et al.*, 2009). In contrast to myelin antigens such as MBP and PLP, which are not exposed, MOG is expressed on the surface of the myelin sheath and is exposed to antibodies penetrating the CNS. MOG is a minor antigen of the CNS which is strongly immunogenic and induces autoantibodies that can potentially be a target for chronic demyelination in EAE (Lebar *et al.*, 1986b). Studies from MOG knockout mice highlighted the importance of the protein as a self-antigen and its necessity for development of EAE (Delarasse *et al.*, 2003; Liñares *et al.*, 2003). MOG IgG autoantibodies are sometimes present in cerebrospinal fluid (CSF) of MS patients and provides evidence supporting their importance in MS pathogenesis (Xiao *et al.*, 1991). The physiological function of MOG is unknown, however evidence suggests a role in myelin maturation and maintenance due to its late expression during development (Scolding *et al.*, 1989).

MOG-specific antibodies were developed to study the effects of circulating anti-myelin antibodies on clinical and pathological course of EAE, which leads to extensive demyelination in the presence of an inflammatory disease that produces BBB dysfunction (Linington *et al.*, 1988). Several clones of MOG-specific antibody have been produced and characterised to further investigate their demyelinative potential and to characterise the immune response in EAE (Piddlesden *et al.*, 1993). The Z12 clone (mouse IgG2a monoclonal antibody) produces the most severe demyelination and a significant increase in deposition of membrane attack-complex of complement due to its

enhanced ability of the IgG2a isotype to activate complement (Piddlesden *et al.*, 1993). It was later shown that the effects of antibody-mediated damage are associated with an increased recruitment of mononuclear cells into the CNS in mice, probably in response to complement-mediated killing of cells, an effect which requires activation of complement (Morris-Downes *et al.*, 2002). This enhanced degree of damage could lead to an increase of severity of EAE that could result in death of the mice (D Baker, personal communication). This suggested that in contrast to the rat, mouse EAE may be too severe to augment demyelination using complement fixing MOG-specific mAb (Linington *et al.*, 1988).

3.1.4 CD4-specific antibodies

CD4 antibodies were extensively studied as a tool to modify the pathogenesis of EAE and gain a greater understanding of the inflammatory components of disease. CD4-specific mAb suppress T cell dependant responses and have been shown to prevent the development of neurological EAE (O'Neill *et al.*, 1993). Administration of YTS191.1 (CD4-specific mAb) led to a rapid reduction of CD4+ T cells in the peripheral blood and lymphoid tissue by a complement mediated mechanism (Cobbold *et al.*, 1984). The basis of CD4-specific mAb immunomodulation is not completely understood but it is thought to prevent the function of activated effector cells (Sedgwick & Mason, 1986). YTS177, a non-depleting CD4 mAb, results in the down regulation of CD4 and thus cannot cause interaction of CD4 with MHC class II antigens, which is required for T cell activation following engagement of the TCR with the MHC antigen complex (O'Neill *et al.*, 1993). YTS177 has also been used to reduce the established inflammation present in non-obese diabetic mice and prevents the onset of type 1 diabetes (Thompson *et al.*, 2004).

3.1.5 Aims and Objectives

The aim was to produce and refine an immunisation protocol, which results in optimal disease activity that can be manipulated for drug studies. Initial studies were aimed at investigating the effects of using classical immunological adjuvants such as PTX and MOG in CFA, which have previously been used in EAE experiments and also in this model (Bettelli *et al.*, 2003). Following this the immunisation protocol was refined using Z12 MOG-specific mAb and modulated with CD4-specific mAb to produce disease with maximum axonal and RGC loss but without paralysis typically associated with EAE.

3.2 Materials and Methods

3.2.1 Animals

MOG^{TCR}x*Thy1*CFP transgenic mice as described earlier were used for all experiments. All experiments were performed according to UK Animals (Scientific Procedures) Act 1986.

3.2.2 Immunisation

Animals were either injected intraperitoneally (i.p.) on day 0 and 2 with 150ng *Bordetella pertussis* toxin (PTX) (1) (Sigma-Aldrich Ltd, Poole, Dorset, UK) or subcutaneously (s.c.) with 100µg MOG (2) in complete Freund's adjuvant (CFA) (3) (Difco Laboratories, West Molesey, Surrey, UK).

(1) PTX (Sigma-Aldrich Ltd, Poole, Dorset, UK) was reconstituted in 500µl PBS. To prepare 1ml of 150ng/100µl PTX, 67µl of reconstituted PTX was dissolved in 933µl distilled water.

(2) 200µg/ml of MOG 35-55 peptide was prepared by adding 100µg MOG 35-55 to 5ml PBS.

(3) CFA was prepared by adding 8mg *Mycobacterium tuberculosis* H37Ra to 10ml incomplete Freund's adjuvant (Difco Laboratories, West Molesey, Surrey, UK).

(4) 100µg MOG in CFA was prepared by adding 5ml of 200µg/ml of MOG 35-55 peptide (2) to 5ml CFA (3). An emulsion was formed by rapidly pumping the mixture through a 1ml syringe for around 15 minutes. The consistency was tested by placing a droplet onto the surface of water and observing dispersion from the droplet.

On day 14 animals were injected with 0.1-1.0mg MOG-specific Z12 monoclonal antibody in 200µl sterile PBS. In subsequent studies animals were injected with 100µl of anti-CD4 YTS177 monoclonal antibody ascites (O'Neill *et al.*, 1993) to reduced disease severity and axonal loss to study demyelination. CD4 is a primary co-ligand for T cell activation; therefore anti-CD4 mAb reduces T cell activation and CNS infiltration.

Animals developing EAE were weighed and scored daily using a five-point EAE scale (Figure 3.1). During the paralytic phase animals are fed on a soaked diet. In accordance with the Home Office animal care protocols, several end points are specified due to the severity of this procedure.

Animals must be euthanized when they reach the following endpoints: a weight loss of greater than 35% of initial weight, prolapsed penis for more than 2 days, loss of bladder control, hypothermia (temperature below 31°C), 5 days of complete hind limb paralysis (without weight gain), 7 days of complete hind limb paralysis (with weight gain) (Al-Izki *et al.*, 2011). A small percentage of animals (>1%) will show signs of distress due to visual disturbance and may rub their eyes beyond what is considered normal grooming, in these cases the animals are also euthanised.

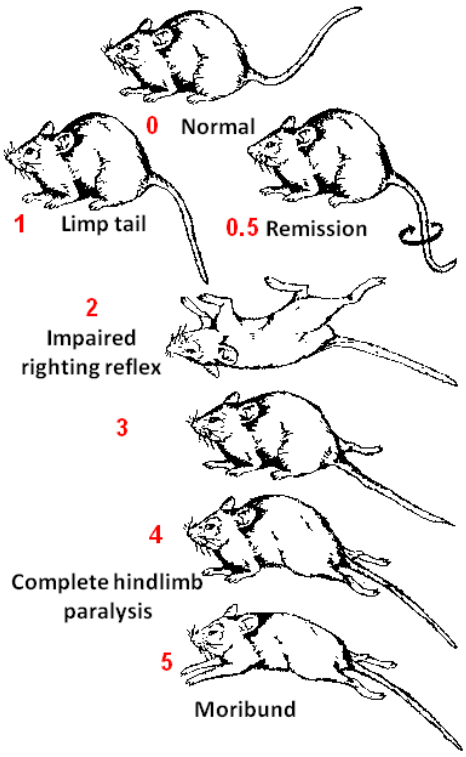

Clinical Score	Description
0	Normal
1	Fully flaccid tail, the tail is completely paralysed. If the tail does not lift but has some tone the score is 0.5.
2	Impaired righting reflex. The animal is turned on its back, it will not right itself. If the animal rights itself slowly the score is 1.5.
3	Hind limb paresis. If the animals only have a hind limb gait disturbance, the score is 2.5.
4	Complete hind limb paralysis. If the limbs are virtually paralysed but have some minor movement, the score is 3.5.
5	Moribund/Death. If the animals' forelimbs become paralysed in addition to the hind limbs then the animal must be euthanised (in accordance with UK home office legislation).

Figure 3.1 ***EAE scoring scale****. Animals scored on a scale of 1-5 (Al-Izki et al., 2011). Each clinical score has been defined and described to allow accurate scoring.*

3.2.3 Hybridomas

3.2.3.1 Growing hybridomas

Hybridomas secreting Z12 MOG-specific mAb (mouse IgG2a monoclonal antibody) (Piddlesden *et al.*, 1993) were used to produce antibodies. A frozen sample of Z12 clone was removed from liquid nitrogen and grown in RPMI 1640 medium (containing L-glutamine) (Invitrogen, Paisley, UK). 150ml of RPMI medium was poured into a 250ml filter unit and additional medium components were added (Table 3.1). The solution was filtered with 0.22µm sterile filter and added back to the original 500ml bottle of RPMI medium.

Medium components	Final concentration
58ml Foetal calf serum (heat inactivated) (Invitrogen, Paisley, UK)	10% FCS
5.8ml Pen/Strep (100x stock) (Sigma, Poole, Dorset, UK)	100 units/ml Penicillin G, 100µg/ml streptomycin
5.8ml insulin (Invitrogen, Paisley, UK)	5µg/ml insulin
5.8ml sodium pyruvate (Sigma, Poole, Dorset, UK)	1mM sodium pyruvate
0.5ml 0.1% β-mercaptoethanol (Sigma, Poole, Dorset, UK) from freshly made 1000x stock (7µl into 10mls distilled H_2O)	0.0001% β-mercaptoethanol

Table 3.1 ***Medium components for growing hybridomas.*** *Concentration and volumes of components added to 500ml RPMI medium 1640.*

A 24 well plate was prepared by adding 0.5ml RPMI medium to the middle 8 wells and was left to equilibrate in a 37°C (5/10% CO_2) incubator for one hour. A Z12 sample was removed from liquid nitrogen and thawed in 37°C water bath. Cells were mixed with 10ml pre-warmed medium and spun at 1000xg for 10 minutes. The medium was decanted and cells re-suspended in 0.5ml RPMI 1640 medium. The re-suspended cells were divided between 4 centre wells and left to incubate overnight in a 37°C (5/10% CO_2) incubator. Once the cells were 30-50% confluent, fresh medium was added from neighbouring wells and fresh medium was added to eight empty wells. After 1-3 days the cells were confluent and a pipette was used to take up the cells and split into 8 wells. Three 150cm^2 flasks were prepared by adding 50ml medium and placing in incubator. When all 8 wells were confluent, the cells were pipetted up and down and re-suspended in 15 ml tube. The

cells were split between the flasks. To propagate, cells were fed everyday by doubling the medium. Once fully confluent, the bottles were stood up and left for 2 weeks with occasional agitation. The supernatant was removed and purified.

3.2.3.2 Purifying monoclonal antibodies

Monoclonal antibodies were purified using protein A affinity chromatography, a chromatography matrix that allows interaction between the Fc portion of protein A and antibody, which can be reversed to isolate antibody of interest. To prepare the sample for purification, the supernatant was centrifuged to remove cell debris (10,000g for 10 minutes) and filtered to remove particulate matter (0.45µm filter).

A HiTrap™ Protein A High Performance 1ml column (GE Healthcare Life Sciences, Buckinghamshire, UK) was used to purify hybridomas. Binding, elution and neutralisation buffer were prepared (Table 3.2).

Buffer	Chemical	pH
Binding buffer	0.02M sodium phosphate (Sigma, Poole, Dorset, UK)	7.0
Elution buffer	0.1M citric acid (Sigma, Poole, Dorset, UK)	4.5-5.5
Neutralisation buffer	1M Tris-HCL (Calbiochem, Merck, Nottingham, UK)	9.0

Table 3.2 ***Buffers used in antibody purification.*** *Binding, elution and neutralisation buffer composition and pH for purifying hybridomas on a Protein A column.*

The column was linked to a peristaltic pump (Pharmacia, Stockholm, Sweden) and equilibrated with 10ml binding buffer at a rate of 1ml/min. The supernatant was pumped through the column at a rate of 3ml/min, followed by 10ml binding buffer at 1ml/min. The antibody was eluted with 5ml elution buffer and collected with 60-200µl neutralisation buffer. To reuse the column, it was re-equilibrated with 10ml binding buffer and washed with 20% ethanol to prevent microbial growth and stored at 4-8°C for future use. The concentration of the antibody was tested by placing a 1µl sample onto a Nanodrop Spectrophotometer (Thermo Scientific, Wilmington, Delaware, USA) and measuring its absorbance at 280nm.

3.2.4 Statistical analysis

Statistical analysis was performed using SigmaStat 3.1. Results were presented as mean values ± standard error of mean. Differences between two groups were analysed by Students t-test following normality tests. Differences between multiple groups were analysed by one way analysis of variance (ANOVA) tests. Results were considered significantly different if the probability level $P<0.05$ (*), $P<0.01$(**) or $P<0.001$(***) was reached between groups.

3.3 Results

3.3.1 Pertussis toxin and MOG in CFA immunisation

Following on from work by Bettelli *et al* 2003, which described the potential use of an immunising protocol, the development of an immunisation protocol to allow sufficient disease to be obtained in MOG^{TCR} mice was explored. Animals were either injected with 150ng PTX on day 0 and 2 or immunized with 50µg MOG peptide in CFA on day 0 (Figure 3.2). Animals were euthanised after 14 days , which has been reported to be the time of maximum disease (Guan *et al.*, 2006) and optic nerves and eyes were removed and analysed. None of these animals developed neurological EAE.

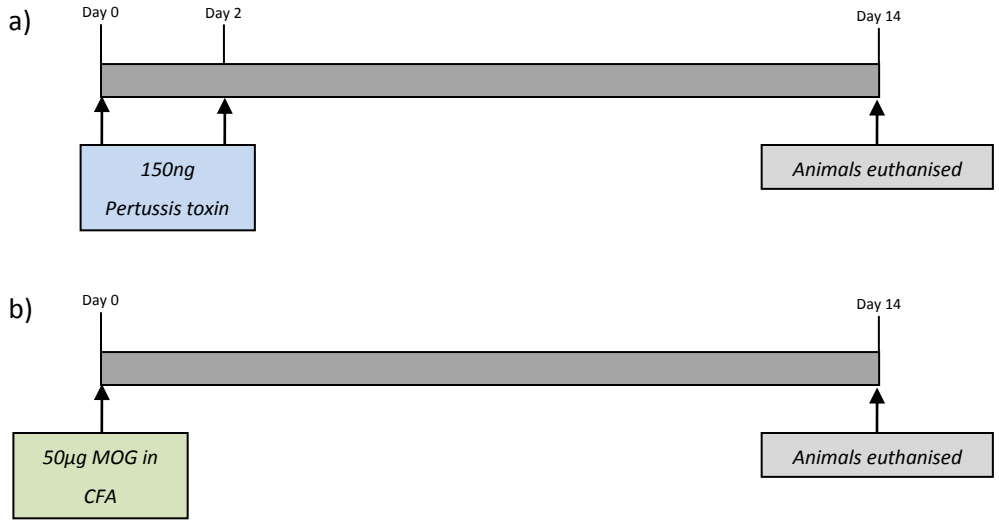

Figure 3.2 ***Timeline of experimental design for investigating immunisation with PTX and MOG in CFA.***
a) Animals immunised with 150ng Pertussis toxin on day 0 and 2. b) Animals immunised with 50µg MOG in CFA on day 0. All animals were euthanised on day 14.

Optic nerves were analysed and the number of myelinated axons in a cross section were counted. The number of myelinated axons decreased in optic nerves taken from animals immunised with PTX or MOG in CFA (Figure 3.3). Both PTX and MOG in CFA immunisation groups showed a decrease in the number of myelinated axons. However, the decrease in the number of myelinated axons was not statistically significantly different in immunised groups when compared to controls. This was possibly due to the small numbers in each group but this clearly was associated with the large deviations within the groups, suggesting that some animals were non-responders. Low availability of MOG^{TCR} mice necessitated the use of wildtype littermate C57BL/6 controls. However, in other experiments the number of axons in C57BL/6 mice was not different from normal C57BL/6 MOG^{TCR} mice.

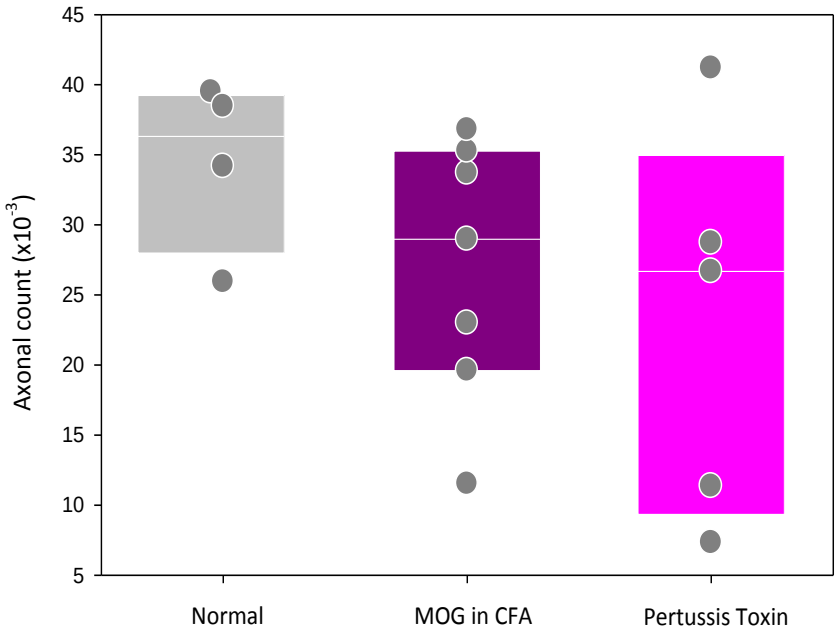

Figure 3.3 ***Axonal counts from optic nerves of normal and diseased MOG^{TCR} mice induced to develop ON using PTX or immunised with MOG peptide in CFA***. *Axonal counts from normal animals (n=4),* MOG^{TCR} *animals immunised with 100µg MOG in CFA (n=5) and* MOG^{TCR} *animals immunised with 150ng PTX (n=7). Animals were euthanized on day 14 and perfused with Karnovsky's Fixative. Tissue was embedded in resin and semi-thin sections (0.7µm) were cut and stained with toluidine blue. Control animals were wildtype C57BL/6 animals of a similar age. Axons were randomly counted from a cross section using stereology software. Boxes show 25th and 75th percentile and median line. Circles show results from individual animals.*

The retina was analysed and RGC were counted along a cross section of the RNFL. The number of RGC was estimated from animals immunized with PTX or MOG in CFA. Both PTX and MOG in CFA immunisation groups showed a decrease in the number of RGC (Figure 3.4). The decrease in RGC was significantly ($P<0.05$) different in immunised groups when compared to controls. This suggested that analysis of RGC number may be more reliable than analysis of the optic nerve.

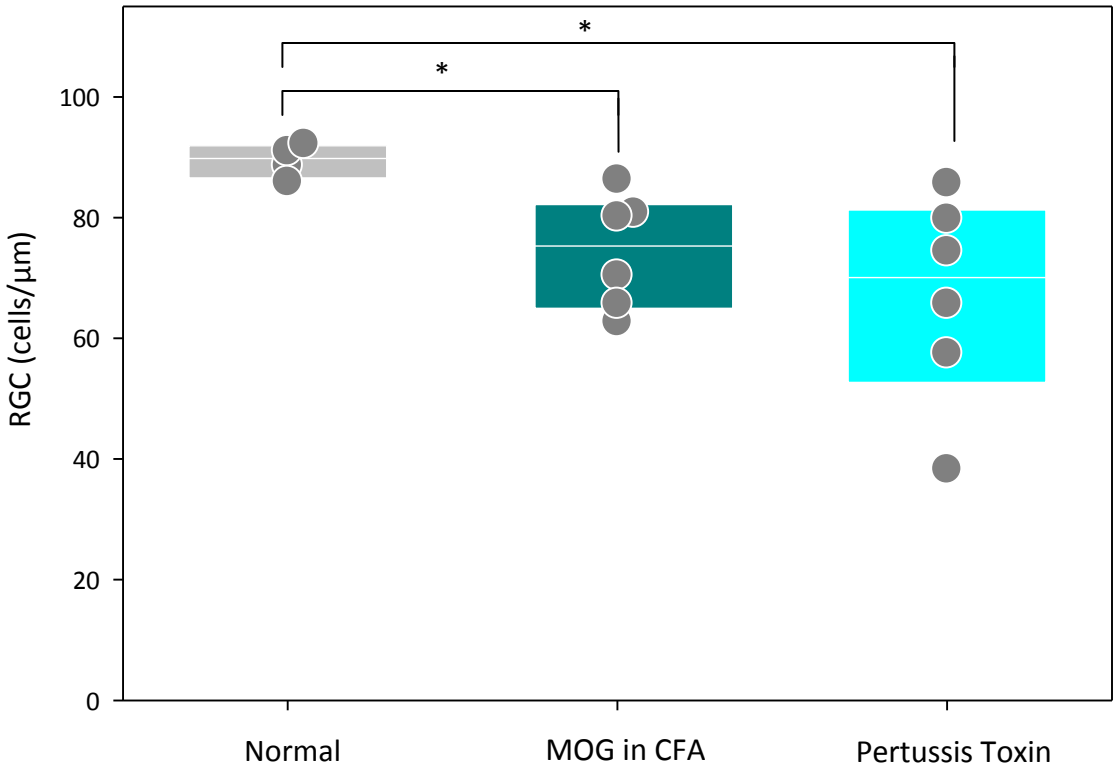

Figure 3.4 **RGC counts from retina of normal and diseased MOG^{TCR} mice induced to develop ON using PTX or immunised with MOG peptide in CFA**. *RGC counts from normal animals (n=4),* MOG^{TCR} *animals immunised with 100µg MOG in CFA (n=5) and* MOG^{TCR} *animals immunised with 150ng PTX (n=7). Animals were euthanized on day 14 and perfused with Karnovsky's Fixative. Tissue was embedded in resin and semi-thin sections (0.7µm) were cut and stained with toluidine blue. Control animals were wildtype C57BL/6 animals of a similar age. RGC were counted along a cross-section of retina and density calculated by measuring the length of retina using sterology software. Boxes show 25th and 75th percentile and median line. Circles show results from individual animals. *P<0.05 compared to controls.*

The percentage of axonal loss and RGC loss following immunisation suggests immunisation was effective at incidence of disease in the majority of MOG^{TCR} transgenic mice (Table 3.3). Immunisation with PTX showed a greater percentage of axonal loss and RGC loss when compared with MOG in CFA immunisation. RGC loss was statistically significant in both PTX and MOG in CFA immunised animals compared to control animals. Axonal loss was not statistically significant in PTX and MOG in CFA immunised animals compared to normal animals. However, there was a large standard error, suggesting a considerable variability between animals in the same group. This was probably due to the suggestion that some animals failed to develop disease, as there was an overlap of RGC and axonal numbers between disease transgenic and normal wildtype mice.

	Pertussis toxin Mean ± SEM	**MOG in CFA** Mean ± SEM
% Axonal loss	33±18	22±10
% RGC loss	25±8*	17±4*

Table 3.3 Percentage ***of mean axonal and RGC loss in normal and diseased MOG^{TCR} mice induced to develop ON using PTX or immunised with MOG peptide in CFA****. MOG^{TCR} mice were immunised with PTX (Day 0 and 2) (n=7) or MOG in CFA (Day 0) (n=6) and were euthanised on Day 14. The % axonal loss and RGC loss was calculated by % mean reduction of MOG-TCR animals immunised compared to wildtype littermates. The largest axonal loss and RGC loss were seen in PTX treated animals. *P<0.05 compared to control animals.*

To gain a greater understanding of the underlying pathology, semi-thin cross sections of the optic nerve and retina stained with toluidine blue were examined (Figure 3.5). Optic nerves from PTX and MOG in CFA treated groups show axonal loss and limited evidence of demyelination.

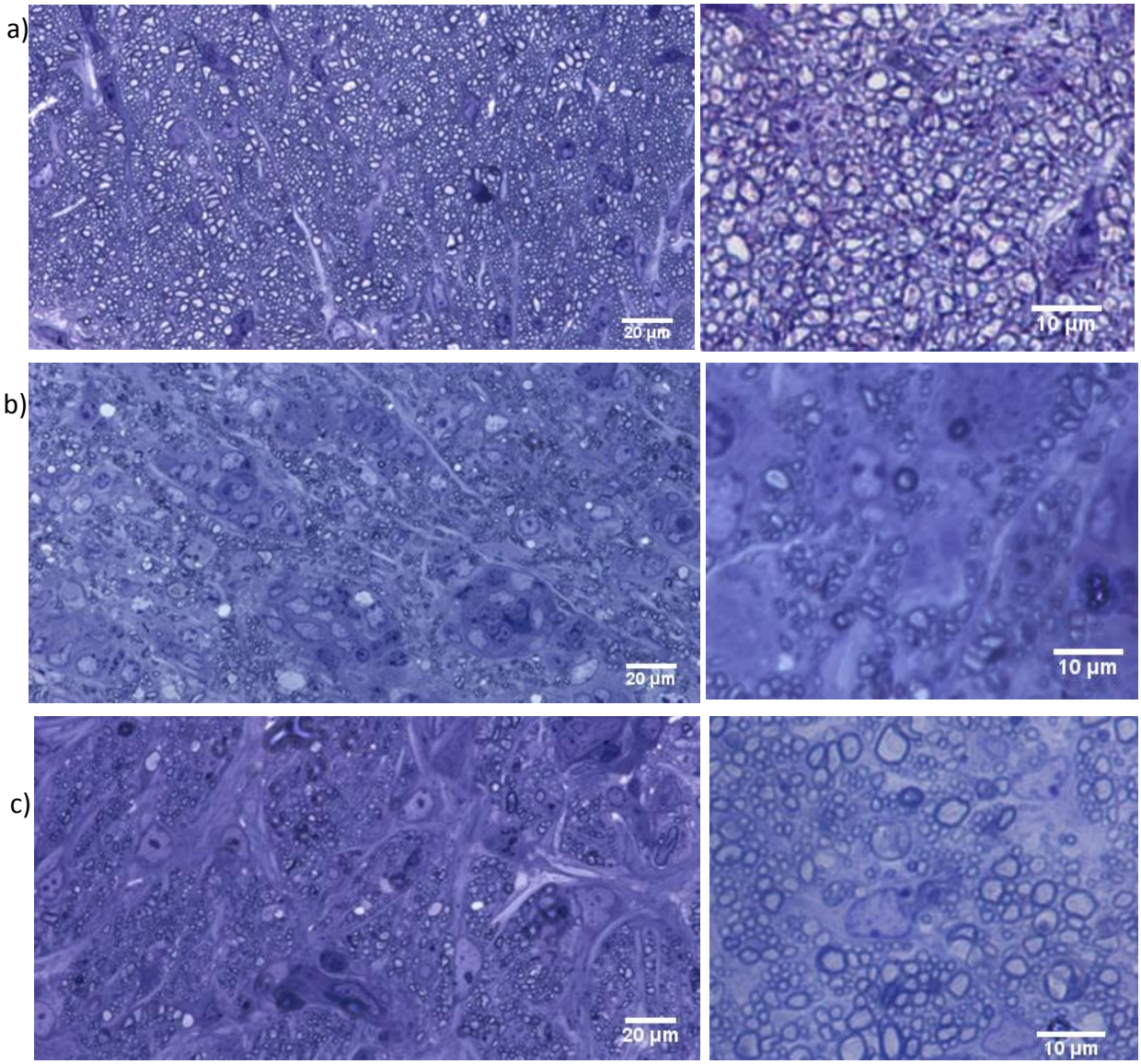

Figure 3.5 ***Cross sections of optic nerves from normal and diseased MOG^{TCR} mice induced to develop ON using PTX or immunised with MOG peptide in CFA.*** *Animals euthanised after 2 weeks of immunisation and wildtype controls were age-matched. Animals were perfused and tissue was fixed in Karnovsky's Fixative. Tissue was embedded in resin and semi-thin sections (0.7µm) were cut and stained with Toluidine blue. a,d) Cross section of optic nerve from wildtype, C57BL/6 mouse shows uniformly myelinated axons and no evidence of optic neuritis. b,e) Cross section of optic nerve from MOG^{TCR} mice immunised with PTX (Day 0 and 2) showed large areas of axonal loss and signs of ON. c,f) Cross section of optic nerve from MOG^{TCR} mice immunised with MOG in CFA (Day 0) showed large areas of axonal loss.*

The retina from control animals showed uniformly rounded RGC with closely packed nuclei, which are typical characteristics of healthy RGC (Figure 3.6a). The retina from PTX and MOG in CFA immunised animals were not uniform in appearance and were sporadically organised (Figure 3.6b,c).

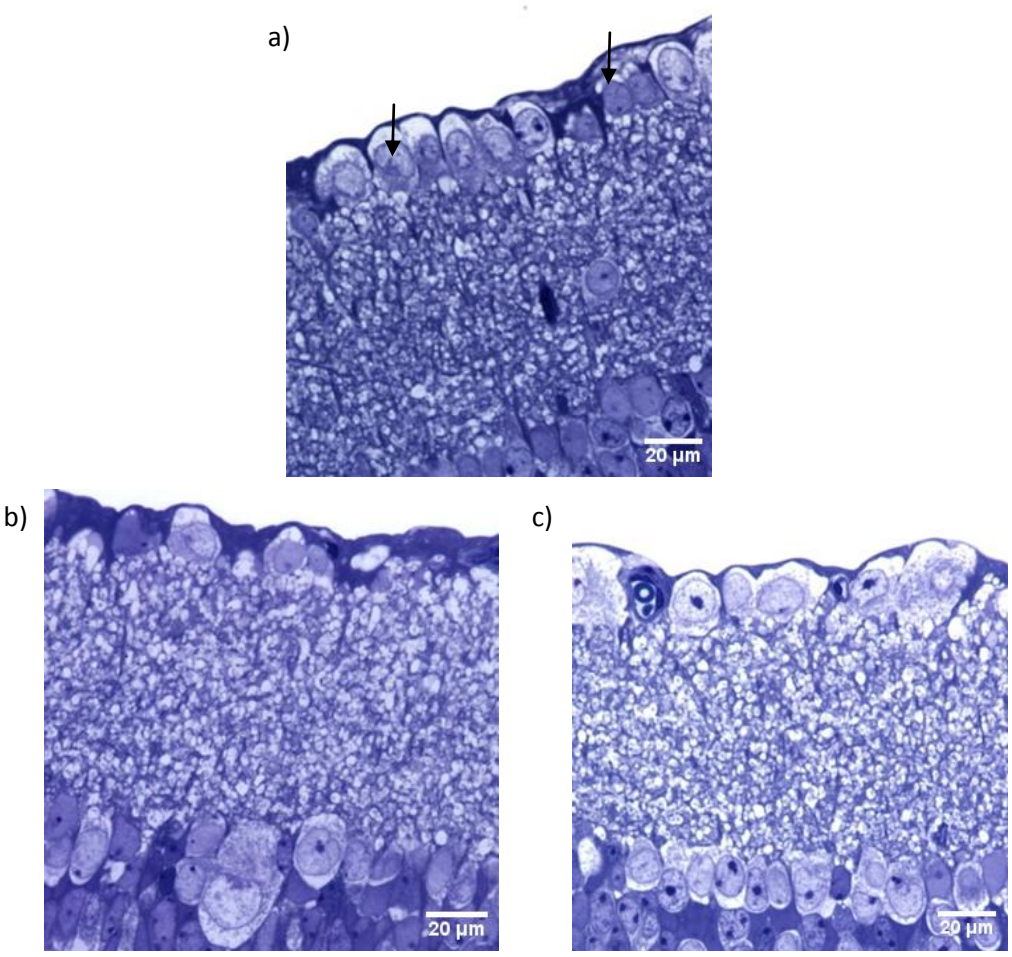

Figure 3.6 ***Cross sections of retina from normal and diseased MOG^{TCR} mice induced to develop ON using PTX or immunised with MOG peptide in CFA.*** *Animals were perfused and tissue was fixed in Karnovsky's Fixative. Tissue was embedded in resin and semi-thin sections (0.7µm) were cut and stained with toluidine blue and RGC (arrows) were counted. a) Cross section of retina from wildtype, C57BL/6 mouse showed uniform RGC. b) Cross section of retina from MOG^{TCR} mice immunised with PTX (Day 0 and 2) showed irregular RGC distribution. c) Cross section of retina from MOG^{TCR} mice immunised with MOG in CFA (Day 0) showed irregular RGC. All images are at 60x objective lens magnification. Animals euthanised after 2 weeks of immunisation and wildtype controls were age-matched.*

Ultra-thin sections were stained with lead citrate and uranyl acetate and were examined with an electron microscope (Figure 3.7). Optic nerves from control animals looked normal with densely packed, uniform myelination surrounding the axon (Figure 3.7a,b). In the immunised animals, the optic nerve contains few axons, some of which appear to be demyelinated but these were infrequent and not easy to distinguish from glial cell processes (Figure 3.7c,d).

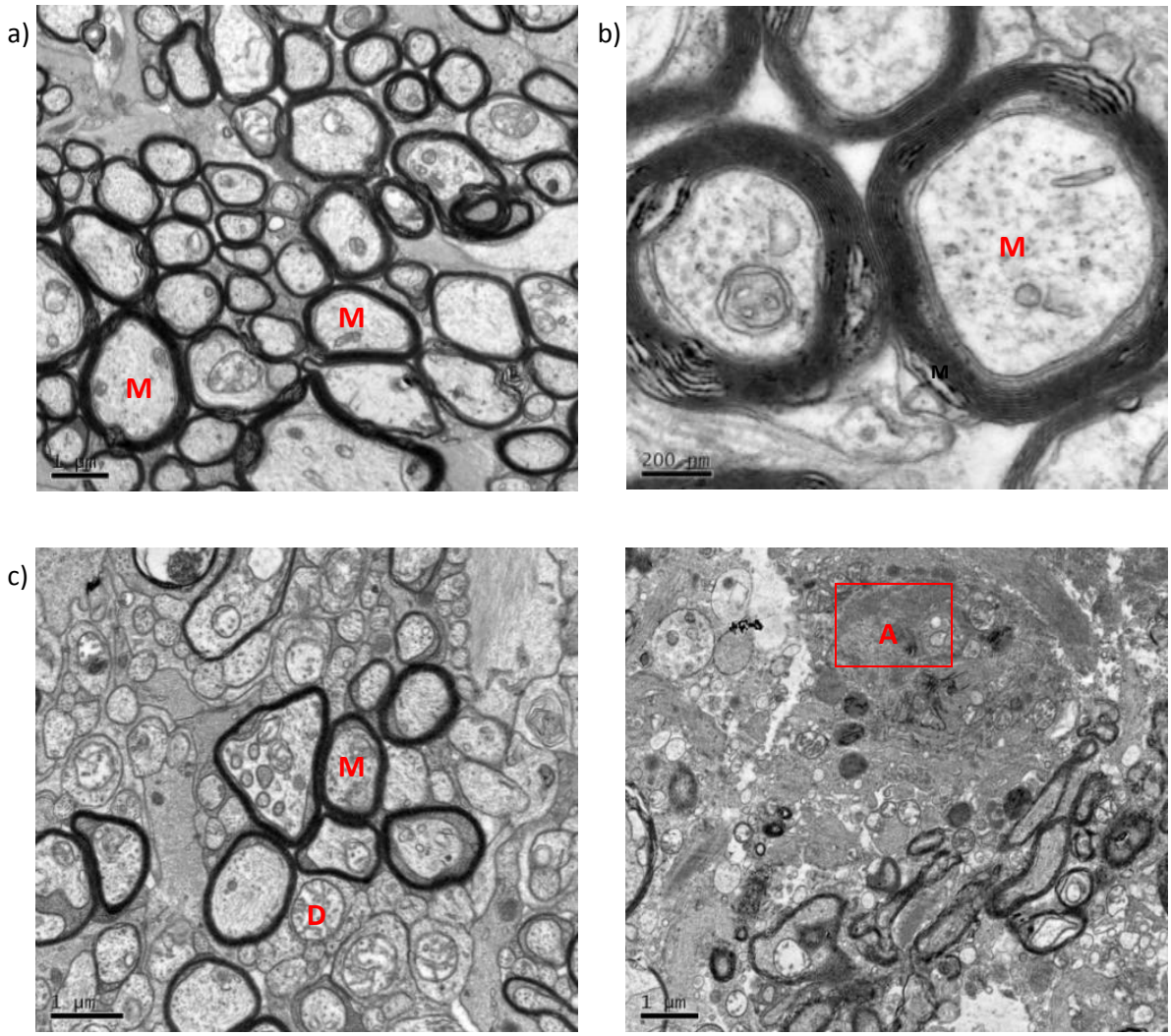

Figure 3.7 ***Electron microscopy of optic nerves from normal and diseased MOG^{TCR} mice induced to develop ON using PTX or immunised with MOG peptide in CFA****. Animals euthanised after 2 weeks of immunisation and wildtype controls were age-matched. Animals were perfused and tissue was fixed in Karnovsky's Fixative. Tissue was embedded in resin and ultra-thin sections (90nm) were cut and stained with Lead citrate. a,b) Cross section of optic nerve from Wildtype, C57BL/6 mice showed uniformly myelinated axons (M). c) Cross section of optic nerve from MOG^{TCR} mice immunised with PTX (Day 0 and 2) showed evidence of demyelination (D) and axonal loss. Demyelinated axons can be differentiated from other cell types by the characteristic stippled cytoplasm surrounded by faintly stained thin line, corresponding to the axonal membrane. d) Cross section of optic nerve from MOG^{TCR} mice immunised with MOG in CFA (Day 0) showed large areas of axonal loss (A).*

These results clearly show a difference between control mice and MOG^{TCR} mice immunised with PTX or MOG in CFA. Therefore, from this study it can be concluded that PTX has a greater effect on RGC and axonal loss compared to animals immunised with MOG in CFA. Future studies should employ immunisation of animals with PTX for optimal results.

3.3.2 Pertussis toxin followed by Z12 MOG-specific mAb at different times

Studies in rats have shown that injection of complement fixing antibody can augment demyelination (Linington *et al.*, 1988). In classic EAE in the mouse, this can augment clinical disease (Morris-Downes *et al.*, 2002) such that it can cause death. As spinal EAE was not a feature of ON, a combination of PTX and anti-MOG Z12 mAb (monoclonal mouse IgG2a) was used in immunised MOG^{TCR} mice in an attempt to amplify demyelination in the optic nerve. Injection of Z12 MOG-specific mAb when the BBB was compromised, would therefore facilitate entry of antibody into the CNS and induce complement-dependant lysis of oligodendrocytes to induce demyelination (Morris-Downes *et al.*, 2002). Initial studies investigated the optimal timing of Z12 MOG-specific mAb injection. Animals were immunised with 150ng PTX on day 0 and 2 followed by i.p. injection of 1.0mg Z12 MOG-specific mAb on day 14 or 21, animals were euthanised on 7 days post Z12 MOG-specific mAb injection (Figure 3.8).

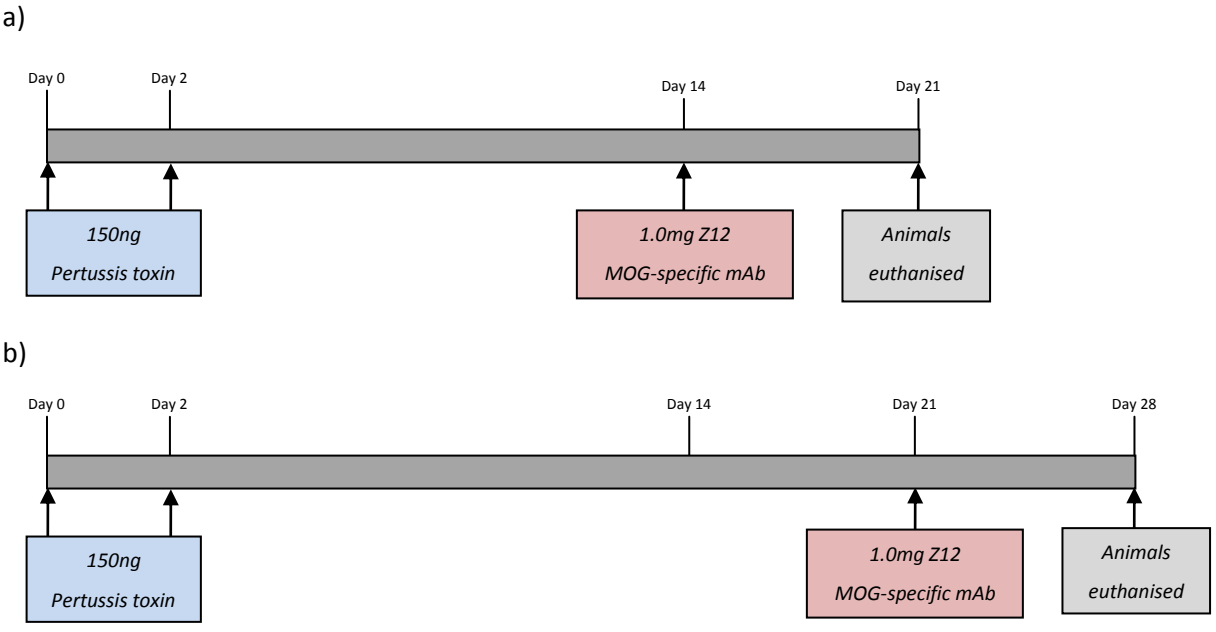

Figure 3.8 ***Timeline of experimental design for investigating the timing of Z12 MOG-specific mAb.***
a) Animals immunised with 150ng Pertussis toxin on day 0 and 2 and 1.0mg Z12 MOG-specific mAb at day 14 and euthanised on day 21. b) Animals immunised with 150ng Pertussis toxin on day 0 and 2 and 1.0mg Z12 MOG-specific mAb at day 21 and euthanised on day 28.

The majority of animals developed neurological EAE (approximately 86%). The average maximal neurological EAE score for animals immunised with Z12 MOG-specific mAb after 14 days and 21 days was 3.2±1.0 and 2.8±0.8 respectively. There was no significant difference between maximal neurological EAE scores when immunised with Z12 MOG-specific mAb on day 14 or 21. Comparison of axonal loss in optic nerve sections following Z12 MOG-specific mAb injection at day 14 showed no significant difference between Z12 MOG-specific mAb injection at day 21 (Figure 3.9). However, Z12 MOG-specific mAb injection at Day 21 shows more variability in axonal counts compared to day 21 post-disease induction. The results are comparable to neurological EAE scores as the group immunised at 14 days show less variability. Therefore, there is no significant difference between axonal loss after Z12 MOG-specific mAb injection on day 14 and day 21 post-disease induction. From these results it would suggest that future immunising protocols should use Z12 MOG-specific mAb at day 14, to ensure a shorter and more concise development of disease.

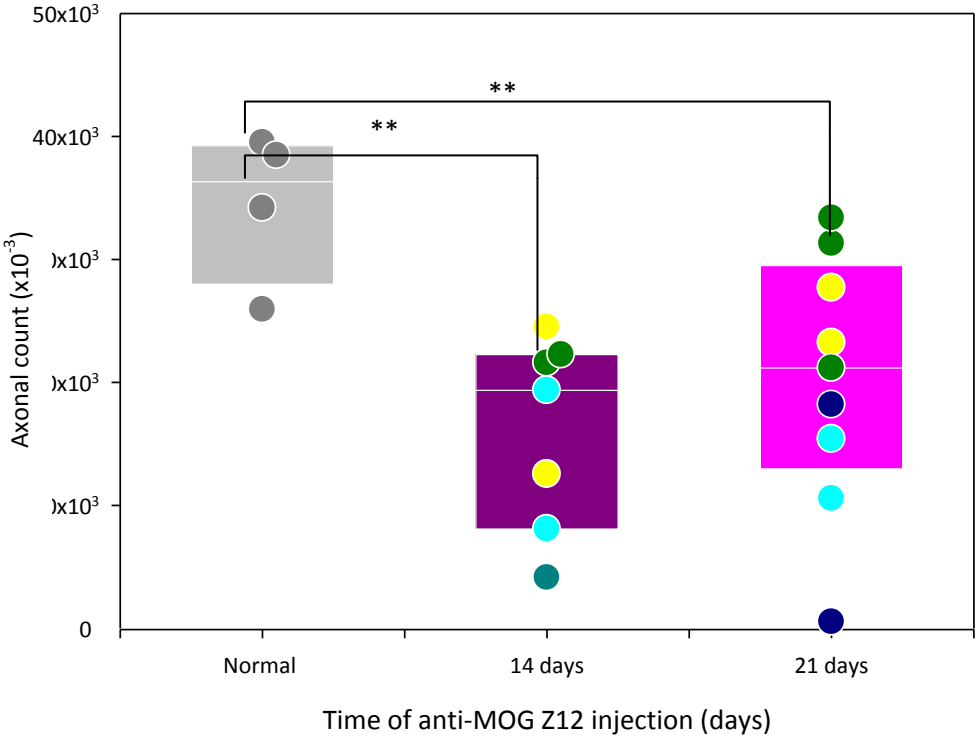

Figure 3.9 ***Axonal counts from optic nerve of normal and MOG^{TCR} mice induced to develop ON following administration with Z12 MOG-specific mAb****. Axonal counts taken in optic nerves from normal animals (n=4) and MOG^{TCR} animals immunised with 150ng PTX (Day 0 and 2) and injected i.p. 1mg MOG-specific Z12 on Day 14 (n=7) or Day 21 (n=9) post-disease induction. Animals were sacrificed at 4 (cyan), 7 (blue), 11(yellow) or 14(green) days post MOG-specific Z12 injection. Animals were perfused and tissue was fixed in Karnovsky's Fixative. Tissue was embedded in resin and semi-thin sections (0.7µm) were cut and stained with toluidine blue. Data was compared with normal animals, which were wildtype C57BL/6 animals of a similar age. Axons were randomly counted from a cross section using stereology software. Grey boxes show 25th and 75th percentile and median line. Circles show results from individual animals. *P<0.01 compared to normal animals.*

3.3.3 Pertussis toxin followed by Z12 MOG-specific mAb at different doses

Different doses of Z12 MOG-specific mAb were administered to establish an immunising protocol that would achieve optimal frequency of ON but limited development of neurological EAE and amount of antibody used. Animals were immunised with PTX on day 0 and 2 followed by i.p. injection of 0.1, 0.5 or 1.0mg of Z12 MOG-specific mAb on day 14 post-disease induction, mice were euthanised on day 28 post-disease induction (Figure 3.10).

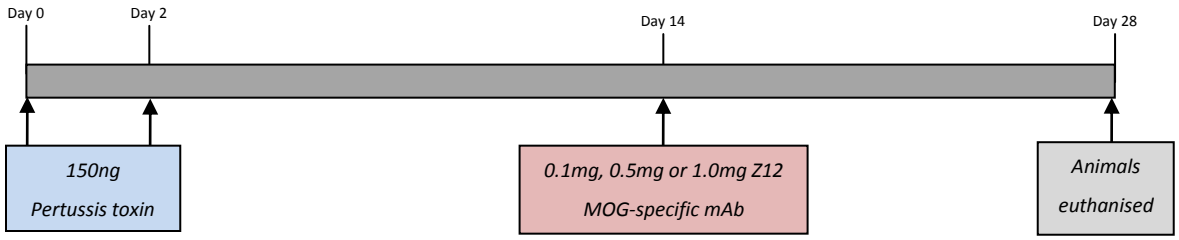

Figure 3.10 ***Timeline of experimental design for investigating different doses of Z12 MOG specific mAb.*** *a) Animals immunised with 150ng Pertussis toxin on day 0 and 2 and 0.1mg, 0.5mg or 1.0mg Z12 MOG-specific mAb on day 14, animals euthanised on day 28.*

The average weight of animals remained constant following different doses of Z12 MOG-specific mAb (Figure 3.11). The percentage of animals developing neurological EAE and the maximal EAE score increased following increasing doses of Z12 MOG-specific mAb (Figure 3.12, Table 3.4).

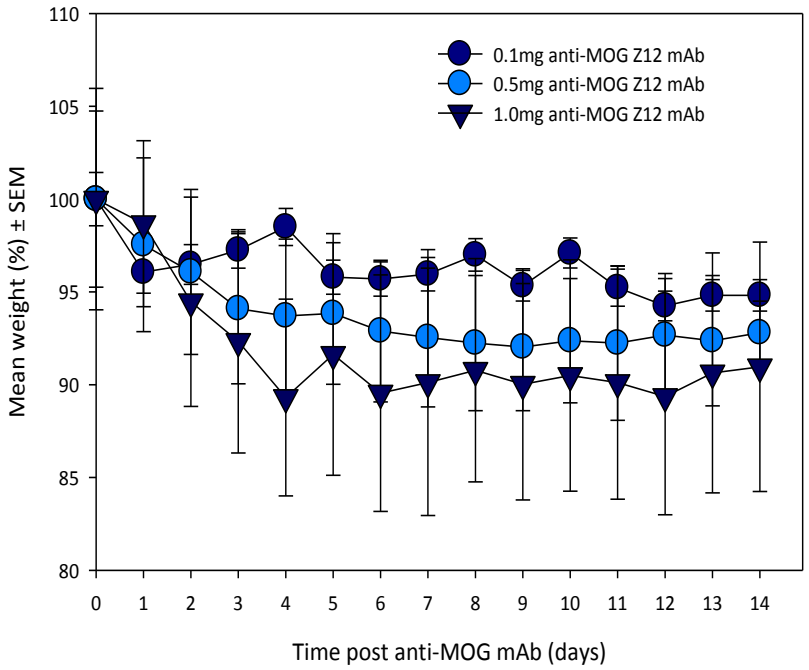

Figure 3.11 ***Mean weight changes in MOG^{TCR} mice induced to develop ON following administration with Z12 MOG-specific mAb at different doses***. *MOG^{TCR} animals were immunised with PTX (Day 0 and 2) and 0.1mg (n=8), 0.5mg (n=8) or 1mg (n=7) MOG-specific Z12 mAb on Day 14. Animals were weighed daily following Z12 MOG-specific mAb injection. The % weight change was calculated from the mean weight on day 0 of Z12 MOG-specific mAb injection.*

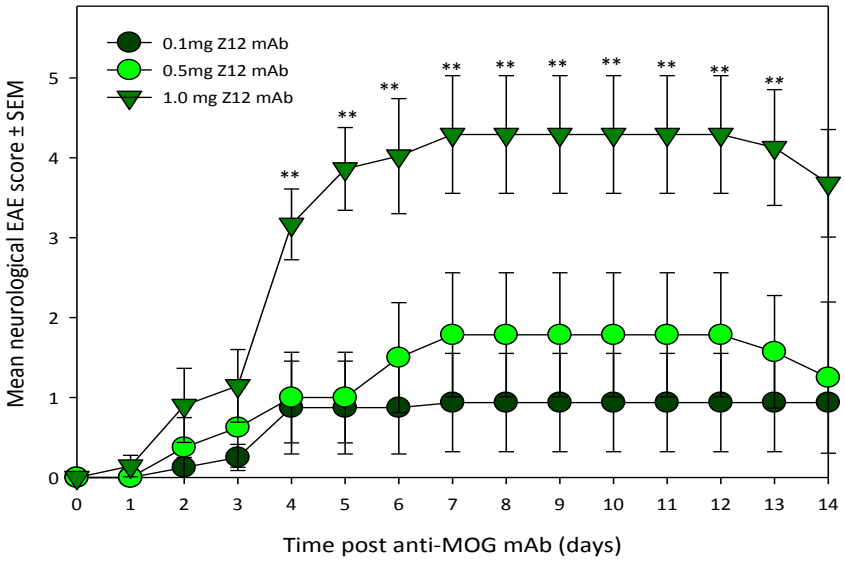

Figure 3.12 ***Neurological EAE develops in MOG^{TCR} mice induced to develop ON following administration with Z12 MOG-specific mAb at different doses.*** *MOG^{TCR} animals were immunised with 200ng PTX (Day 0 and 2). Animals were injected i.p. with 0.1mg (n=8), 0.5mg (n=8) and 1.0mg (n=7) Z12 MOG specific mAb on day 14 post-disease induction. Animals were scored daily following MOG-specific Z12 mAb injection. The results represent the mean daily neurological EAE score ± SEM. ** P<0.01 compared to animals receiving no Z12 mAb.*

The number of surviving RGC following administration of different concentrations of Z12 MOG-specific mAb were significantly reduced compared to untreated control MOG^{TCR} mice (figure 3.13). There appeared to be an increased variability of RGC loss at the lower doses of 0.1mg Z12 MOG-specific mAb. However, the average RGC counts were not significantly different for each concentration of Z12 MOG-specific mAb.

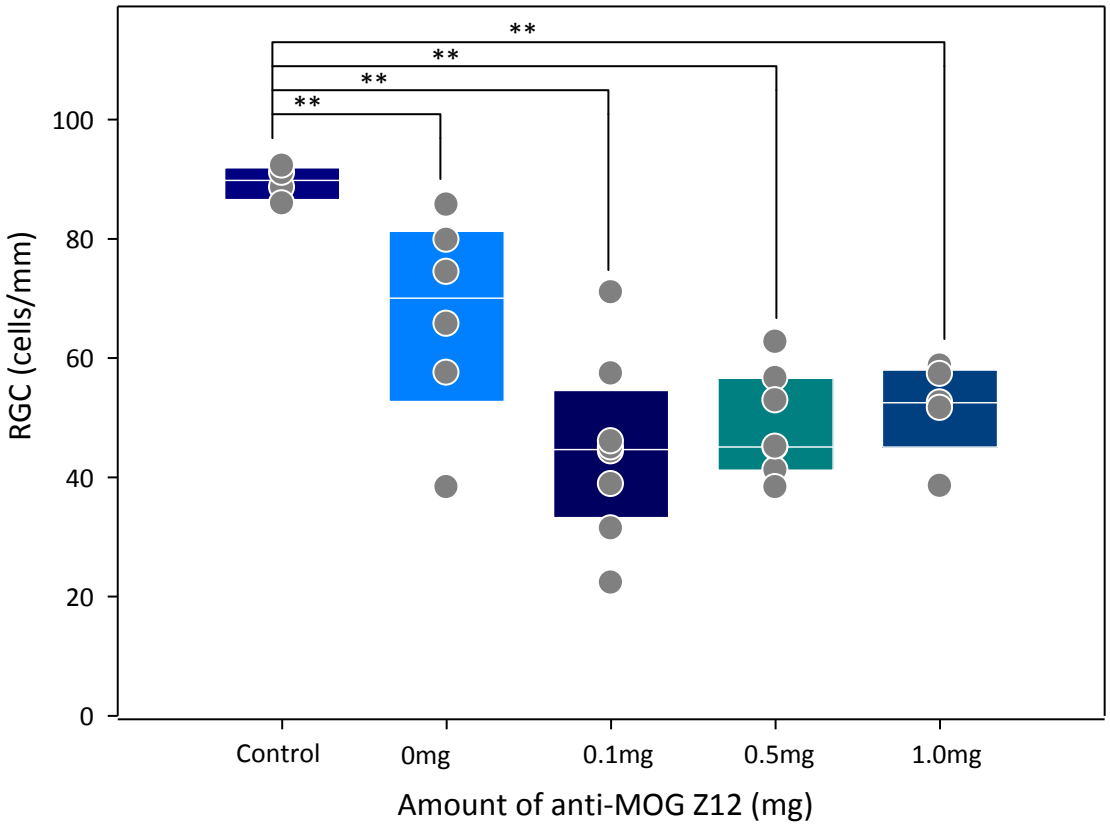

Figure 3.13 ***Administration of Z12 MOG-specific mAb augments RGC loss following induction of ON in MOG^{TCR} mice.*** *Animals were immunised with 150ng PTX (Day 0 and 2) and injected i.p. with 0.1mg (n=8), 0.5mg (n=7) or 1mg (n=5) MOG-specific Z12 mAb on Day 14 post-disease induction. Eyes were removed and embedded in resin and 0.7µm sections were made. The RGC number per unit length of retina was counted under light microscopy. Data was compared with control animals, which were wildtype C57BL/6 littermates. Results represent individual RGC counts (circle) and the boxes represent mean and 25 and 75 percentiles. ** P<0.01 compared to normal animals.*

Treatment	% MOG^{TCR} mice developing neurological EAE	Maximal EAE Score Mean ± SEM	RGC density (RGC/mm) Mean ± SEM
0.0mg Z12 MOG-specific mAb	0	0	67±7
0.1mg Z12 MOG-specific mAb	25	0.9±0.6	45±5
0.5mg Z12 MOG-specific mAb	38	1.3±0.7	50±3
1.0mg Z12 MOG-specific mAb	60	3.2±0.7	52±3

Table 3.42 ***Development of neurological EAE in MOG^{TCR} mice induced to develop ON following administration of different concentrations of MOG-specific mAb.*** *MOG^{TCR} mice were immunised with PTX (Day 0 and 2) followed by 0.1mg (n=8), 0.5mg (n=7) or 1.0mg (n=5) Z12 MOG-specific mAb (Day 14) and were sacrificed on Day 21 post-disease induction. Neurological EAE score was assessed daily and % incidence of neurological EAE was calculated by the number of animals developing any signs of neurological EAE (score 1-5) compared to the total number of animals in the group. The results show the maximal EAE clinical score of all animals within the group and the RGC density.*

Therefore, increasing doses of Z12 MOG-specific mAb had a significant effect on the development of neurological EAE but did not appear to influence the amount of RGC loss. Therefore, a lower dose between 0.1mg and 0.5mg of Z12 MOG-specific mAb could be used to achieve optimal RGC loss whilst minimising the incidence and severity of neurological EAE.

3.3.4 Pertussis toxin, Z12 MOG-specific mAb and anti-CD4 modulation

The previous data suggested that whilst addition of Z12 MOG-specific mAb augmented RGC loss, the disease was so aggressive that axonal loss rather than demyelination was the predominant histological feature. Therefore in an attempt to generate more robust demyelination such that it may be feasible to investigate remyelination strategies rather than purely neuroprotective agents, immunosupression was administered to reduce the level of the inflammatory response. The CD4-specific YTS177 mAb has been shown to cause down regulation of CD4 antigen and rapidly inhibits EAE (O'Neill *et al.*, 1993).

Animals were injected with 150ng PTX on day 0 and 2, followed by 0.25mg MOG-specific Z12 mAb day 14 post-disease induction. Animals were also injected with 100µl i.p. CD4-specific ascites fluid mAb on day 14 or day 16 post-disease induction (Figure 3.14). This contains about 0.5mg of specific mAb and is sufficient to induce the down regulation of CD4 on all T cells within 3 hours of antibody administration (O'Neill *et al.*, 1993). Animals were euthanised at day 21 post-disease induction.

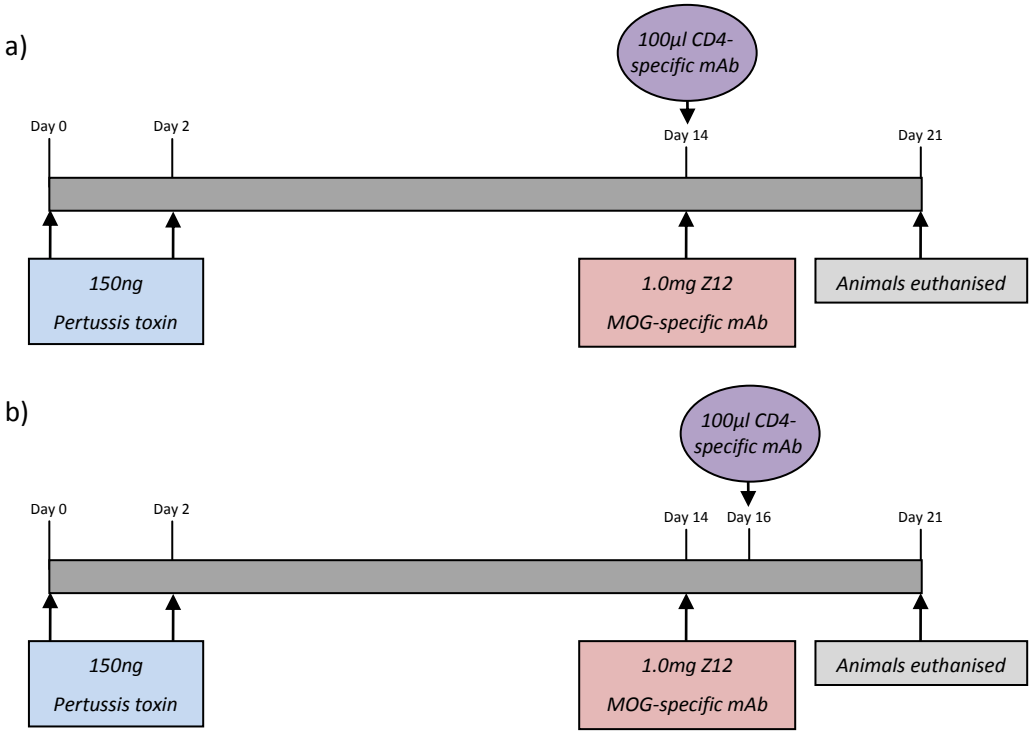

Figure 3.14 ***Timeline of experimental design for investigating immunomodulation with anti-CD4.*** *Animals immunised with 150ng Pertussis toxin on day 0 and 2 and 0.25mg Z12 MOG-specific mAb on day 14 a) animals injected with 100µl CD4-specific ascites on day 14. b) Animals injected 100µl CD4-specific ascites on day 16. Animals were euthanised on day 21.*

The average weight remained relatively constant despite the development of EAE in some animals (Figure 3.15, Table 3.5). The severity of the neurological EAE score was reduced following injection with CD4-specific mAb when compared with animals in previous studies which were not injected with anti-CD4 mAb (Figure 3.16).

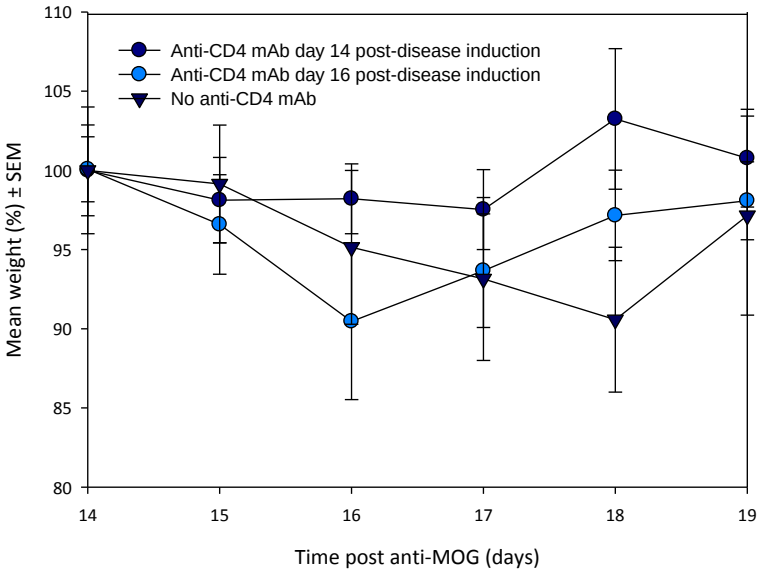

Figure 3.15 ***Mean weight changes in MOG^{TCR} mice administered with Z12 MOG-specific mAb and CD4-specific mAb.*** *Animals were immunised with 150ng PTX (Day 0 and 2) and 0.25mg Z12 MOG-specific mAb at day 14 post-disease induction. MOG-specific TCR animals were given CD4-specific mAb at day 14 post-disease induction (n=5) or day 16 post disease induction (n=4) and compared with animals without CD4-specific mAb (n=4). Animals were weighed daily following injection of Z12 MOG-specific mAb. The % weight change was recorded from the day of Z12 MOG-specific mAb injection.*

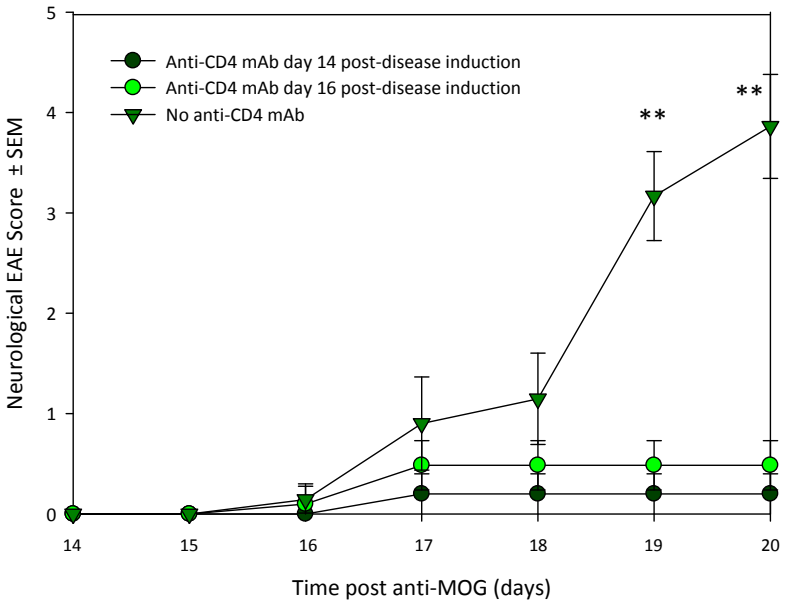

Figure 3.16 ***Neurological EAE development in immunised MOG^{TCR} mice following administration of MOG specific mAb and CD4-specific mAb.*** *Animals were immunised with 150ng PTX (Day 0 and 2) and 0.25mg Z12 MOG-specific mAb at day 14 post disease induction. MOG-specific TCR animals were given CD4-specific mAb at day 14 post-disease induction (n=5) or day 16 post disease induction (n=4) and compared with animals without CD4-specific mAb (n=4). The results represent the mean daily neurological EAE score ± SEM.*

	% MOG^{TCR} mice developing neurological EAE	Maximal EAE Score Mean ± SEM	RGC density (RGC/mm) Mean ± SEM
No CD4-specific mAb	60	3.2±0.7	52±3
CD4-specific mAb day 1	20	0.4±0.1	46±6
CD4-specific mAb day 3	60	0.2±0.2	45±9

Table 3.5 ***Development of neurological EAE and RGC loss induced by injection of MOG-specific mAb in MOG^{TCR}.*** *Animals were immunised with 150ng PTX (Day 0 and 2) and 0.25mg anti-MOG Z12 (Day 14). CD4-specific mAb was injected i.p. on either day 14 post-disease induction (n=5) or day 16 post-disease induction (n=5). Animals were sacrificed on Day 21 post-disease induction. Neurological EAE score was assessed daily and % neurological EAE was calculated by the number of animals developing any signs of neurological EAE*

There was no statistically significant difference in RGC loss in immunised MOG^{TCR} mice injected with CD4-specific mAb on day 14 and day 16, and without injection of CD4-specific mAb (Figure 3.17). These results suggest that the CD4-specific mAb injected at the time of Z12 MOG-specific mAb injection has no effect on the disease process in the optic nerve and retina in contrast to that occurring in the spinal cord, which is associated with the development of neurological EAE.

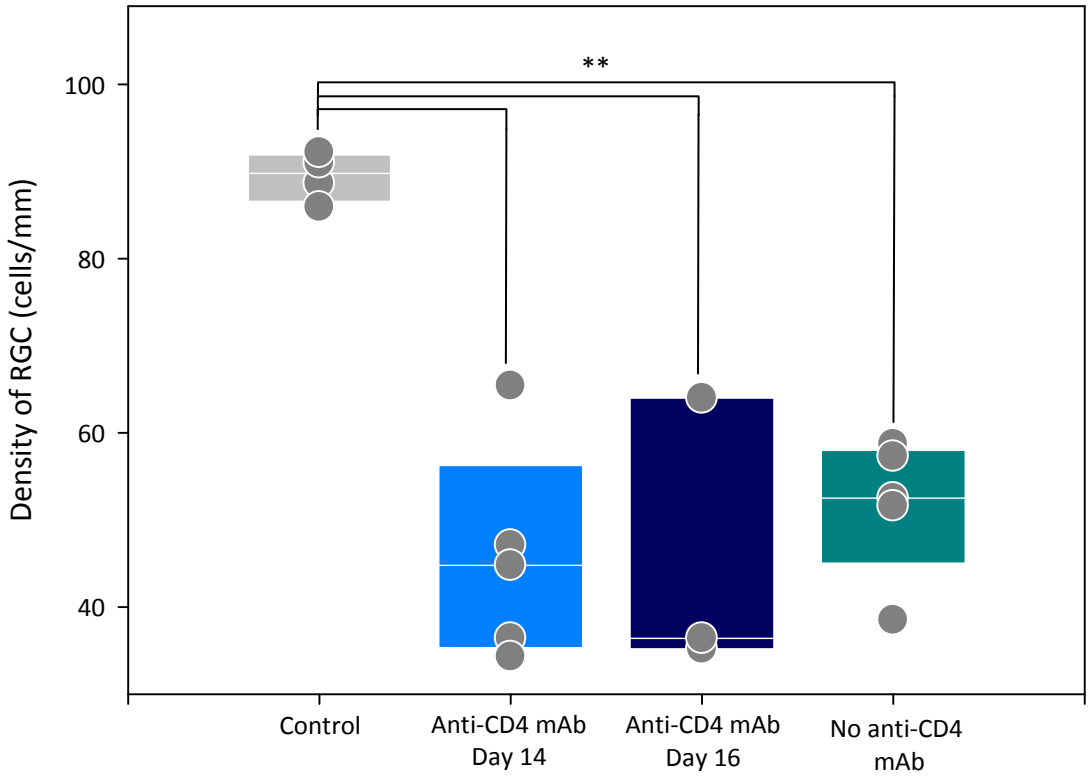

Figure 3.17 ***CD4-specific mAb does not inhibit RGC loss induced by injection of MOG-specific mAb in MOG^{TCR} immunised to develop optic neuritis.*** *Animals were immunised with 150ng of PTX (Day 0 and 2) and 0.25mg anti-MOG Z12 (Day 14). CD4-specific mAb was injected i.p. on either day 14 post-disease induction (n=5) or day 16 post-disease induction (n=5). Control animals were wildtype C57BL/6 animals of a similar age. The eyes were removed and fixed in Karnovsky's fixative and embedded in resin. Sections of 0.7µm were cut and stained with toluidine blue at the level of the optic nerve head. The number of RGC was counted and expressed as number of cells per mm of retina. The results show individual values (circles) and boxes show mean and 25% and 75% percentiles. **P<0.01 compared to control animals.*

Toluidine blue stained optic nerves were studied to look for evidence of demyelination in the optic nerve (Figure 3.18). The pathology of the optic nerves from mice treated with CD4-specific mAb showed no evidence of demyelination and ranged from moderate to severe axonal loss. Optic nerves from mice without CD4-specific mAb treatment showed extensive axonal loss without demyelination.

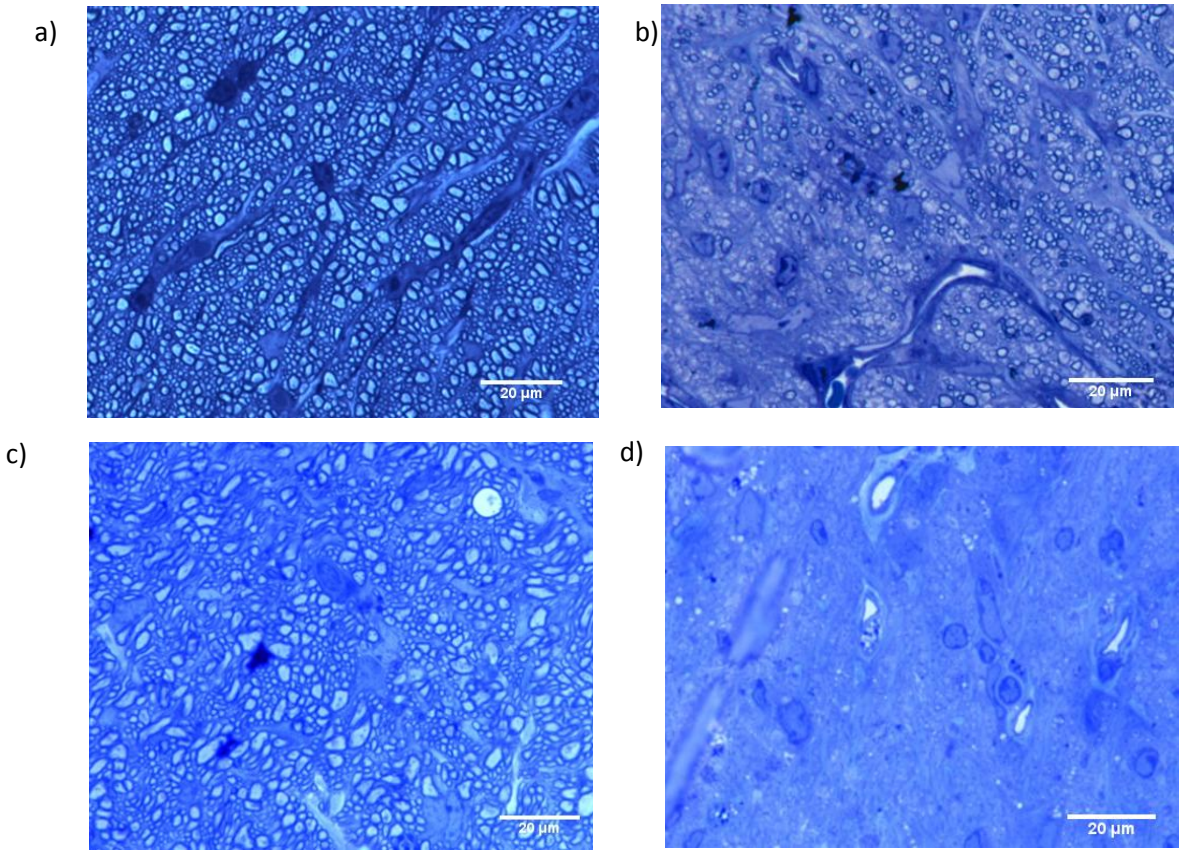

Figure 3.18 ***CD4-specific mAb prevents axonal loss in the optic nerve induced by treatment with MOG-specific mAb in MOG^{TCR} mice induced to develop ON****. Animals were immunised with 150ng PTX (Day 0 and 2) and injected i.p. 0.25mg MOG-specific Z12 at day 14 post-disease induction. One group of animals were injected i.p. with CD4-specific mAb day 16 post-disease induction and compared with animals without CD4-specific mAb. a) Optic nerve taken from normal C57BL/6 wildtype animal. b) Optic nerve taken from MOG^{TCR} specific animal immunised with PTX and MOG-specific mAb without CD4-specific treatment. c) Optic nerve taken from MOG^{TCR} animal immunised with PTX and MOG-specific mAb with CD4-specific treatment shows moderate axonal loss. d) Optic nerve taken from MOG^{TCR} animal immunised with PTX and MOG-specific mAb with CD4-specific treatment shows severe axonal loss and no myelinated axons.*

Treatment with CD4-specific mAb had a significant ameliorating effect on neurological EAE score. However, this immunosuppression had no effect on RGC counts, which were similar in animals injected with CD4-specific mAb and without CD4-specific mAb. Optic nerves were also comparable to early studies without CD4-specific mAb, showing little evidence of demyelination and widespread axonal loss.

To allow CD4-specific mAb to have a greater effect on reducing the extent of axonal loss, the CD4-specific mAb was administered at an earlier stage of the disease process (Figure 3.19). Animals were injected with 150ng PTX on day 0 and 2, followed by 0.25mg MOG-specific Z12 mAb on day 6, day 8 or day 10. Animals were also injected with 100µl i.p. CD4-specific ascites fluid on day 6, day 8 or day 10. Animals were euthanized 7 days after MOG-specific Z12 mAb injection.

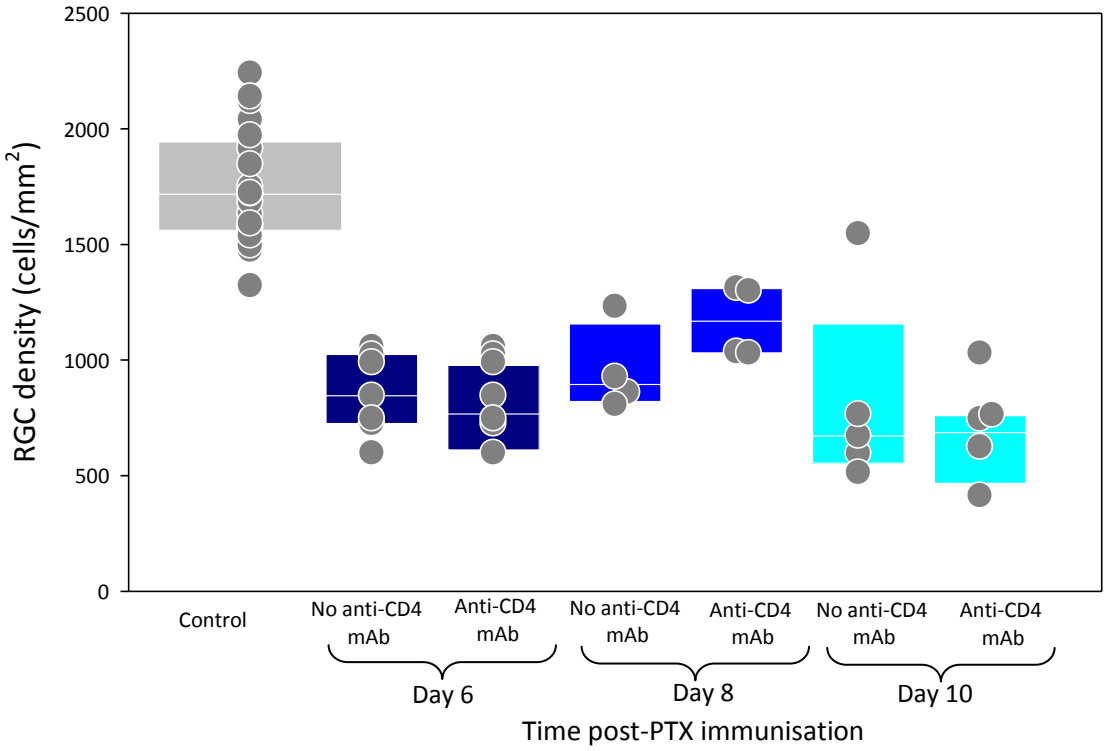

Figure 3.19 ***CD4-specific mAb injection at an early stage in disease does not inhibit RGC loss induced by injection of MOG-specific mAb in MOG^{TCR} immunised to develop optic neuritis****. Animals were immunised with 150ng of PTX (Day 0 and 2). Animals were injected with 0.25mg anti-MOG Z12 on day 6 post-disease induction (n=7), day 8 post-disease induction (n=4) or day 10 post-disease induction (n=5). Another sample of animals were injected with with 0.25mg anti-MOG Z12 and CD4-specific mAb on day 6 post-disease induction (n=7), day 8 post-disease induction (n=4) or day 10 post-disease induction (n=5). Control animals were wildtype C57BL/6 animals of a similar age. The eyes were removed and fixed in Karnovsky's fixative and embedded in resin. Sections of 0.7µm were cut and stained with toluidine blue at the level of the optic nerve head. The number of RGC was counted and expressed as number of cells per mm^2 of retina. The results show individual values (circles) and boxes show mean and 25% and 75% percentiles.*

The difference in RGC loss between animals with and without injection of anti-CD4 mAb at day 6, day 8 and day 10 was insignificant. This result suggests that administration of anti-CD4 mAb was not sufficient early enough to produce immunosupression and was therefore incapable of protecting the loss of RGC. It appears from these results that the timing of administering anti-CD4 mAb needs to be earlier in disease to produce an effect that would promote demyelination and prevent the rapid axonal loss and the accompanied RGC loss. Therefore, further studies are needed to establish an optimal time for CD4-specific mAb administration to prevent severe damage to optic nerve and RGC loss.

3.3.5 Immunisation of the double transgenic MOG^{TCR}x*Thy1*CFP model

Once the two transgenic strains had been successfully crossed to produce the double transgenic MOG^{TCR}x*Thy1*CFP, the immunising protocol which was developed in previous studies was investigated. Mice were immunised with 150ng PTX on day 0 and 2 followed by 0.25mg Z12 MOG-specific mAb on day 14 post-disease induction. Animals were euthanised on day 21 post-disease induction and perfused with 4% PFA. Retinae were dissected and flatmounted. The weight of the animals following immunisation with PTX slightly increased as animals aged, the weight then decreased following MOG-specific mAb injection once clinical signs of EAE occurred (Figure 3.20). In this particular experiment, all animals developed neurological EAE (n=7). The neurological EAE score increased after Z12 MOG-specific mAb immunsiation on day 14 post-disease induction (figure 3.21).

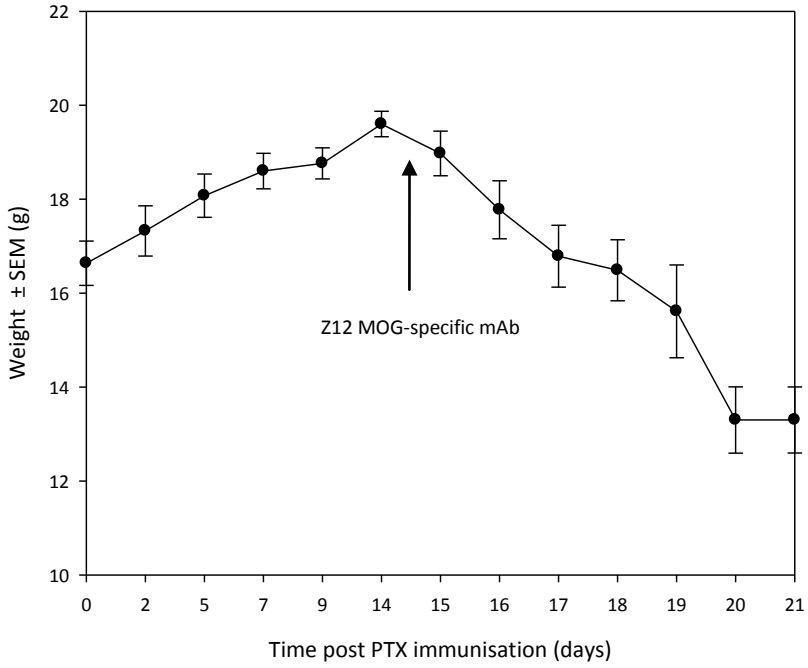

Figure 3.20 ***Changes in weight following immunisation of MOG^{TCR}xThy1CFP mice induced with MOG-specific mAb to develop ON****. Animals were immunised with 150ng PTX (Day 0 and 2) and injected i.p. with 0.25mg MOG-specific Z12 mAb at day 14 post-disease induction (n=7). Animals were weighed daily following PTX immunisation.*

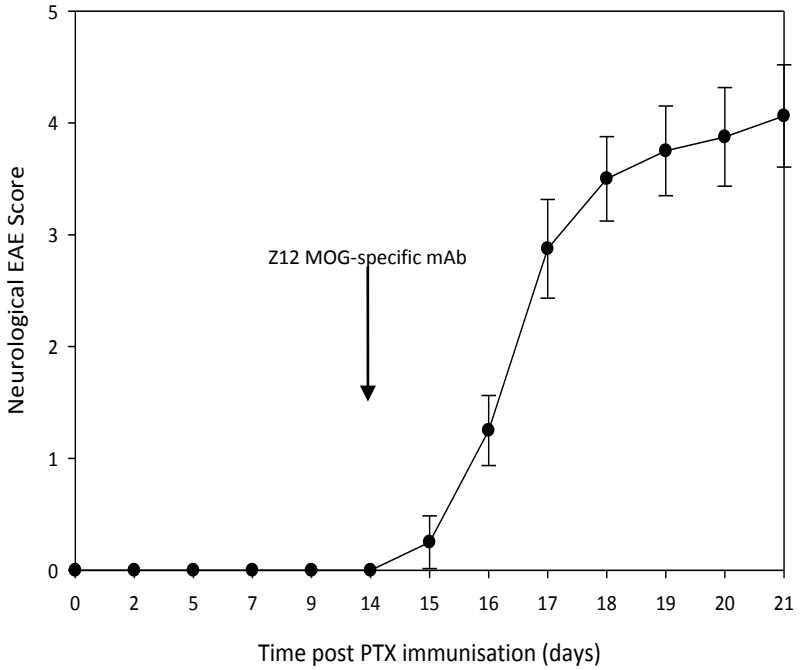

Figure 3.21 ***Neurological EAE score following immunisation of MOG^{TCR}xThy1CFP mice induced with MOG-specific mAb to develop ON****. Animals were immunised with 150ng PTX (Day 0 and 2) and injected i.p. with 0.25mg MOG-specific Z12 mAb at day 14 post-disease induction (n=7). Neurological EAE score was assessed daily (score 1-5) following PTX immunisation.*

RGC were counted from the retinal flatmounts and RGC densities were calculated. The RGC loss following 0.25mg Z12 MOG-specific mAb immunisation was approximately 34% and was significantly different compared to untreated animals (Figure 3.22). The average RGC count in mice immunised with 0.25mg MOG-specific mAB was 955±45 cells/mm^2 compared to 1456±59 cells/mm^2 in the control animals, which did not show any overlap in RGC numbers.

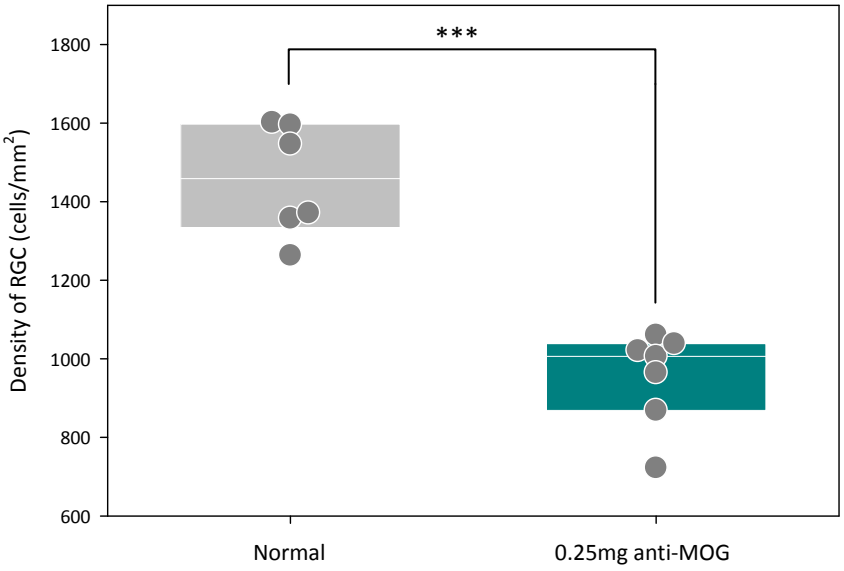

Figure 3.22 ***RGC loss following immunisation of MOG^{TCR}xThy1CFP mice induced with MOG-specific mAb to develop ON****. Animals were immunised with 150ng PTX on day 0 and 2 and injected i.p. with 0.25mg MOG-specific mAb at day 14 post-disease induction (n=7). Data were compared with normal Thy1CFP animals, which were littermates of the MOG^{TCR}xThy1CFP mice (n=6). Animals were sacrificed one week after MOG-specific mAb injection and retina dissected and placed in 4% PFA overnight. Retina were flatmounted and RGC counted using fluorescence microscope.*

3.4 Discussion

This chapter details the steps taken to refine the immunising protocol for MOG-specific TCR transgenic mouse which results in optimum disease activity so the model can be ultimately used for studies of neuroprotective compounds.

Initial studies investigated the efficiency of producing disease in the MOG^{TCR} model by immunising with MOG in CFA or PTX. Using MOG in CFA did not result in a significant reduction in RGC loss or axonal loss in the optic nerve and was therefore not pursued as an immunising protocol for the MOG^{TCR} model. Using CFA would have also been disadvantageous as CFA can cause granulomas in the host animal and can sometimes ulcerate. Injection with PTX produced a more severe disease progression with a greater degree of RGC loss. It appears that PTX stimulates the immune response and the development of ON but is not sufficient to induce EAE, this suggests that PTX activates T cells, which interact with MOG leading to autoimmunity exclusively to the optic nerve. The promising results achieved from immunising MOG^{TCR} mice with PTX supports the use of PTX as an immune adjuvant in future experiments. To increase the severity of disease in the MOG^{TCR} model, injection of Z12 MOG-specific mAb following PTX immunisation led to greater axonal and RGC loss and exacerbated neurological deficits as shown by the increase in incidence and severity of EAE and ON. Normally, a solo injection of Z12 MOG-specific mAb would be excluded from the CNS and would therefore have no effect. However, PTX immunisation generates an inflammatory response in the CNS that is sufficient to compromise the BBB and therefore allow Z12 MOG-specific mAb to access the CNS. This appears to exacerbate the inflammatory response and leads to further degeneration of nerves, rather than produce demyelinated axons. The lack of pathological evidence showing demyelination and the large degree of axonal loss found in this model is consistent with the limited demyelination observed in 'classical' EAE models in C57BL/6 mice where neurodegeneration predominates (Jones *et al.*, 2008). Z12 MOG-specific mAb modulates CNS inflammation via the complement system, a biochemical cascade, which activates proteases that cleave proteins to release cytokines, which amplify the cascade leading to further cleavage. The end result is a massive amplification and activation of the membrane attack complex (MAC) which binds to the plasma membrane on myelin/oligodendrocyte surface and leads to lysis of the oligodendrocyte cell membrane and disruption of myelin (Mead *et al.*, 2002). This role has been demonstrated using cobra venom factor which inhibits the complement cascade and reduces the ability of anti-MOG Z12 to enhance inflammation and mediate demyelination (Morris-Downes

et al., 2002). Therefore disease in MOG^{TCR} mice can be initiated by immunisation with PTX and CNS inflammation increased by injection of Z12 MOG-specific mAb at a later time point.

The MOG^{TCR} model is therefore currently a valuable model to study axonal loss; however, it would be advanageous to adapt the model so this model can be used to study demyelination and remyelination. To accomplish this, the disease severity needs to be attenuated to avoid widespread axonal loss in favour of areas of demyelination. The approach taken was to administer a CD4-specific mAb antibody to modulate the immune response following immunisation with PTX and Z12 MOG-specific mAb. In the MOG^{TCR} model the mice were given CD4-specific mAb on the same day as Z12 MOG-specific mAb treatment (i.e. before any signs of neurological EAE but during sub-clinical disease period). This resulted in a reduced severity and incidence of animals developing neurological EAE. However, CD4-specific mAb had no effect on disease severity in the optic nerve and retina and animals showed significant RGC and axonal loss again with limited demyelination. These results suggest CD4-specific mAb was administered too late to have an effect on CD4 T cells in the optic nerve but in sufficient time to prevent spinal cord damage and development of neurological EAE. Further investigation into the effect of administering anti-CD4 mAb at earlier time points was also inadequate to promote immunosupression. To resolve this issue, future experiments should take advantage of the confocal scanning laser ophthalmoscope to longitudinally measure RGC loss, therefore reducing the need for many animals to be taken at different time points. This would then enable the optimal timing for administering CD4-specific mAb antibody to modulate the immune response and promote demyelination in favour of axonal loss to be determined.

Once an immunising protocol had been developed (PTX on day 0 and 2, Z12 MOG-specific mAb day 14), the protocol was used to immunise MOG^{TCR}x*Thy1*CFP double transgenic mice, which express the MOG-specific TCR and fluorescent RGC. The MOG^{TCR}x*Thy1*CFP allowed easy visualisation of the RGC and a rapid method to evaluate RGC loss at the end of an experiment, which was significantly lower in mice immunised to develop ON. Therefore the MOG^{TCR}x*Thy1*CFP is an ideal model to study neuroprotective capabilities of drugs by analysing the effect of the drug on the survival of RGC in the retina, as quantified by retinal flatmounts. Ideally the model could be used to also study remyelinative strategies, however further research needs to be undertaken to identify if demyelination occurs and the possibility of a time window of demyelination.

Chapter 4

Development of methods to measure visual dysfunction

4.1 Introduction

To test the hypothesis that axonal loss correlates with neurological deficit, methods need to be developed that measure visual dysfunction that can be compared with underlying pathology. Recording VEP and the behavioural assessment of visual-tracking with a rotating drum are two methods, which can be used to measure the integrity of the visual system (Porciatti *et al.*, 1999; Thaung *et al.*, 2002a).

4.1.1 Electrophysiology

The visual system can be functionally assessed by measuring flash-evoked VEPs. The VEP measures changes in electrical potential over the visual cortex in response to a visual stimulus to assess post-retinal function. The VEP is only produced when the optic nerve is intact and can therefore be used to assess visual pathway diseases, such as optic neuritis (Trip *et al.*, 2005). The use of VEP to measure RGC loss during ON was described in Section 1.3.5.

The use of the VEP in animals has been demonstrated in a range of species to study the electrophysiology of the optic nerve (Maertz *et al.*, 2006; Mozafari *et al.*, 2010; Soto *et al.*, 2004). The currents that generate the VEP have been studied in primates and cats, which was found to result from activity of neurons in the geniculo-cortical pathway and the visual cortex (Kraut *et al.*, 1985; Rose & Lindsley, 1968). Although the VEP is often used in mice to detect pathological changes, the precise origin and cellular organisation of the neuronal response of the VEP in the mouse has not been studied comprehensively. Sufficient evidence is available to show that the flash VEP can be used to assess the signal processing through the visual pathway from the retina to the visual cortex (Ridder & Nusinowitz, 2006). Measuring VEP can be used as an objective method to detect pathological changes in the optic nerve. Demyelination in the optic nerve has reported to increase the response latency, as demonstrated in PLP knockout mice (Chow *et al.*,

2005). The VEP has been used to demonstrate transgenic mice with enhanced myelination in the optic nerve display faster VEP responses (Yu *et al.*, 2011). Limited studies have been performed on EAE models, however, one study reported a correlation between measured VEP response and RGC counts (Hobom *et al.*, 2004).

4.1.2 Visual Acuity

The visual acuity of mice can be assessed using an optokinetic (OKN) drum, which is a rapid, reliable and reproducible method of measuring visual acuity. The OKN drum measures the OKN nystagmus, an involuntary mechanism that is part of the vestibulo-ocular reflex that is elicited by a moving field, which results in the head tracking of movement when the body is stationary (Buttner & Kremmyda, 2007). The OKN is sensitive to defects in the visual pathway and can be used to detect pathological changes. The OKN drum was one of the first approaches used to measure optokinetic response in rats (Cowey & Franzini, 1979) and has been adapted for use in many species including mice (Thaung *et al.*, 2002a). The visual-tracking drum consists of a motorised rotating vertical grate surrounding the mouse, which is on a stationary platform. The head tracking response of the animal can be measured to assess visual acuity and quantitatively analysed by varying parameters such as grating width, contrast and illumination (Cahill & Nathans, 2008).

In mice with severe loss of visual function, the OKN drum protocol does not evoke any behavioural response and partly for this reason is thought to be a good marker of visual function. Furthermore, the technique is not influenced by other sensory information (auditory or tactile) (Thaung *et al.*, 2002b). This method has been used accurately to assess visual function in mice (Thaung *et al.*, 2002a), rats (Coffey *et al.*, 2002; Schmucker *et al.*, 2005) and fish (Haug *et al.*, 2010). The visual acuity drum has been tested in a variety of mouse strains, the C57BL/6 strain successfully demonstrated head tracking movements reflective of visual acuity (Puk *et al.*, 2008). The OKN drum can also be modified to allow monocular visual assessment (Thomas *et al.*, 2004). Therefore the OKN drum is an ideal, non-invasive, method to assess visual acuity in mice.

4.1.3 Aims and objectives

The aim of this chapter was to develop objective methods that could be used to measure visual dysfunction in immunised MOG^{TCR}x*Thy1*CFP mouse model. To achieve this aim, recording of the VEP following a flash stimulus and head tracking movements in the OKN drum were assessed for their potential to detect changes occurring in the optic nerve. Both methods are minimally invasive and allow longitudinal measurement of the disease process.

4.2 Materials and Methods

4.2.1 Animals

MOG^{TCR}x*Thy1*CFP transgenic mice as described earlier were used for all experiments. All experiments were performed according to UK, Animals (Scientific Procedures) Act 1986.

4.2.2 Anaesthesia

Animals were anaesthetised with an intraperitoneal injection of 75mg/kg Ketamine and 1mg/kg Medetomidine in normal saline, a dose of 100µl (35µl Ketamine + 50µl Medetomidine + 15µl saline) was administered to each animal. To reverse the anaesthetic, animals were injected with a 100µl dose of 1mg/kg Atipamezole in normal saline (10µl Aptemazole + 90µl saline) and were left to recover under a heated lamp and supplied with soaked diet.

4.2.3 Electrophysiological setup

The pupils were dilated with Mydriacyl® 1% (active ingredient tropicamide. Alcon, Hemel Hempstead, Hertfordshire, UK) and drops of Viscotears® (active ingredient carbomer, polyacylic acid. Novartis, Basel, Switzerland) were used to prevent the eyes from drying out and clouding during the recording. The animals were secured in a stereotaxic frame and body temperature was maintained at 35˚C with a small heating plate with built in Resistance Temperature Detector (RTD) sensor (World Precision Instruments, Stevenage, Hertfordshire, UK) connected to a DC direct temperature controller (ATC1000. World Precision Instruments, Stevenage, Hertfordshire, UK). The active electrode was a needle electrode placed subcutaneously over the visual cortex and the reference electrode was a needle electrode placed subcutaneously in the snout. The signal was amplified 10,000x (NL104A AC Amplifier. Digitimer Ltd, Hertfordshire, UK). A flash stimulus of 10ms duration every 300ms from a stand-alone monocular ganzfield photic stimulator (MGS-2, LKC Technologies Inc, Gaithersburg, MD, USA) was presented approximately 20cm from the eyes. Signals were band pass filtered at 5Hz and 1kHz and sampled at 1000 Hz. Flash recordings were available at +5dB (decibel), 0dB, -5dB, -10dB, -20dB and -25dB. Recordings were made with sweep-based data capture software (Signal v3.11, Cambridge Electronic Design, Cambridge, UK). For each recording, 5-200 stimuli were captured and consecutive sweeps averaged to produce a VEP response.

4.2.4 Visual Acuity

Visual acuity was measured using a custom-built visual tracking drum (supplied by Prof. P Coffey, Institute of Ophthalmology, UCL, London) that was setup as in Figure 4.1. Two lamps were used to illuminate the drum to allow the mouse to be videoed from an aerial position using a tripod for support. An individual mouse was placed on a stationary platform located in the centre of the visual tracking drum, which was rotated on a vertical axis. The drum was motored by an electric DC motor and the direction of rotation could be changed with a mechanical flick switch connected to the power supply.

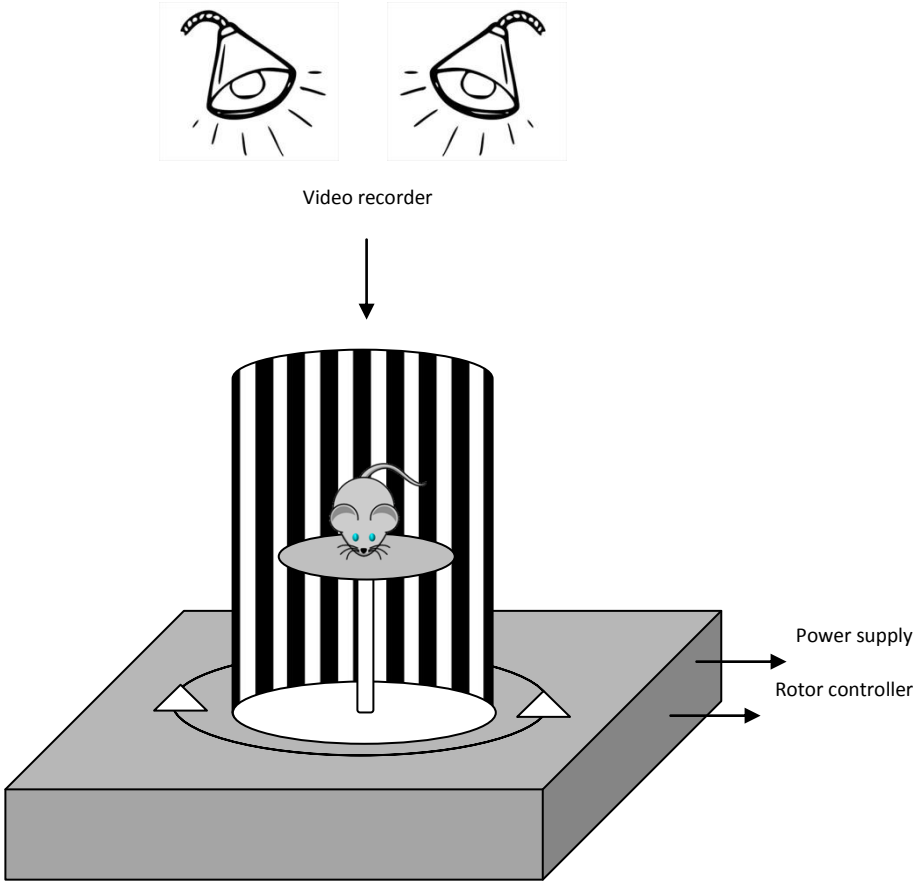

Figure 4.1 ***Schematic diagram of visual tracking drum****. Setup of visual tracking drum used to monitor visual acuity in mice. Mice are placed in centre of the drum, which rotates in clockwise and anti-clockwise directions. The head movements are recorded as a measure of visual acuity.*

A pattern of clockwise and anti-clock wise rotations with intermediary breaks were performed based upon previous experimental design (personal communication with Dr. P. Lundh von Leithner, Institute of Ophthalmology, UCL, London) (Table 4.1). The initial 30 second pause is required to allow the mouse to familiarise with the environment. Additional pauses and alternation of the direction of rotation were used to prevent habituation of the mouse in its environment. The platform was washed in between each mouse to minimise any odour related behaviour, which would distract the mouse from the rotating drum. The experiments were filmed using a video recorder to enable post-hoc measurements of head tracking movements of the mouse.

Time	Action
30 seconds	Pause
60 seconds	Clockwise rotation
30 seconds	Pause
60 seconds	Clockwise rotation
30 seconds	Pause
60 seconds	Anti-clockwise rotation
30 seconds	Pause
60 seconds	Anti-clockwise rotation
30 seconds	Pause
Total time = 6 minutes 30 seconds	

Table 4.1 ***Pattern of rotations of optokinetic drum used to measure visual acuity in mice****. Rotations subjected to each mouse tested using the visual acuity drum to incorporate both clockwise and anti-clockwise rotations and pauses.*

Successful head tracking movement was characterised as a horizontal head movement in the direction of rotation and the same speed as the visual tracking drum. Analysis of head tracking movements was performed by replaying video using Windows Media Player. Animal videos were coded and the observer was blinded to treatment to allow unbiased reporting. The number of head movements in both directions was noted and the net movement in positive tracking directions was calculated (Positive head movements – Negative head movements = Net positive head movements).

4.2.5 Statistical analysis

Statistical analysis was performed using SigmaStat 3.1. Results were presented as mean values ± SEM. Differences between amplitude and latency were analysed by one-way repeated measures ANOVA with Dunnett's post test. Differences between the two groups (binocular and monocular vision, day 0 and day 21) were analysed using a paired t test. For the visual acuity testing, the differences between the two groups (control and ON) at different time points were analysed using a two-way ANOVA. Each time point was further analysed using a Student's t-test. Results was considered significantly different if the probability level $P<0.05$ (*), $P<0.01$(**) or $P<0.001$(***) was reached between groups.

4.3 Results

4.3.1 Electrophysiology

4.3.1.1 Characterising the normal VEP response

To examine the changes in electrophysiological function of the optic nerve in MOG-specific TCR immunised mice, VEP recordings in response to a flash stimulus were recorded. Initially, VEP responses of wildtype C57BL/6 mice to a flash stimulus were obtained. The typical VEP pattern observed using recordings from the scalp showed an initial major negative peak followed by a major positive peak (Figure 4.2). From this VEP pattern, several key data points could be extracted and used to measure changes in the visual system. Factors which can be measured include peak to peak amplitude (from negative trough to positive peak), time delay of first negative peak and the latency.

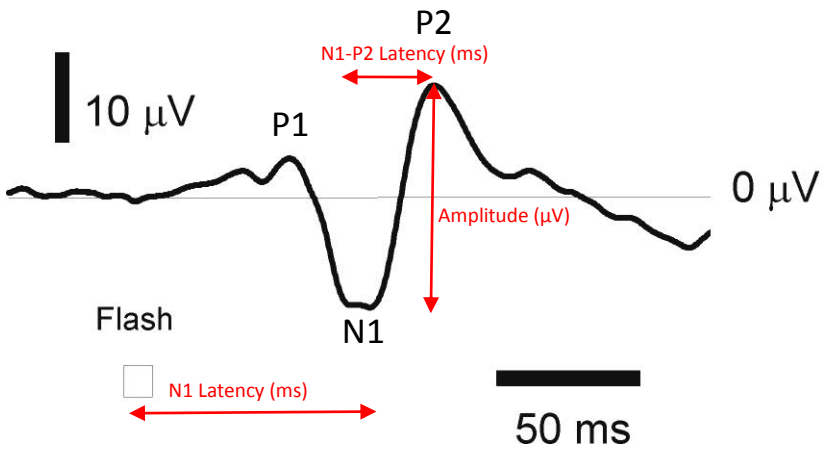

Figure 4.2 ***Typical flash VEP pattern****. Animal were anaesthetised and the VEP was recorded at a flash stimulus of +5dB for 10ms duration averaged over 200 consecutive sweeps. P1 (first positive peak), N1 (first negative peak), P2 (second positive peak). Red text shows measurements taken for N1 latency, N1-P2 latency and amplitude.*

4.2.1.2 VEP response to different light intensities

The electrophysiological setup allowed flash intensities to be set over a wide range, from a maximum of +5dB to a minimum of -25dB (Table 4.2). The VEP response pattern from each flash intensity varied in amplitude, timing of first negative peak and latency with decreasing flash intensity (Figure 4.3).

Flash Intensities (dB)	Flash Intensities (cd/m^2)
5	7.743
0	2.448
-5	0.7691
-10	0.2436
-15	0.07685
-20	0.02443
-25	0.007674

Table 4.2 ***Range of flash intensities produced from ganzfield photic stimulator****. Flash intensities expressed in dB and cd/m2 of flash stimulus used to produce VEP.*

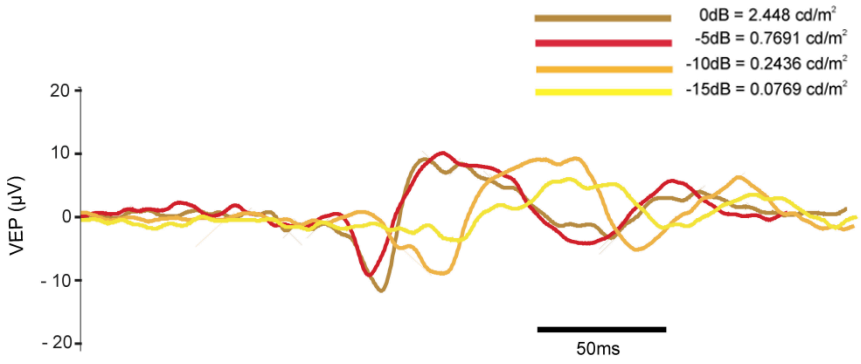

Figure 4.3 ***VEP at different flash intensities****. Averaged VEP recording from a normal mouse using flash stimulus of 0dB, -5dB, -10dB and -15dB.*

The VEP response was recorded at different flash intensities in a stepwise fashion and changes in amplitude and N1 latency were recorded (Figure 4.4, Figure 4.5). An overall significant increase in amplitude ($P<0.001$) and decrease in N1 latency ($P<0.001$) was observed with decreasing flash intensities. Initially the mean amplitude increased with decreasing flash intensity (observed between +5dB and -5dB), which would suggest the flash stimulus was saturated and too large to produce a constant maximal VEP response (Figure 4.4). The mean amplitude reached a maximum of 32.6µV at a flash intensity of -5dB, which appeared to be the most appropriate flash intensity to produce an optimal response. The mean amplitude subsequently decreased at -15, -20 and -25dB and was significantly reduced compared to the mean amplitude at the maximum response. At the minimum producible flash intensity it was still possible to elicit a VEP response. The mean N1 latency showed a trend towards increasing with decreasing flash intensity, which reflects the delay in the visual system processing weaker flash intensities (Figure 4.5). Therefore decreasing the flash intensity decreases the mean amplitude and increases the N1 latency. These results show a decreased response to a decreased flash intensity and represent a functional response to light.

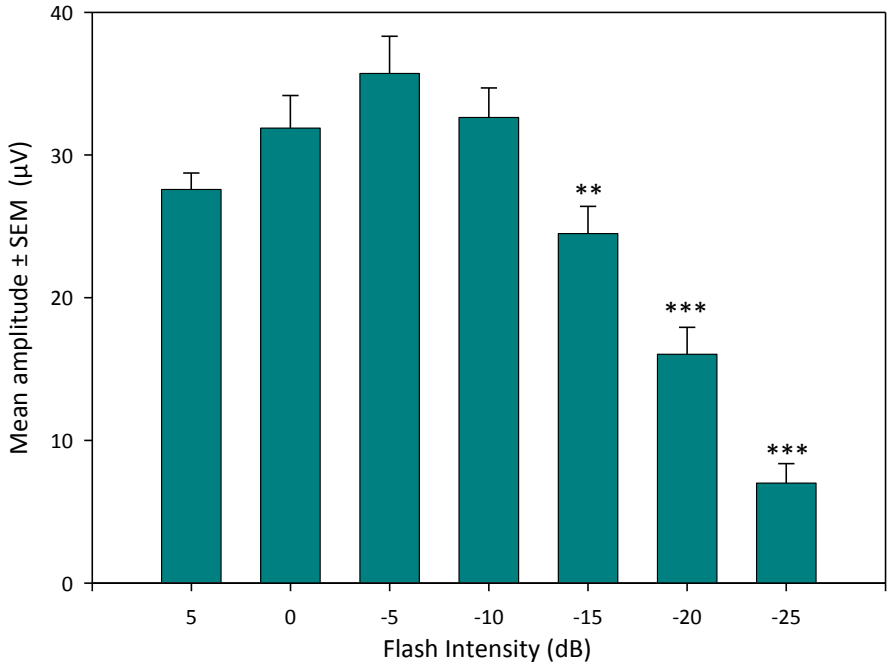

Figure 4.4 ***Decrease in mean amplitude of VEP with decreased flash intensity****. Animals were anaesthetised and the VEP was recorded (n=8) at +5dB, 0dB, -5dB, -10dB, -15dB, -20dB and -25dB flash intensity. Animals were dark adapted for 30 minutes. Results represent the mean ± SEM of amplitude.**P<0.01 and ***P<0.001 compared to VEP response at +5dB light intensity.*

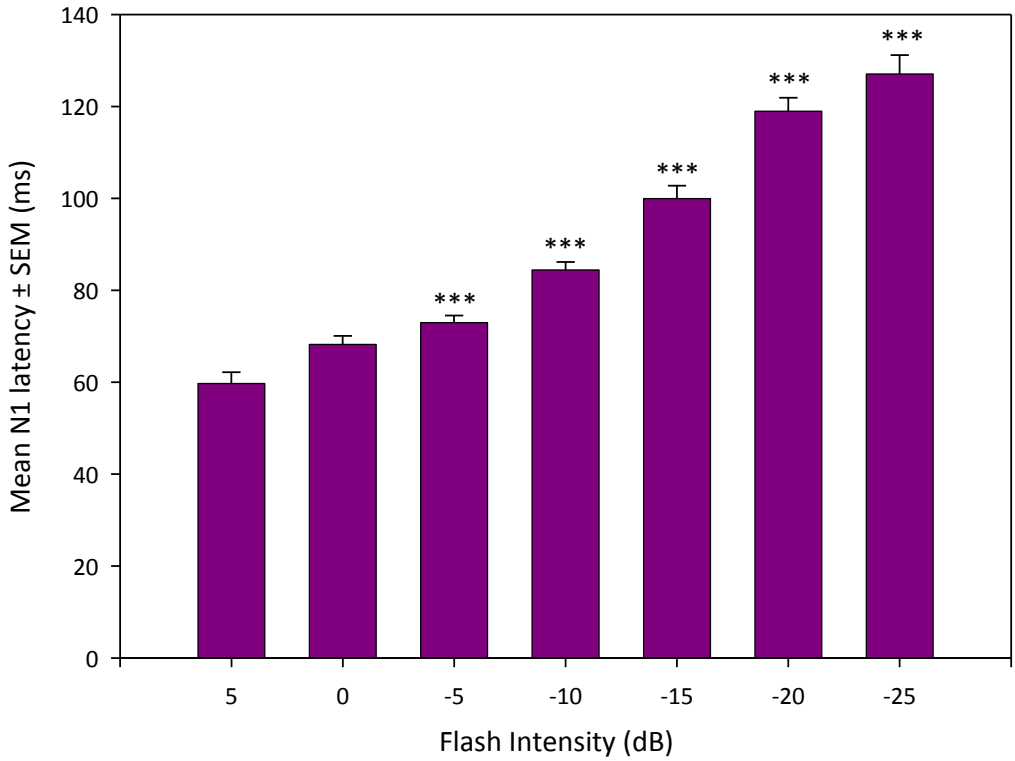

Figure 4.5 ***Increase in N1 latency of VEP with decreased flash intensity****. Animals were anaesthetised and the VEP was recorded (n=8) at +5dB, 0dB, -5dB, -10dB, -15dB, -20dB and -25dB flash intensity. Animals were dark adapted for 30 minutes. Results represent the mean ± SEM of latency N1 ***P<0.001 compared to response at +5dB light intensity.*

4.3.1.3 VEP response to visual impairment

To further characterise the VEP response, the setup was used to test the differences in mean amplitude and N1 latency of the VEP response in mice with both eyes (binocular vision) or with one eye occluded (monocular vision). It is hypothesised that occluding one eye resulted in halving the amount of light that enters the visual system and is processed in the visual cortex. The occlusion of one eye (monocular vision) lead to a decrease in the mean amplitude of the VEP response (Figure 4.6). The difference in amplitude between monocular and binocular vision was significant at a flash intensity of -10dB and resulted in a 37% reduction. The results also show that monocular vision increases the mean N1 latency by 9% compared to binocular vision (Figure 4.7).

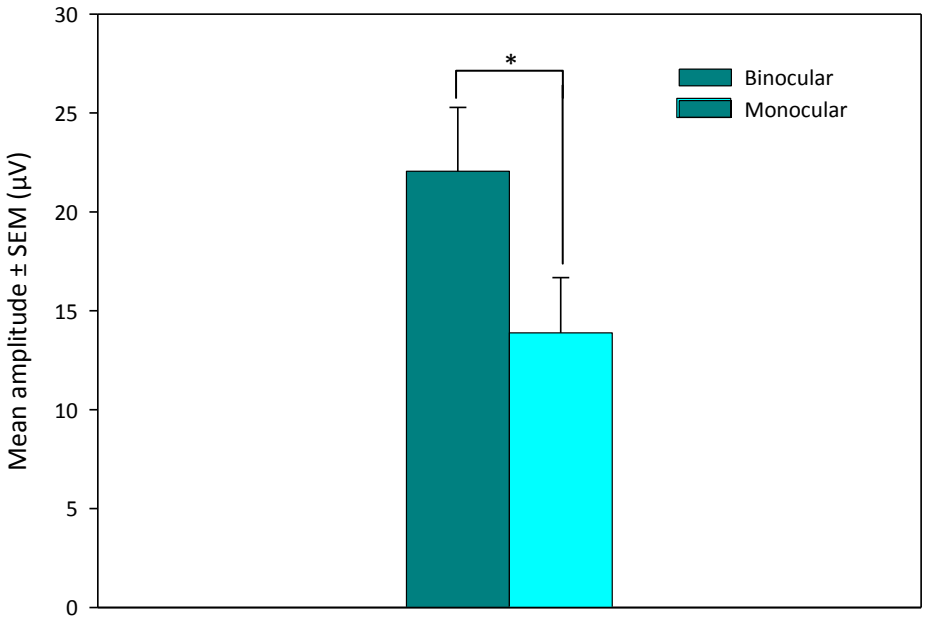

Figure 4.6 ***Decrease in mean VEP amplitude following occlusion of one eye****. Animals were anaesthetised and the amplitude of the VEP was recorded (n=5) at -10dB flash intensity. The VEP measurements were repeated with one eye being visually impaired by covering with foil. Animals were dark adapted for 30 minutes. Results represent the mean ± SEM of amplitude *P<0.05 between binocular and monocular vision (paired t test).*

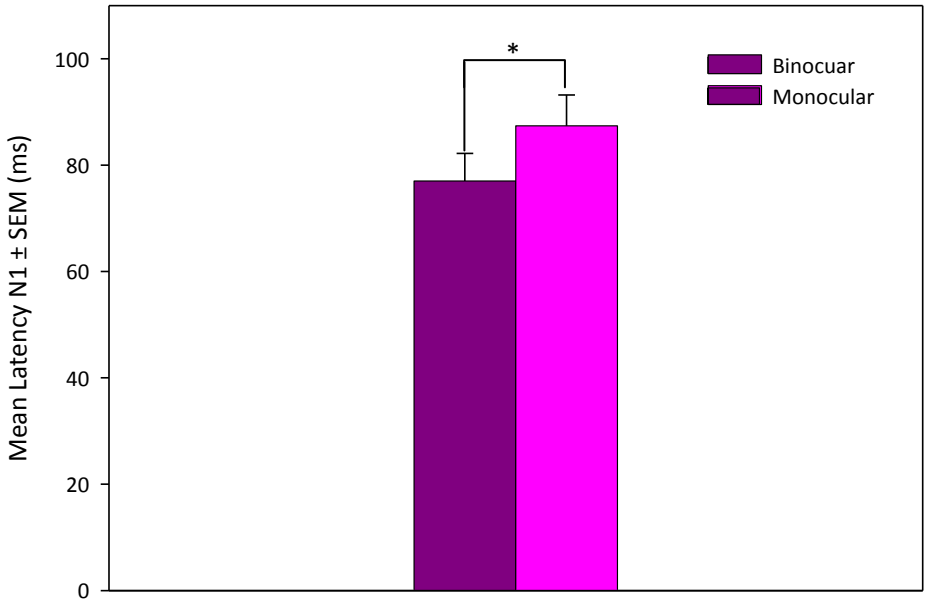

Figure 4.7 ***Increase in the mean N1 latency of VEP response following occlusion of one eye****. Animals were anaesthetised and the time of first peak of VEP was recorded (n=5) at -10dB flash intensity. The VEP measurements were repeated with one eye being visually impaired by covering with foil. Animals were dark adapted for 30 minutes. Results represent the mean ± SEM of N1 latency. *P<0.05 between binocular and monocular vision (paired t test).*

Therefore, these results show that by significantly reducing the amount of light that enters the visual pathway, the amplitude is decreased and the latency shows signs of increasing. These changes in the characteristic VEP signal reflect the reduced input of light into the visual system, therefore producing a reduced response in the visual cortex showing signs of delay. These results provide evidence that the experimental setup is sensitive and capable of detecting dysfunctional changes in the mouse eye and therefore can be used to test the dysfunction occurring in the visual system of MOG^{TCR}x*Thy1*CFP mice.

4.3.1.4 VEP response following immunisation to develop ON

The VEP response was examined in MOG^{TCR}x*Thy1*CFP immunised mice to determine the electrophysiological changes occurring in the optic nerve through the disease progress, which has been described in detail in previous chapters. Animals were tested on day 0 (before disease onset) and day 21 (after disease onset) of disease induction and VEP recorded at a flash intensity of -10dB to assess changes occurring through the development of ON (Figure 4.8, Figure 4.9 and Figure 4.10). This study showed that VEP recordings trended towards a reduction in mean amplitude between day 0 and day 21 (Figure 4.8). The difference between mean amplitudes before and after development of ON observed at a flash intensity of -10dB showed a mean amplitude before disease of 31.8µV and after disease of 18.5µV, representing a 42% reduction in mean amplitude.

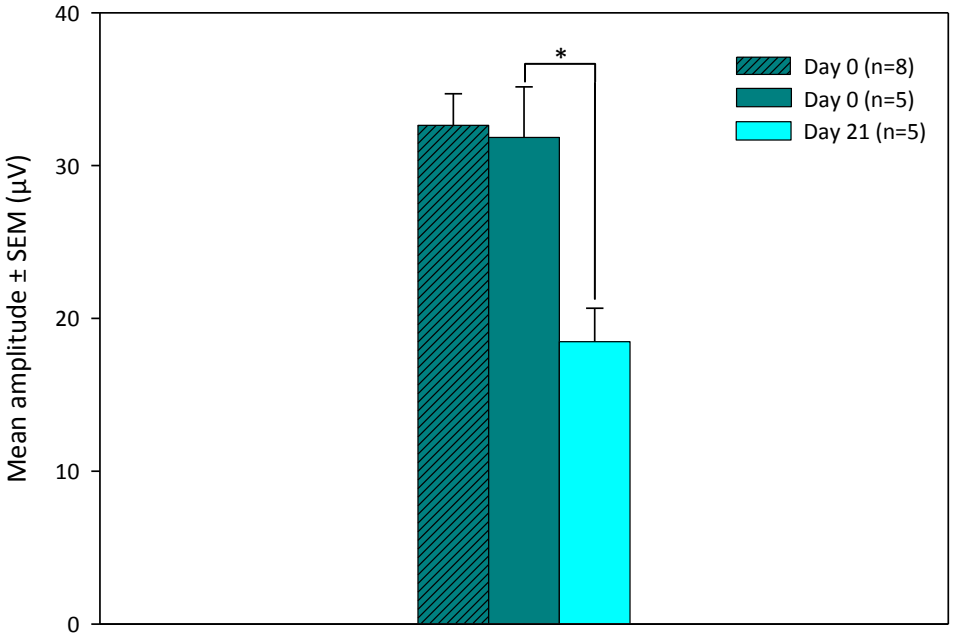

Figure 4.8 ***Decrease in mean VEP amplitude following immunisation to develop ON****. MOG^{TCR} x Thy1CFP transgenic mice were immunised with 150ng PTX on day 0 and 2 followed by injection of 0.25mg Z12 MOG-specific mAb at day 14 post-disease induction. Animals were anaesthetised and the amplitude of the VEP was recorded before the development of ON at day 0 (n=8) and after the development of ON at day 21 (n=5) at a flash intensity of -10dB. To allow comparison by paired t-test, day 0 was plotted (n=5) as a direct comparison with day 21 (n=5). Animals were dark adapted for 30 minutes. Results represent the mean ± SEM of amplitude. *P<0.05 between day 0 (n=5) and day 21 (n=5) (paired t test).*

A decrease in the mean N1 latency (Figure 4.9) and an increase in mean N1-P2 latency between day 0 and day 21 were observed (Figure 4.10). These results suggest that the VEP response following disease induction is prolonged due to the slow processing of the visual stimulus as a result of the damage occurring in the optic nerve.

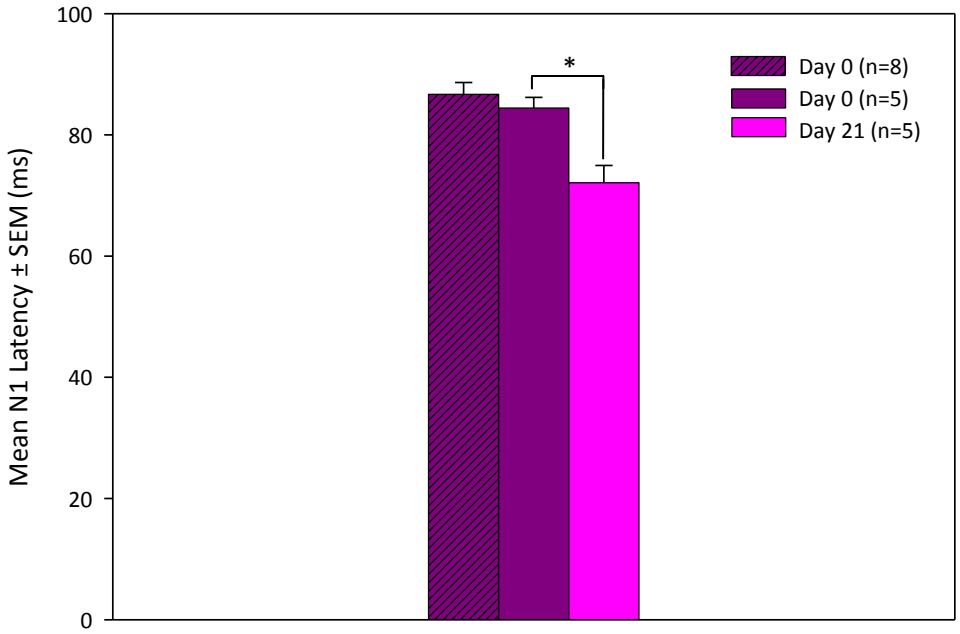

Figure 4.9 ***Decreased N1 latency of VEP response following immunisation to develop ON****. MOG^{TCR}xThy1CFP transgenic mice were immunised with 150ng PTX on day 0 and 2 followed by injection of 0.25mg Z12 MOG-specific mAb on day 14 post-disease induction. Animals were anaesthetised and the mean time of the first peak of the VEP was recorded before the development of ON at day 0 (n=8) and after the development of ON at day 21 (n=5). Animals were dark adapted for 30 minutes. Results represent the mean ± SEM of N1 latency. *P<0.05 between day 0 (n=5) and day 21 (n=5) (paired t test).*

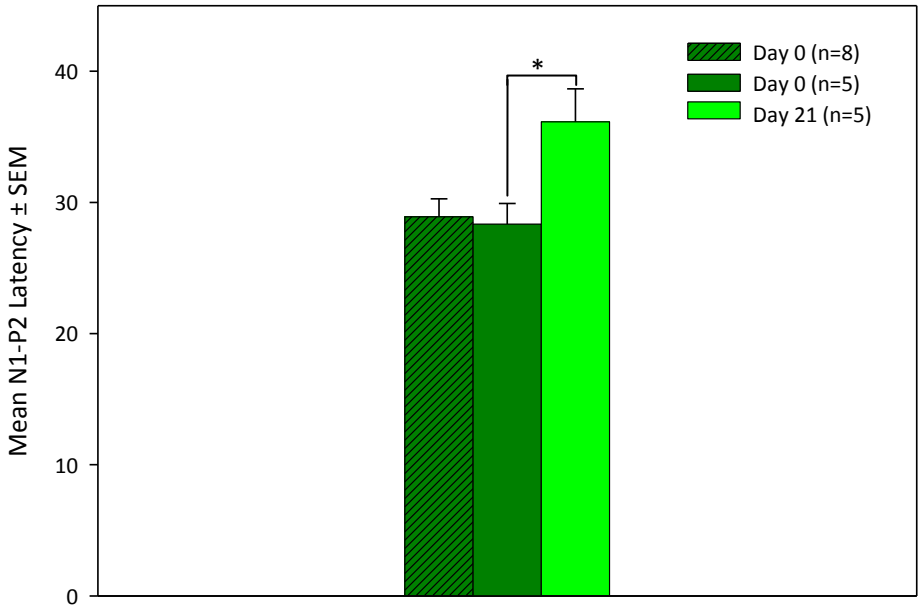

Figure 4.10 ***Increased N1-P2 latency of VEP amplitude following immunisation to develop ON****. MOG^{TCR}xThy1CFP transgenic mice were immunised with 150ng PTX on day 0 and 2 followed by injection of 0.25mg Z12 MOG-specific mAb at day 14 post-disease induction. Animals were anaesthetised and the latency of the VEP was recorded before the development of ON at day 0 (n=8) and after the development of ON at day 21 (n=5) at a flash intensity of -10dB. Animals were dark adapted for 30 minutes. Results represent the mean ± SEM of N1-P2 latency. *P<0.05 between day 0 (n=5) and day 21 (n=5) (paired t test).*

This data indicate that the electrophysiological function of the optic nerve is dysfunctional at day 21 due to the disease activity resulting in reduced amplitude. The data also indicates that although the signal is disrupted, the visual pathway is still sufficiently intact to allow nerve impulse transmission from the retina to the visual cortex. The reduction in VEP amplitude and minimal change in latency suggests axonal loss rather than demyelination occurs in the optic nerve, although the small increase in N1-P2 latency of 22% could suggest demyelination is slowing the VEP response.

4.3.2 Visual Acuity

The visual acuity of animals was tested by monitoring their behaviour in a visual tracking drum. Animals were divided into two groups; one group were used as a control and the other group were immunised on day 0 and 2 with PTX and day 14 with Z12 MOG-specific mAb to develop ON. Animals were tested on 0, 7, 14 and 21 days post-PTX immunisation (Figure 4.11).

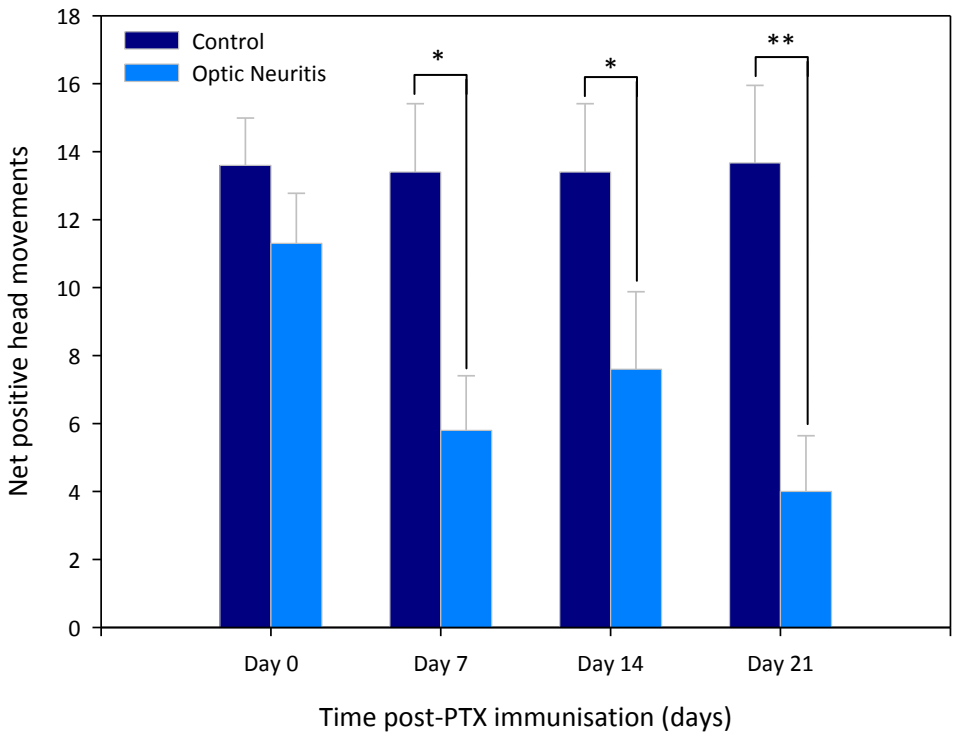

Figure 4.11 ***Decrease in positive head tracking movements following MOG^{TCR} immunisation****. Animals were divided into two groups a) control group (n=10), b) MOGTCR immunised with PTX on day 0 and 2 and Z12 MOG-specific mAb on day 14 to produce optic neuritis (n=10). Animals were observed in the visual tracking drum on days 0, 7, 14 and 21 for four times 60 seconds with 30 second intervals in both clockwise and anti-clockwise direction. Results represent the mean ± SEM of net positive head movements.*

The mice withstood sitting on the stationary platform and although some mice showed signs of leaning over, no mice jumped off the platform and remained calm and appeared unstressed throughout the process. However, one of the fundamental problems with this method was the difficulty in observing head tracking movements as they were short in length and often interrupted due to examining and grooming behaviour. To resolve this, both positive and negative head movements were counted and a net positive head movement in the direction of the rotating drum was calculated. There was a significant difference ($P<0.01$) between the control group and the optic neuritis group, with a lower incidence of positive head movements occurring in the ON group. This differences between the Control group and ON group was observed from day 7 (Figure 4.11), proposing a rapid onset of disease and the threshold for disease activity observable using the OKN drum had already been reached at this early stage. At the end of the study, animals were sacrificed and the RGC density was calculated from retinal flatmounts (Figure 4.12). A reduction in RGC density was observed in the ON group compared to the control, although this was not significant.

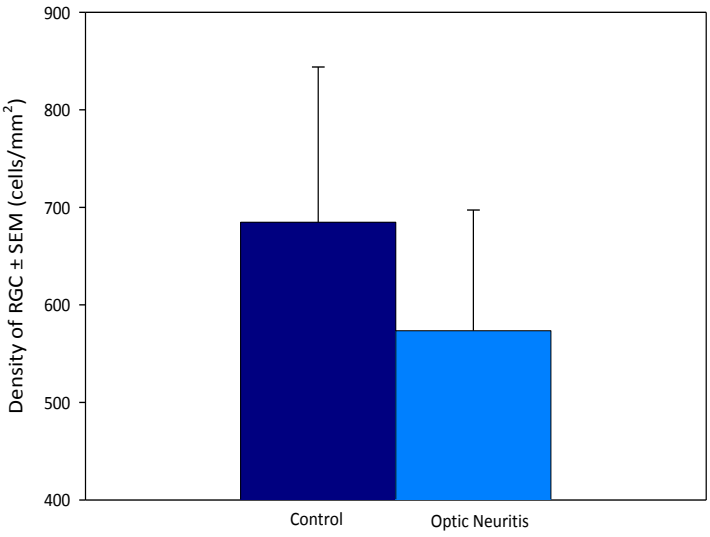

Figure 4.12 ***RGC loss in immunised MOG^{TCR} mice.*** *Animals were divided into two groups a) control group (n=9), b) MOGTCR immunised with PTX on day 0 and 2 and Z12 MOG-specific mAb on day 14 to produce ONs (n=10). Mice were sacrificed on day 21. Eyes were flatmounted and RGC were counted using stereology software. Results represent mean ± SEM of density of RGC.*

It is clear from these results that the level of accuracy of determining the visual acuity of mice using the visual tracking drum is variable but is capable of detecting a difference between the control and ON group. The results also suggest visual acuity is reduced by day 7 therefore showing the rate of degeneration following PTX treatment is rapid and occurs in the early stages of disease.

4.4 Discussion

This chapter investigated two methods, which can be used to objectively assess the visual system in MOG^{TCR}x*Thy1*CFP mice. These methods have been used to detect visual dysfunction following immunisation of MOG^{TCR}x*Thy1*CFP mice and can be used in future studies to correlate with optic nerve pathology and determine the beneficial effect of potential neuroprotective therapies.

Recording the VEP in MOG^{TCR}x*Thy1*CFP mice allowed a measure of synaptic activity in the visual cortex, which was altered during the disease process of optic neuritis. Although the electrophysiology setup was capable of detecting a decrease in the VEP amplitude, the variability between individual mouse recordings could hide the significance of the results due to the large degree of variation. The method used to measure VEP in this study employed needle electrodes which are minimally invasive and easily placed into the skin. However, several previous studies used intracranial electrodes implanted following craniotomies, which allow direct recording from the visual cortex (Tebano *et al.*, 1999). This results in an increased signal to noise ratio allowing for a more accurate VEP signal to be recorded. The major advantage is the increased reliability of the measurements as repeated tests would be conducted in exactly the same cortical area, unlike the needle electrode method which is open to variability. However, the most significant disadvantage would be the invasive surgical nature of this method, which would require greater time to carry out the experiment and increased attention for the welfare of the animal due to the possibility of increased suffering. Previous studies using needle electrodes have supported the use of this method and consider the effect of the skull thickness on the evoked potential amplitude to be minimal, therefore allowing adequate extracranial recordings (Hobom *et al.*, 2004; Porciatti *et al.*, 1999; Strain & Tedford, 1993). In this study, the non-invasive needle electrode method appears to be sensitive enough to detect changes in amplitude of the VEP, but not sufficiently sensitive to detect any changes in the latency of the VEP, expected to be associated with demyelination (Chow *et al.*, 2005). This could be attributed to the variability of positioning of the needle electrode. To reduce this level of variability, methods need to be developed to allow more reproducible positioning of the extracranial needle electrodes. Another variable to take into consideration is the effect of anaesthesia on the VEP response, which is capable of augmenting the VEP amplitude and increasing the latency (Hetzler & Oaklay, 1981). The evidence suggests that this effect could be due to a drop in body temperature as a result of the anaesthetic (Dyer & Boyes, 1983). In this

study, the body temperature was maintained using a heat pad at a constant level of 35°C for all the VEP studies described in this chapter, and therefore is unlikely to have an effect on the variability of the VEP response. A greater insight into the dysfunction of the visual system in MOG^{TCR}x*Thy1*CFP mice may be found by using the electrophysiology setup to record the VEP in each eye individually, which may give further insight into the changes occurring in the visual system. Assessment of the visual system could also be extended by analysing the pattern VEP, which can detect the response to spatial features of a stimulus (Porciatti *et al.*, 1999; Strain & Tedford, 1993). Another method which could be tested in the MOG^{TCR}x*Thy1*CFP mice is recording the ERG from the corneal surface. The ERG measures the massed response of the retina to light stimulation, recorded from the corneal surface (Peachey & Ball, 2003). The ERG is a good assessment to measure restricted sets of neurons and can therefore offer further information compared to the VEP, which is limited to measurement of the overall visual function.

The advantage of using the visual tracking drum as a behavioural technique to measure visual acuity in the mouse is that animals do not need any training or time to customise to their surroundings. The technique is also non-invasive and the animals are allowed to move freely and are not restricted. The disadvantage of this technique is the difficulty in assessing head tracking movements and the subjective variability as a result. Mice show very minimal head movements in comparison to rats, which are easier to assess due to their exaggerated head movements. The technique has been frequently used to demonstrate head tracking behaviour in rats (Fuller, 1985; Thomas *et al.*, 2004). To overcome this issue the results were analysed blinded to avoid the induction of bias and animals were observed on video at a slower speed which allowed all head movements to be counted. Variability also occurs according to the positioning of the mouse, which is free to roam on a small platform and therefore the distance between the mouse and the rotating drum does not remain constant. The OKN drum could be adapted to allow additional testing of acuity and contrast sensitivity by changing light illumination, grating size and stripe contrast to determine thresholds of vision. The development of virtual reality optomoter systems have allowed the frequency, contrast and velocity of horizontal stripes to be easily manipulated allowing further examination of the mouse visual system (Prusky *et al.*, 2004). This data suggests that loss of visual acuity occurs quickly following the development of disease and is perhaps consistent with the rapid loss of RGC following induction as shown following CD4 antibody treatment.

Using electrophysiology to measure the VEP response and the OKN drum to measure visual acuity has profound implications on the 3Rs. These techniques allow longitudinal measurement of changes in the visual system of animals, which ultimately reduce the number of animals required to conduct an experiment. In addition, the OKN drum eliminates the need of an anaesthetic, further reducing potentially harmful manipulations. Both the methods studied in this chapter can be related to techniques used in humans to monitor a dysfunctional visual system in people with MS. The visual acuity in people with MS is normally quantitatively measured using a low-contrast visual test (Balcer & Frohman, 2011) and has been proven to correlate with expanded disability status scale (EDSS) scores in people with SPMS (Balcer, 2001). The optokinetic reflex has been used to study visual impairment in people with MS, which showed delays in the optokinetic reflex in response to drum movements (Todd *et al.*, 2001). This method has also been proposed as a method to diagnose MS and to evaluate the efficacy of new drugs in clinical trials (Prasad & Galetta, 2010). The VEP response is known to be delayed in patients with MS (Corallo *et al.*, 2005; Naismith *et al.*, 2009) and is used as a complimentary tool for the diagnosis of MS. Therefore both the methods studied in this chapter show correlation with techniques used in humans to monitor MS. To conclude, two methods to study the visual dysfunction occurring in the MOG^{TCR}x*Thy1*CFP have been developed with the potential to longitudinally measure changes in the visual system. Although both methods were carried out as independent studies, future studies could utilise both methods to allow correlation between visual acuity and visual function.

Chapter 5

Development of methods to measure RGC loss

5.1 Introduction

To take full advantage of the MOG^{TCR}x*Thy1*CFP mouse model, it is essential to be able to serially measure RGC loss. The cSLO and OCT are two technologies that are used in humans to study ON and can be used to serially assess RGC loss in the MOG^{TCR}x*Thy1*CFP model.

5.1.1 Confocal scanning laser ophthalmoscope (cSLO)

The cSLO is a non-invasive device used to image the eye. The technique is based on the standard scanning laser microscope, which is capable of producing detailed images of the retina. The method was first developed by (Webb *et al.*, 1980), by adapting a conventional ophthalmoscope to produce a focused laser beam capable of producing high quality images. The most common clinical use of the cSLO is to use fluorescent dyes to label cells and monitor the dynamics of cells (Hassenstein & Meyer, 2009), tomographic imaging (Weinreb, 1993) and fluorescein and indocyanine green angiography for the diagnosis of retinal and choroidal disorders (Marmor & Ravin, 2011).

Due to the small size of the mouse eye, the cSLO has only recently been developed and adapted to visualise the mouse retina. The cSLO has been used in mice to study retinal and choroidal circulation (Xu *et al.*, 2002), visualisation of RGC (Paques *et al.*, 2006) and mononuclear phagocytes (Eter *et al.*, 2008). Therefore the SLO is a valuable tool which can be used in biomedical research to investigate the eye in detail and reduces the need for histology and large numbers of animals in experiments. To examine *Thy1*-CFP expressing RGC, a modified blue-light cSLO (bCSLO, 460 nM excitation and 490 nm detection) has been used to allow quantification of RGC loss (Leung *et al.*, 2008b), without the need to surgically label the RGC. This study showed that co-localisation of RGC from images taken from a live animal using a cSLO are comparable with a retinal flatmount image from the same animal. This therefore demonstrates that the cSLO detects RGC with good reliability and that fluorescent non-RGC (such as amacrine cells) are not an issue when considering the value of the model for detecting RGC loss (Leung *et al.*, 2008a). These

results therefore support the use of a modified blue light cSLO to monitor RGC loss in MOG^{TCR}x*Thy1*CFP mice.

5.1.2 Optical coherence tomography (OCT)

OCT is a non-invasive retinal imaging tool that can be used to measure the microstructure of the retina. OCT was introduced in 1991 (Huang *et al.*, 1991) and revolutionised the field of ophthalmic imaging to allow non-invasive visualisation of the retina, which is used for medical diagnosis.

OCT is analogous to ultrasound but is based upon the principle of low coherence interferometry instead of ultrasound waves. OCT omits a light source, which is split into two beams: a reference beam and a sample beam. The reference beam is received and reflected by a reference mirror and the sample beam is focused into the eye and reflected back by the different layers of the retina. The reflected light from the two pathways converge to induce an interference signal detected by a photodetector, which uses an interferometer to produce a cross-sectional depth image of the retina (Fercher, 2010). The Stratus OCT (Carl Zeiss Meditec) is an example of a first generation OCT system, which offers axial resolutions of up to 10µm and 400 axial-scans per second (A-scans/s). The speed and sensitivity of OCT has been increased by using Fourier domain technology, which are capable of measuring all echoes of light from different delays simultaneously to produce Spectral-Domain OCT (SD-OCT) (Drexler *et al.*, 2003). SD-OCT allows axial resolutions of less than 5µm and a 50 fold higher acquisition speed compared to time-domain SD (Alam *et al.*, 2006), with speeds capable of 312,500 A-scans/s (Potsaid *et al.*, 2008). The development of SD-OCT allowed comprehensive visualisation and mapping of retinal structures at a higher speed and resolution, which led to improved diagnosis and disease monitoring. Ultrahigh-resolution OCT (UHR-OCT) is also being developed, which uses bandwidth as a low coherence light source and gives much greater resolutions, which almost allows cellular visualisation of the retinal layer (Wojtkowski *et al.*, 2005). These improvements and developments in OCT technology will allow early patient diagnosis and contribute to knowledge on the pathogenesis of eye disease.

This technique is frequently used as a primary outcome in clinical trials to monitor MS disease progress due to its capability to detect RNFL thinning as a result of axonal loss in MS patients (Parisi *et al.*, 1999; Urano *et al.*, 2011). Due to its low variability and high reliability, OCT is a valuable technology to evaluate disease activity and neuroprotection. The first study of MS

patients using OCT, demonstrated that MS patients who had previously suffered with ON showed a significant reduction in the RNFL thickness compared to healthy controls (Parisi *et al.*, 1999). Detection of RNFL thinning with OCT has also been found in MS patients without any prior episodes of ON, therefore suggesting OCT is a marker of global neuronal degeneration in MS (Gordon-Lipkin *et al.*, 2007). OCT has also been shown to distinguish between disease subtypes (RRMS, PPMS and SPMS) based upon RNFL thickness (Pulicken et al., 2007). Some evidence suggests that ultimately using OCT to measure RNFL thinning maybe a more useful evaluation to measure neuronal loss than conventional MRI (Frohman et al., 2009). MRI has been shown to have poor correlation with MS disease outcome when monitored over a short period of time (Daumer et al., 2008). Therefore, there is significant evidence to suggest OCT could be used in future neuroprotection clinical trials in MS to monitor changes in the rate of neurodegeneration (Greenberg, 2010).

The development of SD-OCT and UHR-OCT has also allowed the technology to be used in animal research (Ruggeri et al., 2007). Using OCT in rodent models allows monitoring of disease progress without the need to sacrifice large numbers of animals at different time points for histological analysis. OCT has been used on mice to evaluate retinal degeneration in retinal degeneration slow mice (Horio et al., 2001; Li et al., 2001). Studies using OCT in mouse models are limited due to the small size of the mouse pupil in comparison to the rat. The small pupil size makes OCT measurements difficult and also limits the amount of reflected light from the retina and the signal-to-noise ratio. OCT can produce high resolution images, which are comparable to stained histology samples (Kim et al., 2008) and has been used to evaluate RGC loss following optic nerve crush (Gabriele *et al.*, 2011).

5.1.3 Aims and Objectives

The aim of this chapter was to develop methods to measure RGC loss in the MOG^{TCR}x*Thy1*CFP transgenic model, thus providing an animal model correlate to concurrent human studies using ophthalmic devices. To achieve this aim, the non-invasive SLO and OCT methods were investigated for their potential to monitor longitudinal RGC loss following immunisation of MOG^{TCR}x*Thy1*CFP transgenic mice to develop ON.

5.2 Materials and Methods

5.2.1 Animals

MOG^{TCR}x*Thy1*CFP transgenic mice as described earlier were used for all experiments. All experiments were performed according to UK Animals (Scientific Procedures) Act 1986.

5.2.2 Histology

Animals were perfused, tissue fixed and embedded, sections cut and stained with toluidine blue as described in Section 2.2.3. Using Stereo Investigator software the ganglion cell layer (GCL) was measured at 100µm sections across the retina (Figure 5.1).

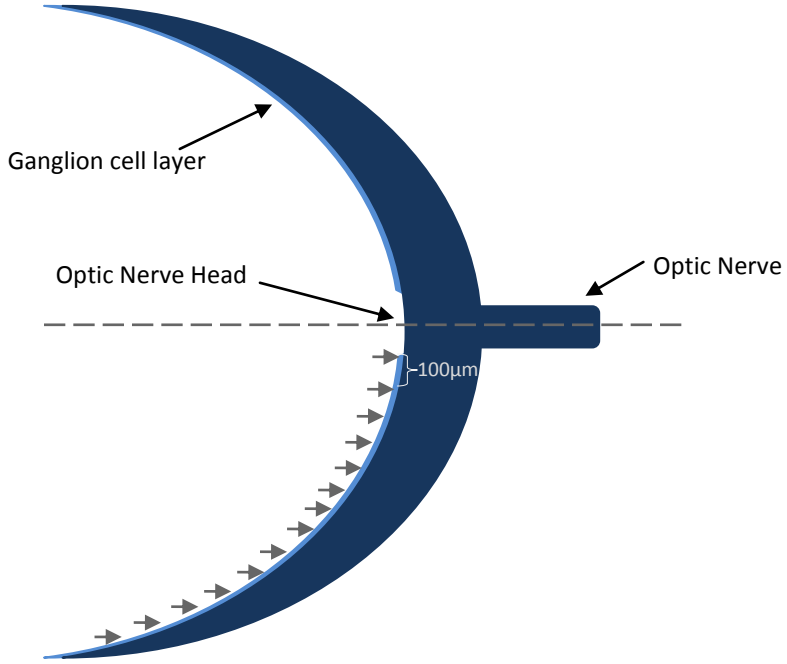

Figure 5.1 ***Cross-section of retina****. Measurements taken at 100µm sections from a cross section of retina to estimate changes in the thickness of GCL.*

5.2.3 Immunisation

MOG^{TCR}x*Thy1*CFP transgenic mice were immunised as described in Section 3.2.2 with 150ng PTX (day 0 and 2) and 1mg MOG-specific Z12 monoclonal antibody (day 14). Animals were sacrificed on day 21.

5.2.4 Multiline OCT

A Spectralis® HRA + OCT from Heidelberg Engineering, Inc (Heidelberg, Germany) was modified to allow imaging of CFP and adapted to comply with mouse optics. The modifications resulted in the Spectralis® being unsuitably certified for human use and was therefore renamed Multiline OCT for animal use only.

5.2.4.1 Modifications of Multiline OCT

Modifications include changes to the diameter of the exciting laser beam, which was reduced to 2mm to allow more efficient coupling of laser light into the small animal aperture. The patient fixation light was removed as the filter slot was required for alternative filters. The standard chin rest was replaced with a special animal mount (custom built by Workshop, Institute of Ophthalmology, UCL) to allow the animal to be positioned correctly (Figure 5.2). A +25 diopter add-on lens was used to correct for the characteristic hyperopia seen in rodents. The machine consisted of a 4 slot filter wheel with different filters:

Figure 5.2 ***Setup of Multiline OCT.*** *A Spectalis HRA + OCT from Heidelberg Engineering was modified to allow imaging of MOG^{TCR}xThy1CFP mice.*

Filter #1 – Standard Heidelberg retina angiograph (HRA) filter, which has a high blocking of laser wavelengths between 450nm and 488nm and a high transmission between 498nm and 720nm.

Filter #2 – RazorEdge® ultrasteep long-pass filter, transmits between 458 and 670nm (LP02-458RS-25, Semrock, Baltimore, USA) to allow detection of CFP (Figure 5.3).

Filter #3 - 510/20 nm BrightLine® single-band bandpass filter, transmits between 510 and 520nm (FF02 510/20-25, Semrock, Baltimore, USA) to allow detection of GFP (Figure 5.4).

Filter #4 - 525/50 nm BrightLine® single-band bandpass filter, transmits between 525 and 550nm (FF02-525/50-25, Semrock, Baltimore, USA) to allow detection of YFP (Figure 5.5).

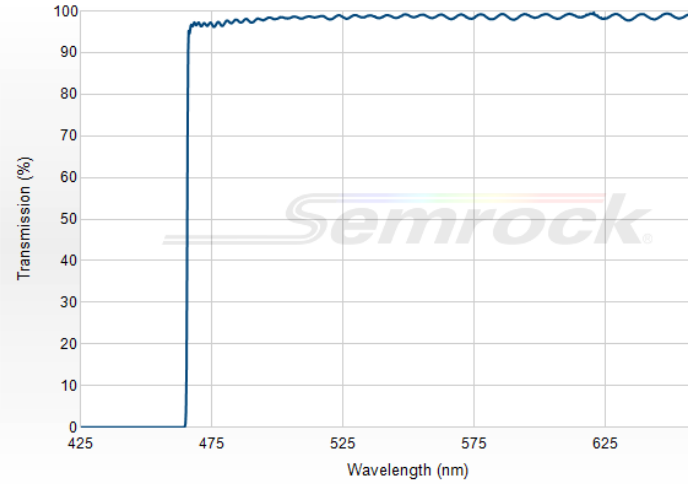

Figure 5.3 ***458nm RazorEdge® ultrasteep long-pass filter.*** *Filter positioned in Filter #2 transmits between 458 and 670nm to detect CFP excitation.*

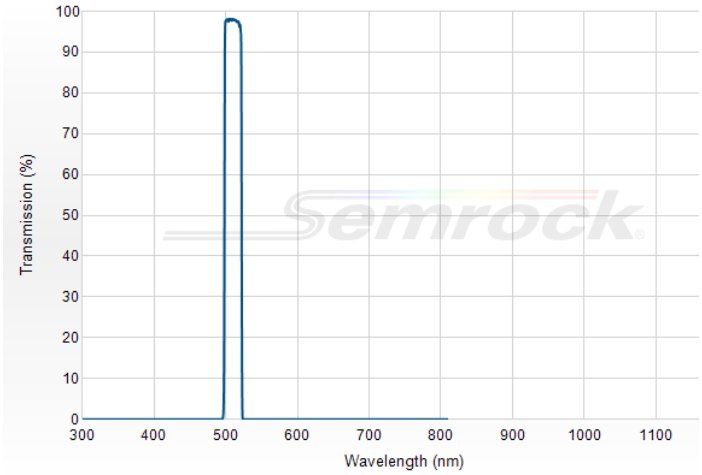

Figure 5.4 ***510/20 nm BrightLine® single-band bandpass filter.*** *Filter positioned in Filter #3 transmits between 510 and 520nm to detect GFP.*

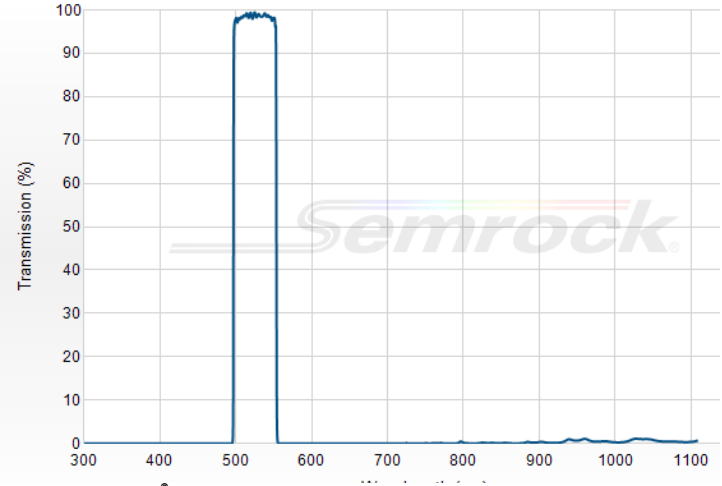

Figure 5.5 ***525/50 nm BrightLine® single-band bandpass filter****. Filter positioned in Filter #4 transmits between 525 and 550nm to detect YFP.*

5.2.4.2 Preparing animals

Animals were anaesthetised as described in Section 4.2.2. Eyes were dilated with one drop of Tropicamide (Minims® Tropicamide 1% w/v, Bausch & Lomb, Surrey, UK) and one drop of phenylephrine hydrochloride (Minims® phenylephrine hydrochloride 2.5% w/v, Bausch & Lomb, Surrey, UK). A polymethylmethacrylate contact lens (Cantor & Nissel, Northamptonshire, UK) or a drop of 2% hydroxypropyl methylcellulose (HPMC, Sigma-Aldrich Ltd, Poole, Dorset, UK) was used to prevent the mouse eyes from drying out during anaesthesia.

5.2.4.3 Capturing OCT images

Previous studies have reported imaging of the eye without the use of anaesthetic (Leung *et al.*, 2009), however this method was insufficient to allow a quality image of the eye to be obtained. Therefore, to capture an OCT image, animals were anaesthetised and placed on the animal mount and an infra red (IR) reflection image with the optic nerve head in a centralised position was achieved with optimal focus, which generally occurred at a refraction setting of +18.0 dioptres. The machine was switched to IR&OCT mode and the reference arm length was adjusted to bring the OCT image into the acquisition frame and to find the optimal position to acquire an OCT image. Examinations were recorded in both the right eye (oculus dextrus, OD) and the left eye (oculus sinister, OS) of each animal. A RNFL Single Exam using the Automatic Real Time (ART) mode (allows averaging of 100 recordings) was produced for each mouse eye, which measured RNFL thickness (µm) in a circle with the optic nerve head in the centre (Figure 5.6). Results were compared to a normative database (normative database was automatically set by Heidelberg and compiled of 201 Caucasian subjects who were considered to have 'normal' eyes as diagnosed by an ophthalmologist) and were colour coded with green (within normal limits), yellow (borderline) and red (outside normal limits). These results were therefore not applicable to examination of mouse eyes, however current communication with Heidelberg is being undertaken to investigate the possibility of a normative database consisting of C57BL/6 data. Examinations also generated an OCT Thickness Profile Map, which measured a detailed total thickness of the RNFL over a 15°x15° sample area (Figure 5.7).

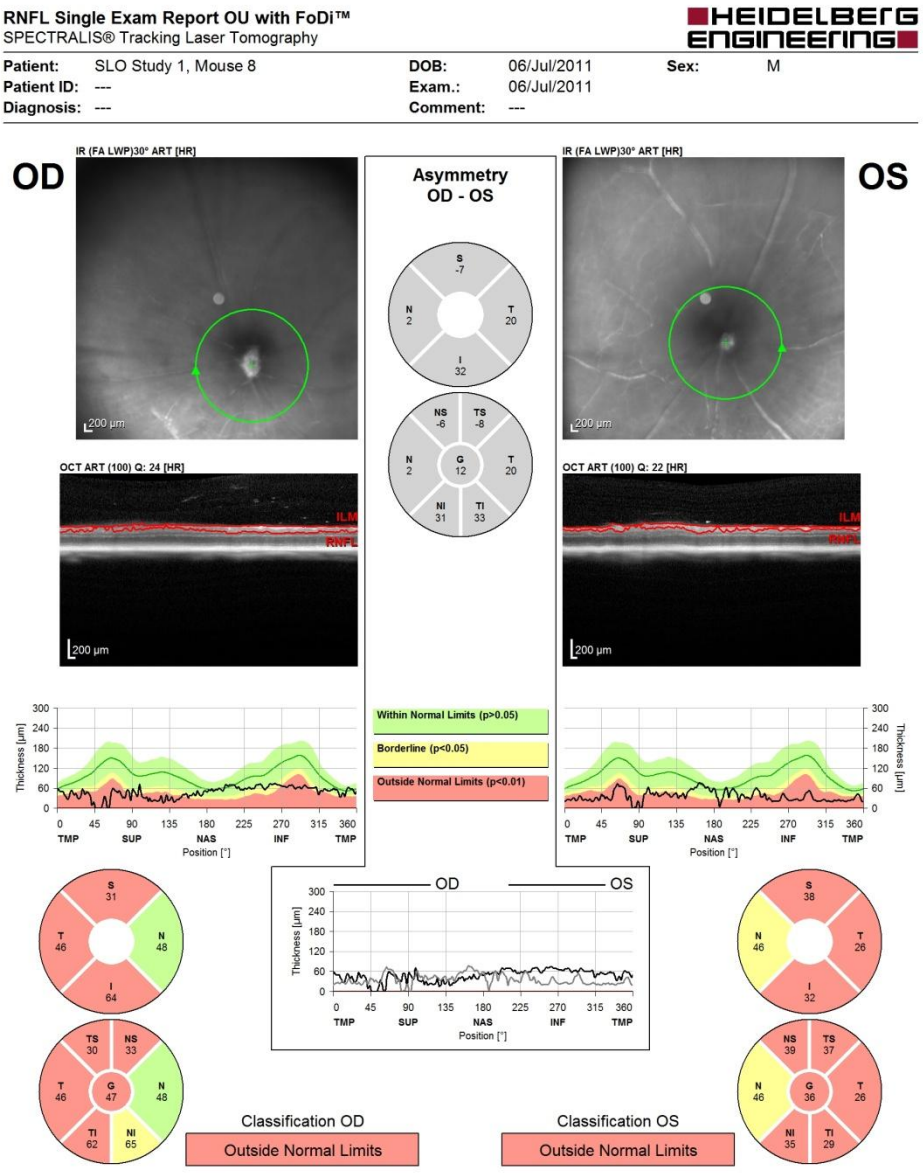

Figure 5.6 ***Example of OCT RNFL Single Exam Report****. RNFL single exam report measures the thickness of the RNFL surrounding the optic nerve head in OD (right eye) and OS (left eye). Report shows IR image of the retina and green circle shows the area measured by OCT. The Heidelberg Eye Explorer software automatically detects the RNFL (highlighted by red lines labelled ILM, internal limiting membrane and RNFL, retinal nerve fibre layer). RNFL Thickness Graph displays RNFL measurements along the calculation circle compared to a normative database. The results are simplified in a RNFL Quadrant which shows the average thickness in 6 segments surrounding the eye: nasal superior (NS), nasal (N), nasal inferior (NI), temporal inferior (TI), temporal (T), temporal superior (TS) and a global average (G). Differences between OD and OS measurements are recorded in the RNFL Quadrant and RNFL Thickness Graph (grey) in the centre.*

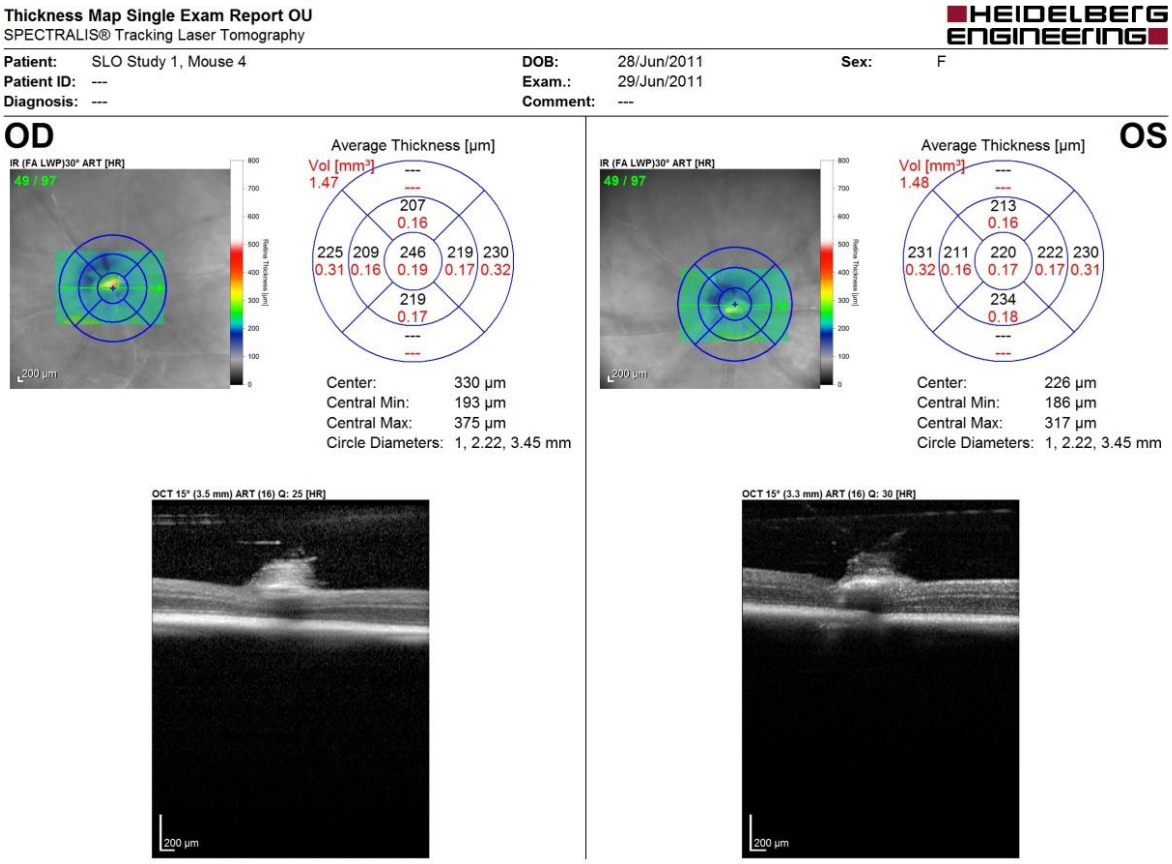

Figure 5.7 ***Example of OCT Thickness Map Single Exam Report****. Thickness Map Single Exam Report measures the thickness of the retina in a detailed 15°x15° area centralised over the optic nerve head in the OD (right eye) and OS (left eye). Report shows IR image with detail area of measurement and topographical display of RNFL with a thickness map. Average thickness of retina (µm) (black text) and volume of macular (mm^3) (red text) (not applicable to the mouse eye, which lack a macula region) are summarised in the circle diagram. OCT image shows a horizontal scan through the centre of the optic nerve head.*

5.2.4.4 Capturing SLO images

To capture an SLO image, an IR reflection image was achieved as described in the previous section. Once an IR image had been acquired, the CFP (450nm) laser was selected and the CFP-expressing RGC were visualised. A constant sensitivity of 80% and a field view of 30° were maintained for each eye examined. For each eye a minimum of 10 recordings were made at different refractions settings using the average real time (ART) mode to capture an average of 50 images for each recording. A montage of all recordings was produced using Heidelberg Eye Explorer software.

To calculate the RGC density, images were analysed in a blinded fashion using Image J software. Assumptions on the area of retina observed were made from (Leung et al., 2009), who estimated 1° of field is subtended by 30µm of retina, therefore, a 30° field of view is subtended by 900µm area of retina. The image resolution analysed with Image J software had a resolution of 48pixels/inch with an image width of 16.33 inches, therefore the total image width was 783.84 pixels = 1 pixel/1.148µm. The number of RGC was counted in the Superior, Nasal, Inferior and Temporal quadrants of a box overlaid on the image of the retina (Figure 5.8) and the density of RGC calculated in terms of mm^2.

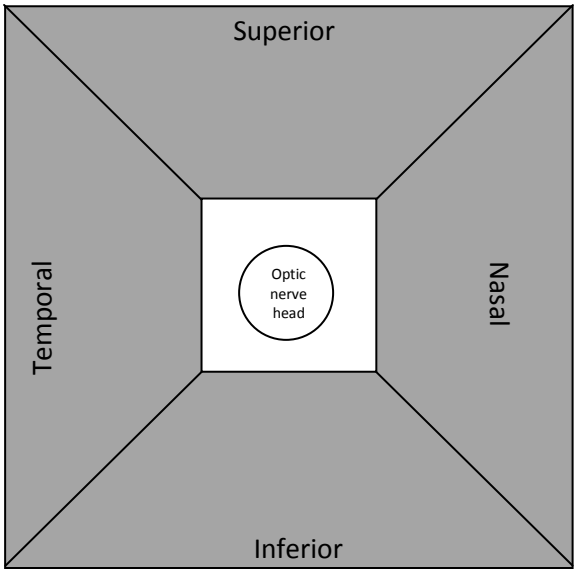

Figure 5.8 ***Area of retina used to count RGC to calculate RGC density****. A 12 x 12 inch box (equivalent to 0.437mm^2) was divided into 4 quadrants and a 4 x 4 inch box (equivalent to 0.048mm^2) was placed in the centre over the optic nerve head. RGC were counted in grey areas in the Superior, Nasal, Inferior and Temporal quadrants. The total area of retina counted is equivalent to 0.389mm^2.*

5.2.5 Statistical analysis

Statistical analysis was performed in SigmaStat 3.1. Results were presented as mean values ± standard error of mean. In preliminary experiments using histological data, differences between the RGC density in control and MOG^{TCR}x*Thy1*CFP immunised mice were analysed by Student t tests. Differences between RGC density and thickness of GCL between control and MOG^{TCR}x*Thy1*CFP immunised mice at different distances from the optic nerve head were analysed using a two-way ANOVA with Tukey post-hoc analysis. For OCT, differences between the two groups (Day 0 and Day 21) at different segments were analysed using a two-way paired ANOVA with Tukey post-hoc analysis and were further analysed using a paired t test. For SLO, differences between the two groups (Day 0 and Day 21) were analysed using a paired t test and compared with histological data using a Student t test. Correlations were analysed using the Pearson product moment correlation. Results was considered significantly different if the probability level $P<0.05$ (*), $P<0.01$(**) or $P<0.001$(***) was reached between groups.

5.3 Results

5.3.1 Preliminary data for OCT

To test the feasibility of an OCT machine being able to detect RNFL thinning in the MOG^{TCR}x*Thy1*CFP mouse model, a preliminary study investigated the thickness of the RGC layer using histological sections. As described previously, mice were immunised with 150ng PTX on day 0 and 2 followed by 0.25mg Z12 MOG-specific mAb on day 14. Animals were sacrificed on day 21, retinae was fixed, resin embedded and stained with toluidine blue to allow identification of RGC structure. The RGC density in MOG-specific TCR mice was significantly reduced compared to control mice (Figure 5.9).

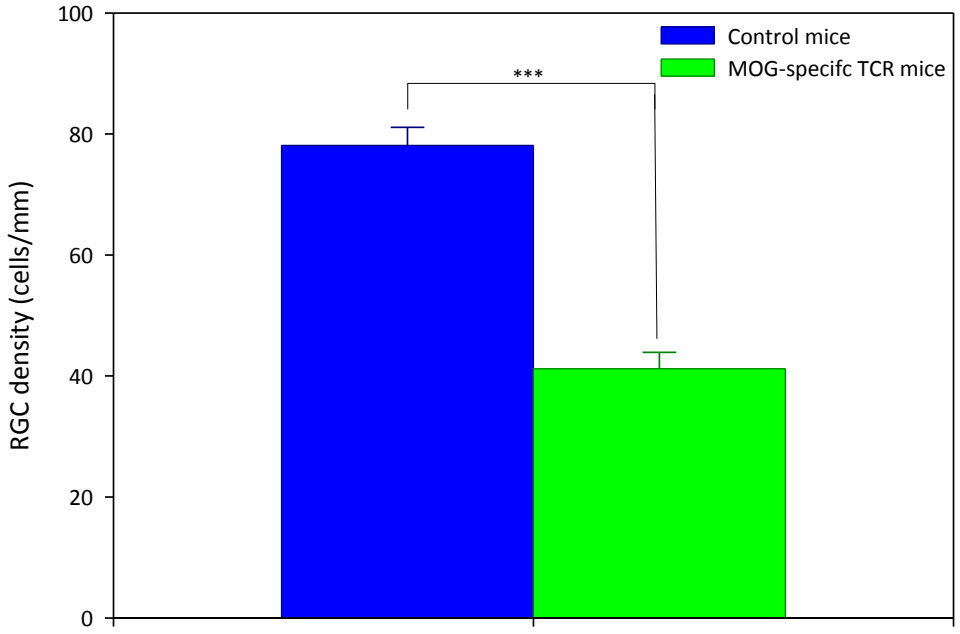

Figure 5.9 ***RGC loss following immunisation of MOG-specific TCR mice****. Animals were immunised with 150ng PTX on day 0 and 2 and injected i.p. with 0.25mg MOG-specific mAb at day 14 post-disease induction (n=5). Data was compared with control C57BL/6 animals, which were Wildtype littermates of the MOG-specific TCR mice (n=5). Animals were sacrificed on day 21 and perfused with Karnovsky's Fixative. Tissue was embedded in resin and semi-thin sections (0.7µm) were cut and stained with toluidine blue. The number of RGC in a cross section was counted and the length was measured to calculate RGC density using stereology software.*

The RGC density in 100µm sections was measured at intervals from the optic nerve head. RCG density in MOG^{TCR}x*Thy1*CFP mice was significantly reduced compared to control mice (P<0.001), which showed the RGC density is reduced throughout the retina with more significant loss observed closer to the optic nerve head (Figure 5.10).

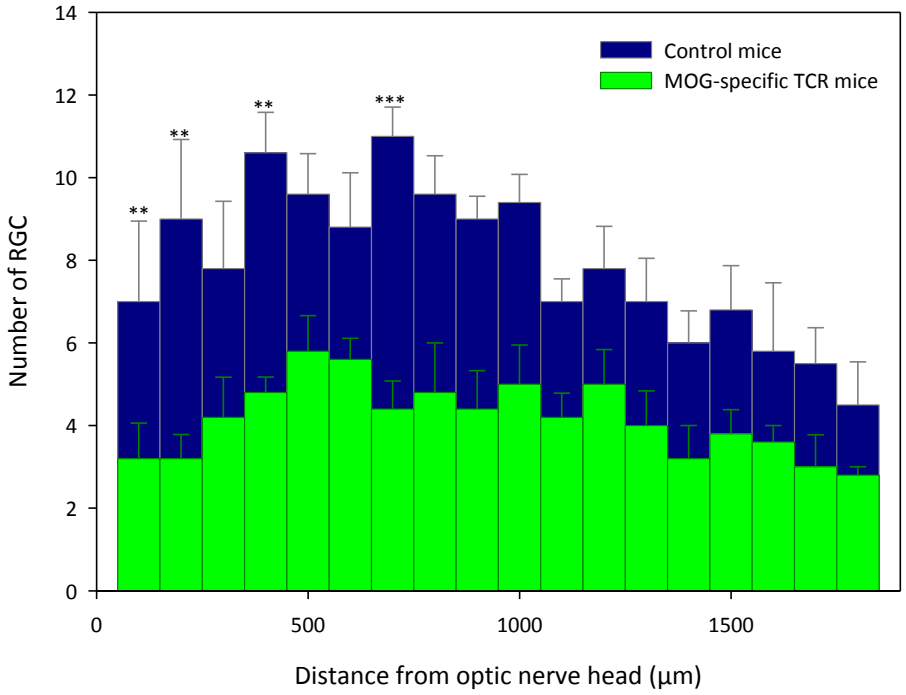

Figure 5.10 ***RGC loss following immunisation of MOG-specific TCR mice at intervals from the optic nerve head****. Animals were immunised with 150ng PTX on day 0 and 2 and injected i.p. with 0.25mg MOG-specific mAb at day 14 post-disease induction (n=5). Data was compared with control C57Bl/6 animals, which were wildtype littermates of the MOG-specific TCR mice (n=5). Animals were sacrificed on day 21 and perfused with Karnovsky's Fixative. Tissue was embedded in resin and semi-thin sections (0.7µm) were cut and stained with toluidine blue. The number of RGC in a 100µm section was counted at intervals starting at the optic nerve head using stereology software. **P<0.01 and ***P<0.001 between control mice and MOG-specific TCR mice at the same distance from optic nerve head.*

Although it is clear from these results that RGC density is significantly reduced in MOG^{TCR}x*Thy1*CFP, for the OCT to be able to detect any changes there must also be a significant reduction in the thickness of the GCL. Using stereology software it was possible to measure the thickness of the GCL at 100µm sections throughout the retina, which was found to be significantly reduced in MOG^{TCR}x*Thy1*CFP mice immunised to develop ON compared to control (P<0.001) (Figure 5.11). The greatest reduction in GCL thickness was observed in close proximity to the optic nerve head, with minimal reduction in the outer periphery of the retina.

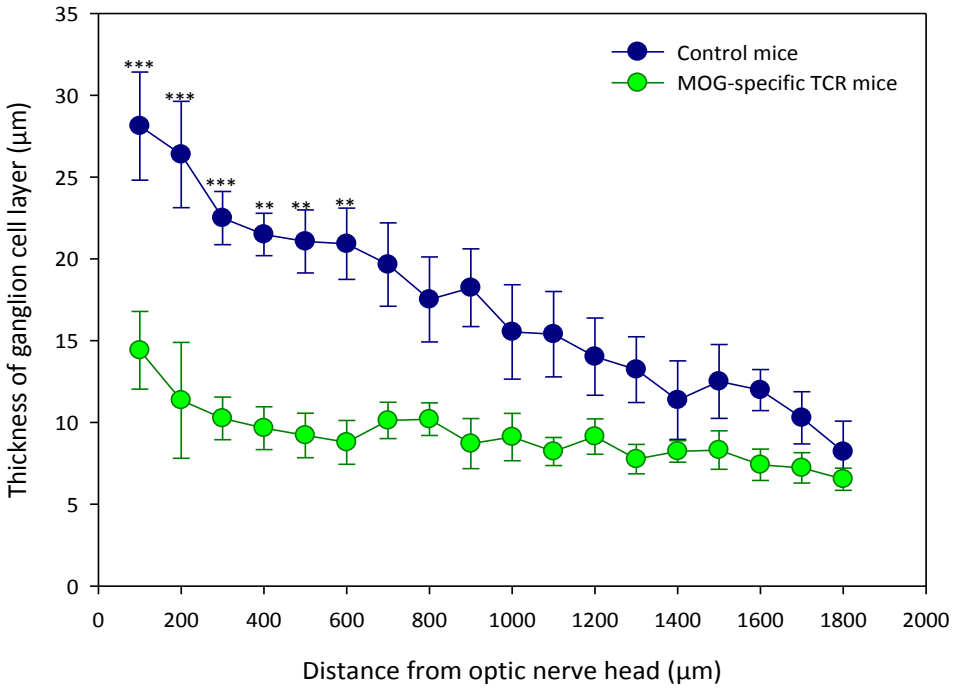

Figure 5.11 ***Comparison of RGC layer thickness****. Changes in the thickness of RGC layer in normal animals (n=5) and MOGTCR animals (n=5) immunised with 150ng PTX day 0 and 2 and anti-MOG Z12 mAb at day 14. Animals were perfused with Karnovsky's Fixative and tissue was fixed. Tissue was embedded in resin and semi-thin sections (0.7µm) were cut and stained with toluidine blue. Thickness of RGC layer was counted at 100µm sections starting from the optic nerve head using stereology software. Results represent the mean ± SEM of RGC layer thickness. **P<0.01 and ***P<0.001 between control mice and MOG-specific TCR mice at the same distance from optic nerve head.*

The resolution of the OCT machine is crucial, as the resolution needs to be great enough to detect a difference in RNFL in mice. The mean reduction in RNFL thickness found in this study was 8µm with a maximum difference of 13.7µm and a minimum difference of 1.7µm. Table 5.1 shows the smallest measurable changes recorded in three commercially available machines (data taken from Heidelberg Engineering website) (Wolf-Schnurrbusch *et al.*, 2009) and their coefficient of variation. The results of this study (Wolf-Schnurrbusch *et al.*, 2009) clearly show that the Spectralis® OCT manufactured by Heidelberg Engineering produces the greatest resolution and reliability compared with 5 other commercially available OCT instruments. This data would also suggests that the Spectralis® OCT machine would be capable of detecting changes in RNFL thickness; the smallest measurable change the machine can detect is 1µm and the smallest difference recorded in this preliminary study of histological sections was 1.7µm.

Manufacturer	Device	Smallest measurable change	Coefficient of Variation
Heidelberg Engineering, Inc	Spectralis®	1µm	0.46%
Opko/OTI, Inc	OCT SLO™	5µm	2.23%
Carl Zeiss Meditec, Inc	Cirrus™	9µm	3.33%

Table 5.1 ***Comparison of OCT machines****. Comparison of measurements of retinal thickness and reproducibility in commercially available OCT machines (Wolf-Schnurrbusch et al., 2009)*

Therefore, the available literature proposes that the Heidelberg Spectralis® OCT machine would be the only OCT machine commercially available that would be capable of detecting changes in the thickness of RNFL in mice.

5.3.2 Measuring RGC loss with OCT

To assess the ability of the OCT to measure changes in retina thickness, MOG^{TCR}x*Thy1*CFP animals were monitored on Day 0 (before disease induction) and Day 21 (end of experiment) to analyse the impact of disease on the reduction of thickness of the retina as a result of RGC loss. Using OCT, a detailed density map of total retina thickness was created in a 15°x15° area surrounding the optic nerve head. The density map calculated the average thickness of the retina in four segments (superior, nasal, inferior and temporal) surrounding the optic nerve head (Figure 5.13). A decrease in the total retina thickness of 10µm was observed following immunisation of MOG^{TCR}x*Thy1*CFP animals to develop ON (Figure 5.12). In particular, a statistical difference was noted in the nasal and inferior segments ($P<0.05$ and $P<0.01$ respectively) and an overall decrease in the thickness of the retina of 4% was observed ($P<0.05$).

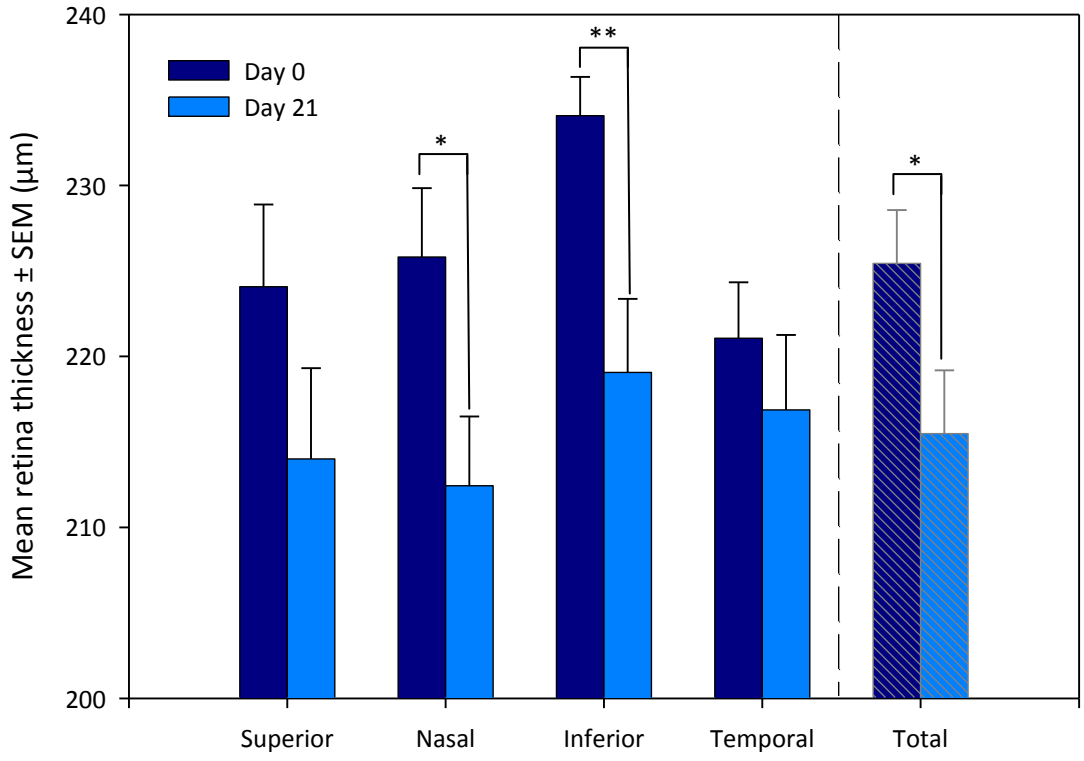

Figure 5.12 ***Decrease in mean retina thickness following immunisation of MOG^{TCR}xThy1CFP mice.*** *Animals were immunised with 150ng PTX on day 0 and 2 and injected i.p. with 0.25mg MOG-specific mAb at day 14 post-disease induction (n=8). OCT images of retina were acquired on Day 0 and Day 21 of disease induction and total retina thickness was calculated in four segments: superior, nasal, inferior and temporal. Results represent mean ± SEM of retina thickness.*

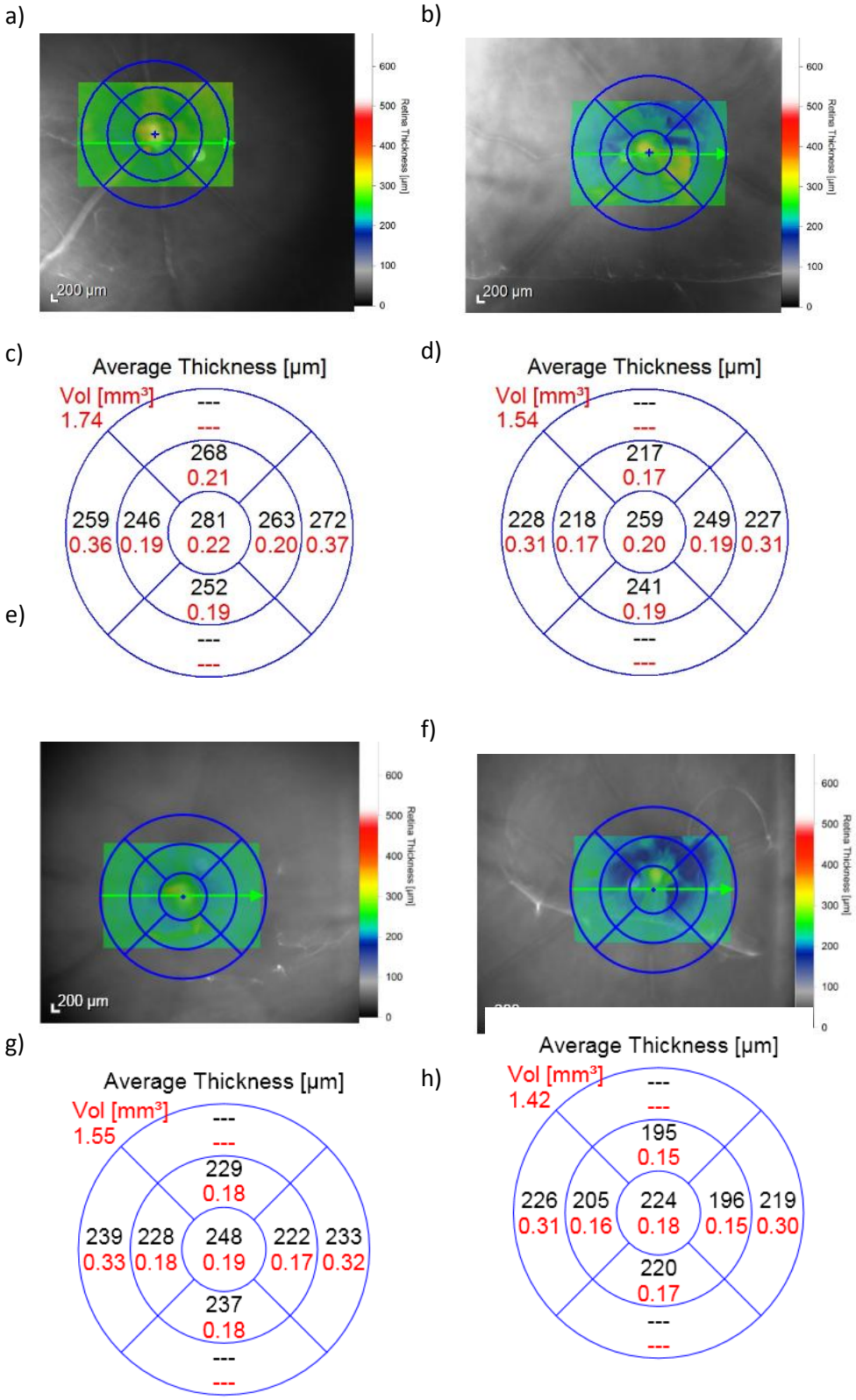

Figure 5.13 ***Density map of OCT measured mean thickness of retina following immunisation of MOG^{TCR}xThy1CFP mice.*** *A MOG^{TCR}xThy1CFP mouse was immunised with 150ng PTX on day 0 and 2 and injected i.p. with 0.25mg MOG-specific mAb at day 14. OCT images of retina were acquired on Day 0 (right eye a, c and left eye b, d) and Day 21 (right eye e, g and left eye f, h) of disease induction. Numbers in black show average thickness (µm) and numbers in red show volume (mm^3).*

To further analyse the decrease in thickness of the retina, the OCT was used to observe the RNFL thickness in a circle surrounding the optic nerve head (Figure 5.15), which calculated the average thickness of the RNFL in four segments (S, N, I, T segments) (Figure 5.13). A 12µm decrease in the RNFL thickness was observed following immunisation of MOG^{TCR}x*Thy1*CFP animals to develop ON (Figure 5.14). Each segment (with the exception of the temporal segment) showed a decrease in RNFL thickness and an overall decrease in the thickness of the retina of 33% ($P<0.05$).

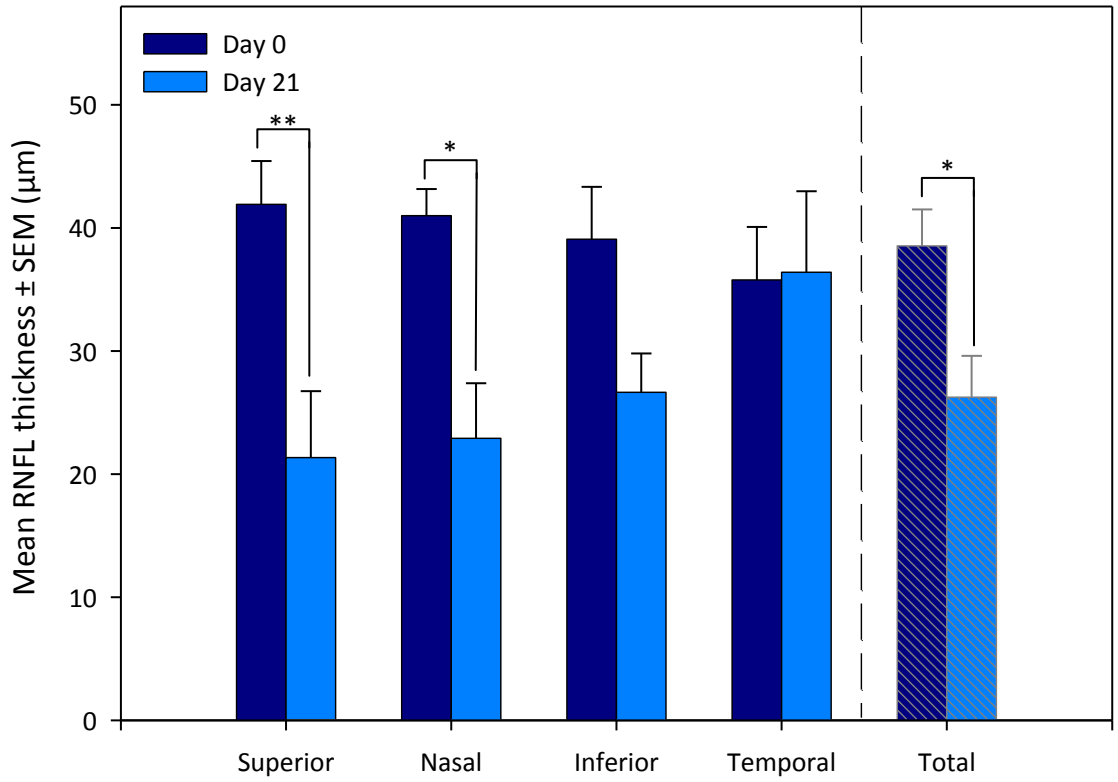

Figure 5.14 ***Decrease in measured RNFL thickness following immunisation of MOG^{TCR}xThy1CFP mice.*** *Animals were immunised with 150ng PTX on day 0 and 2 and injected i.p. with 0.25mg MOG-specific mAb at day 14 post-disease induction (n=8). OCT images of retina were acquired on Day 0 and Day 21 of disease induction and total retina thickness was calculated in four segments: superior, nasal, inferior and temporal. Plots show mean ± SEM of RNFL thickness.*

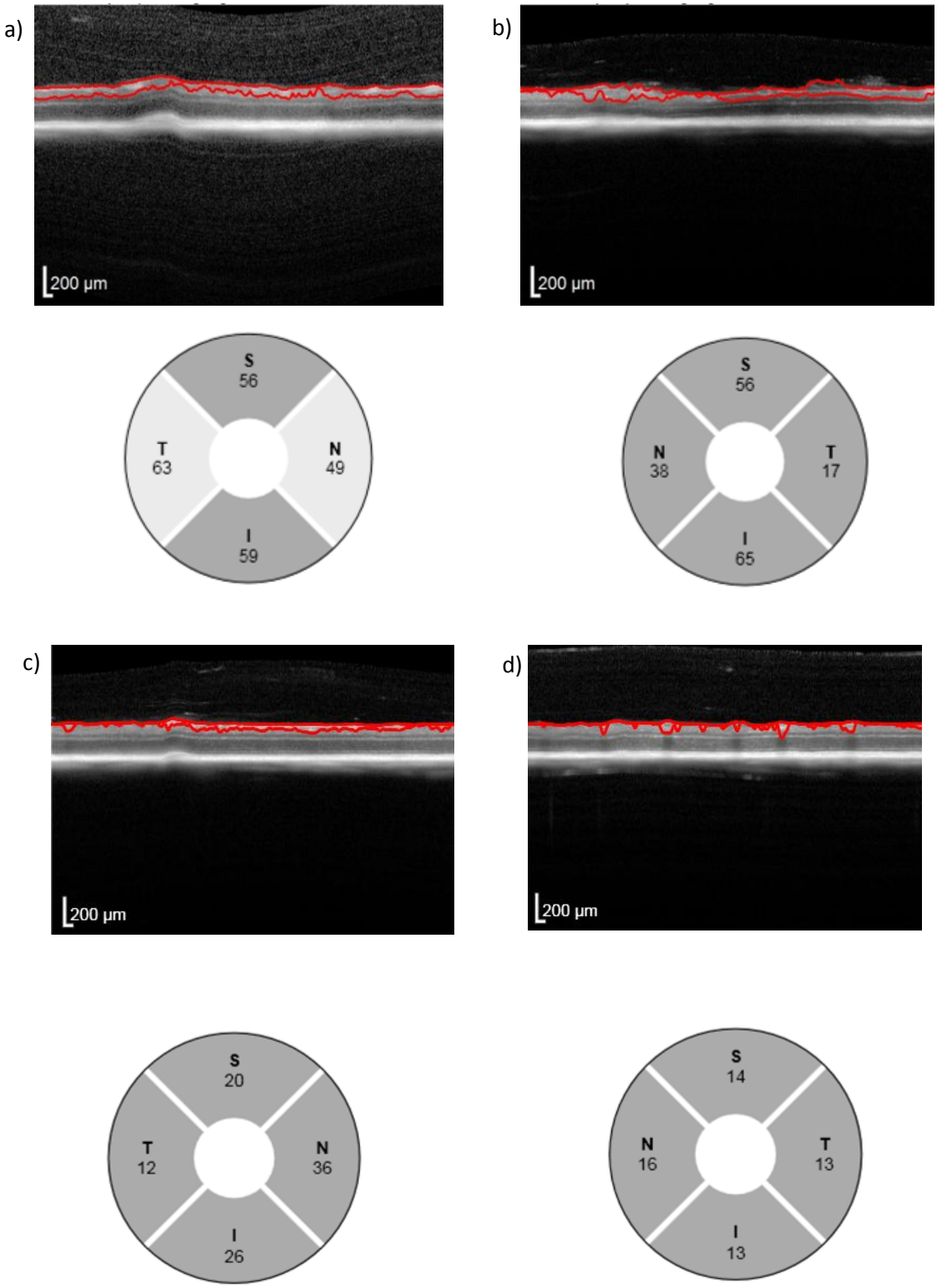

Figure 5.15 ***RNFL thickness using RNFL examination with OCT following immunisation of MOG^{TCR}xThy1CFP mice.*** *A MOG^{TCR}xThy1CFP mouse was immunised with 150ng PTX on day 0 and 2 and injected i.p. with 0.25mg MOG-specific mAb at day 14. OCT images of retina were acquired on Day 0 (right eye, a and left eye b) and Day 21 (right eye, c and left eye, d) of disease induction. Red lines indicate RNFL measured. Numbers indicate average RNFL thickness (µm) at superior (S), temporal (T), inferior (I) and nasal (N).*

Both the results of total retina thickness and RNFL thickness using OCT showed a decrease of 10µm and 12µm following immunisation of MOG^{TCR}x*Thy1*CFP mice to develop ON. There was a positive correlation between measuring changes in total retina thickness and RNFL thickness ($P>0.05$). The decrease in total retina thickness was small (4%) compared to the observed decrease in RNFL thickness (33%), which reflects the small proportion of RNFL in the total retina. Both these methods could therefore be used to assess RNFL thinning following the development of ON.

These results show the capability of the OCT to detect small changes in the RNFL of MOG^{TCR}x*Thy1*CFP mice immunised to develop ON, as predicted with the preliminary data and the high resolution of the Heidelberg Spectralis OCT. This technique can therefore be used as a longitudinal method to assess RGC damage and to study neuroprotective therapies.

5.3.3 Measuring RGC loss with cSLO

The cSLO was used to take images of the retina of MOG^{TCR}x*Thy1*CFP on day 0 and day 21, which allowed RGC density to be quantified before and after disease induction (Figure 5.16). RGC density was also quantified at the end of the experiment using retinal flatmounts. There was a significant difference between RGC density on day 0 and day 21 as quantified from cSLO images ($P<0.05$) (Figure 5.17).

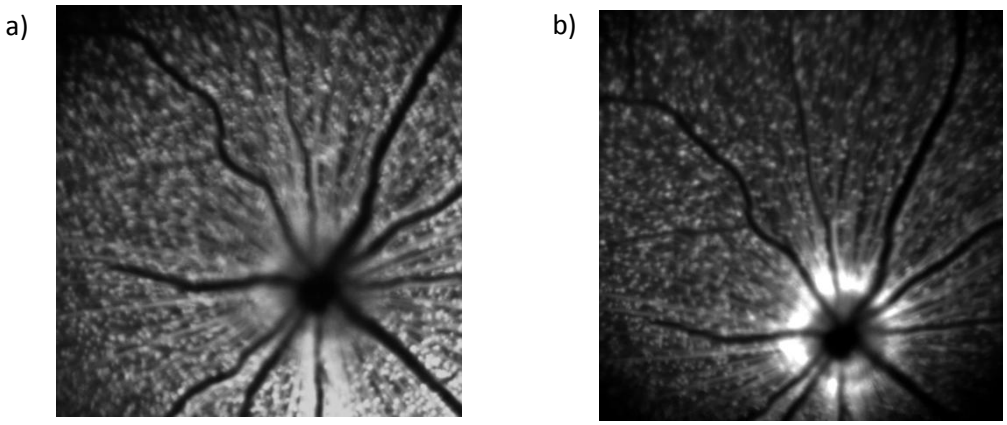

Figure 5.16 ***In vivo cSLO image of retina from MOG^{TCR}xThy1CFP mouse before and after disease induction.*** *Animals were immunised with 150ng PTX on day 0 and 2 and injected i.p. with 0.25mg MOG-specific mAb at day 14 post-disease induction. Animals were anaesthetised and retina viewed using SLO. a) Retina before disease induction on day 0, b) Retina after disease induction on day 21. Images taken over a 30° field of view and a contrast sensitivity of 80%.*

The RGC density was quantified on day 21 by cSLO images and histology images (retinal flatmounts) and were positively correlated ($P<0.05$). The density of RGC assessed by cSLO was 935±193 cells/mm^2 and the density of RGC assessed by histology was 791±173 cells/mm^2. Therefore, using the cSLO to quantify RGC loss appears to be an accurate method and is in agreement with results obtained from histological methods.

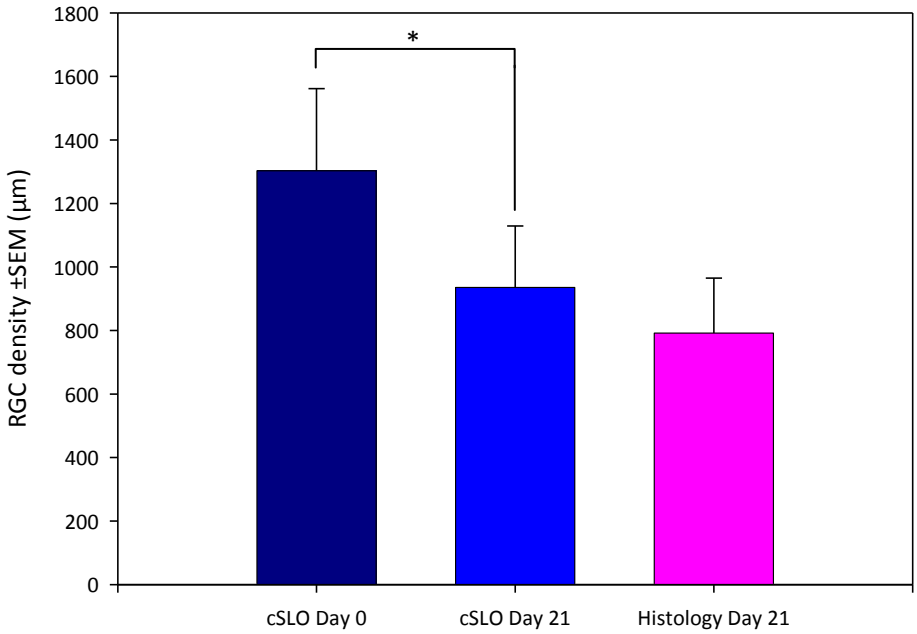

Figure 5.17 ***Decrease in RGC density measured by cSLO following immunisation of MOG^{TCR}xThy1CFP.*** *Animals were immunised with 150ng PTX on day 0 and 2 and injected i.p. with 0.25mg MOG-specific mAb at day 14 post-disease induction (n=8). RGC density of retina was quantified using images taken with cSLO on Day 0 and Day 21 of disease induction. Mice were sacrificed on day 21. Eyes were flatmounted and RGC were counted using stereology software. Plots show mean ± SEM of RGC density.*

Using the 15° field of view the cSLO can be used to detect individual RGC and can be used to detect areas of RGC loss by using the topography of the blood vessels to locate RGC (Figure 5.18).

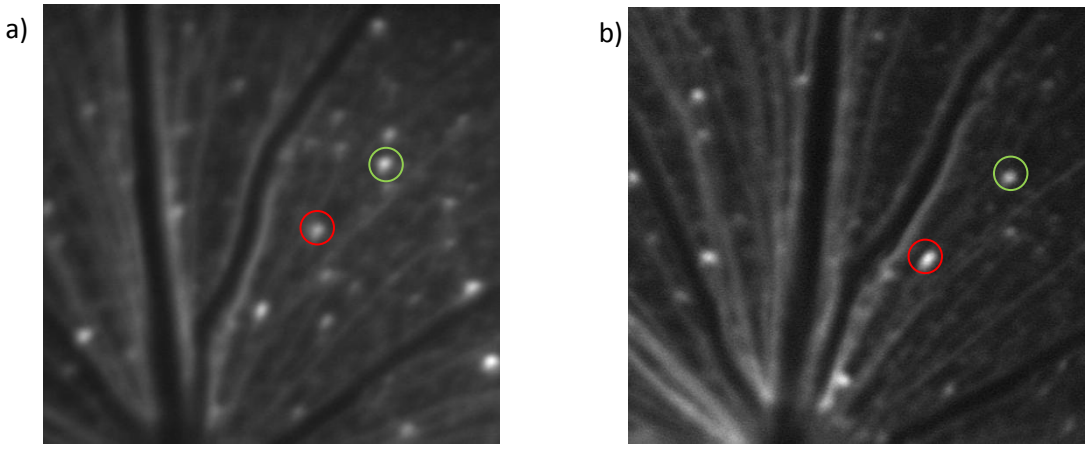

Figure 5.18 ***Repeated SLO image of retina from MOG^{TCR}xThy1CFP mouse before and after disease induction shows loss of RGC.*** *Animals were immunised with 150ng PTX on day 0 and 2 and injected i.p. with 0.25mg MOG-specific mAb at day 14 post-disease induction. Animals were anaesthetised and retina viewed using SLO. a) Example of retina before disease induction on day 0 b) Example of retina after disease induction on day 21, with fewer surviving RGC. Images taken over a 15° field of view and a contrast sensitivity of 80%. Red and green circles highlight repeated imaging of surviving RGC.*

The results acquired using the OCT and cSLO to study the level of RGC loss in MOG^{TCR}x*Thy1*CFP mice are concurrent; the decrease in the thickness of the RNFL using OCT was 32% and the decrease in RGC density using cSLO was 29%. This therefore provides further evidence that measuring RGC loss using cSLO and RNFL thinning using OCT are accurate methods to assess the disease process.

5.4 Discussion

To allow the MOG^{TCR}x*Thy1*CFP model to be used to its full potential, methods to measure RGC loss needed to be developed. This chapter investigated the ability of the cSLO and OCT to longitudinally measure RGC loss in MOG^{TCR}x*Thy1*CFP immunised to develop ON. Each of these methods successfully showed the capability to monitor disease progression and could therefore be used to study new drug therapies and assess their neuroprotective potential by serially measuring disease progression.

The preliminary data gained to assess the feasibility of using OCT to monitor RGC loss were confirmed by the positive results achieved with the Multiline OCT, which had a resolution great enough to detect small changes in the thickness of the RNFL. Capturing an OCT image of the mouse retina proved to be a quick and rapid method to understand the pathology without the killing of animals at multiple points for histological purposes. By using the cSLO to quantify RGC before disease induction on day 0 and subsequently after disease induction on day 21, will result in a more accurate assessment of the disease progression. Previous results could only take into consideration the density of RGC on day 21 using retinal flatmounts and therefore no methods were available to fully assess the degree of RGC loss. Both the cSLO and OCT results correlated well with each other signifying the loss of RGC occurs in accordance with the thinning of the RNFL. The RGC density quantified from the cSLO was also comparable with the RGC density quantified by retinal flatmounts, therefore showing an accurate method to quantify RGC density and therefore evaluate the degeneration in the visual system.

There are multiple advantages of using the cSLO and OCT to monitor RGC loss, which offers a refinement over current methods and a reduction in the number of animals used in experiments. These methods are non-invasive and result in minimal harm to the animals. The methods can be used to longitudinally monitor disease progression and therefore animals do not have to be sacrificed at time points to analyse RGC loss. In particular, the OCT could potentially be used without the need for anaesthetic therefore allowing very rapid evaluation of RNFL.

Using OCT as a method to detect RNFL thinning in the MOG^{TCR}x*Thy1*CFP offers a direct correlate of human studies, which use OCT as an outcome measure. OCT is becoming increasingly popular as an outcome measure for clinical trials in MS (Garcia-Martin et al., 2011; Keltner et al., 2011).

Evaluation of disease in mice developing optic neuritis using OCT would therefore be a valuable asset and correlate to neuroprotective clinical trials currently being carried out in humans.

However, one of the major limitations of this study is the development of media opacity during the experiment due to the anaesthetic (Calderone *et al.*, 1986). Although 2% HPMC drops were used to protect the eye from drying out, occasionally opacity was detected in mice which were examined for long periods of the time. Several lines of evidence suggest that blue light exposure can induce apoptosis both *in vivo* (Wu *et al.*, 1999) and *in vitro* (Osborne *et al.*, 2008) and may contribute to a decrease in colour contrast sensitivity (Berninger *et al.*, 1989). However, the duration of blue light exposure in this system is very short (several minutes) and rapid and therefore unlikely to induce long-term cell damage (Feng *et al.*, 2000). All the studies reported in this chapter required the use of anaesthesia to ensure the animal remained stable to allow an image to be acquired. Previous papers describe the technique without use of anaesthetic (Leung *et al.*, 2009). Although this could be easily feasible to acquire an OCT image, the cSLO currently requires a longer period of time due to the large amount of time required to scan the eye and produce a feasible image, which can be used to quantify RGC. However, rapid screening would allow serial monitoring at multiple time points. Also for convenience and to improve animal welfare, future experiments should aim to acquire images without the need for anaesthesia.

Using the cSLO it was possible to detect animals with a low number of RGC before immunisation with PTX and Z12 MOG-specific mAb, which reflects the development of spontaneous ON in a small percentage of animals, which confirmed previous reports suggesting ON occurred in 30% of MOG-specific TCR animals (Bettelli *et al.*, 2003). Therefore in future studies, exclusion criteria should be set to remove animals developing spontaneous ON from the study to reduce the variability in baseline density of RGC and allow more accurate analysis of potential drug interventions.

In summary, the OCT and cSLO offer a non-invasive method to study the CNS and longitudinally measure RGC loss throughout the development of ON in the MOG^{TCR}x*Thy1*CFP model. These methods will allow the MOG^{TCR}x*Thy1*CFP model to be studied in greater detail to understand the disease progression and will also allow new therapies to be rapidly screened for their potential neuroprotective properties.

Chapter 6

Neuroprotective treatments in MOG^{TCR}xT*hy*1CFP model

6.1 Introduction

There is clear evidence to show that axonal degeneration is a major contributor to the progressive stages of MS. Axonal loss has been shown to be related to neurological deficit (Wujek *et al.*, 2002), therefore supporting research focusing on developing protective strategies. Axonal damage and loss has also been implicated in early stages of disease (Kuhlmann *et al.*, 2002). Therefore it is crucial that research is aimed at finding neuroprotective treatments to prevent axonal damage and is used at the earliest stages of disease.

6.1.1 Voltage gated sodium channels and sodium channel blockers

Voltage gated sodium channels are present in the cell membrane of electrically excitable cells and contribute to the generation of action potentials. Sodium channels exist in several functional states: resting state, channel pore is closed; open state, channel pore is open; inactivated state, channel pore is open but unable to conduct (Catterall, 1995). There are nine different types of sodium channels, which all share a common overall motif but are expressed in different areas and have different voltage dependencies and kinetics; $Na_v1.1$, $Na_v1.3$, $Na_v1.6$, $Na_v1.9$ (neuronal), $Na_v1.4$ (muscle) and $Na_v1.5$ (cardiac) (Catterall *et al.*, 2005).

Sodium channel modulation therapy therefore has wide implications across many disorders, including affective disorders, anxiety disorders, behavioural disorders, cardiovascular disorders, CNS and PNS degenerative disorders, CNS injuries, cerebral ischemia's, chemical injuries, cognitive disorders, eyes disease and pain. In particular, sodium channel blockers have been used as therapeutic agents in a range of CNS diseases, including epilepsy, neuropathic pain, spasticity and potentially neurodegeneration (Tarnawa *et al.*, 2007). These conditions are characterised by a neuronal over-excited state, leading to an abnormal increase in sodium channel activity, which can be relieved by the blockade of sodium channels with sodium channel blockers.

6.1.1.1 The role of sodium channel blockers in neuroprotection

Mature CNS axons predominantly express $Na_v1.6$, which are the main target for neuroprotection and the focus of current research (Caldwell *et al.*, 2000). Sodium channels are clustered on the axon at a high density at the nodes of Ranvier (approximately $1000\mu m^{-2}$) and are also located at internodal domains at a lower density ($25\mu m^{-2}$) (Waxman, 1977). During demyelination $Na_v1.6$ is overexpressed and clustered within the nodal membrane (Black *et al.*, 2006). Voltage-gated sodium channels have been shown to play a significant role in the injury cascade, which leads to axonal damage and loss (Figure 6.1). During demyelination, sodium channels are redistributed and the density is reduced leading to conduction failure. Disruption of sodium channels during demyelination results in the persistent opening and an increased influx of sodium into the axon ultimately leading to axonal injury (Waxman, 2006).

In addition to the direct neuroprotective effects of sodium channel blockers, they have also been implicated in a parallel mechanism reducing the inflammatory damage. The sodium channel $Na_v1.6$ is also expressed on macrophages and microglia (Craner *et al.*, 2005). Cultured microglia treated with TTX showed a 40% reduction in phagocytic activity and Med mice, lacking functional $Na_v1.6$, show reduced activation of microglia. The role of sodium channels in inflammatory cells is unclear and is the focus of current research but could prove to be an additional target for sodium channel blockers.

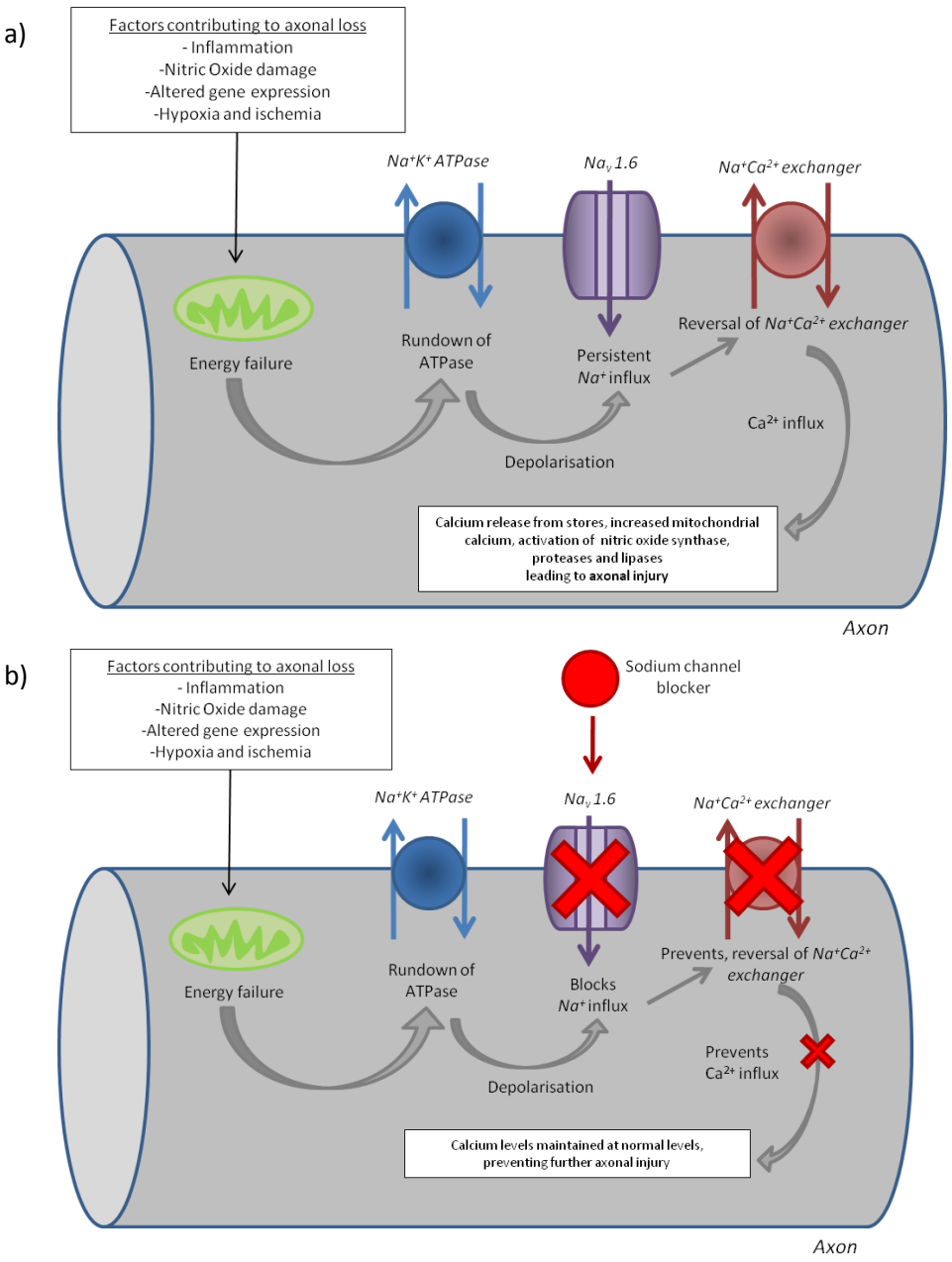

Figure 6.1 ***The role of sodium channel $Na_v1.6$ in the axonal injury cascade****. a) Several factor contribute towards the injury cascade (inflammation, nitric oxide damage, altered gene expression, hypoxia and ischemia), which lead to energy failure within the axon. Energy failure leads to the rundown of the Na^+K^+ATPase leading to depolarisation and activated $Na_v1.6$ channels, which results in persistent Na^+influx. As a result, the Na^+Ca^{2+} exchanger runs in reverse and increases intracellular Ca^{2+}levels. The rise in intracellular Ca^{2+} levels is also increased by Ca^{2+}-induced Ca^{2+} release from intracellular stores. Increased levels of Ca^{2+} are damaging to the axon and leads to activation of nitric oxide synthase, proteases and lipases resulting in axonal injury. b) Blocking of the sodium channels with a sodium channel blocker prevents the persistent Na^+ influx and the consequential reversal of Na^+Ca^{2+} exchanger and the resulting axonal injury. Figure adapted from (Black & Waxman, 2008; Waxman, 2008)*

6.1.1.2 Sodium channel blockers in EAE

There is evidence to show sodium channel blockers are effective in animal models of EAE. The sodium channel blockers phenytoin and carbamazepine were investigated in the animal model EAE for their potential to prevent axon degeneration (Black *et al.*, 2007a; Black & Waxman, 2008). Phenytoin and carbamazepine prevented axon degeneration, preserved action potential conductance and also reduced neurological deficit. However, both studies noted worsening of EAE clinical signs upon withdrawal of sodium channel blockers, which has raised doubt into the potential of sodium channel blockers to treat MS. Sodium channel blockers flecanide and lamotrigine have also been tested in rat chronic-relapsing EAE models and demonstrated protection of axons (Bechtold *et al.*, 2004; Bechtold *et al.*, 2006).

6.1.1.3 Sodium channel blockers in MS

Sodium channel blockers were initially used in MS to control positive symptoms such as trigeminal neuralgia, a pain caused by lesions on the trigeminal nerve leading to propagation of ectopic impulses (Hooge & Redekop, 1995; Sakurai & Kanazawa, 1999). However, treatment with sodium channel blockers can also lead to an increase in negative symptoms such as weakness caused by conduction block and was reported in a clinical trial of sodium channel blockers (Solaro *et al.*, 2005). The role of sodium channels in the pathogenesis of MS was highlighted by the upregulation of Nav1.6 in acute MS lesions (Waxman, 2006), which is associated with increased loading of calcium leading to damaging effects (Waxman, 2008).

A Phase II clinical trial on lamotrigine was conducted to investigate the neuroprotective effect in patients with SPMS (Kapoor *et al.*, 2010), based upon animal studies showing a neuroprotective role for lamotrigine preventing axonal damage and preserving electrophysiological function (Bechtold *et al.*, 2006). However, the results of the trial showed no change in EDSS score and the primary outcome measured changes of partial cerebral volume with no significant changes. Changes in brain volume were complex and raised questions about the underlying mechanisms and its relationship with neurodegeneration. The negative outcome of this trial was partially attributed to the limited tolerability of lamotrigine, the high dropout rate and also the observed pseudoatrophy in the treated group, probably secondary to an anti-inflammatory effect that reduced oedema.

6.1.2 Apoptosis and caspases

Apoptosis is a form of cell suicide characterised by distinct cellular changes (condensation and fragmentation of nuclear chromatin, membrane blebbing, dilation of endoplasmic reticulum, decrease in cell volume and changes in plasma membrane permeability) which result in phagocytosis of apoptotic cells (Arends & Wyllie, 1991).

6.1.2.1 The role of caspases in neuroprotection

Caspases (cysteine-dependant aspsartate-directed proteases) are a family of cysteine proteases that are involved in the apoptotic pathway, triggered by pro-apoptotic signals leading to the disassembly of the cell (Thornberry & Lazebnik, 1998). There are 12 caspases in total which each share an oligomerisation motif for the caspase recruitment domain and death effector domain.

Caspases are synthesised as inactive pro-caspases and are activated following cleavage at aspartate cleavage sites and hydrolyze key proteins in the progression of apoptosis (Cohen, 1997; Weaver et al., 1996). There are two types of caspases; initiators (cleave inactive effector caspases to activate) and effectors (cleave other proteins in apoptotic cascade). Caspases also have non-death functions, including maturation of red blood cells and skeletal muscle myoblasts (Lamkanfi et al., 2006).

Caspase 2 (ICH-1/Nedd2) acts as both an 'initiator' and an 'effector' caspase and was originally identified as a down regulated gene in neural precursor cells during development of the mouse brain (Kumar et al., 1992). It was later identified to show sequence conservation at the active site with caspase-1 (Kumar et al., 1994). There are several other lines of evidence to suggest caspase 2 is involved in apoptosis; caspase 2 induces cell death when over expressed (Wang et al., 1994), is activated early in the apoptotic pathway (Harvey et al., 1997) and caspase 2 inhibition results in delayed cell death (Kumar, 1995).

6.1.2.2 Caspases in disease

Caspases have been implicated in apoptotic cell death in a range of neurodegenerative disorders. Studies have shown that neurons exposed to degeneration lacking caspase 2 result in inhibition of apoptosis and ultimately increased neuronal survival (Tiwari et al., 2011). Caspase 1 and 3 have

been shown to mediate axonal damage and cell death in EAE and in particular, caspase 3 has been proposed as an important target for caspase 3 inhibitors to prevent neurodegeneration in MS (Ahmed et al., 2002). In Alzheimer's disease, caspase 2 is upregulated, suggesting neuronal damage occurs by an apoptotic dependant manner and also proposing a target for caspase inhibitors (Shimohama et al., 1999).

In this particular study, the focus is upon the role of caspase 2 in RGC death occurring in the retina following ON. Previous studies show morphological changes occurring during RGC death (chromatin condensation and formation of apoptotic bodies) are evidence that cell death occurs by apoptosis and revealed an important role for the caspase family in the execution phase (Quigley et al., 1995). Specifically, it has been demonstrated that caspase 2 was expressed in RGC undergoing apoptosis following ischemia injury and plays an important role in apoptotic mechanisms (Kurokawa et al., 1999).

6.1.3 Aims and Objectives

The objective of this chapter was to test whether the MOG^{TCR}x*Thy1*CFP transgenic model was responsive to drug therapy; the further aim was to identify therapeutic strategies which could potentially be developed towards a drug candidate for future clinical trials in MS patients. The two main neuroprotective strategies which were investigated in this model were sodium channel blockers and small interfering RNA (siRNA) against Caspase-2.

6.2 Materials and Methods

6.2.1 Animals

MOG^{TCR}x*Thy1*CFP transgenic mice as described in Chapter 3 were used for all experiments. All experiments were performed according to UK Animals (Scientific Procedures) Act 1986.

6.2.2 Immunisation

MOG^{TCR}x*Thy1*CFP transgenic mice were immunised as described in Chapter 3 to achieve optimal disease activity to study neuroprotective drugs. Animals were immunised with a combination of PTX and Z12 MOG-specific mAb (Figure 6.2).

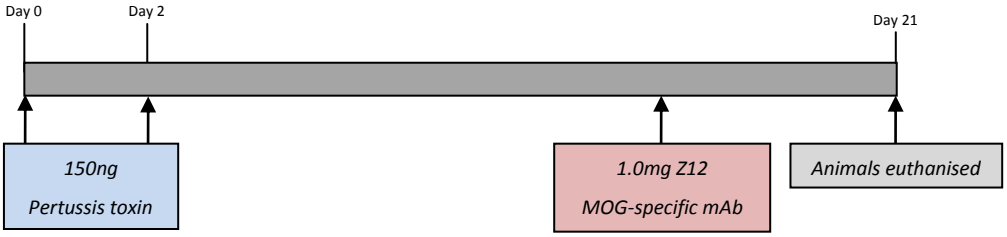

Figure 6.2 ***Immunising protocol used to immunise MOG^{TCR}xThy1CFP mice.*** *Animals immunised with 150ng PTX on day 0 and 2, injected with 1mg Z12 MOG-specific mAb on day 14. All animals were sacrificed on day 21.*

The primary experimental outcome was quantification of RGC loss and the secondary outcome was the neurological EAE score.

6.2.3 Drug preparations

Several sodium channel blockers were studied for their neuroprotective potential in the MOG^{TCR}x*Thy1*CFP mouse.

6.2.3.1 Carbamazepine

Carbamazepine (CBZ) (5H-Dibenz[b,f]azepine-5-carboxamide) blocks voltage sensitive sodium channels in their inactivated state, which are responsible for the propagation of action potentials (Schauf *et al.*, 1974; Willow & Catterall, 1982) (Figure 6.3). CBZ is an anticonvulsant and mood stabilising drug primarily used for the treatment of epilepsy, bipolar disorders and trigeminal neuralgia. CBZ is available as a white powder and is insoluble in water but soluble in ethanol.

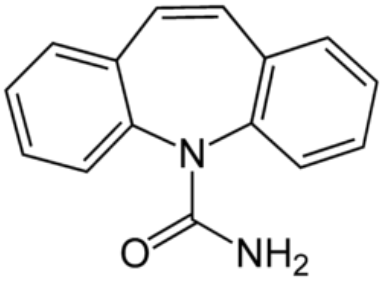

Figure 6.3 ***Chemical structure of Carbamazepine****. Empirical formula $C_{15}H_{12}N_2O$.*

CBZ (Sigma-Aldrich Ltd, Poole, Dorset, UK) was diluted in a 1:1 dilution of PBS and DMSO (dimethyl sulfoxide) (Sigma-Aldrich Ltd, Poole, Dorset, UK) and administered i.p. daily in 100µl at a concentration of 10mg/kg from day 0. Animals treated with vehicle were injected i.p. with 100µl of 1:1 dilution of PBS and DMSO. This vehicle had been used in ABH mice previously without adverse influences on onset of severity of EAE (Polak *et al.*, 2005).

6.2.3.2 Oxcarbazepine

Oxcarbazepine (OXC) (10,11-Dihydro-10-oxo-5h-dibenz[b,f]azepine-5-carboxamide) is structurally related to CBZ, with the addition of ketone in the dibenzazepine ring (Figure 6.4). OXC was developed as a valuable alternative from CBZ to reduce its associated adverse effects but retain its neurologic effect and is used as a primary treatment of epilepsy (Dam *et al.*, 1989). OXC is not oxidatively metabolised and therefore does not induce hepatic enzymes, leading to fewer unwanted drug-drug interactions and breakdown of the compound as found with CBZ (Scwabe, 1994). OXC is poorly soluble in water, ethanol and ether and is partly soluble in acetone,

chloroform, dichloromethane and methanol. OXC is a pro-drug, which is metabolised to eslicarbazepine (Dulsat *et al.*, 2009) and the pharmacological effect is mediated through its monohydroxy molecule (MHD), which induces blockade of voltage sensitive sodium channels. This leads to inhibition of repetitive neuronal discharges and reduces the propagation of synaptic pulses.

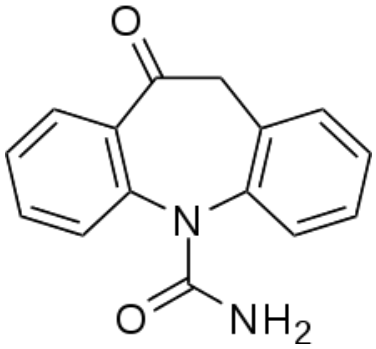

Figure 6.4 ***Chemical structure of Oxcarbazepine****. Systematic name 10,11-dihydro- 10-oxo- 5*H*-dibenz(b,f)azepine- 5-carboxamide. Empirical formula* $C_{15}H_{12}N_2O$

Oxcarbazepine (Sigma-Aldrich Ltd, Poole, Dorset, UK) was diluted in a 1:1 dilution of PBS and DMSO (dimethyl sulfoxide) and administered i.p. daily in 100µl at a concentration of 10mg/kg from day 0. Animals treated with vehicle were injected i.p. with 100µl of 1:1 dilution of PBS and DMSO.

6.2.3.3 CFM1604

Newly designed and synthesised sodium channel blockers based on first generation sodium channel blockers (carbamazepine, lamotrigine, phenytoin) have been developed with more potent and selective neuroprotective activity (Clutterbuck *et al.*, 2009). From these studies, a new compound CFM1604 was formulated and supplied by Dr. David Selwood, Biological and Medicinal Chemistry, The Wolfson Institute for Biomedical Research, UCL, London, UK. CFM1604 is an indazole derivative (Figure 6.5), which has potential as a neuroprotective voltage dependant sodium channel modulator. CFM1604 is a high affinity, non-selective, state dependant sodium channel blocker, which is only active during the inactive phase of voltage-gated sodium channel modulation (Table 6.1).

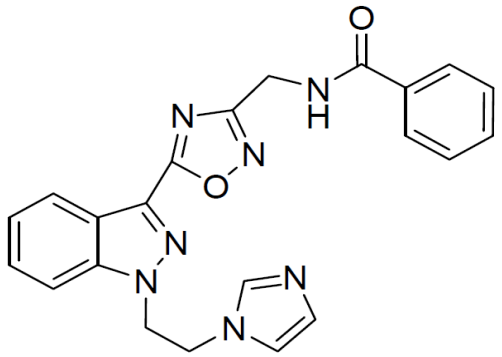

Figure 6.5 ***Chemical structure of CFM1604.*** *Systematic name N-((5-(2-(2-(1h-imidazol-1-yl)ethyl)-2h-indazol-3-l)-1,2,4-oxadiazol-3-yl)methyl)-3-methylbenzamide. CFM1604 is an idazole derivative based upon the above structure. Derivatives are made by substitutions of chemical groups onto R^1 to R^4 branches.*

Physical Properties		**Value**
Rotational bonds lipophilicity	LogP	1.8
Total polar surface area	tPSA	100Å^2
Aqueous solubility	LogS	-5.5
Affinity in inactivated state Nav1.1 Nav1.3 Nav1.5 Nav1.6 Nav1.7 Nav1.8	IC_{50} (µm)	 19.66 26.49 21.39 21.31 14.68 27.52

Table 6.1 ***Physical properties of CFM1604****. Physical properties of lipophilicity, polar surface area, aqueous solubility and receptor affinities.*

CFM1604 was diluted in a 1:1:16 dilutions of ethanol (Sigma-Aldrich Ltd, Poole, Dorset, UK), cremaphore (Sigma-Aldrich Ltd, Poole, Dorset, UK) and PBS and administered i.p. daily in 100µl at a concentration of 5mg/kg from day 0. Animals treated with vehicle were injected i.p. with 100µl of 1:1:16 dilution of ethanol, cremaphore and PBS.

6.2.3.4 Vehicles

A study was conducted to investigate the potential unwanted neuroprotective effects of vehicles. The following vehicles were used:

1) Ethanol, cremaphore and PBS (Sigma-Aldrich Ltd, Poole, Dorset, UK) in a 1:1:16 dilution.

2) 0.5% hydroxypropyl methylcellulose (HPMC) (Sigma-Aldrich Ltd, Poole, Dorset, UK) and 0.25% Tween.

3) Dimethyl sulfoxide (DMSO) and PBS (Sigma-Aldrich Ltd, Poole, Dorset, UK) in a 1:1 dilution.

6.2.4 Immunohistochemistry

Eyes were dissected and cryoprotected as described in Section 2.2.4.1. Frozen sections were thawed for 30 minutes at room temperature and then immunostained using the following protocol:

1) Samples were fixed in 100% ethanol for 1 minute and washed 2 x 5 minutes in PBS.
2) Samples were permabilised in 0.1% Triton X-100 in PBS for 10 minutes and washed 3 x 5 minutes in PBS.
3) Blocked in 3% bovine serum albumin (BSA) in PBS containing 0.05% Tween 20.
4) Primary antibody was added to samples and incubated overnight at 4°C followed by a wash 3 x 5 minutes in PBS. Two different primary antibodies were used:
    a. Active Caspase-2 at a 1 in 200 dilution rabbit polyclonal IgG (ab2251 - Abcam, Cambridge, UK).
    b. Total Caspase-2 at a 1 in 400 dilution rabbit polyclonal IgG (sc-623 Santa Cruz
5) Secondary antibody Alexa Fluor 488 donkey anti-rabbit IgG (H+L) at a 1 in 1000 dilution (A-21206 – Invitrogen, Paisley, UK) added was added to samples and incubated for one hour at room temperature and washed 3 x 5 minutes in PBS.
6) Sections were placed on slides and mounted in Vectashield with DAPI.
7) Sections were imaged using a Zeiss LSM 510 confocal laser scanning microscope.

6.2.5 Intravitreal injections

Caspase-2 small interfering RNA (siRNA) and control nonsense siRNA were provided by Quark Pharmaceuticals, California, USA in collaboration with Dr. Zubair Ahmed, University of Birmingham. A fine tip glass pipette was used to inject the siRNA into the mouse eye. Using a P2 micropipette and a long fine tip, the glass pipette was loaded with 2µl of siRNA. The mouse was briefly anaesthetised in an isofluorane chamber until eye flick response had stopped and the mouse showed signs of slowed breathing. The mouse was removed from the chamber and a small nose cone was used to maintain a low level of anaesthesia throughout the procedure. Using forceps the eye was exposed and the glass pipette needle was inserted into the vitreous (Figure 6.6). The glass pipette tip was attached to rubber tubing connected to a syringe which was compressed to allow the siRNA to be injected into the vitreous. The glass pipette tip was removed and the animal was left to recover in its cage. Animals were injected in both eyes on day 0 and 10 of disease.

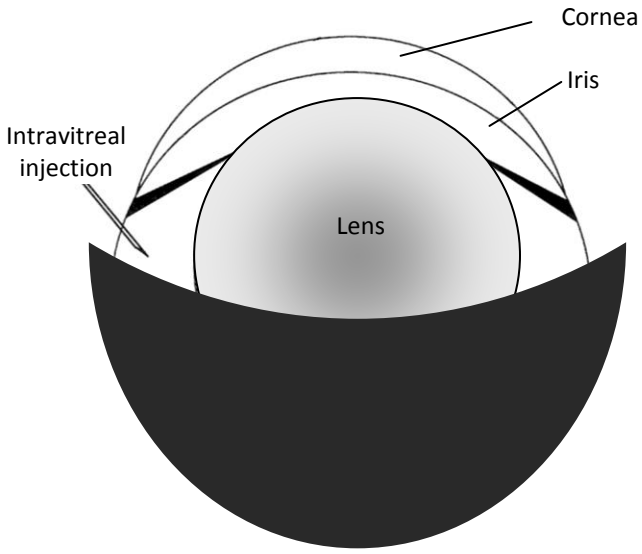

Figure 6.6 ***Schematic diagram of intravitreal injection into the mouse eye.*** *Using forceps the eye is exposed and the needle is inserted through the eye into the vitreous cavity.*

6.2.6 Statistical analysis

Statistical analysis was performed in SigmaStat 3.1. Results were presented as mean values ± standard error of mean. Differences between EAE scores in multiple groups was analysed by Kruskal-Wallis non-parametric ANOVA tests with Dunn's post test. Differences between RGC loss in multiple groups was analysed by one-way ANOVA with Bonferonni post-test. Results was considered significantly different if the probability level $P<0.05$ (*), $P<0.01$(**) or $P<0.001$(***) was reached between groups.

6.3 Results

6.3.1 Carbamazepine treatment

The neuroprotective effect of CBZ treatment was investigated in immunised MOG^{TCR}x*Thy1*CFP mice. Animals were divided into three groups; MOG^{TCR}x*Thy1*CFP no treatment, vehicle treatment and CBZ treatment. Treatment with CBZ reduced the severity, onset and the number of animals developing neurological EAE (Figure 6.7). Animals receiving no treatment showed signs of a weight decrease following Z12 MOG-specific mAb on day 14; however the other two groups remained relatively constant despite the development of EAE in several animals (Figure 6.7).

The difference in the density of RGC following treatment with CBZ was not statistically different to vehicle treated groups or MOG^{TCR}x*Thy1*CFP controls (Figure 6.8). However, the CBZ treated group showed a greater average density of RGC compared to MOG^{TCR}x*Thy1*CFP, suggesting a trend towards neuroprotection with CBZ.

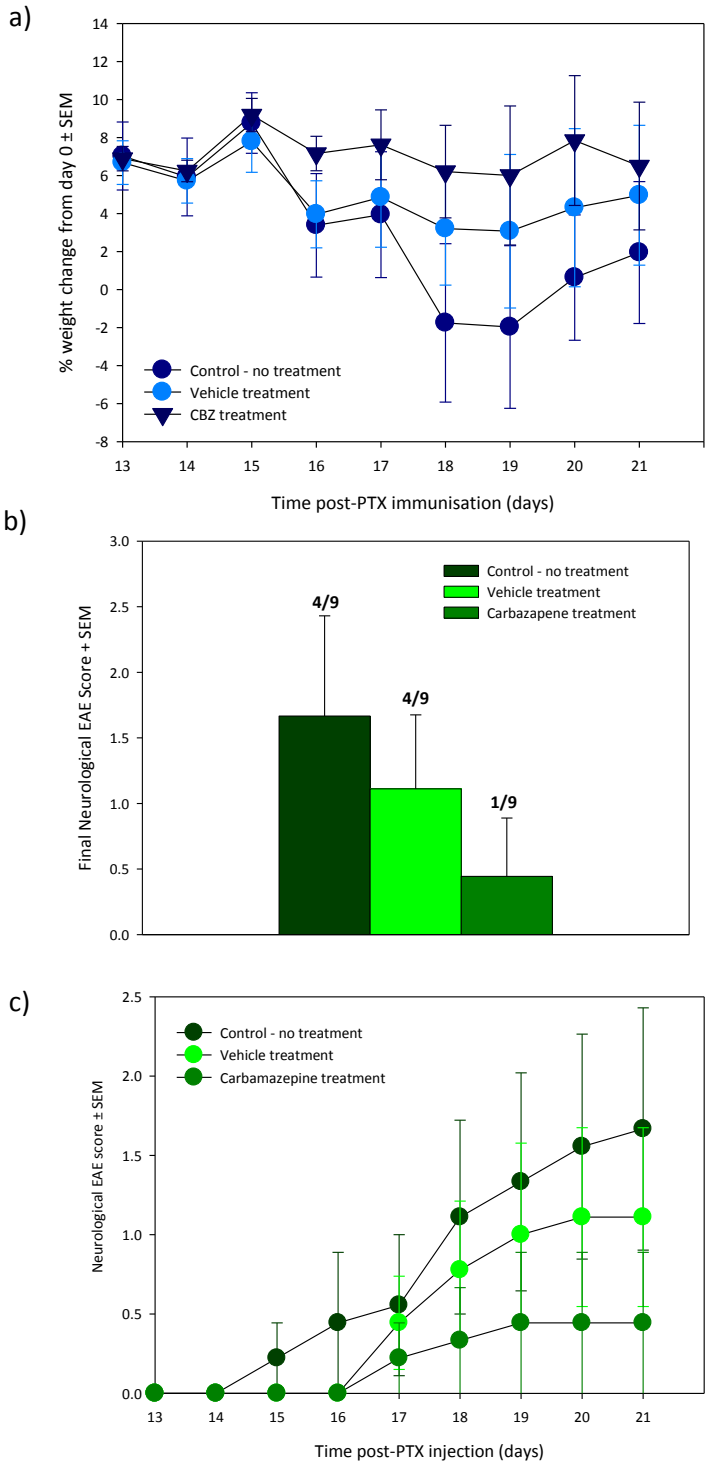

Figure 6.7 ***Neurological EAE development and weight changes in immunised MOG^{TCR}xThy1CFP mice following injection of CBZ and vehicle.*** *MOG^{TCR}xThy1CFP transgenic mice were immunised with 150ng* Pertussis toxin *on day 0 and 2, followed by 0.25mg Z12 MOG-specific mAb on day 14 post-disease induction. Groups of mice received the following: no treatment (n=9), 100µl daily dose of vehicle (50% PBS:DMSO) (n=9) or 100µl 10mg/kg Carbamazepine (dissolved in 50% PBS:DMSO) (n=9). Mice were sacrificed on day 21. a) Percentage weight changes following Z12 MOG-specific mAb, b) Final neurological EAE scores on day 21, c) Development of EAE following Z12 MOG-specific mAb.*

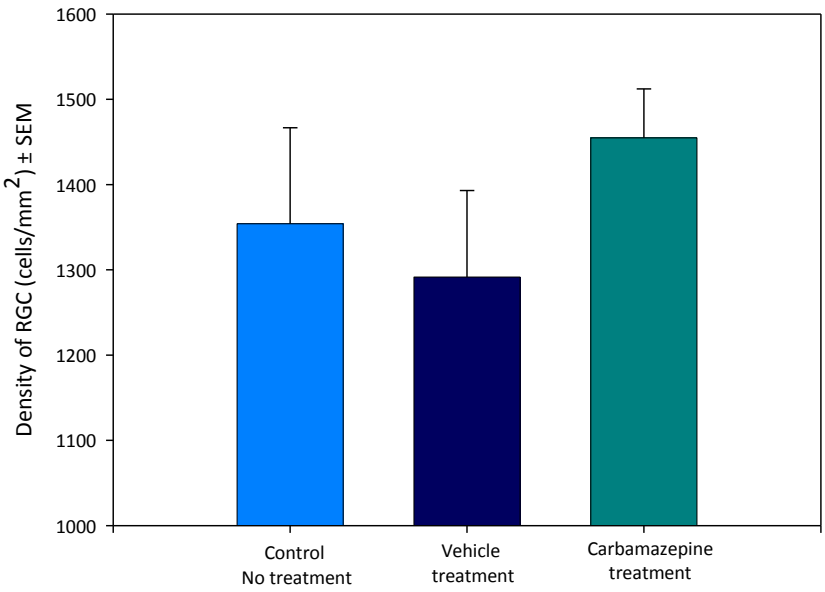

Figure 6.8 ***RGC loss in immunised MOG^{TCR}xThy1CFP mice following injection of CBZ and vehicle****. MOG^{TCR}xThy1CFP transgenic mice were immunised with 150ng* Pertussis toxin *on day 0 and 2, followed by 0.25mg Z12 MOG-specific mAb on day 14 post-disease induction. Groups of mice received the following: no treatment (n=9), 100µl daily dose of vehicle (50% PBS:DMSO) (n=9) or 100µl 10mg/kg Carbamazepine (dissolved in 50% PBS:DMSO) (n=9). Mice were sacrificed on day 21. Eyes were flatmounted and RGC were counted using stereology software. Plots show mean ± SEM of RGC density.*

These results suggest that CBZ showed signs of neuroprotection against EAE and RGC loss in the retina. However, the neuroprotective capability was minimal and not significant to conclude a neuroprotective role of CBZ. The failure to produce a significant effect could be due to the high level of non-responders in the vehicle group, leading to a high average RGC density with a large amount of error. This suggested a vehicle effect of CBZ that has not been seen when the agent had been used in EAE studies in Biozzi ABH mice (Al-Izki et al., unpublished).

6.3.2 Oxcarbazepine treatment

Based on previous results with CBZ showing signs of neuroprotection, the derivative OXC was investigated for its neuroprotective effects. Animals were divided into three groups; MOG^{TCR}x*Thy1*CFP untreated control, vehicle treatment and CBZ treatment. Treatment with OXC significantly reduced the severity of animals developing neurological EAE with little effect on the number of animals developing neurological EAE (Figure 6.9). The weight remained relatively constant in each group despite the development of EAE in a small minority of animals (Figure 6.9).

The difference in density of RGC following treatment with OXC was statistically different ($P<0.05$) compared to vehicle treated groups and MOG^{TCR}x*Thy1*CFP controls (Figure 6.10). The higher density of RGC in the OXC treated group demonstrates a neuroprotective effect of OXC. There is also a higher density of RGC in the vehicle treated group compared to the MOG^{TCR}x*Thy1*CFP control. A higher RGC density in the vehicle treated group could be explained by a neuroprotective effect of the vehicle, DMSO (Di Giorgio *et al.*, 2008).

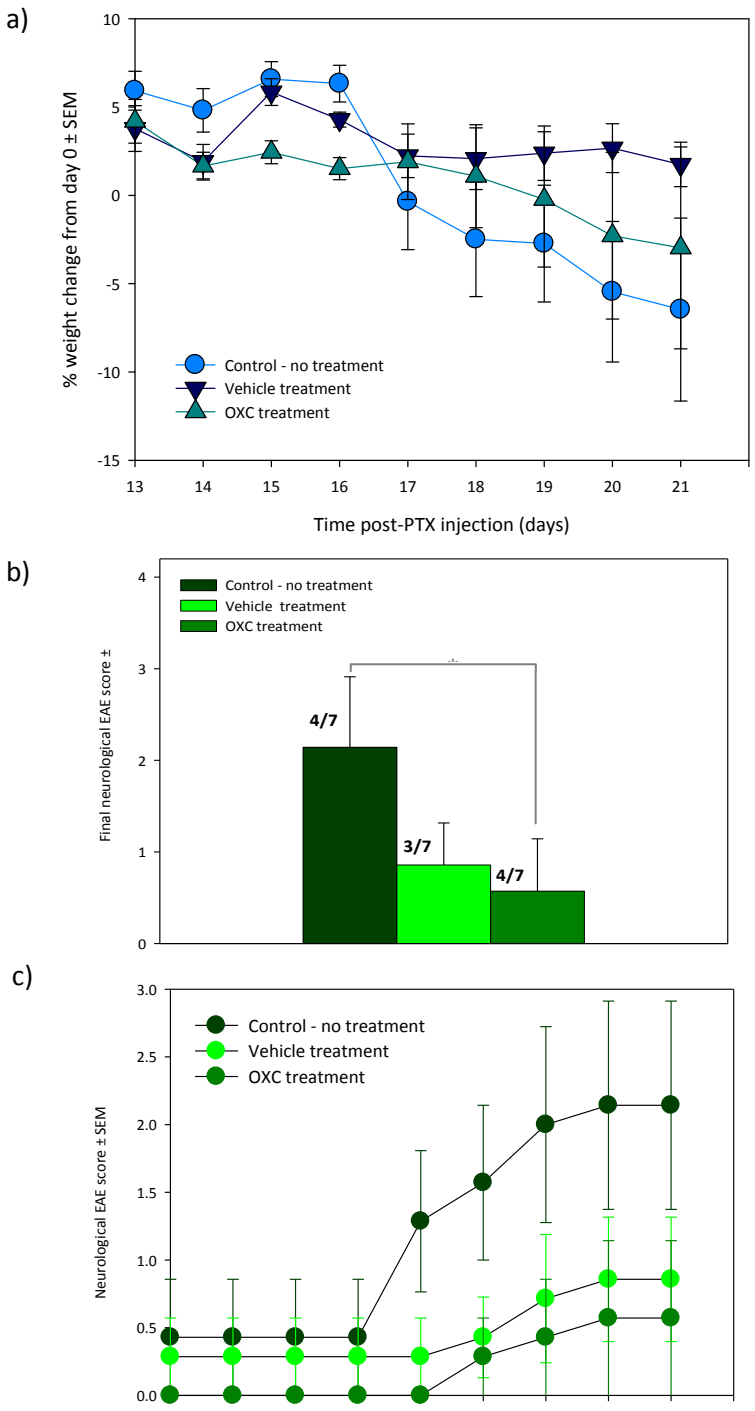

Figure 6.9 ***Neurological EAE development and weight changes in immunised MOG^{TCR}xThy1CFP mice following injection of OXC and vehicle.*** *MOG^{TCR}xThy1CFP transgenic mice were immunised with 150ng PTX on day 0 and 2 followed by 0.25mg Z12 MOG-specific mAb at day 14 post-disease induction. Groups of mice received the following: no treatment (n=7), 100µl daily dose of vehicle (50% PBS:DMSO) (n=7) or 100µl 10mg/kg Oxcarbazepine (dissolved in 50% PBS:DMS) (n=7). Mice were sacrificed on day 21. a) Percentage weight changes following Z12 MOG-specific mAb, b) Final neurological EAE scores on day 21, c) Development of EAE following Z12 MOG-specific mAb*

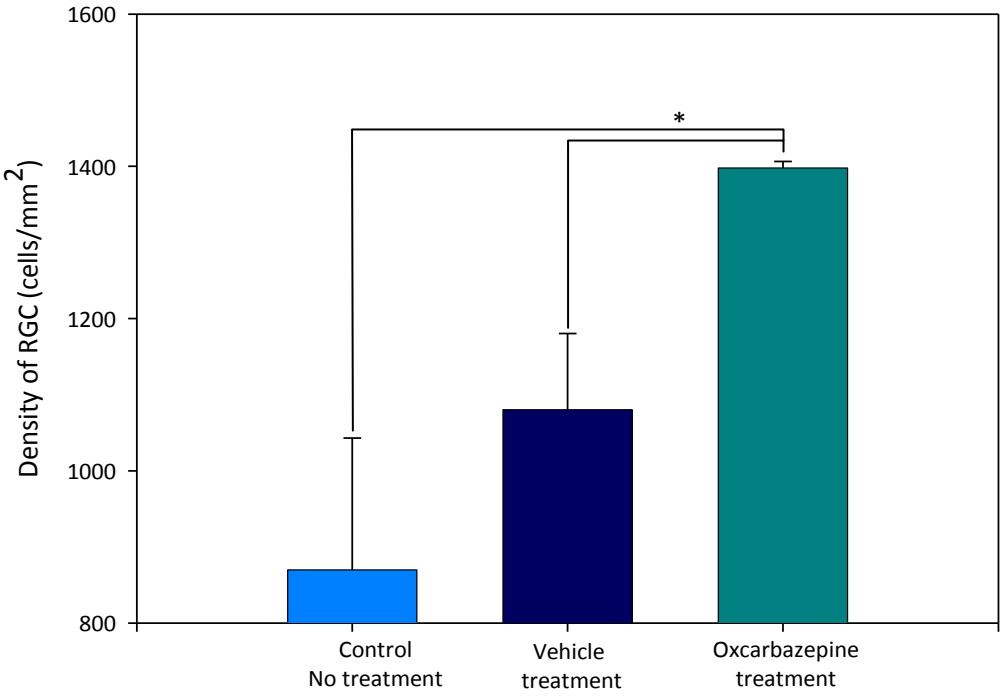

Figure 6.10 ***RGC loss in immunised MOG^{TCR}x*Thy1*CFP mice following injection of OXC and vehicle****. MOG^{TCR}x*Thy1*CFP transgenic mice were immunised with 150ng* PTX *on day 0 and 2 followed by 0.25mg Z12 MOG-specific mAb on day 14 post-disease induction. Groups of mice received the following: no treatment (n=7), 100µl daily dose of vehicle (50% PBS:DMSO) (n=7) or 100µl 10mg/kg Oxcarbazepine (dissolved in 50% PBS:DMSO) (n=7). Mice were sacrificed on day 21. Eyes were flatmounted and RGC were counted using stereology software. Plots show mean ± SEM of RGC density. *P<0.05 compared to PTX treated controls.*

Therefore, these results demonstrate that OXC has beneficial neuroprotective effects on the survival of RGC following immunisation in MOG^{TCR}x*Thy1*CFP mice developing optic neuritis. OXC also appears to have a greater neuroprotective effect than CBZ.

6.3.3 CFM1604

The novel compound CFM1604, a derivative of conventional sodium channel blockers, with CNS-targeted for its neuroprotective effects in the MOG^{TCR}x*Thy1*CFP model. Animals were divided into three groups; MOG^{TCR}x*Thy1*CFP untreated control, vehicle treatment and CFM1604 treatment. Treatment with CFM1604 had no effect on the severity and number of animals developing neurological EAE compared to untreated and vehicle treated MOG^{TCR}x*Thy1*CFP mice (Figure 6.11). The weight remained relatively constant in each group despite the development of EAE (Figure 6.11).

There was a significant difference in RGC density in the group treated with CFM1604 compared to treatment with vehicle (Figure 6.12). However the positive neuroprotective result of CFM1604 was not significantly different to the untreated group which appeared to have a large RGC density with a high level of error. Therefore it is difficult to conclude a neuroprotective role of CFM1604 based upon the uncertainty of the high RGC density in the untreated group.

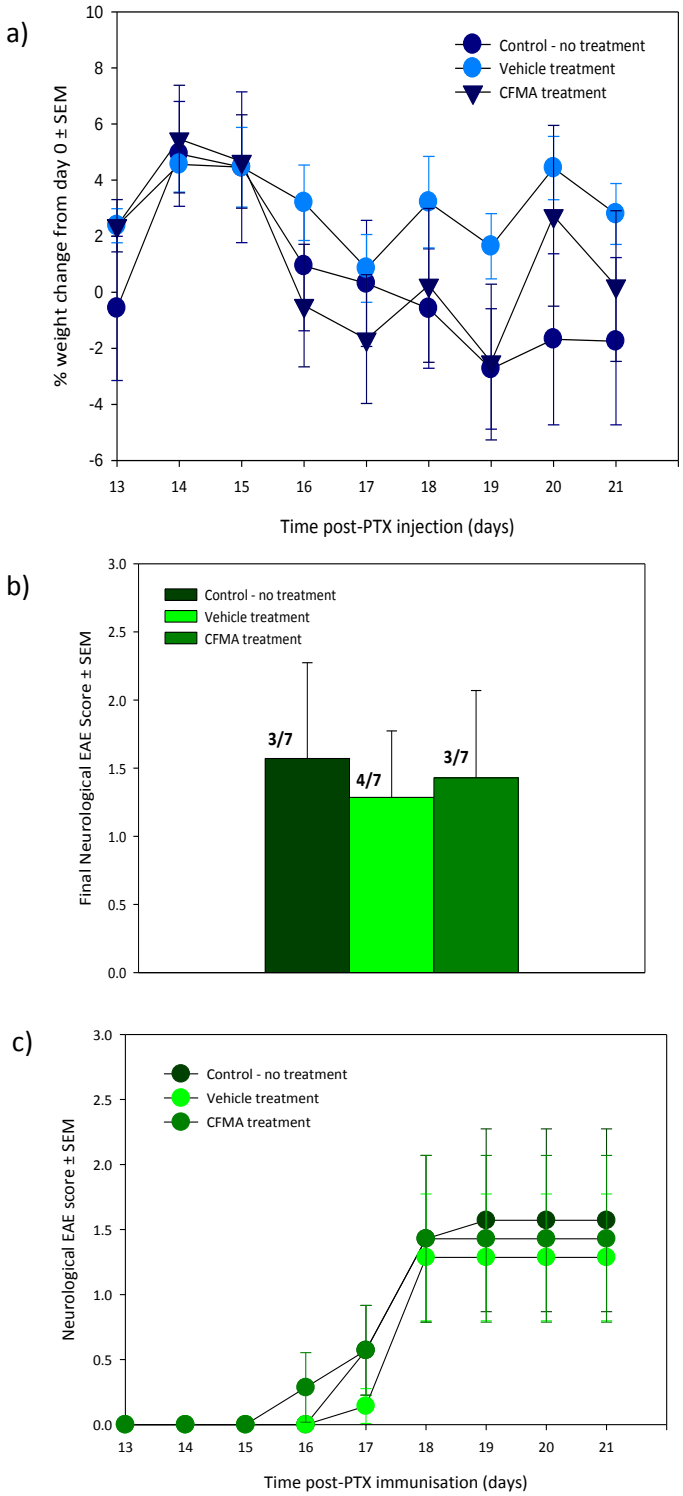

Figure 6.11 ***Neurological EAE development and weight changes in immunised MOG^{TCR}xThy1CFP mice following injection of CFM1604 and vehicle.*** *MOG^{TCR}x*Thy1*CFP transgenic mice were immunised with 150ng Pertussis toxin on day 0 and 2 followed by 0.25mg Z12 MOG-specific mAb at day 14 post-disease induction. Groups of mice received the following: MOGTCR x Thy1CFP control (n=7), 100µl daily dose of vehicle (1:1:16 alcohol, cremaphore, PBS) (n=7) or 100µl 5mg/kg CFM1604 (dissolved in 1:1:16 alcohol, cremaphore, PBS) (n=7). Mice were sacrificed on day 21. a) Percentage weight changes following Z12 MOG-specific mAb, b) Final neurological EAE scores on day 21, c) Development of EAE following Z12 MOG-specific mAb.*

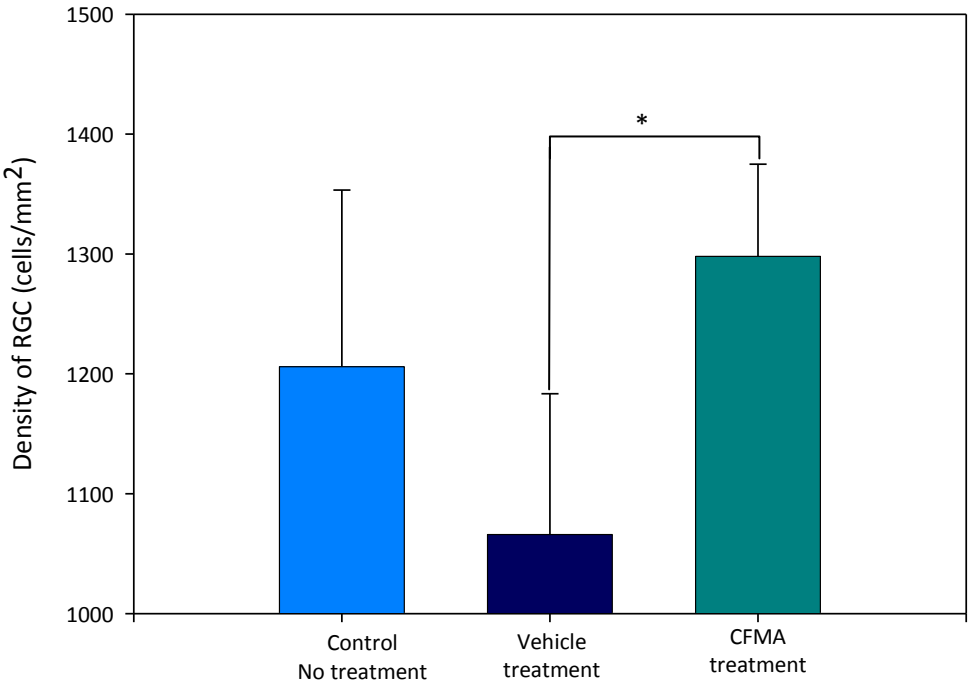

Figure 6.12 ***RGC loss in immunised MOG^{TCR}x*Thy1*CFP mice following injection of CFM1604 and vehicle****. MOG^{TCR}x*Thy1*CFP transgenic mice were immunised with 150ng* PTX *on day 0 and 2 followed by 0.25mg Z12 MOG-specific mAb on day 14 post-disease induction. Groups of mice received the following: no treatment (n=7), 100µl daily dose of vehicle (1:1:16 alcohol, cremaphore, PBS) (n=7) or 100µl 5mg/kg CFM1604 (dissolved in 1:1:16 alcohol, cremaphore, PBS) (n=7). Mice were sacrificed on day 21. Eyes were flatmounted and RGC were counted using stereology software. Plots show mean ± SEM of RGC density. *P<0.05 compared to vehicle treatment.*

6.3.4 Caspase 2 siRNA

The potential neuroprotective effect of targeting the anti-apoptotic pathway by using caspase-2 siRNA was investigated in MOG^{TCR}x*Thy1*CFP mice.

6.3.3.1 Caspase-2 staining

To establish the pathways involved in RGC death in the retinae of MOG^{TCR}x*Thy1*CFP model, immunohistochemistry was carried out on retina sections to identify factors which could potentially be targeted or neuroprotection. Based upon previous data (Personal communication with Dr. Zubair Ahmed, University of Birmingham) caspase-2 was suggested as a key factor in the apoptotic pathway in RGC (Ahmed, 2011 #1509). Therefore, immunohistochemistry with both activated and total caspase-2 staining was carried out (Figure 6.13). Activated caspase-2 recognised the carboxyterminals aspartate D316 on activated caspase-2 and total caspase-2 recognised the propeptide of caspase 2 (i.e. before caspase activation).

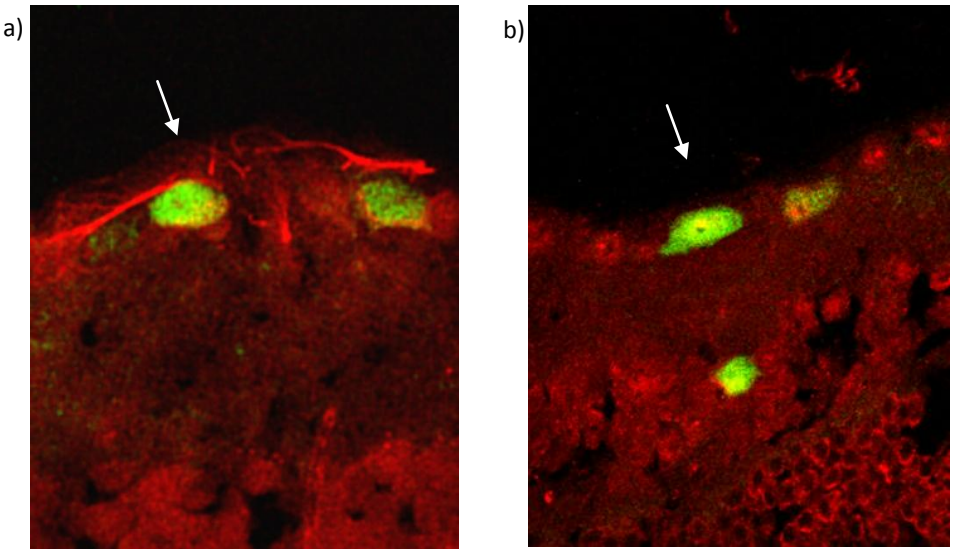

Figure 6.13 ***Total and activated caspse-2 staining in RGC.*** *MOG^{TCR}x*Thy1*CFP transgenic mice were immunised with 150ng* PTX *on day 0 and 2 followed by 0.25mg Z12 MOG-specific mAb at day 14 post-disease induction. Mice were sacrificed on day 21. Eyes were cryoprotected and sectioned. Cross sections of the retina were stained with a) total caspase-2, b) active caspase-2 and both were secondary labelled with Alex fluor 568 (Red). RGC are shown in green (arrow).*

The results show that total caspase-2 is present in the RNFL and in particular is seen in the axons and cell bodies of RGC in MOG^{TCR}x*Thy1*CFP mice. Activated caspase-2, is difficult to analyse as staining in the RGC is dependent upon capturing the correct timing in the apoptotic pathway. However, it appears that activated caspase-2 in Figure 6.13b is present and can be seen in both RGC and areas where RGC have degenerated. From these results it can be concluded that casapase-2 plays an important role in the apoptotic pathway of RGC degeneration in the MOG^{TCR}x*Thy1*CFP model of disease. Therefore future strategies should be developed to target caspase-2 activation.

6.3.3.2 Caspase-2 intravitreal injections

As the previous results showed a role of caspase-2 in the apoptotic pathway of RGC, siRNA against caspase-2 was used and its neuroprotective potential analysed. Animals were divided into three groups; untreated, vehicle treatment (scrambled siRNA) and capase-2 siRNA treatment. Treatment with caspase-2 siRNA and control siRNA appeared to reduced the severity and number of animals developing neurological EAE compared to untreated MOG^{TCR}x*Thy1*CFP mice (Figure 6.14).

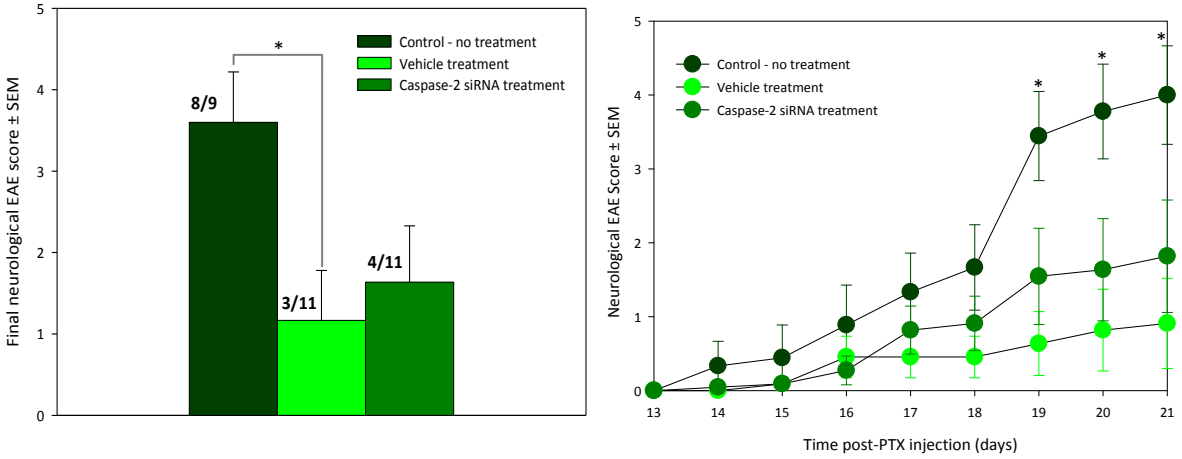

Figure 6.14 ***Neurological EAE development in immunised MOG^{TCR}xThy1CFP mice following intravitreal injection of caspase-2 siRNA and vehicle siRNA.*** *MOG^{TCR}x*Thy1*CFP transgenic mice were immunised with 150ng* Pertussis toxin *on day 0 and 2 followed by 0.25mg Z12 MOG-specific mAb on day 14 post-disease induction. Groups of mice received the following: no treatment (n=9), 2µl control siRNA (vehicle treated) on day 0 and 10 (n=11) or 2µl caspase-2 siRNA (n=11). Mice were sacrificed on day 21. Final neurological EAE scores expressed as mean ± SEM.*

Treatment with capase-2 siRNA had a highly significant effect on the increased survival of RGC compared to MOG^{TCR}x*Thy1*CFP mice with no treatment (Figure 6.15). However, these results also show animals treated with control siRNA promoted the survival of RGC and a clear vehicle effect (RGC density of vehicle was 834 cells/mm^2 compared to control, which was 296 cells/mm^2), which needs to be taken into consideration.

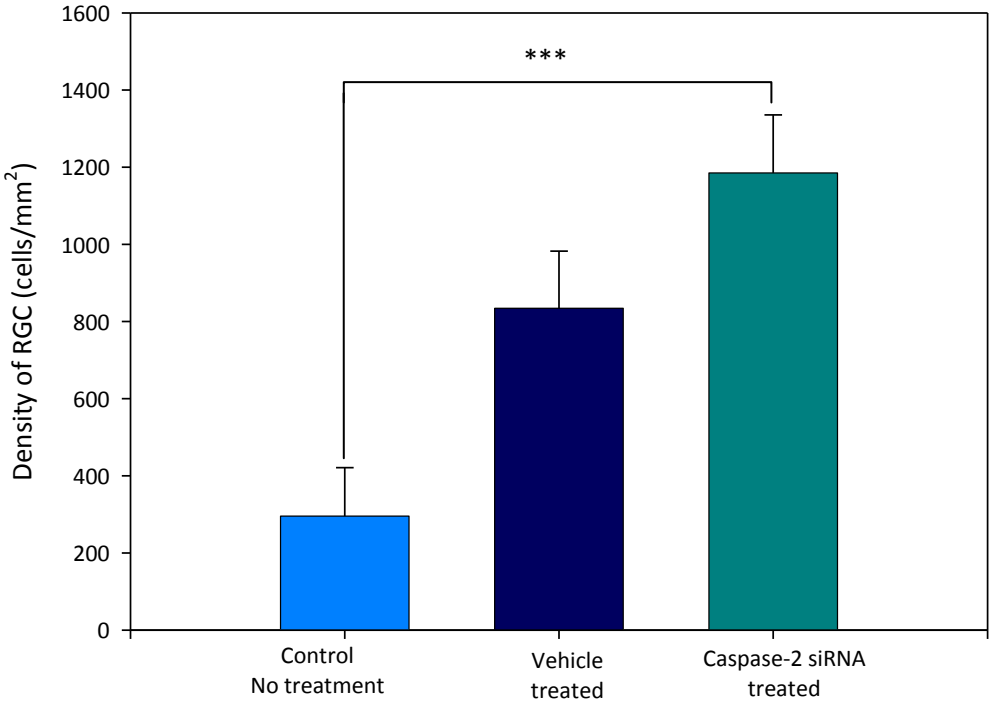

Figure 6.15 ***RGC loss in immunised MOG^{TCR}xThy1CFP mice following intravitreal of caspase-2 sRNA****. MOG-TCR x Thy1CFP transgenic mice were immunised with 150ng PTX on day 0 and 2 followed by 0.25mg Z12 MOG-specific mAb at day 14 post-disease induction. Groups of mice received the following: untreated (n=8), 2µl control siRNA (vehicle) at Day 0 and 10 (n=10) or 2µl caspase-2 siRNA at Day 0 and 10 (n=10). Mice were sacrificed on day 21. Eyes were flatmounted and RGC were counted using stereology software. Plots show mean ± SEM of RGC density. ***P<0.001 compared to PTX treated control.*

In conclusion, caspase-2 siRNA shows the potential to increase the survival of RGC and be neuroprotective. However, these results need to be interoperated with caution due to the high neuroprotective effect of the vehicle treated group. The vehicle effect could possibly be due to damage caused by intravitreal injection leading to an inflammatory response and the activation of growth factors, which offer a form of neuroprotection. Therefore, the vehicle effect needs to be addressed and approaches made in future experiments to reduce this effect.

6.3.5 Neuroprotective effects of vehicles

Some of the previous results suggested a disease modifying neuroprotective effect of vehicles, therefore the effect of different vehicles on development of EAE was analysed. To determine the vehicle with the least neuroprotective effect, the following vehicles were investigated for their properties to attenuate the development of neurological EAE compared to daily treatment with OXC; Vehicle 1 (0.5% HPMC, 0.25% Tween in dH2O), vehicle 2 (ethanol, cremaphore, PBS 1:1:16), vehicle 3 (DMSO, PBS 1:1) (Figure 6.16).

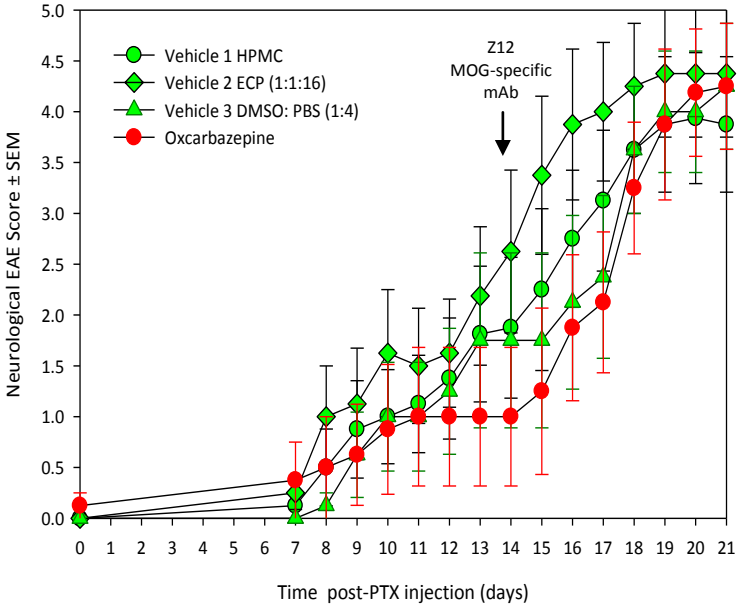

Figure 6.16 ***Neurological EAE development in immunised MOG^{TCR}xThy1CFP mice following injection of OXC and vehicle.*** *MOG^{TCR}xThy1CFP transgenic mice were immunised with 150ng PTX on day 0 and 2 followed by 0.25mg Z12 MOG-specific mAb on day 14 post-disease induction. Groups of mice received the following: Vehicle 1 (100µl daily dose of 0.5% HPMC, 0.25% Tween in dH$_2$O) (n=8), Vehicle 2 (100µl daily dose of Ethanol, cremaphore, PBS 1:1:16) (n=8), Vehicle 3 (100µl daily dose of DMSO, PBS 1:1) (n=8), Oxcarbazepine (100µl daily dose of 10mg/kg OXC dissolved in 0.5% HPMC, 0.25% Tween in dH$_2$O) (n=8). Mice were sacrificed on day 21. Neurological EAE scores expressed as mean ± SEM.*

The results show that vehicle 3 (DMSO, PBS 1:1) reduced the onset of neurological EAE to a similar extent of treatment of MOG^{TCR} animals with OXC. This suggests that DMSO is exerting an anti-inflammatory neuroprotective effect and reducing the development of neurological EAE. The results also show that vehicle 2 (ethanol, cremaphore, PBS 1:1:16) had the least effect on the development of neurological EAE. Therefore, future drug study experiments should use ethanol, cremaphore and PBS (1:1:16) as a vehicle which displays limited effect on disease activity.

6.4 Discussion

The MOG^{TCR}x*Thy1*CFP is a valuable mouse model, which can be used to test the neuroprotective properties of treatment strategies. This chapter investigated the neuroprotective properties of two conventional sodium channel blockers (CBZ and OXC), a novel sodium channel blocker (CFM1604) and a novel therapeutic strategy (caspase 2 siRNA). Each of these treatment strategies showed signs of neuroprotection and prevented RGC loss to a varying degree.

In some of these neuroprotective studies it was difficult to determine the potential of these drugs as the vehicle effect compromised any results obtained. Sodium channel blockers are highly hydrophobic and therefore have limited solubility in water, which leads to difficulties in selecting an appropriate vehicle. Both OXC and CBZ were tested using the organic solvent DMSO as a vehicle. However, both experiments showed DMSO had a moderate neuroprotective effect, which reduced the ability to make conclusions about the neuroprotective potential of the sodium channel blockers being tested. This effect has been noticed in several other studies and compounded the results of the neuroprotective treatment under investigation (Di Giorgio *et al.*, 2008). The neuroprotective effect of DMSO has been demonstrated to reduce the neurological deficit in rodent (Bardutzky *et al.*, 2005) and monkey models of cerebral ischemia (de la Torre & Surgeon, 1976) and tested in patients with severe head trauma (Karaca *et al.*, 1991). The mechanism of neuroprotection by DMSO is not clearly understood and is postulated to be due to its radical scavenging properties, which lead to a reduction in oxidative stress (Repine *et al.*, 1981). To overcome the vehicle effects of DMSO, several other vehicles were tested and found to have less of a neuroprotective effect compared to DMSO. It is therefore essential to carefully select future vehicles appropriate for the strain used, which are capable of dissolving hydrophobic drugs but still remain to have no effect.

A vehicle effect was also observed in the caspase-2 siRNA study using intravitreal injections, which highlights the complex relationship between inflammation and neuroprotection. It appears from the results that mechanical injury at the injection site can result in neuroprotection, possibly by an inflammatory mechanism. Previous studies have demonstrated a T-cell dependant neuroprotective response following immunisation of MBP-specific T cells after optic nerve crush (Moalem *et al.*, 1999). The mechanism of neuroprotection as a consequence of inflammation is postulated to be due to the release of neurotrophic factors (Hammarberg *et al.*, 2000), which is supported by other studies providing evidence that immune cells can produce NGF (Ehrhard *et al.*,

1993) and brain derived neurotrophic factor (Braun *et al.*, 1999). Similar studies have also reported the phenomenon of the immune response slowing down degeneration following ocular injections of gene therapy (Reichel *et al.*, 2001). Therefore there is a need to exclude the possibility that the immune response to intravitreal injections is responsible for neuroprotection in the MOG^{TCR}x*Thy1*CFP model. This effect could potentially be minimised with more experience resulting in a greater accuracy of intravitreal injections without leading to damage of surrounding areas and the consequential inflammation driven neuroprotection.

An observation made throughout the neuroprotective studies of MOG^{TCR}x*Thy1*CFP mice was the decreasing RGC density in untreated groups and increased frequency and severity of neurological EAE (MOG^{TCR}x*Thy1*CFP mice immunised with PTX and Z12 MOG-specific mAb). The cause of increased severity of disease is not obvious, although there are several possible explanations. There could potentially be phenotypic variability as the breeding colony develops; animals are bred with an increased copy number of the MOG^{TCR} transgene, which potentiate the susceptibility of animals to PTX and the severity and incidence of disease. However, the increased copy number of the transgene does not typically correlate with increased expression, as expression is dependent upon the integration site of the transgene. To resolve this issue, the qPCR techniques developed in Section 2.2.2.3 could be used to determine the copy number of MOG^{TCR} transgene and correlate with the development of neurological EAE and RGC density. There are also techniques which have been developed and can be used to correlate transgene copy number with expression using reverse transcription to quantify levels of transgene mRNA (Ringel *et al.*, 1998). An alternative explanation for the increased severity and incidence of disease is the presence of infections in the breeding colony of MOG^{TCR}x*Thy1*CFP mice. The compromised immune system in MOG^{TCR}x*Thy1*CFP mice would make them more susceptible to infections showing clinical signs compared to wildtype C57BL/6 mice. Pathogens present in the breeding colony include Murine norovirus (MNV), which commonly circulates in laboratory mice and is harmless to wildtype mice but can cause complications in immune deficient mice (Mumphrey *et al.*, 2007). Presence of MNV in the breeding colony could explain the increased incidence of disease in MOG^{TCR}x*Thy1*CFP mice. This issue could be resolved by re-deriving the MOG^{TCR}x*Thy1*CFP breeding colony to produce a clean, virulent free strain, which is currently being undertaken. Both of these hypotheses (increased transgene expression and presence of infections) could explain the increased incidence and severity of disease in MOG^{TCR}x*Thy1*CFP mice and they could also be working in combination to produce a noticeable effect.

The results from this chapter provide promising evidence for support of sodium channel blockers as a neuroprotective therapy in MS. Although the first large scale trial of a sodium channel blocker failed to show any significant benefit (Kapoor *et al.*, 2010) the potential of other sodium channel blockers should still be investigated. The trial targeted the late stage of disease and raised questions about the ideal phase of MS to start a neuroprotective therapy. Future clinical trials have been proposed to start treatment at the earliest signs of MS when patients present with ON who may progress on to developing MS. In summary, the results provide promising pre-clinical evidence for the use of sodium channel blockers in MS. Although it initially seems that finding a neuroprotective therapy is ambitious due to the poorly understood mechanisms of neurodegeneration, it is clear that drug treatments existing for other disorders could be used to treat people with MS.

Chapter 7

General Discussion and Conclusions

7.1 Key findings

This project met the aim to develop and characterise a novel transgenic mouse model for the study of neuroprotection and repair strategies in autoimmune disease. Initial studies defined and characterised the MOG-specific TCR transgenic mouse and an immunising protocol, to produce an appropriate model for studying neurodegeneration. The subsequent crossing with a *Thy1*CFP transgenic mouse allowed the axonal loss to be easily monitored using CFP-expressing RGC in the retina. Several *in vivo* methods were developed to longitudinally study visual dysfunction including electrophysiology, visual tracking drum, OCT and cSLO. These methods were developed as a correlate to techniques currently used to study disease progress in people with MS. The MOG^{TCR}x*Thy1*CFP mouse model was used to study the potential of sodium channel blockers for the treatment of MS and ON. Two conventional sodium channel blockers (CBZ and OXC) and a novel sodium channel blocker (CFM1604) were studied for their neuroprotective properties. The pre-clinical evidence using these drugs showed promising results; CBZ increased RGC survival by 11%, OXC increased RGC survival by 23% and CFM increased survival by 18% compared to vehicle control. These findings could potentially be translated into a treatment for people with MS.

7.2 Value of the MOG^{TCR}x*Thy1*CFP mouse model

The MOG^{TCR}x*Thy1*CFP mouse model offers multiple advantages over current animal models of autoimmune diseases and is a valuable model to study axonal loss and neuroprotection. Due to the rapid onset of disease and the short nature of experiments (approximately 21 days), new drugs can be studied and evaluated in a shorter time and their potential for further development can be assessed quickly.

Following on from the preliminary data presented in Chapters 2 and 3, the project was successfully funded by the National Centre for the Replacement, Refinement and Reduction of Animals in Research (NC3Rs) to allow methods to be developed to measure RGC loss in the animal model

therefore offering a refinement and reduction opportunity over the EAE animal model of MS. The immunising protocol developed for the MOG^{TCR}x*Thy1*CFP model results in reduced paralysis typically associated with classical EAE, therefore resulting in minimal weight loss. The system primarily affected in the MOG^{TCR}x*Thy1*CFP model is the visual system, which seems to be well tolerated by the animals and does not result in any welfare issues due to the nocturnal nature of mice, which do not rely on the visual system as a primary sense. The induction of disease in the MOG^{TCR}x*Thy1*CFP model offers a reduction of substantial procedures and is considerably milder than the typical immunising protocol used to induce EAE consisting of CFA. The development of methods to non-invasively measure disease progress reduced need for time-consuming histology and also reduced the number of animals required in an experiment. The methods also allow objective outcomes to be recorded in contrast to the subjective clinical scoring routinely carried out on EAE animals, therefore increasing the statistical power of detecting a change.

As is common with many experimental situations, this model currently has several limitations that need to be addressed. The most significant limitation of the model at this stage is the limited degree of demyelination observed in the pathology of disease, therefore preventing the model from being used to study drugs for remyelination. The results from all the experiments suggest the disease is rapid and axonal loss prevails over demyelination. To overcome this, future work would need to be carried out to adapt the immunisation protocol using immunomodulating antibodies to reduce the severity of disease to promote demyelination. Previously, this was difficult to study as it required a significant number of animals to be sacrificed at different time points to gain an understanding of the stages of the disease process. With the addition of the SLO, the disease progress can now be studied in the MOG^{TCR}x*Thy1*CFP mouse non-invasively and a greater understanding of the timing of RGC death can be achieved. Further studies to measure demyelination by measuring latency delay in the VEP response will be carried out. However, as an alternative we may adapt these protocols towards disease in the rat by administration of demyelinating antibodies resulting in marked demyelination with preservation of axons (Linington *et al.*, 1988).

A significant weakness of the MOG^{TCR}x*Thy1*CFP mouse model throughout the project was the limited number of animals available due to problems with the breeding of a double transgenic strain, resulting in experiments with low n numbers. The breeding problems with the MOG^{TCR}x*Thy1*CFP appeared to become exaggerated when a higher percentage of homozygous

mice for the MOG-specific TCR transgene were included in the breeding colony, a trend which has been observed previously in other transgenic strains (Olivares-Villagomez *et al.*, 1998). To prevent further problems occurring, the colony will require close observation and selection of healthy, robust animals as breeders. To further enhance the breeding success, immune intervention could prevent the frequency of spontaneous disease developing and improve the general health of breeding animals. Another limitation of the model which made several of the methods difficult to develop was the restrictions imposed by the size of the mouse eye. However, these difficulties were successfully overcome by adapting the lens on the cSLO/OCT machine to allow imaging of the mouse eye. In addition, with all animal models of disease there may be discrepancies between the physiology and anatomy of the mouse in comparison with the human, which may restrict the translation between the two species.

The generation of the MOG^{TCR}x*Thy1*CFP mouse model has many implications for work undertaken in this field of research and the development of drugs for people with MS. The novel model also has many implications for the welfare of animals and the way animals are used to screen new drugs. Although the current immunising protocol of the MOG^{TCR}x*Thy1*CFP mouse does not appear to result in a prolonged phase of demyelination, the model has many implications for the study of neuroprotective therapies and the drugs that were tested focused primarily on their neuroprotective potential. The need for neuroprotective therapies for MS patients is still a primary goal, even though the majority of RRMS patients are being treated more effectively with immunomodulatory drugs. Evidence shows that axonal loss occurs at early stages of MS (Filippi *et al.*, 2003) and emphasises the importance of intervening in early stages of MS. Additionally, there is demand for neuroprotective therapies for SPMS and PPMS, which is an area deprived of drug treatment. Therefore, the generation of the MOG^{TCR}x*Thy1*CFP mouse model will have significant implications on the development of neuroprotective therapies by providing a rapid screening tool to identify potential drug candidates for clinical trials and molecular targets for drug development.

7.4 Future work

There are several lines of future work that could potentially be investigated to improve and refine the MOG^{TCR}x*Thy1*CFP mouse model and the methods used to study the model. The most significant part of the model which needs modifying is the level of demyelination that occurs. Future work could utilise the cSLO and OCT to detect the critical time points of RGC damage and loss and identify a window for promotion of demyelination. Once demyelination has been established, alternative electrophysiological methods will be investigated to monitor demyelination (Cambiaghi *et al.*, 2011) and the MOG^{TCR}x*Thy1*CFP mouse model could therefore be employed to study remyelination strategies.

To achieve an animal model of demyelination, a rat model of optic neuritis could be used as the rat model of EAE has been shown to have a greater degree of demyelination and would therefore be valuable to study remyelination therapies (Meyer *et al.*, 2001). Using a rat model would also offer many advantages over the mouse due to the larger size of the eye and the methods developed in this project could be developed for a rat model. Several of the methods would be easier to use with rats, for example the head tracking behaviour of rats is more evident than mice and this would therefore be easier to detect changes in visual acuity. In addition the transfer of Z12 antibody is likely to be more demyelinating in rat compared to the degeneration in mice. However, the drawback to using a rat model is the lack of fluorescent transgenic rats available. Therefore to use the SLO to visualise the RGC it would require injection of fluorescent dye. In the future, appropriate transgenic rats could be generated and it may be feasible to generate transgenic rats that mimic the MOG^{TCR}x*Thy1*CFP mouse model. Similar transgenic rats to the *Thy1*CFP strains of mice have been developed to study axons *in vivo* (Magill *et al.*, 2010).

Another avenue of research would be to use the cSLO to complement current studies by using it to study neuroinflammation and neurodegeneration in greater detail. During the modification of the cSLO by Heidelberg Engineering, the spare filter positions were fitted with filters capable of detecting GFP and YFP. This would allow both GFP and YFP to be detected in the retina of animals. One example of how this additional capability of the cSLO could be used in the future is to detect YFP to study the degeneration process of axons and dendrites in the eye (Leung *et al.*, 2011; Li *et al.*, 2011). The transgenic mouse B6.Cg-TgN(*Thy1*-YFP)16Jrs expresses YFP under the *Thy1* promoter specifically in axons and dendrites, with limited expression in the RGC (less than 1%)

(Feng *et al.*, 2000). The *Thy1*-YFP transgenic mouse can be monitored serially using the cSLO to measure cell body area, axon diameter, dendritic field and branching complexity (Li *et al.*, 2011). From these measurements, the degree of dendritic shrinkage can be used as an early sign of RGC dysfunction (Shou *et al.*, 2003) and can therefore be used as a sensitive method to monitor neuronal degeneration and identify potential neuroprotective therapies. Taking into consideration dendritic and axonal behaviours, this method would be a more accurate evaluation of RGC degeneration, as the presence of a cell body does not directly represent a functional and an intact RGC.

The methods developed could also be used to monitor blood retinal barrier function in models of experimental autoimmune uveitis (EAU). This model can therefore be used to address the activity of agents before confirmation of activity of optimal formation to prevent neurodegeneration in EAE (Pryce *et al.*, 2003). Loss of photoreceptor cells in EAU could be monitored using OCT to measure changes in the thickness of the retina, which would be within the resolution limits of the OCT.

7.5 Conclusions

This project successfully met the aim to develop and characterise a novel transgenic mouse model for the study of neuroprotection and repair strategies in autoimmune diseases.

1. The MOG-specific TCR transgenic mouse was successfully crossed with the *Thy1*CFP transgenic mouse to produce the novel MOG^{TCR}x*Thy1*CFP mouse model that expresses fluorescent RGC and develops ON.

2. An immunisation protocol for the MOG^{TCR}x*Thy1*CFP model was developed and refined, which resulted in optimum disease activity and extensive RGC and axonal loss so the model can be ultimately for studies of neuroprotective compounds.

3. Non-invasive methods were developed which allowed the study of visual dysfunction by measuring the VEP using electrophysiology and measuring head tracking movements using the OKN drum.

4. Methods were developed to measure RGC loss by measuring thinning of RNFL using OCT and RGC density using cSLO. These methods provide an animal model correlate to concurrent human studies using cSLO and OCT.

5. Neuroprotective therapies were investigated in the form of two conventional sodium channel blockers (CBZ and OXC), a novel sodium channel blocker (CFM1604) and a novel therapeutic strategy (caspase 2 siRNA). These treatment strategies showed signs of neuroprotection and prevented RGC loss in the MOG^{TCR}x*Thy1*CFP model.

Reference List

Adelmann, M, Wood, J, Benzel, I, Fiori, P, Lassmann, H, Matthieu, JM, Gardinier, MV, Dornmair, K, Linington, C (1995). The N-terminal domain of the myelin oligodendrocyte glycoprotein (MOG) induces acute demyelinating experimental autoimmune encephalomyelitis in the Lewis rat. *Journal of Neuroimmunology* **63:** 17-27.

Ahern, GP, Hsu, S-F, Klyachko, VA, Jackson, MB (2000). Induction of Persistent Sodium Current by Exogenous and Endogenous Nitric Oxide. *Journal of Biological Chemistry* **275:** 28810-28815.

Ahmed, Z, Doward, AI, Pryce, G, Taylor, DL, Pocock, JM, Leonard, JP, Baker, D, Cuzner, ML (2002). A Role for Caspase-1 and -3 in the Pathology of Experimental Allergic Encephalomyelitis : Inflammation Versus Degeneration. *American Journal Pathology* **161:** 1577-1586.

Al-Izki, S, Pryce, G, Jackson, SJ, Giovannoni, G, Baker, D (2011). Immunosuppression with FTY720 is insufficient to prevent secondary progressive neurodegeneration in experimental autoimmune encephalomyelitis. *Multiple Sclerosis Journal* **17:** 939-948.

Alcina, A, Fedetz, Ma, Ndagire, D, FernÃ¡ndez, O, Leyva, L, Guerrero, M, Abad-Grau, MaM, Arnal, C, Delgado, Cn, Lucas, M, Izquierdo, G, Matesanz, F (2009). IL2RA/CD25 Gene Polymorphisms: Uneven Association with Multiple Sclerosis (MS) and Type 1 Diabetes (T1D). *PLoS ONE* **4:** e4137.

Alnemri, ES, Livingston, DJ, Nicholson, DW, Salvesen, G, Thornberry, NA, Wong, WW, Yuan, J (1996). Human ICE/CED-3 Protease Nomenclature. *Cell* **87:** 171-171.

Alotaibi, S, Kennedy, J, Tellier, R, Stephens, D, Banwell, B (2004). Epstein-Barr Virus in Pediatric Multiple Sclerosis. *JAMA: The Journal of the American Medical Association* **291:** 1875-1879.

Arends, M, Wyllie, A (1991). Apoptosis: mechanisms and roles in pathology. *International Review Experimental Pathology* **32:** 223-54.

Arnon, R, Teitelbaum, D, Sela, M (1989). Suppresion of experimental allergic encephalomyelitis by COP1 - relevance to multiple sclerosis. *Israel Journal Medical Science* **25:** 686-9.

Arquint, M, Roder, J, Chia, L, Down, J, Wilkinson, D, Bayley, H, Braun, P, Dunn, R (1987). Molecular cloning and primary structure of myelin-associated glycoprotein. *Proc Natl Acad Sci U S A.* **84:** 600-4.

Babbe, H, Roers, A, Waisman, A, Lassmann, H, Goebels, N, Hohlfeld, R, Friese, M, Schroder, R, Deckert, M, Schmidt, S, Ravid, R, Rajewsky, K (2000). Clonal Expansions of CD8+ T Cells Dominate the T Cell Infiltrate in Active Multiple Sclerosis Lesions as Shown by Micromanipulation and Single Cell Polymerase Chain Reaction. *Journal Experimental Medicine* **192:** 393-404.

Babinet, C, Morello, D, Renard, J (1989). Transgenic mice. *Genome* **31:** 938-49.

Balcer, LJ (2001). Clinical outcome measures for research in multiple sclerosis. *Journal of Neuro-Ophthalmology* **21:** 296-301.

Balcer, LJ, Frohman, EM (2011). Evaluating loss of visual function in multiple sclerosis as measured by low-contrast letter acuity. *Neurology* **74:** S16-S23.

Banik, N, McAlhaney, W, Hogan, E (1985). Calcium-stimulated proteolysis in myelin: evidence for a Ca2+-activated neutral proteinase associated with purified myelin of rat CNS. *Journal Neurochemistry* **45:** 581-8.

Banwell, B, Krupp, L, Kennedy, J, Tellier, R, Tenembaum, S, Ness, J, Belman, A, Boiko, A, Bykova, O, Waubant, E, Mah, JK, Stoian, C, Kremenchutzky, M, Bardini, MR, Ruggieri, M, Rensel, M, Hahn, J, Weinstock-Guttman, B, Yeh, EA, Farrell, K, Freedman, M, Iivanainen, M, Sevon, M, Bhan, V, Dilenge, M-E, Stephens, D, Bar-Or, A (2007). Clinical features and viral serologies in children with multiple sclerosis: a multinational observational study. *The Lancet Neurology* **6:** 773-781.

Bar-Or, A, Calabresi, PAJ, Arnold, D, Markowitz, C, Shafer, S, Kasper, LH, Waubant, E, Gazda, S, Fox, RJ, Panzara, M, Sarkar, N, Agarwal, S, Smith, CH (2008). Rituximab in relapsing-remitting multiple sclerosis: A 72-week, open-label, phase I trial. *Annals of Neurology* **63:** 395-400.

Barcellos, LF, Oksenberg, JR, Begovich, AB, Martin, ER, Schmidt, S, Vittinghoff, E, Goodin, DS, Pelletier, D, Lincoln, RR, Bucher, P, Swerdlin, A, Pericak-Vance, MA, Haines, JL, Hauser, SL (2003). HLA-DR2 Dose Effect on Susceptibility to Multiple Sclerosis and Influence on Disease Course. *The American Journal of Human Genetics* **72:** 710-716.

Bardutzky, J, Meng, X, Bouley, J, Duong, TQ, Ratan, R, Fisher, M (2005). Effects of intravenous dimethyl sulfoxide on ischemia evolution in a rat permanent occlusion model. *Journal Cerebral Blood Flow Metabolism* **25:** 968-977.

Barkhof, F, Calabresi, PA, Miller, DH, Reingold, SC (2009). Imaging outcomes for neuroprotection and repair in multiple sclerosis trials. *Nature Review Neurology* **5:** 256-266.

Barkhof, F, Filippi, M, Miller, DH, Scheltens, P, Campi, A, Polman, CH, Comi, G, Ader, HJ, Losseff, N, Valk, J (1997). Comparison of MRI criteria at first presentation to predict conversion to clinically definite multiple sclerosis. *Brain* **120:** 2059-2069.

Barnstable, CJ, Dräger, UC (1984). Thy-1 antigen: A ganglion cell specific marker in rodent retina. *Neuroscience* **11:** 847-855.

Bartsch, S, Montag, D, Schachner, M, Bartsch, U (1997). Increased number of unmyelinated axons in optic nerves of adult mice deficient in the myelin-associated glycoprotein (MAG). *Brain Research* **762:** 231-234.

Batoulis, H, Addicks, K, Kuerten, S (2010). Emerging concepts in autoimmune encephalomyelitis beyond the CD4/TH1 paradigm. *Annals of Anatomy - Anatomischer Anzeiger* **192:** 179-193.

Bechtold, D, Kapoor, R, Smith, K (2004). Axonal protection using flecainide in experimental autoimmune encephalomyelitis. *Annals of Neurology* **55:** 607-616.

Bechtold, D, Miller, S, Dawson, A, Sun, Y, Kapoor, R, Berry, D, Smith, K (2006). Axonal protection achieved in a model of multiple sclerosis using lamotrigine. *Journal of Neurology* **253:** 1542-1551.

Bechtold, DA, Yue, X, Evans, RM, Davies, M, Gregson, NA, Smith, KJ (2005). Axonal protection in experimental autoimmune neuritis by the sodium channel blocking agent flecainide. *Brain* **128:** 18-28.

Beck, R, Arrington, J, Murtagh, F, Cleary, PA, Kaufman, DI (1993a). Brain magnetic resonance imaging in acute optic neuritis. Experience of the Optic Neuritis Study Group. *Archives of Neurology* **50:** 841-6.

Beck, R, Gal, R, Bhatti, M, Brodsky, M, Bucci, MG, Chrousos, G, Corbett, J, Eggenberger, E, Goodwin, J, Katz, B, Kaufman, DI, Keltner, J, Kupersmith, MJ, Miler, N, Moke, P, Nazarian, S, Orengo-Nania, S, Savino, P, Shults, W, Smith, C, Trobe, JD, Wall, M, Xing, D (2004). Visual function more than 10 years after optic neuritis: experience of the optic neuritis treatment trial. *American Journal of Ophthalmology* **137:** 77-83.

Beck, RW (1988). The Optic Neuritis Treatment Trial. *Archives of Ophthalmology* **106:** 1051-1053.

Beck, RW, Cleary, PA, Anderson, MM, Keltner, JL, Shults, WT, Kaufman, DI, Buckley, EG, Corbett, JJ, Kupersmith, MJ, Miller, NR, Savino, PJ, Guy, JR, Trobe, JD, McCrary, JA, Smith, CH, Chrousos, GA, Thompson, HS, Katz, BJ, Brodsky, MC, Goodwin, JA, Atwell, CW (1992). A Randomized, Controlled Trial of Corticosteroids in the Treatment of Acute Optic Neuritis. *New England Journal of Medicine* **326:** 581-588.

Beck, RW, Cleary, PA, Trobe, JD, Kaufman, DI, Kupersmith, MJ, Paty, DW, Brown, CH, The Optic Neuritis Study, G (1993b). The Effect of Corticosteroids for Acute Optic Neuritis on the Subsequent Development of Multiple Sclerosis. *New England Journal of Medicine* **329:** 1764-1769.

Berne, RM, Levy, MN (2000). Principles of Physiology. *Mosby; 3rd Edition*

Berninger, TA, Canning, CR, Gunduz, K, Strong, N, Arden, GB (1989). Using Argon Laser Blue Light Reduces Ophthalmologists' Color Contrast Sensitivity: Argon Blue and Surgeons' Vision. *Arch Ophthalmol* **107:** 1453-1458.

Bettelli, E, Pagany, M, Weiner, HL, Linington, C, Sobel, RA, Kuchroo, VK (2003). Myelin Oligodendrocyte Glycoprotein-specific T Cell Receptor Transgenic Mice Develop Spontaneous Autoimmune Optic Neuritis. *Journal Experimental Medicine* **197:** 1073-1081.

Billiau, A, Matthys, P (2001). Modes of action of Freund's adjuvants in experimental models of autoimmune diseases. *Journal of Leukocyte Biology* **70:** 849-860.

Bitsch, A, Schuchardt, J, Bunkowski, S, Kuhlmann, T, Bruck, W (2000). Acute axonal injury in multiple sclerosis: Correlation with demyelination and inflammation. *Brain* **123:** 1174-1183.

Bjartmar, C, Wujek, JR, Trapp, BD (2003). Axonal loss in the pathology of MS: consequences for understanding the progressive phase of the disease. *Journal of Neurological Sciences* **206:** 165-171.

Black, J, Liu, S, Carrithers, M, Carrithers, L, Waxman, S (2007a). Exacerbation of experimental autoimmune encephalomyelitis after withdrawal of phenytoin and carbamazepine. *Annals of Neurology* **62:** 21-33.

Black, J, Newcombe, J, Trapp, BD, Waxman, S (2007b). Sodium channel expression within chronic multiple sclerosis plaques. *Journal Neuropathology & Experimental Neurology* **66:** 828-37.

Black, JA, Waxman, SG (2008). Phenytoin protects central axons in experimental autoimmune encephalomyelitis. *Journal of the Neurological Sciences* **274:** 57-63.

Black, JA, Waxman, SG, Smith, KJ (2006). Remyelination of dorsal column axons by endogenous Schwann cells restores the normal pattern of Nav1.6 and Kv1.2 at nodes of Ranvier. *Brain* **129:** 1319-1329.

Blakemore, WF (1973). Demyelination of the superior cerebellar peduncle in the mouse induced by cuprizone. *Journal of the Neurological Sciences* **20:** 63-72.

Blakemore, WF (1982). Ethidium bromide induced demyelination in the spinal cord of the cat. *Neuropathology and Applied Neurobiology* **8:** 365-75.

Blakemore, WF (1978). Observations on remyelination in the rabbit spinal cord follwoing demyelination induced by lysolecithin. *Neuropathology and Applied Neurobiology* **4:** 47-59.

Blakemore, WF, Franklin, RJM (2008). Remyelination in experimental models of tocin-induced demyelination. *Current Topics Microbiolgy & Immunology* **318:** 193-212.

Blüthmann, H, Kisielow, P, Uematsu, Y, Malissen, M, Krimpenfort, P, Berns, A, von Boehmer, H, Steinmetz, M (1988). T-cell-specific deletion of T-cell receptor transgenes allows functional rearrangement of endogenous α- and β-genes. *Nature* **334:** 156-159.

Bornstein, M, Miller, A, Slagle, S, Weitzman, M, Crystal, H, Drexler, E, Keilson, M, Merriam, A, Wassertheil-Smoller, S, Spada, V (1987). A pilot trial of Cop 1 in exacerbating-remitting multiple sclerosis. *New England Journal of Medicine* **13:** 408-14.

Brady, CM, DasGupta, R, Dalton, C, Wiseman, OJ, Berkley, KJ, Fowler, CJ (2004). An open-label pilot study of cannabis-based extracts for bladder dysfunction in advanced multiple sclerosis. *Multiple Sclerosis* **10:** 425-433.

Brahic, M, Bureau, J-Fo, Michiels, T (2005). The genetics of the persistent infection and demyelinating disease caused by Theiler's virus. *Annual Review of Microbiology* **59:** 279-298.

Brand-Schieber, E, Werner, P (2004). Calcium channel blockers ameliorate disease in a mouse model of multiple sclerosis. *Experimental Neurology* **189:** 5-9.

Braun, A, Lommatzsch, M, Mannsfeldt, A, Neuhaus-Steinmetz, U, Fischer, A, Schnoy, N, Lewin, GR, Renz, H (1999). Cellular Sources of Enhanced Brain-Derived Neurotrophic Factor Production in a Mouse Model of Allergic Inflammation. *American Journal Respiratory Cell & Molecular Biology* **21:** 537-546.

Bray, P, Bloomer, L, Salmon, V, Bagley, M, Larsen, P (1983). Epstein-Barr virus infection and antibody synthesis in patients with multiple sclerosis. *Archives of Neurology* **40:** 406-8.

Brines, ML, Ghezzi, P, Keenan, S, Agnello, D, de Lanerolle, NC, Cerami, C, Itri, LM, Cerami, A (2000). Erythropoietin crosses the blood brain barrier to protect against experimental brain injury. *Proceedings of the National Academy of Sciences of the United States of America* **97:** 10526-10531.

Bringmann, A, Pannicke, T, Grosche, J, Francke, M, Wiedemann, P, Skatchkov, SN, Osborne, NN, Reichenbach, A (2006). Müller cells in the healthy and diseased retina. *Progress in Retinal and Eye Research* **25:** 397-424.

Brinkmann, V, Cyster, J, Hla, T (2004). FTY720: Sphingosine 1-Phosphate Receptor-1 in the Control of Lymphocyte Egress and Endothelial Barrier Function. *American Journal of Transplantation* **4:** 1019-1025.

Broman, T (1964). Blood-brain barrier damage in multiple sclerosis supravital test-observations. *Acta Neurologica Scandinavica* **40:** 21-4.

Brousil, JA, Roberts, RJ, Schlein, AL (2006). Cladribine: An Investigational Immunomodulatory Agent for Multiple Sclerosis. *Annals of Pharmacotherapy* **40:** 1814-1821.

Brunner, C, Lassmann, H, Waehneldt, T, Matthieu, J, Linington, C (1989). Differential ultrastructural localization of myelin basic protein, myelin/oligodendroglial glycoprotein, and 2',3'-cyclic nucleotide 3'-phosphodiesterase in the CNS of adult rats. *Journal of Neurochemistry* **52:** 296-304.

Brusaferri, F, Candelise, L (2000). Steriods for multiple sclerosis and optic neuritis: a meta-analysis of randomized controlled clinical trials. *Journal of Neurology* **247:** 435-442.

Budde, K, Schmouder, RL, Brunkhorst, R, Nashan, B, LÃcker, PW, Mayer, T, Choudhury, S, Skerjanec, A, Kraus, G, Neumayer, HH (2002). First Human Trial of FTY720, a Novel Immunomodulator, in Stable Renal Transplant Patients. *Journal of the American Society of Nephrology* **13:** 1073-1083.

Buemi, M, Cavallaro, E, Floccari, F, Sturiale, A, Aloisi, C, Trimarchi, M, Corica, F, Frisina, N (2003). The pleiotropic effects of erythropoietin in the central nervous system. *Journal Neuropathology & Experimental Neurology* **62:** 228-36.

Burton, E, Greenberg, S, Frohman, E (2010). Optic neuritis: A mechanistic view. *Pathophysiology* **18:** 81-92.

Buttner, U, Kremmyda, O (2007). Smooth pursuit eye movements and optokinetic nystagmus. *Developments in Ophthalmology* **40:** 76-89.

Caccia, N, Kronenberg, M, Saxe, D, Haars, R, Bruns, GAP, Goverman, J, Malissen, M, Willard, H, Yoshikai, Y, Simon, M, Hood, L, Mak, TW (1984). The T cell receptor [beta] chain genes are located on chromosome 6 in mice and chromosome 7 in humans. *Cell* **37:** 1091-1099.

Cahill, H, Nathans, J (2008). The optokinetic reflex as a tool for quantitative analyses of nervous system function in mice: application to genetic and drug-induced variation. *PLoS ONE* **3:** e25055.

Calderone, L, Grimes, P, Shalev, M (1986). Acute reversible cataract induced by xylazine and by ketamine-xylazine anesthesia in rats and mice. *Experimental Eye Research* **42:** 331-337.

Caldwell, JH, Schaller, KL, Lasher, RS, Peles, E, Levinson, SR (2000). Sodium channel Nav1.6 is localized at nodes of Ranvier, dendrites, and synapses. *Proceedings of the National Academy of Sciences of the United States of America* **97:** 5616-5620.

Cambiaghi, M, Teneud, L, Velikova, S, Gonzalez-Rosa, JJ, Cursi, M, Comi, G, Leocani, L (2011). Flash visual evoked potentials in mice can be modulated by transcranial direct current stimulation. *Neuroscience* **185:** 161-165.

Cannella, B, Pitt, D, Capello, E, Raine, CS (2000). Insulin-Like Growth Factor-1 Fails to Enhance Central Nervous System Myelin Repair during Autoimmune Demyelination. *American Journal Pathology* **157:** 933-943.

Cantorna, MT, Hayes, CE, DeLuca, HF (1996). 1,25-Dihydroxyvitamin D3 reversibly blocks the progression of relapsing encephalomyelitis, a model of multple sclerosis. *Proceedings of the National Academy of Sciences of the United States of America* **93:** 7861-7864.

Carson, DA, Wasson, DB, Taetle, R, Yu, A (1983). Specific toxicity of 2-chlorodeoxyadenosine toward resting and proliferating human lymphocytes. *Blood* **62:** 737-743.

Cassan, C, Piaggio, E, Zappulla, JP, Mars, LT, Couturier, N, Bucciarelli, F, Desbois, S, Bauer, J, Gonzalez-Dunia, D, Liblau, RS (2006). Pertussis Toxin Reduces the Number of Splenic Foxp3+ Regulatory T Cells. *Jounral Immunology* **177:** 1552-1560.

Catterall, WA (1995). Structure and function of voltage-gated ion channels. *Annual Review of Biochemistry* **64:** 493-531.

Catterall, WA, Goldin, AL, Waxman, SG (2005). International Union of Pharmacology. XLVII. Nomenclature and Structure-Function Relationships of Voltage-Gated Sodium Channels. *Pharmacological Reviews* **57:** 397-409.

Chalfie, M, Tu, Y, Euskirchen, G, Ward, W, Prasher, D (1994). Green fluorescent protein as a marker for gene expression. *Science* **263:** 802-5.

Chang, B, Heckenlively, JR, Hawes, NL, Roderick, TH (1993). New Mouse Primary Retinal Degeneration (rd-3). *Genomics* **16:** 45-49.

Chen, X, Winkler-Pickett, RT, Carbonetti, NH, Ortaldo, JR, Oppenheim, JJ, Howar, OM (2006). Pertussis toxin as an adjuvant suppresses the number and function of CD4+CD25+ T regulatory cells. *European Journal of Immunology* **36:** 671-680.

Chothia, C, Boswell, DR, Lesk, AM (1988). The outline structure of the T-cell alpha beta receptor. *EMBO* **7:** 3745-55.

Chow, E, Mottahedeh, J, Prins, M, Ridder, W, Nusinowitz, S, Bronstein, JM (2005). Disrupted compaction of CNS myelin in an OSP/Claudin-11 and PLP/DM20 double knockout mouse. *Molecular and Cellular Neuroscience* **29:** 405-413.

Clark, AJ, Ware, MA, Yazer, E, Murray, TJ, Lynch, ME (2004). Patterns of cannabis use among patients with multiple sclerosis. *Neurology* **62:** 2098-2100.

Clutterbuck, LA, Posada, CG, Visintin, C, Riddall, DR, Lancaster, B, Gane, PJ, Garthwaite, J, Selwood, DL (2009). Oxadiazolylindazole Sodium Channel Modulators are Neuroprotective toward Hippocampal Neurones. *Journal of Medicinal Chemistry* **52:** 2694-2707.

Cobbold, SP, Jayasuriya, A, Nash, A, Prospero, TD, Waldmann, H (1984). Therapy with monoclonal antibodies by elimination of T-cell subsets in vivo. *Nature* **312:** 548-551.

Coffey, PJ, Girman, S, Wang, SM, Hetherington, L, Keegan, DJ, Adamson, P, Greenwood, J, Lund, RD (2002). Long-term preservation of cortically dependent visual function in RCS rats by transplantation. *Nature Neuroscience* **5:** 53-56.

Cohen, GM (1997). Caspases: the executioners of apoptosis. *Biochemical Journal* **326:** 1-16.

Cohen, JA, Barkhof, F, Comi, G, Hartung, H-P, Khatri, BO, Montalban, X, Pelletier, J, Capra, R, Gallo, P, Izquierdo, G, Tiel-Wilck, K, de Vera, A, Jin, J, Stites, T, Wu, S, Aradhye, S, Kappos, L (2010). Oral Fingolimod or Intramuscular Interferon for Relapsing Multiple Sclerosis. *New England Journal of Medicine* **362:** 402-415.

Cohen, JA, Chun, J (2011). Mechanisms of fingolimod's efficacy and adverse effects in multiple sclerosis. *Annals of Neurology* **69:** 759-777.

Coles, A, Compston, D, Selmaj, K (2008). Alemtuzumab vs. Interferon Beta-1a in Early Multiple Sclerosis. *New England Journal of Medicine* **359:** 1786-1801.

Compston, A (1996). Remyelination of the central nervous system. *Multiple Sclerosis* **1:** 388-92.

Confavreux, C, Vukusic, S (2004). Non-specific immunosuppressants in the treatment of multiple sclerosis. *Clinical Neurology and Neurosurgery* **106:** 263-269.

Conway, BR (2009). Color Vision, Cones, and Color-Coding in the Cortex. *Neuroscientist* **15:** 274-290.

Corallo, G, Cicinell, S, Papdia, M, Bandini, F, Uccelli, A, Calabria, G (2005). Conventional perimetry, short-wavelength automated perimetry, frequency-doubling technology, and visual evoked potentials in the assessment of patients with multiple sclerosis. *European Journal of Ophthalmology* **15:** 730-8.

Costello, F, Coupland, S, Hodge, W, Lorello, G, Koroluk, J, Pan, Y, Freedman, M, Zackon, D, Kardon, R (2006). Quantifying axonal loss after optic neuritis with optical coherence tomography. *Annals of Neurology* **59:** 963-969.

Cowey, A, Franzini, C (1979). The retinal origin of uncrossed optic nerve fibres in rats and their role in visual discrimination. *Experimental Brain Research* **2:** 443-55.

Craner, M, Damarjian, T, Liu, S, Hains, B, Lo, A, Black, J, Newcombe, J, Cuzner, M, Waxman, S (2005). Sodium channels contribute to microglia/macrophage activation and function in EAE and MS. *Glia* **49:** 220-229.

Craner, MJ, Hains, BC, Lo, AC, Black, JA, Waxman, SG (2004a). Co-localization of sodium channel Nav1.6 and the sodium-calcium exchanger at sites of axonal injury in the spinal cord in EAE. *Brain* **127:** 294-303.

Craner, MJ, Newcombe, J, Black, JA, Hartle, C, Cuzner, ML, Waxman, SG (2004b). Molecular changes in neurons in multiple sclerosis: Altered axonal expression of Nav1.2 and Nav1.6 sodium channels and Na+/Ca2+ exchanger. *Proceedings of the National Academy of Sciences of the United States of America* **101:** 8168-8173.

Cross, AH, Manning, PT, Keeling, RM, Schmidt, RE, Misko, TP (1998). Peroxynitrite formation within the central nervous system in active multiple sclerosis. *Journal of Neuroimmunology* **88:** 45-56.

Cua, DJ, Sherlock, J, Chen, Y, Murphy, CA, Joyce, B, Seymour, B, Lucian, L, To, W, Kwan, S, Churakova, T, Zurawski, S, Wiekowski, M, Lira, SA, Gorman, D, Kastelein, RA, Sedgwick, JD (2003). Interleukin-23 rather than interleukin-12 is the critical cytokine for autoimmune inflammation of the brain. *Nature* **421:** 744-748.

Dal Canto, M, Rabinowitz, S (1982). Experimental models of virus-induced demyelination of the central nervous system. *Annals of Neurology* **11:** 109-27.

Dalton, CM, Brex, PA, Miszkiel, KA, Fernando, K, MacManus, DG, Plant, GT, Thompson, AJ, Miller, DH (2003). Spinal cord MRI in clinically isolated optic neuritis. *Journal of Neurology, Neurosurgery & Psychiatry* **74:** 1577-1580.

Dalton, DK, Haynes, L, Chu, C-Q, Swain, SL, Wittmer, S (2000). Interferon Eliminates Responding Cd4 T Cells during Mycobacterial Infection by Inducing Apoptosis of Activated Cd4 T Cells. *The Journal of Experimental Medicine* **192:** 117-122.

Dam, M, Ekberg, R, Løyning, Y, Waltimo, O, Jakobsen, K (1989). A double-blind study comparing oxcarbazepine and carbamazepine in patients with newly diagnosed, previously untreated epilepsy. *Epilepsy Research* **3:** 70-6.

Dandekar, AA, Wu, GF, Pewe, L, Perlman, S (2001). Axonal Damage Is T Cell Mediated and Occurs Concomitantly with Demyelination in Mice Infected with a Neurotropic Coronavirus. *Journal of Virology.* **75:** 6115-6120.

Daumer, M, Neuhaus, O, Morrissey, S, Hintzen, RQ, Ebers, GC (2008). MRI as an outcome in multiple sclerosis clinical trials. *Neurology* **72:** 705-11.

Davie, CA, Barker, GJ, Webb, S, Tofts, PS, Thompson, AJ, Harding, AE, McDonald, WI, Miller, DH (1995). Persistent functional deficit in multiple sclerosis and autosomal dominant cerebellar ataxia is associated with axon loss. *Brain* **118:** 1583-1592.

Davto, AF, Pamela, SO, Valerie, AW, Marco, S, Tak, WM (1990). Transgenic Mice as an in vivo Model for Self-Reactivity. *Immunological Reviews* **118:** 257-283.

De Jager, PL, Baecher-Allan, C, Maier, LM, Arthur, AT, Ottoboni, L, Barcellos, L, McCauley, JL, Sawcer, S, Goris, A, Saarela, J, Yelensky, R, Price, A, Leppa, V, Patterson, N, de Bakker, PIW, Tran, D, Aubin, C, Pobywajlo, S, Rossin, E, Hu, X, Ashley, CW, Choy, E, Rioux, JD, Pericak-Vance, MA, Ivinson, A, Booth, DR, Stewart, GJ, Palotie, A, Peltonen, L, Dubois, Bnd, Haines, JL, Weiner, HL, Compston, A, Hauser, SL, Daly, MJ, Reich, D, Oksenberg, JR, Hafler, DA (2009). The role of the CD58 locus in multiple sclerosis. *Proceedings of the National Academy of Sciences United States America* **106:** 5264-5269.

de la Torre, JC, Surgeon, JW (1976). Dexamethasone and DMSO in experimental transorbital cerebral infarction. *Stroke* **7:** 577-583.

de Melo Reis, R, Ventura, A, Schitine, C, de Mello, M, de Mello, F (2008). Müller Glia as an Active Compartment Modulating Nervous Activity in the Vertebrate Retina: Neurotransmitters and Trophic Factors. *Neurochemical Research* **33:** 1466-1474.

De Stefano, N, Matthews, PM, Fu, L, Narayanan, S, Stanley, J, Francis, GS, Antel, JP, Arnold, DL (1998). Axonal damage correlates with disability in patients with relapsing- remitting multiple sclerosis. Results of a longitudinal magnetic resonance spectroscopy study. *Brain* **121:** 1469-1477.

Debouverie, M, Pittion-Vouyovitch, S, Louis, S, Roederer, T, Guillemin, F (2007). Increasing incidence of multiple sclerosis among women in Lorraine, Eastern France. *Multiple Sclerosis* **13:** 962-967.

Delarasse, C, daubas, P, Mars, LT, Vizler, C, Litzenburger, T, Iglesias, A, Bauer, J, Della Gaspera, B, Schubart, A, Decker, L, Dimitri, D, Roussel, G, Dieraich, A, Amor, S, Dautigny, A, Liblau, R, Pham-Dinh, D (2003). Myelin/oligodendrocyte glycoprotein-deficient (MOG-deficient) mice reveal lack of immune tolerance to MOG in wild-type mice. *Journal of Clinical Investigations* **112:** 544-553.

DeLuca, GC, Williams, K, Evangelou, N, Ebers, GC, Esiri, MM (2006). The contribution of demyelination to axonal loss in multiple sclerosis. *Brain* **129:** 1507-1516.

Dembic, Z, Haas, W, Weiss, S, Kiefer, H, von Bohemer, H, Steinmetz, H (1986). Transfer of specificity by murine alpha and beta T cell receptor genes. *Nature* **320:** 232-238.

Di Giorgio, AM, Hou, Y, Zhao, X, Zhang, B, Lyeth, BG, Russell, MJ (2008). Dimethyl sulfoxide provides neuroprotection in a traumatic brain injury model. *Restorative Neurology and Neuroscience* **26:** 501-507.

Diem, R, Sattler, MB, Merkler, D, Demmer, I, Maier, K, Stadelmann, C, Ehrenreich, H, Bahr, M (2005). Combined therapy with methylprednisolone and erythropoietin in a model of multiple sclerosis. *Brain* **128:** 375-385.

Diem, R, Tschirne, A, Bähr, M (2003). Decreased amplitudes in multiple sclerosis patients with normal visual acuity: a VEP study. *Journal of Clinical Neuroscience* **10:** 67-70.

Drexler, W, Sattmann, H, Hermann, B, Ko, TH, Stur, M, Unterhuber, A, Scholda, C, Findl, O, Wirtitsch, M, Fujimoto, JG, Fercher, AF (2003). Enhanced Visualization of Macular Pathology With

the Use of Ultrahigh-Resolution Optical Coherence Tomography. *Archives of Ophthalmology* **121:** 695-706.

Dulsat, C, Mealy, N, Castaner, R, Bolos, J (2009). Eslicarbazepine acetate. *Drugs of the Future* **34:** 189.

Dutta, R, McDonough, J, Yin, X, Peterson, J, Chang, A, Torres, T, Gudz, T, Macklin, WB, Lewis, DA, Fox, RJ, Rudick, R, Mirnics, K, Trapp, BD (2006). Mitochondrial dysfunction as a cause of axonal degeneration in multiple sclerosis patients. *Annals of Neurology* **59:** 478-489.

Dyer, R, Boyes, W (1983). Hypothermia and chloropent anesthesia differentially affect the flash evoked potentials of hooded rats. *Brain Research Bulletin* **10:** 825-31.

Ebers, G, Sadovnick, A, Risch, N (1995). A genetic basis for familial aggregation in multiple sclerosis. *Nature* **377:** 150-151.

Ebers, GC (2008). Environmental factors and multiple sclerosis. *The Lancet Neurology* **7:** 268-277.

Ehrenreich, H, Fischer, B, Norra, C, Schellenberger, F, Stender, N, Stiefel, M, Siren, A-L, Paulus, W, Nave, K-A, Gold, R, Bartels, C (2007). Exploring recombinant human erythropoietin in chronic progressive multiple sclerosis. *Brain* **130:** 2577-2588.

Ehrhard, P, Erb, P, Graumann, U, Otten, U (1993). Expression of nerve growth factor and nerve growth factor receptor tyrosine kinase Trk in activated CD4-positive T-cell clones. *Proceedings of the National Academy of Sciences United States America* **90:** 10984-10988.

El-behi, M, Rostami, A, Ciric, B (2010). Current views on the roles of Th1 and Th17 cells in experimental auotimmune encephalomyelitis. *Journal of Neuroimmune Pharmacology* **5:** 189-197.

El-Remessy, AB, Khalil, IE, Matragoon, S, Abou-Mohamed, G, Tsai, N-J, Roon, P, Caldwell, RB, Caldwell, RW, Green, K, Liou, GI (2003). Neuroprotective Effect of(-)[Delta]9-Tetrahydrocannabinol and Cannabidiol in N-Methyl-d-Aspartate-Induced Retinal Neurotoxicity: Involvement of Peroxynitrite. *The American Journal of Pathology* **163:** 1997-2008.

Espir, M, Millac, P (1970). Treatment of paroxysmal disorders in multiple sclerosis with carbamazepine (Tegretol). *Journal of Neurolgy, Neurosurgery & Psychiatry* **33:** 528-31.

Eter, N, Engel, DR, Meyer, L, Helb, H-M, Roth, F, Maurer, J, Holz, FG, Kurts, C (2008). In Vivo Visualization of Dendritic Cells, Macrophages, and Microglial Cells Responding to Laser-Induced Damage in the Fundus of the Eye. *Investigative Ophthalmology & Visual Science* **49:** 3649-3658.

Farina, C, Weber, MS, Meinl, E, Wekerle, H, Hohlfeld, R (2005). Glatiramer acetate in multiple sclerosis: update on potential mechanisms of action. *The Lancet Neurology* **4:** 567-575.

Feng, G, Mellor, RH, Bernstein, M, Keller-Peck, C, Nguyen, QT, Wallace, M, Nerbonne, JM, Lichtman, JW, Sanes, JR (2000). Imaging Neuronal Subsets in Transgenic Mice Expressing Multiple Spectral Variants of GFP. *Neuron* **28:** 41-51.

Fercher, AF (2010). Optical coherence tomography - development, principles, applications. *Zeitschrift für Medizinische Physik* **20:** 251-276.

Ferguson, B, Matyszak, MK, Esiri, MM, Perry, VH (1997). Axonal damage in acute multiple sclerosis lesions. *Brain* **120:** 393-399.

Fern, R, Ransom, BR, Stys, PK, Waxman, SG (1993). Pharmacological protection of CNS white matter during anoxia: actions of phenytoin, carbamazepine and diazepam. *Journal of Pharmacology and Experimental Therapeutics* **266:** 1549-1555.

Figlewicz, D, Quarles, R, Johnson, D, Barbarash, G, Sternberger, N (1982). Biochemical demonstration of the myelin-associated glycoprotein in the peripheral nervous system. *Journal of Neurochemistry* **37:** 749-58.

Filippi, M, Bozzali, M, Rovaris, M, Gonen, O, Kesavadas, C, Ghezzi, A, Martinelli, V, Grossman, RI, Scotti, G, Comi, G, Falini, A (2003). Evidence for widespread axonal damage at the earliest clinical stage of multiple sclerosis. *Brain* **126:** 433-437.

Fisher, JB, Jacobs, DA, Markowitz, CE, Galetta, SL, Volpe, NJ, Nano-Schiavi, ML, Baier, ML, Frohman, EM, Winslow, H, Frohman, TC, Calabresi, PA, Maguire, MG, Cutter, GR, Balcer, LJ (2006). Relation of Visual Function to Retinal Nerve Fiber Layer Thickness in Multiple Sclerosis. *Ophthalmology* **113:** 324-332.

Forrester, JV, Peters, A (1967). Nerve fibres in optic nerve of rat. *Nature* **15:** 245-7.

Freund, J, McDermott, K (1942). Sensitization to horse serum by means of adjuvants. *Proceedings of the Society of Experimental Biological Medicine* **49:** 548-553.

Freund, J, Stern, E, Pisani, T (1947). Isoallergic encephalomyelitis and radiculitis in guinea pigs after one injection of brain and Mycobacteria in water-in-oil emulsion. *Journal of Immunology* **57:** 179-94.

Fridkis-Hareli, M, Neveu, JM, Robinson, RA, Lane, WS, Gauthier, L, Wucherpfennig, KW, Sela, M, Strominger, JL (1999). Binding Motifs of Copolymer 1 to Multiple Sclerosis- and Rheumatoid Arthritis-Associated HLA-DR Molecules. *Journal of Immunology* **162:** 4697-4704.

Frohman, EM, Costello, F, Stuve, O, Calabresi, P, Miller, DH, Hickman, SJ, Sergott, R, Conger, A, Salter, A, Krumwiede, KH, Frohman, TC, Balcer, L, Zivadinov, R (2008a). Modeling Axonal Degeneration Within the Anterior Visual System: Implications for Demonstrating Neuroprotection in Multiple Sclerosis. *Archives of Neurology* **65:** 26-35.

Frohman, EM, Dwyer, MG, Frohman, T, Cox, JL, Salter, A, Greenberg, BM, Hussein, S, Conger, A, Calabresi, P, Balcer, LJ, Zivadinov, R (2009). Relationship of optic nerve and brain conventional and non-conventional MRI measures and retinal nerve fiber layer thickness, as assessed by OCT and GDx: A pilot study. *Journal of the Neurological Sciences* **282:** 96-105.

Frohman, EM, Fujimoto, JG, Frohman, TC, Calabresi, PA, Cutter, G, Balcer, LJ (2008b). Optical coherence tomography: a window into the mechanisms of multiple sclerosis. *Nature Clinical Practice Neurology* **4:** 664-675.

Frohman, EM, Racke, MK, Raine, CS (2006). Multiple Sclerosis - The Plaque and Its Pathogenesis. *The New England Journal of Medicine* **354:** 942-955.

Fruttiger, M, Montag, D, Schachner, M, Martini, R (1995). Crucial role for the myelin-associated glycoprotein in the maintenance of axon-myelin integrity. *European Journal of Neuroscience* **7:** 511-5.

Fuller, JH (1985). Eye and head movements in the pigmented rat. *Vision Research* **25:** 1121-1128.

Gabriele, ML, Ishikawa, H, Schuman, JS, Ling, Y, Bilonick, RA, Kim, JS, Kagemann, L, Wollstein, G (2011). Optic Nerve Crush Mice Followed Longitudinally with Spectral Domain Optical Coherence Tomography. *Investigative Ophthalmology & Visual Science* **52:** 2250-2254.

Gale, CR, Martyn, CN (1995). Migrant studies in multiple sclerosis. *Progress in Neurobiology* **47:** 425-448.

Garcia-Martin, E, Pueyo, V, Pinilla, I, Ara, J-R, Martin, J, Fernandez, J (2011). Fourier-Domain OCT in Multiple Sclerosis Patients: Reproducibility and Ability to Detect Retinal Nerve Fiber Layer Atrophy. *Investigative Ophthalmology & Visual Science* **52:** 4124-4131.

Gardinier, MV, Amiguet, P, Linington, C, Matthieu, JM (1992). Myelin/oligodendrocyte glycoprotein is a unique member of the immunoglobulin superfamily. *Journal of Neuroscience Research* **33:** 177-87.

Garthwaite, G, Goodwin, DA, Batchelor, AM, Leeming, K, Garthwaite, J (2002). Nitric oxide toxicity in CNS white matter: an in vitro study using rat optic nerve. *Neuroscience* **109:** 145-155.

Gensert, JM, Goldman, JE (1997). Endogenous Progenitors Remyelinate Demyelinated Axons in the Adult CNS. *Neuron* **19:** 197-203.

Gilgun-Sherki, Y, Panet, H, Melamed, E, Offen, D (2003). Riluzole suppresses experimental autoimmune encephalomyelitis: implications for the treatment of multiple sclerosis. *Brain Research* **989:** 196-204.

Giovannoni, G, Comi, G, Cook, S, Rammohan, K, Rieckmann, P, Sorensen, PS, Vermersch, P, Chang, P, Hamlett, A, Musch, B, Greenberg, SJ, the, CSG (2010). A Placebo-Controlled Trial of Oral Cladribine for Relapsing Multiple Sclerosis. *New England Journal of Medicine***362:** 416-426.

Gold, R, Linington, C, Lassmann, H (2006). Understanding pathogenesis and therapy of multiple sclerosis via animal models: 70 years of merits and culprits in experimental autoimmune encephalomyelitis research. *Brain* **129:** 1953-1971.

Gordon-Lipkin, E, Chodkowski, B, Reich, DS, Smith, SA, Pulicken, M, Balcer, LJ, Frohman, EM, Cutter, G, Calabresi, PA (2007). Retinal nerve fiber layer is associated with brain atrophy in multiple sclerosis. *Neurology* **69:** 1603-1609.

Goverman, J, Woods, A, Larson, L, Weiner, LP, Hood, L, Zaller, DM (1993). Transgenic mice that express a myelin basic protein-specific T cell receptor develop spontaneous autoimmunity. *Cell* **72:** 551-560.

Grazioli, E, Zivadinov, R, Weinstock-Guttman, B, Lincoff, N, Baier, M, Wong, JR, Hussein, S, Cox, JL, Hojnacki, D, Ramanathan, M (2008). Retinal nerve fiber layer thickness is associated with brain MRI outcomes in multiple sclerosis. *Journal of the Neurological Sciences* **268:** 12-17.

Greenberg, BM (2010). Optical coherence tomography as a potential readout in clinical trials. *Therapeutic Advances in Neurological Disorders* **3:** 153-60.

Gronseth, GS, Ashman, EJ (2000). Practice parameter: The usefulness of evoked potentials in identifying clinically silent lesions in patients with suspected multiple sclerosis (an evidence-based review): Report of the Quality Standards Subcommittee of the American Academy of Neurology. *Neurology* **54:** 1720-1725.

Grossman, RI, Gonzalez-Scarano, F, Atlas, SW, Galetta, S, Silberberg, DH (1986). Multiple sclerosis: gadolinium enhancement in MR imaging. *Radiology* **161:** 721-725.

Guan, Y, Shindler, KS, Tabuena, P, Rostami, AM (2006). Retinal ganglion cell damage induced by spontaneous autoimmune optic neuritis in MOG-specific TCR transgenic mice. *Journal of Neuroimmunology* **178:** 40-48.

Guzman, NJ, Fang, MZ, Tang, SS, Ingelfinger, JR, Garg, LC (1995). Autocrine inhibition of Na+/K(+)-ATPase by nitric oxide in mouse proximal tubule epithelial cells. *The Journal of Clinical Investigation* **95:** 2083-2088.

Haeryfar, SMM, Hoskin, DW (2004). Thy-1: More than a Mouse Pan-T Cell Marker. *Journal of Immunology***173:** 3581-3588.

Hafezi, F, Grimm, C, Simmen, BC, Wenzel, A, Reme, CE (2000). Moelcular ophthalmology: an update on animal models for retinal degenerations and dystrophies. *British Journal of Ophthalmology* **84:** 922-927.

Hammarberg, H, Lidman, O, Lundberg, C, Eltayeb, SY, Gielen, AW, Muhallab, S, Svenningsson, A, LindÃ¥, H, van der Meide, PH, Cullheim, S, Olsson, T, Piehl, F (2000). Neuroprotection by Encephalomyelitis: Rescue of Mechanically Injured Neurons and Neurotrophin Production by CNS-Infiltrating T and Natural Killer Cells. *The Journal of Neuroscience* **20:** 5283-5291.

Hampson, AJ, Grimaldi, M, Axelrod, J, Wink, D (1998). Cannabidiol and (â^')Î"9-tetrahydrocannabinol are neuroprotective antioxidants. *Proceedings of the National Academy of Sciences* **95:** 8268-8273.

Handunnetthi, L, Ramagopalan, SV (2010). UV radiation, vitamin D, and multiple sclerosis. *Proceedings of the National Academy of Sciences* **107:** E130.

Hardin-Pouzet, H, Krakowski, M, Bourbonniére, L, Didier-Bazes, M, Tran, E, Owens, T (1997). Glutamate metabolism is down-regulated in astrocytes during experimental allergic encephalomyelitis. *Glia* **20:** 79-85.

Hartung, H-P (2009). New cases of progressive multifocal leukoencephalopathy after treatment with natalizumab. *The Lancet Neurology* **8:** 28-31.

Harvey, NL, Butt, AJ, Kumar, S (1997). Functional activation of Nedd2/ICH-1 (caspase-2) is an early process in apoptosis. *Journal of Biological Chemistry* **272:** 13134-13139.

Hassen, G, Feliberti, J, Kesner, L, Stracher, A, Mokhtarian, F (2008). Prevention of axonal injury using calpain inhibitor in chronic progressive experimental autoimmune encephalomyelitis. *Brain Research* **1236:** 206-215.

Hassenstein, A, Meyer, CH (2009). Clinical use and research applications of Heidelberg retinal angiography and spectral-domain optical coherence tomography – a review. *Clinical & Experimental Ophthalmology* **37:** 130-143.

Haug, M, Biehlmaier, O, Mueller, K, Neuhauss, S (2010). Visual acuity in larval zebrafish: behavior and histology. *Frontiers in Zoology* **7:** 8.

Hauser, SL, Oksenberg, JR (2006). The Neurobiology of Multiple Sclerosis: Genes, Inflammation, and Neurodegeneration. *Neuron* **52:** 61-76.

Hauser, SL, Waubant, E, Arnold, DL, Vollmer, T, Antel, J, Fox, RJ, Bar-Or, A, Panzara, M, Sarkar, N, Agarwal, S, Langer-Gould, A, Smith, CH (2008). B-Cell Depletion with Rituximab in Relapsingâ€“Remitting Multiple Sclerosis. *New England Journal of Medicine* **358:** 676-688.

Hawker, K, O'Connor, P, Freedman, MS, Calabresi, PA, Antel, J, Simon, J, Hauser, S, Waubant, E, Vollmer, T, Panitch, H, Zhang, J, Chin, P, Smith, CH (2009). Rituximab in patients with primary progressive multiple sclerosis: Results of a randomized double-blind placebo-controlled multicenter trial. *Annals of Neurology* **66:** 460-471.

Hemler, ME (1990). VLA Proteins in the Integrin Family: Structures, Functions, and Their Role on Leukocytes. *Annual Review of Immunology* **8:** 365-400.

Henderson, APD, Trip, SA, Schlottmann, PG, Altmann, DR, Garway-Heath, DF, Plant, GT, Miller, DH (2008). An investigation of the retinal nerve fibre layer in progressive multiple sclerosis using optical coherence tomography. *Brain* **131:** 277-287.

Hendriks, JJA, Teunissen, CE, de Vries, HE, Dijkstra, CD (2005). Macrophages and neurodegeneration. *Brain Research Reviews* **48:** 185-195.

Herbert, W (1968). The mode of action of mineral-oil emulsion adjuvants on antibody production in mice. *Immunology* **14:** 301-18.

Hetzler, BE, Oaklay, KE (1981). Dose effects of pentobarbital on evoked potentials in visual cortex and superior colliculus of the albino rat. *Neuropharmacology* **20:** 969-978.

Hickman, SJ, Toosy, AT, Miszkiel, KA, Jones, SJ, Altmann, DR, MacManus, DG, Plant, GT, Thompson, AJ, Miller, DH (2004). Visual recovery following acute optic neuritis. *Journal of Neurology* **251:** 996-1005.

Hide-Aki, S (1983). Morphology of physiologically identified X-, Y-, and W-type retinal ganglion cells of the cat. *The Journal of Comparative Neurology* **221:** 279-288.

Hjelmström, P, Juedes, AE, Ruddle, NH (1998). Cytokines and antibodies in myelin oligodendrocyte glycoprotein-induced experimental allergic encephalomyelitis. *Research in Immunology* **149:** 794-804.

Hobom, M, Storch, MK, Weissert, R, Maier, K, Radhakrishnan, A, Kramer, B, Bähr, M, Diem, R (2004). Mechanisms and Time Course of Neuronal Degeneration in Experimental Autoimmune Encephalomyelitis. *Brain Pathology* **14:** 148-157.

Holder, GE (2004). Electrophysiological assessment of optic nerve disease. *Eye* **18:** 1133-1143.

Hooge, J, Redekop, W (1995). Trigeminal neuralgia in multiple sclerosis. *Neurology* **45:** 1294-6.

Horio, N, Kachi, S, Hori, K, Okamoto, Y, Yamamoto, E, Terasaki, H, Miyake, Y (2001). Progressive Change of Optical Coherence Tomography Scans in Retinal Degeneration Slow Mice. *Archives of Ophthalmology* **119:** 1329-1332.

Hu, Y, Lee, X, Ji, B, Guckian, K, Apicco, D, Pepinsky, RB, Miller, RH, Mi, S (2011). Sphingosine 1-phosphate receptor modulator fingolimod (FTY720) does not promote remyelination in vivo. *Molecular and Cellular Neuroscience* **48:** 72-81.

Huang, D, Swanson, E, Lin, C, Schuman, J, Stinson, W, Chang, W, Hee, M, Flotte, T, Gregory, K, Puliafito, C, Fujimoto, J (1991). Optical Coherence Tomography. *Science* **254:** 1178-81.

Humphries, M, Rancourt, D, Farrar, G, Kenna, P, Hazel, M, Bush, R, Sieving, P, Sheils, D, McNally, N, Creighton, P, Erven, A, Boros, A, Gulya, K, Capecchi, M, Humphries, P (1997). Retinopathy induced in mice by targeted disruption of the rhodopsin gene. *Nature Genetics* **15:** 216-9.

Hutchinson, M, Kappos, L, Calabresi, P, Confavreux, C, Giovannoni, G, Galetta, S, Havrdova, E, Lublin, F, Miller, D, O'Connor, P, Phillips, J, Polman, C, Radue, EW, Rudick, R, Stuart, W, Wajgt, A, Weinstock-Guttman, B, Wynn, D, Lynn, F, Panzara, M, for the, AaSI (2009). The efficacy of natalizumab in patients with relapsing multiple sclerosis: subgroup analyses of AFFIRM and SENTINEL. *Journal of Neurology* **256:** 405-415.

Iglesias, A, Bauer, J, Litzenburger, T, Schubart, A, Linington, C (2001). T- and B-cell responses to myelin oligodendrocyte glycoprotein in experimental autoimmune encephalomyelitis and multiple sclerosis. *Glia* **36:** 220-34.

Imaizumi, T, Kocsis, JD, Waxman, SG (1999). The role of voltage-gated Ca2+ channels in anoxic injury of spinal cord white matter. *Brain Research* **817:** 84-92.

Inoue, H, Ohsawa, I, Murakami, T, Kimura, A, Hakamata, Y, Sato, Y, Kaneko, T, Takahashi, M, Okada, T, Ozawa, K, Francis, J, Leone, P, Kobayashi, E (2005). Development of new inbred transgenic strains of rats with LacZ or GFP. *Biochemical and Biophysical Research Communications* **329:** 288-295.

Ismail, A, Kemp, J, Sharrack, B (2008). Melanoma complicating treatment with Natalizumab (Tysabri) for multiple sclerosis. *Journal of Neurology* **358:** 647-648.

Jack, C, Ruffini, F, Bar-Or, A, Antel, JP (2005). Microglia and multiple sclerosis. *Journal of Neuroscience Research* **81:** 363-373.

Jacobs, L, Munschauer, F, Kaba, S (1991). Clinical and magnetic resonance imaging in optic neuritis. *Neurology* **41:** 15-9.

Jeffery, G (2001). Architecture of the Optic Chiasm and the Mechanisms That Sculpt Its Development. *Physiological Reviews.* **81:** 1393-1414.

John, S, Smith, R, Savinova, O, Hawes, N, Chang, B, Turnbull, D, Davisson, M, Roderick, T, Heckenlively, J (1998). Essential iris atrophy, pigment dispersion, and glaucoma in DBA/2J mice. *Investigative Ophthalmology & Visual Sciences* **39:** 951-62.

Johnson, K, Brooks, B, COhen, J, Ford, C, Goldstein, J, Lisak, R, Myers, L, Panitch, H, Rose, J, Schiffer, R, Vollmer, TL, Weiner, L, Wolinsky, J (2001). Copolymer 1 reduces relapse rate and improves disability in relapsing-remitting multiple sclerosis: results of a phase III multicenter, double-blind, placebo-controlled trial. *Neurology* **57:** S16-24.

Jones, MV, Nguyen, TT, DeBoy, CA, Griffin, JW, Whartenby, KA, Kerr, DA, Calabresi, PA (2008). Behavioral and pathological outcomes in MOG 35-55 experimental autoimmune encephalomyelitis. *Journal of Neuroimmunology* **199:** 83-93.

Kain, S, Adams, M, Kondepudi, A, Yang, T, Ward, W, Kitts, P (1995). Green fluorescent protein as a reporter of gene expression and protein localization. *Biotechniques* **19:** 650-5.

Kalkers, N, Barkhof, F, Bergers, E, van Schijndel, R, Polman, C (2001). The effect of the neuroprotective agent riluzole on MRI parameters in primary progressive multiple sclerosis: a pilot study. *Multiple Sclerosis* **8:** 532-3.

Kanamori, A, Catrinescu, M-M, Traistaru, M, Beaubien, R, Levin, LA (2010). In Vivo Imaging of Retinal Ganglion Cell Axons within the Nerve Fiber Layer. *Investigative Ophthalmology & Visual Science* **51:** 2011-2018.

Kapoor, R, Davies, M, Smith, KJ (1999). Temporary Axonal Conduction Block and Axonal Loss in Inflammatory Neurological Disease: A Potential Role for Nitric Oxide? *Annals of the New York Academy of Sciences* **893:** 304-308.

Kapoor, R, Furby, J, Hayton, T, Smith, KJ, Altmann, DR, Brenner, R, Chataway, J, Hughes, RAC, Miller, DH (2010). Lamotrigine for neuroprotection in secondary progressive multiple sclerosis: a randomised, double-blind, placebo-controlled, parallel-group trial. *The Lancet Neurology* **9:** 681-688.

Kappos, L, Polman, CH, Freedman, MS, Edan, G, Hartung, HP, Miller, DH, Montalban, X, Barkhof, F, Bauer, L, Jakobs, P, Pohl, C, Sandbrink, R, for the, BSG (2006). Treatment with interferon beta-1b delays conversion to clinically definite and McDonald MS in patients with clinically isolated syndromes. *Neurology* **67:** 1242-1249.

Kappos, L, Radue, E-W, O'Connor, P, Polman, C, Hohlfeld, R, Calabresi, P, Selmaj, K, Agoropoulou, C, Leyk, M, Zhang-Auberson, L, Burtin, P, the, FSG (2010). A Placebo-Controlled Trial of Oral Fingolimod in Relapsing Multiple Sclerosis. *New England Journal of Medicine***362:** 387-401.

Karaca, M, Bilgin, U, Akar, M, De la Torre, JC (1991). Dimethly sulphoxide lowers ICP after closed head trauma. *European Journal of Clinical Pharmacology* **40:** 113-4.

Kaufman, DI, Trobe, JD, Eggenberger, ER, Whitaker, JN (2000). Practice parameter: The role of corticosteroids in the management of acute monosymptomatic optic neuritis: Report of the Quality Standards Subcommittee of the American Academy of Neurology. *Neurology* **54:** 2039-2044.

Kaushansky, N, Zhong, M-C, Kerlero de Rosbo, N, Hoeftberger, R, Lassmann, H, Ben-Nun, A (2006). Epitope Specificity of Autoreactive T and B Cells Associated with Experimental Autoimmune Encephalomyelitis and Optic Neuritis Induced by Oligodendrocyte-Specific Protein in SJL/J Mice. *Journal of Immunology***177:** 7364-7376.

Kawamura, S, Tachibanaki, S (2008). Rod and cone photoreceptors: Molecular basis of the difference in their physiology. *Comparative Biochemistry and Physiology - Part A: Molecular & Integrative Physiology* **150:** 369-377.

Keegan, BM, Noseworthy, JH (2002). Multiple Sclerosis. *Annual Review of Medicine* **53:** 285-302.

Keita, M, Magy, L, Heape, A, Richard, L, Piaser, M, Vallat, J (2002). Immunocytological studies of L-MAG expression regulation during myelination of embryonic brain cell cocultures. *Developmental Neuroscience* **24:** 495-503.

Keltner, JL, Cello, KE, Balcer, LJ, Calabresi, PA, Markowitz, CE, Werner, JS (2011). Stratus OCT Quality Control in Two Multi-Centre Multiple Sclerosis Clinical Trials. *Neuro-Ophthalmology* **35:** 57-64.

Kemppinen, A, Sawcer, S, Compston, A (2011). Genome-wide association studies in multiple sclerosis: lessons and future prospects. *Briefings in Functional Genomics* **10:** 61-70.

Kerfoot, SM, Long, EM, Hickey, MJ, Andonegui, G, Lapointe, BM, Zanardo, RCO, Bonder, C, James, WG, Robbins, SM, Kubes, P (2004). TLR4 Contributes to Disease-Inducing Mechanisms Resulting in Central Nervous System Autoimmune Disease. *Journal of Immunology***173:** 7070-7077.

Kezuka, T, Usui, Y, Goto, H (2011). Analysis of the pathogenesis of experimental autoimmune optic neuritis. *Journal of Biomedicine and Biotechnology* **2011**.

Kieseier, B, Wiendl, H, Leussink, V, Stüve, O (2008). Immunomodulatory treatment strategies in multiple sclerosis. *Journal of Neurology* **255:** 15-21.

Kim, KH, PUoris'haag, M, Maguluri, GN, Umino, Y, Cusato, K, Barlow, RB, Boer, JF (2008). Monitoring mouse retinal degeneration with high-resolution spectral-domain optical coherence tomography. *Journal of Vision* **8:** 1-11.

Kirk, J, Plumb, J, Mirakhur, M, McQuaid, S (2003). Tight junctional abnormality in multiple sclerosis white matter affects all calibres of vessel and is associated with blood-brain barrier leakage and active demyelination. *The Journal of Pathology* **201:** 319-327.

Kisielow, P, Bluthmann, H, Staerz, U, Steinmetz, M, Von Boehmer, H (1988). Toelrance in T-cell receptor transgenic mice involves deletion of nonmature CD4+CD8+ thymocytes. *Nature* **333:** 742-6.

Kolappan, M, Henderson, A, Jenkins, T, Wheeler-Kingshott, C, Plant, G, Thompson, A, Miller, D (2009). Assessing structure and function of the afferent visual pathway in multiple sclerosis and associated optic neuritis. *Journal of Neurology* **256:** 305-319.

Kooij, G, van Horssen, J, de Lange, ECM, Reijerkerk, A, van der Pol, SMA, van het Hof, B, Drexhage, J, Vennegoor, A, Killestein, J, Scheffer, G, Oerlemans, R, Scheper, R, van der Valk, P, Dijkstra, CD, de Vries, HE (2010). T lymphocytes impair P-glycoprotein function during neuroinflammation. *Journal of Autoimmunity* **34:** 416-425.

Kouskoff, V, Signorelli, K, Benoist, C, Mathis, D (1995). Cassette vectors directing expression of T cell receptor genes in transgenic mice. *Journal of Immunological Methods* **180:** 273-280.

Kouwenhoven, M, Özenci, V, Gomes, A, Yarilin, D, Giedraitis, V, Press, R, Link, H (2001). Multiple sclerosis: elevated expression of matrix metalloproteinases in blood monocytes. *Journal of Autoimmunity* **16:** 463-470.

Kranz, D, Saito, H, Disteche, C, Swisshelm, K, Pravtcheva, D, Ruddle, F, Eisen, H, Tonegawa, S (1985). Chromosomal locations of the murine T-cell receptor alpha-chain gene and the T-cell gamma gene. *Science* **22:** 941-5.

Kraut, M, Arezzo, J, Vaughan, H (1985). Intracortical generators of the flash VEP in monkeys. *Electromyography & Clinical Neurophysiology* **62:** 300-12.

Krishnamoorthy, G, Wekerle, H (2009). EAE: An immunologist's magic eye. *European Journal of Immunology* **39:** 2031-2035.

Kuhlmann, T, Lingfeld, G, Bitsch, A, Schuchardt, J, BrÃ¼ck, W (2002). Acute axonal damage in multiple sclerosis is most extensive in early disease stages and decreases over time. *Brain* **125:** 2202-2212.

Kumar, S (1995). Inhibition of apoptosis by the expression of antisense Nedd2. *FEBS Letter* **368:** 69-72.

Kumar, S, Kinoshita, M, Noda, M, Copeland, N, Jenkins, N (1994). Induction of apoptosis by the mouse Nedd2 gene, which encodes a protein similar to the product of the Caenorhabditis elegans cell death gene ced-3 and the mammalian IL-1 beta-converting enzyme. *Genes Deb* **8:** 1613-26.

Kumar, S, Tomooka, Y, Noda, M (1992). Identification of a set of genes with developmentally down-regulated expression in the mouse brain. *Biochemical and Biophysical Research Communications* **185:** 1155-1161.

Kurenny, DE, Moroz, LL, Turner, RW, Sharkey, KA, Barnes, S (1994). Modulation of ion channels in rod photoreceptors by nitric oxide. *Neuron* **13:** 315-324.

Kurokawa, T, Katai, N, Shibuki, H, Kuroiwa, S, Kurimoto, Y, Nakayama, C, Yoshimura, N (1999). BDNF Diminishes Caspase-2 but Not c-Jun Immunoreactivity of Neurons in Retinal Ganglion Cell Layer after Transient Ischemia. *Investigative Ophthalmology & Visual Science* **40:** 3006-3011.

Kurtzke, JF (1991). Multiple Sclerosis: changing times. *Neuroepidemiology* **10:** 1-8.

Kurtzke, JF (1975). A reassessment of the disrtibution of multiple sclerosis. *Acta Neurologica Scandinavica* **51:** 110-136.

Kutok, JL, Wang, F (2006). Spectrum of Epstein-Barr Virus-associated diesease. *Annual Review of Pathology: Mechanisms of Disease* **1:** 375-404.

Lafaille, JJ (2004). T-cell receptor transgenic mice in the study of autoimmune diseases. *Journal of Autoimmunity* **22:** 95-106.

Lafaille, JJ, Nagashima, K, Katsuki, M, Tonegawa, S (1994). High incidence of spontaneous autoimmune encephalomyelitis in immunodeficient anti-myelin basic protein T cell receptor transgenic mice. *Cell* **78:** 399-408.

Lai, E, Barth, RK, Hood, L (1987). Genomic organisation of the mouse T-cell receptor beta-chain gene family. *Proceedings of the National Academy of Sciences United States America* **84:** 3846-3850.

Lamkanfi, M, Festjens, N, Declercq, W, Berghe, TV, Vandenabeele, P (2006). Caspases in cell survival, proliferation and differentiation. *Cell Death & Differentiation* **14:** 44-55.

Lando, Z, Teitelbaum, D, Arnon, R (1979). Genetic control of susceptibility to experimental allergic encephalomyelitis in mice. *Immunogenetics* **9:** 435-442.

Lassmann, H, Brück, W, Lucchinetti, C (2001). Heterogeneity of multiple sclerosis pathogenesis: implications for diagnosis and therapy. *Trends in Molecular Medicine* **7:** 115-121.

Lebar, R, Lubetzki, C, Vincent, C, Lombrail, P, Boutry, J (1986a). The M2 autoantigen of central nervous system myelin, a glycoprotein present in oligodendrocyte membrane. *Clinical & Experimental Immunology* **66:** 423-34.

Lebar, R, Lubetzki, C, Vincent, C, Lombrail, P, Boutry, JM (1986b). The M2 autoantigen of central nervous system myelin, a glycoprotein present in oligodendrocyte membrane. *Clinical & Experimental Immunology* **66:** 423-434.

Lee, AG, Beaver, HA, Brazis, PW (2004). Painful ophthalmologic disorders and eye pain for the neurologist. *Neurologic Clinics* **22:** 75-97.

Lester, M, Cioli, F, Uccelli, A, Papadia, M, Bandini, F, Mancardi, GL, Calabria, GA (2009). Retinal nerve fibre layer measurements and optic nerve head analysis in multiple sclerosis patients. *Eye* **23:** 407-412.

Leung, CK-s, Lindsey, JD, Crowston, J, Chen, LJ, Chiang, SWY, Weinreb, RN (2008a). Longitudinal profile of retinal ganglion cell degeneration after optic nerve crush with blue-light confocal scanning laser ophthalmascopy. *Investigative Ophthalmology & Visual Science* **49:** 4898-4902.

Leung, CK-s, Weinreb, RN, Li, ZW, Liu, S, Lindsey, JD, Choi, N, Liu, L, Cheung, CY-l, Ye, C, Qiu, K, Chen, LJ, Yung, WH, Crowston, JG, Pu, M, So, KF, Pang, CP, Lam, DSC (2011). Long-Term In Vivo Imaging and Measurement of Dendritic Shrinkage of Retinal Ganglion Cells. *Investigative Ophthalmology & Visual Science* **52:** 1539-1547.

Leung, CKS, Lindsey, JD, Chen, L, Liu, Q, Weinreb, RN (2009). Longitudinal profile of retinal ganglion cell damage assessed with blue-light confocal scanning laser ophthalmoscopy after ischaemic reperfusion injury. *British Journal of Ophthalmology* **93:** 964-968.

Leung, CKS, Lindsey, JD, Crowston, JG, Ju, W-K, Liu, Q, Bartsch, D-U, Weinreb, RN (2008b). In vivo imaging of murine retinal ganglion cells. *Journal of Neuroscience Methods* **168:** 475-478.

Levin, L, Munger, K, O'Reilly, E, Falk, K, Ascherio, A (2010). Primary infection with the epstein-barr virus and risk of multiple sclerosis. *Annals of Neurology* **67:** 824-830.

Li, C, Tropak, MB, Gerlai, R, Clapoff, S, Abramow-Newerly, W, Trapp, B, Peterson, A, Roder, J (1994). Myelination in the absence of myelin-associated glycoprotein. *Nature* **369:** 747-750.

Li, Q, Timmers, AM, Hunter, K, Gonzalez-Pola, C, Lewin, AS, Reitze, DH, Hauswirth, WW (2001). Noninvasive Imaging by Optical Coherence Tomography to Monitor Retinal Degeneration in the Mouse. *Investigative Ophthalmology & Visual Science* **42:** 2981-2989.

Li, W, Maeda, Y, Yuan, RR, Elkabes, S, Cook, S, Dowling, P (2004a). Beneficial effect of erythropoietin on experimental allergic encephalomyelitis. *Annals of Neurology* **56:** 767-777.

Li, W, Yasuhiro Maeda, Y, Yuan, RR, Elkabes, S, Cook, S, Dowling, P (2004b). Beneficial effect of erythropoietin on experimental allergic encephalomyelitis. *Annals of Neurology* **56:** 767-777.

Li, Z-w, Liu, S, Weinreb, RN, Lindsey, JD, Yu, M, Liu, L, Ye, C, Cui, Q, Yung, W-h, Pang, C-P, Lam, DSC, Leung, CK-s (2011). Tracking Dendritic Shrinkage of Retinal Ganglion Cells after Acute Elevation of Intraocular Pressure. *Investigative Ophthalmology & Visual Science***:** doi:10.1167/iovs.10-6868

Liñares, D, Mañá, P, Goodyear, M, Chow, AM, Clavarino, C, Huntington, ND, Barnett, L, Koentgen, F, Tomioka, R, Bernard, CCA, Freire-Garabal, M, Reid, HH (2003). The magnitude and encephalogenic potential of autoimmune response to MOG is enhanced in MOG deficient mice. *Journal of Autoimmunity* **21:** 339-351.

Lincoln, MR, Montpetit, A, Cader, MZ, Saarela, J, Dyment, DA, Tisslar, M, Ferretti, V, Tienari, PJ, DSadovnick, AD, Peltonen, L, Ebers, GC, Hudson, TJ (2005). A predominant role for the HLA class II region in the association of the MHC region with multiple sclerosis. *Nature Genetics* **37:** 1108-1112.

Linington, C, Bradl, M, Lassmann, H, C., B, Vass, K (1988). Augmentation of demyelination in rat acute allergic encephalomyelitis by circulating mouse monoclonal antibodies directed against a myelin/oligodendrocyte glycoprotein. *American Journal of Pathology* **130:** 443-54.

Linthicum, DS, Frelinger, JA (1982). Acute autoimmune encephalomyelitis in mice. II. Susceptibility is controlled by the combination of H-2 and histamine sensitization genes. *Journal of Experimental Medicine* **156:** 31-40.

Lipton, H, Dal Canto, M (1979). The TO strains of Theiler's viruses case "slow virus-like" infections in mice. *Annals of Neurology* **6:** 25-8.

Lisak, R, Zweiman, B, Blanchard, N, Rorke, L (1983). Effect of treatment with Copolymer 1 (Cop-1) on the in vivo and in vitro manifestations of experimental allergic encephalomyelitis (EAE). *Journal of Neurological Sciences* **62:** 281-93.

Liu, X, Linnington, C, Webster, H, Lassmann, S, Yao, DL, Hudson, L, Wekerle, H, Kreutzberg, G (1997). Insulin-like growth factor-I treatment reduces immune cell responses in acute non-demyelinative experimental autoimmune encephalomyelitis. *Journal of Neuroscience Research* **47:** 531-538.

Lo, AC, Black, JA, Waxman, SGCA (2002). Neuroprotection of axons with phenytoin in experimental allergic encephalomyelitis. *Neuroreport* **13:** 1909-1912.

Lucchinetti, C, Brück, W, Parisi, J, Scheithauer, B, Rodriguez, M, Lassmann, H (2000). Heterogeneity of multiple sclerosis lesions: Implications for the pathogenesis of demyelination. *Annals of Neurology* **47:** 707-717.

Lucchinetti, C, Kiers, L, O'Duffy, A, Gomez, M, Cross, S, Leavitt, J, O'Brien, P, Rodriguez, M (1997). Risk factors for developing multiple sclerosis after childhood optic neuritis. *Neurology* **49:** 1413-8.

Lundmark, F, Duvefelt, K, Iacobaeus, E, Kockum, I, Wallstrom, E, Khademi, M, Oturai, A, Ryder, LP, Saarela, J, Harbo, HF, Celius, EG, Salter, H, Olsson, T, Hillert, J (2007). Variation in interleukin 7 receptor [alpha] chain (IL7R) influences risk of multiple sclerosis. *Nature Genetics* **39:** 1108-1113.

Maertz, NA, Kim, CBY, Nork, TM, Levin, LA, Lucarelli, MJ, Kaufman, PL, Ver Hoeve, JN (2006). Multifocal Visual Evoked Potentials in the Anesthetized Non-human Primate. *Current Eye Research* **31:** 885-893.

Magill, CK, Moore, AM, Borschel, GH, Mackinnon, SE (2010). A New Model for Facial Nerve Research. *Archives of Facial Plastic Surgery* **12:** 315-320.

Maloney, DG, Liles, TM, Czerwinski, DK, Waldichuk, C, Rosenberg, J, Grillo-Lopez, A, Levy, R (1994). Phase I clinical trial using escalating single-dose infusion of chimeric anti-CD20 monoclonal antibody (IDEC-C2B8) in patients with recurrent B-cell lymphoma. *Blood* **84:** 2457-2466.

Mamalaki, C, Elliott, J, Norton, T, Yannoutsos, N, Townsend, A, Chandler, P, Simpson, E, Kioussis, D (1993). Positive and Negative Selection in Transgenic Mice Expressing a T-Cell Receptor Specific for Influenza Nucleoprotein and Endogenous Superantigen *Developmental Immunology* **3:** 159-174.

Marmor, MF, Ravin, JG (2011). Fluorescein Angiography: Insight and Serendipity a Half Century Ago. *Archives of Ophthalmology* **129:** 943-948.

Marrie, RA (2004). Environmental risk factors in multiple sclerosis aetiology. *The Lancet Neurology* **3:** 709-718.

Matute, C, Alberdi, E, Ibarretxe, G, Sánchez-Gómez, MV (2002). Excitotoxicity in glial cells. *European Journal of Pharmacology* **447:** 239-246.

McDonald, W, Compston, A, Edan, G, Goodkin, D, Hartung, H, Lublin, F, McFarland, H, Paty, D, Polman, C, Reingold, S, Sandberg-Wollheim, M, Sibley, W, Thompson, A, van den Noort, S, Weinshenker, B, Wolinsky, J (2001). Recommended diagnostic criteria for multiple sclerosis: guidelines from the International Panel on the diagnosis of multiple sclerosis. *Annals of Neurology* **50:** 121-7.

McDonald, WI (1993). The dynamics of multiple sclerosis. *Journal of Neurology* **240:** 28-36.

McFarland, HF, Martin, R (2007). Multiple sclerosis: a complicated picture of autoimmunity. *Nature Immunology* **8:** 913-919.

McGeachy, MJ, Chen, Y, Tato, CM, Laurence, A, Joyce-Shaikh, B, Blumenschein, WM, McClanahan, TK, O'Shea, JJ, Cua, DJ (2009). The interleukin 23 receptor is essential for the terminal differentiation of interleukin 17-producing effector T helper cells in vivo. *Nature Immunology* **10:** 314-324.

McQualter, JL, Bernard, CCA (2007). Multiple Sclerosis: a battle between destruction and repair. *Journal of Neurochemistry* **100:** 295-306.

Mead, RJ, Singhrao, SK, Neal, JW, Lassmann, H, Morgan, BP (2002). The Membrane Attack Complex of Complement Causes Severe Demyelination Associated with Acute Axonal Injury. *The Journal of Immunology* **168:** 458-465.

Mendel, I, Kerlero de Rosbo, N, Ben-Nun, A (1995). A myelin oligodendrocyte glycoprotein peptide induces typical chronic experimental autoimmune encephalomyelitis in H-2b mice: fine specificity and T cell receptor V beta expression of encephalitogenic T cells. *European Journal of Immunology***25:** 1951-1959.

Meyer, R, Weissert, R, Diem, R, Storch, MK, de Graaf, KL, Kramer, B, Bahr, M (2001). Acute Neuronal Apoptosis in a Rat Model of Multiple Sclerosis. *Journal of Neuroscience* **21:** 6214-6220.

Miller, DH, Khan, OA, Sheremata, WA, Blumhardt, LD, Rice, GPA, Libonati, MA, Willmer-Hulme, AJ, Dalton, CM, Miszkiel, KA, O'Connor, PW, the International Natalizumab Multiple Sclerosis Trial, G (2003). A Controlled Trial of Natalizumab for Relapsing Multiple Sclerosis. *New England Journal of Medicine***348:** 15-23.

Miller, DH, Leary, SM (2007). Primary-progressive multiple sclerosis. *The Lancet Neurology* **6:** 903-912.

Miller, DH, Newton, MR, van der Poel, JC, du Boulay, EPGH, Halliday, AM, Kendall, BE, Johnson, G, MacManus, DG, Moseley, IF, McDonald, WI (1988). Magnetic resonance imaging of the optic nerve in optic neuritis. *Neurology* **38:** 175.

Miron, V, Jung, C, Kim, H, Kennedy, T, Soliven, B, Antel, J (2008). FTY720 modulates human oligodendrocyte progenitor process extension and survival. *Annals of Neurology* **63:** 61-71.

Moalem, G, Leibowitz-Amit, R, Yoles, E, Mor, F, Cohen, I, Schwartz, M (1999). Autoimmune T cells protect neurons from secondary degeneration after central nervous system axotomy. *Nature Medicine* **5:** 49-55.

Mokhtarian, F, McFarlin, DE, Raine, CS (1984). Adoptive transfer of myelin basic protein-sensitized T cells produce chronic relapsing demyelinating disease in mice. *Nature* **309:** 356-8.

Montag, D, Giese, KP, Bartsch, U, Martini, R, Lang, Y, Blüthmann, H, Karthigasan, J, Kirschner, DA, Wintergerst, ES, Nave, K-A, Zielasek, J, Toyka, KV, Lipp, H-P, Schachner, M (1994). Mice deficient for the glycoprotein show subtle abnormalities in myelin. *Neuron* **13:** 229-246.

Mora, JR, Iwata, M, von Andrian, UH (2008). Vitamin effects on the immune system: vitamins A and D take centre stage. *Nature Reviews Immunology* **8:** 685-698.

Moreau, T, Coles, A, Wing, M, Thorpe, J, Miller, D, Moseley, I, Issacs, J, Hale, G, Clayton, D, Scolding, N, Waldmann, H, Compston, A (1996). CAMPATH-1H in multiple sclerosis. *Multiple Sclerosis* **1:** 357-65.

Morgan, I (1947). Allergic encephalomyelitis in monkeys in response to injection of normal monkey nervous tissue. *Journal of Experimental Medicine* **1:** 131-40.

Morris-Downes, MM, Smith, PA, Rundle, JL, Piddlesden, SJ, Baker, D, Pham-Dinh, D, Heijmans, N, Amor, S (2002). Pathological and regulatory effects of anti-myelin antibodies in experimental allergic encephalomyelitis in mice. *Journal of Neuroimmunology* **125:** 114-124.

Morrison, L (1947). Disseminated encephalomyelitis experimentally produced by the use of homologous antigen. *Archives of Neurology & Psychiatry* **58:** 391-416.

Mozafari, S, Sherafat, MA, Javan, M, Mirnajafi-Zadeh, J, Tiraihi, T (2010). Visual evoked potentials and MBP gene expression imply endogenous myelin repair in adult rat optic nerve and chiasm following local lysolecithin induced demyelination. *Brain Research* **1351:** 50-56.

Mumphrey, SM, Changotra, H, Moore, TN, Heimann-Nichols, ER, Wobus, CE, Reilly, MJ, Moghadamfalahi, M, Shukla, D, Karst, SM (2007). Murine Norovirus 1 Infection Is Associated with Histopathological Changes in Immunocompetent Hosts, but Clinical Disease Is Prevented by STAT1-Dependent Interferon Responses. *Journal of Virology.* **81:** 3251-3263.

Naismith, RT, Tutlam, NT, Xu, J, Shepherd, JB, Klawiter, EC, Song, SK, Cross, AH (2009). Optical coherence tomography is less sensitive than visual evoked potentials in optic neuritis. *Neurology* **73:** 46-52.

Neuhaus, O, Kieseier, BC, Hartung, H-P (2007). Immunosuppressive Agents in Multiple Sclerosis. *Neurotherapeutics* **4:** 654-660.

Neumann, H (2003). Molecular mechanisms of axonal damage in inflammatory central nervous system diseases. *Current Opinion in Neurology* **16:** 267-273.

Ng, WP, Cartel, N, Li, C, Roder, J, Lozano, A (1996). Myelin from MAG-deficient mice is a strong inhibitor of neurite outgrowth. *Neuroreport* **22:** 861-4.

Nguyen, T, Mehta, NR, Conant, K, Kim, K-J, Jones, M, Calabresi, PA, Melli, G, Hoke, A, Schnaar, RL, Ming, G-L, Song, H, Keswani, SC, Griffin, JW (2009). Axonal Protective Effects of the Myelin-Associated Glycoprotein. *Journal of Neuroscience* **29:** 630-637.

Niklas, A, Sebraoui, H, Hess, E, Wagner, A, Then Bergh, F (2009). Outcome measures for trials of remyelinating agents in multiple sclerosis: retrospective longitudinal analysis of visual evoked potential latency. *Multiple Sclerosis* **15:** 68-74.

Nikolaeva, MA, Mukherjee, B, Stys, PK (2005). Na+-Dependent Sources of Intra-Axonal Ca2+ Release in Rat Optic Nerve during In Vitro Chemical Ischemia. *Journal of Neuroscience* **25:** 9960-9967.

Nobuhara, H, Kuida, K, Furutani, M, Shiroishi, T, Moriwaki, K, Yanagi, Y, Tada, T (1989). Polymorphism of T-cell receptor genes among laboratory and wild mice: diverse origins of laboratory mice. *Immunogenetics* **30:** 405-13.

Noonan, CW, Kathman, SJ, White, MC (2002). Prevalence estimates for MS in the United States and evidence of an increasing trend for women. *Neurology* **58:** 136-138.

Noseworthy, JH, Lucchinetti, C, Rodriguez, M, Weinshenker, BG (2000). Multiple Sclerosis. *New England Journal of Medicine***343:** 938-952.

O'Neill, JK, Baker, D, Davidson, AN, Allen, SJ, Butter, C, Waldmann, H, Turk, JL (1993). Control of immune-mediated disease of the central nervous system with monoclonal (CD4-specific) antibodies. *Journal of Neuroimmunology* **45:** 1-14.

O'Neill, JK, Baker, D, Morris, MM, Gschmeissner, SE, Jenkins, HG, Butt, AM, Kirvell, SL, Amor, S (1998). Optic neuritis in chronic relapsing experimental allergic encephalomyelitis in Biozzi ABH mice: Demyelination and fast axonal transport changes in disease. *Journal of Neuroimmunology* **82:** 210-218.

Oksenberg, JR, Barcellos, LF (2005). Multiple sclerosis genetics: leaving no stone unturned. *Genes & Immunity* **6:** 375-387.

Olivares-Villagomez, D, Wang, Y, Lafaille, JJ (1998). Regulatory CD4+ T Cells Expressing Endogenous T Cell Receptor Chains Protect Myelin Basic Protein specific Transgenic Mice from Spontaneous Autoimmune Encephalomyelitis. *The Journal of Experimental Medicine* **188:** 1883-1894.

Olney, J (1969). Brain lesions, obesity, and other disturbances in mice treated with monosodium glutamate. *Science* **164:** 719-21.

Optic Neuritis Study, G (1991). The Clinical Profile of Optic Neuritis: Experience of the Optic Neuritis Treatment Trial. *Archives of Ophthalmology* **109:** 1673-1678.

Optic Neuritis Study, G (2008). Visual Function 15 Years after Optic Neuritis: A Final Follow-up Report from the Optic Neuritis Treatment Trial. *Ophthalmology* **115:** 1079-1082.e5.

Orton, SM, Herrera, BM, Yee, IM, Valdar, W, Ramagopalan, SV, Sadovnick, AD, Ebers, GC (2006). Sex ratio of multiple sclerosis in Canada: a longitudinal study. *The Lancet Neurology* **5:** 932-936.

Osborne, NN, Li, G-Y, Ji, D, Mortiboys, HJ, Jackson, S (2008). Light affects mitochondria to cause apoptosis to cultured cells: possible relevance to ganglion cell death in certain optic neuropathies. *Journal of Neurochemistry* **105:** 2013-2028.

Owens, G, Bunge, R (1989). Evidence for an early role for myelin-associated glycoprotein in the process of myelination. *Glia* **2:** 119-28.

Päiväläinen, S, Heape, AM (2007). Myelin-associated glycoprotein and galactosylcerebroside expression in Schwann cells during myelination. *Molecular and Cellular Neuroscience* **35:** 436-446.

Pan, B, Fromholt, SE, Hess, EJ, Crawford, TO, Griffin, JW, Sheikh, KA, Schnaar, RL (2005). Myelin-associated glycoprotein and complementary axonal ligands, gangliosides, mediate axon stability in the CNS and PNS: Neuropathology and behavioral deficits in single- and double-null mice. *Experimental Neurology* **195:** 208-217.

Paques, M, Simonutti, M, Roux, MJ, Picaud, S, Levavasseur, E, Bellman, C, Sahel, J-A (2006). High resolution fundus imaging by confocal scanning laser ophthalmoscopy in the mouse. *Vision Research* **46:** 1336-1345.

Parisi, V, Manni, G, Spadaro, M, Colacino, G, Restuccia, R, Marchi, S, Bucci, MG, Pierelli, F (1999). Correlation between Morphological and Functional Retinal Impairment in Multiple Sclerosis Patients. *Investigative Ophthalmology & Visual Science* **40:** 2520-2527.

Paty, DW, Li, DKB, the, UBCMSMRISG, the, IMSSG (1993). Interferon beta-1b is effective in relapsing-remitting multiple sclerosis: II. MRI analysis results of a multicenter, randomized, double-blind, placebo-controlled trial. *Neurology* **43:** 662.

Peachey, NS, Ball, SL (2003). Electrophysiological analysis of visual function in mutant mice. *Documenta Ophthalmologica* **107:** 13-35.

Peferoen, LAN, Lamers, F, Lodder, LNR, Gerritsen, WH, Huitinga, I, Melief, J, Giovannoni, G, Meier, U, Hintzen, RQ, Verjans, GMGM, van Nierop, GP, Vos, W, Peferoen-Baert, RMB, Middeldorp, JM, van der Valk, P, Amor, S (2009). Epstein Barr virus is not a characteristic feature in the central nervous system in established multiple sclerosis. *Brain***:** e137.

Piddlesden, SJ, Lassmann, H, Zimprich, F, Morgan, BP, Linington, C (1993). The demyelinating potential of antibodies to myelin oligodendrocyte glycoprotein is related to their ability to fix complement. *American Journal of Pathology* **143:** 555-564.

Pierrot-Deseilligny, C (2009). Clinical implications of a possible role of vitamin D in multiple sclerosis. *Journal of Neurology*. **256:** 1468-1479.

Pilz, G, Wipfler, P, Ladurner, G, Kraus, J (2008). Modern multiple sclerosis treatment - what is approved, what is on the horizon. *Drug Discovery Today* **13:** 1013-1025.

Pinto, LH, Enroth-Cugell, C (2000). Tests of the mouse visual system. *Mammalian Genome* **11:** 531-536.

Pircher, H, Bürki, K, Lang, R, Hengartner, H, Zinkernagel, R (1989). Tolerance induction in double specific T-cell receptor transgenic mice varies with antigen. *Nature* **342:** 559-61.

Pitt, D, Werner, P, Raine, CS (2000a). Glutamate excitotoxicity in a model of multiple sclerosis. *Nature Medicine* **6:** 67-70.

Pittock, SJ, McClelland, RL, Mayr, WT, Jorgensen, NW, Weinshenker, BG, Noseworthy, J, Rodriguez, M (2004). Clinical implications of benign multiple sclerosis: A 20-year population-based follow-up study. *Annals of Neurology* **56:** 303-306.

Plumb, J, McQuaid, S, Mirakhur, M, Kirk, J (2002). Abnormal endothelial tight junctions in active lesions and normal-appearing white matter in multiple sclerosis. *Brain Pathology* **12:** 154-69.

Pohl, D (2009). Epstein-Barr virus and multiple sclerosis. *Journal of the Neurological Sciences* **286:** 62-64.

Polak, PE, Kalinin, S, Dello Russo, C, Gavrilyuk, V, Sharp, A, Peters, JM, Richardson, J, Willson, TM, Weinberg, G, Feinstein, DL (2005). Protective effects of a peroxisome proliferator-activated receptor-[beta]/[delta] agonist in experimental autoimmune encephalomyelitis. *Journal of Neuroimmunology* **168:** 65-75.

Pollinger, B, Krishnamoorthy, G, Berer, K, Lassmann, H, Bosl, MR, Dunn, R, Domingues, HS, Holz, A, Kurschus, FC, Wekerle, H (2009). Spontaneous relapsing-remittying EAE in the SJL/J mouse: MOG-reactive transgenic T cells recruit endogenous MOG-specific B cells. *Journal of Experimental Medicine* **206:** 1303-1316.

Polman, CH, O'Connor, PW, Havrdova, E, Hutchinson, M, Kappos, L, Miller, DH, Phillips, JT, Lublin, FD, Giovannoni, G, Wajgt, A, Toal, M, Lynn, F, Panzara, MA, Sandrock, AW, the, AI (2006). A Randomized, Placebo-Controlled Trial of Natalizumab for Relapsing Multiple Sclerosis. *New England Journal of Medicine* **354:** 899-910.

Porciatti, V, Pizzorusso, T, Maffei, L (1999). The visual physiology of the wild type mouse determined with pattern VEPs. *Vision Research* **39:** 3071-3081.

Potter, NT, Bigazzi, PE (1992). Acute optic neuritis associated with immunization with the CNS myelin proteolipid protein. *Investigative Ophthalmology & Visual Science* **33:** 1717-1722.

Pouly, S, Antel, JP (1999). Multiple Sclerosis and Central Nervous System Demyelination. *Journal of Autoimmunity* **13:** 297-306.

Prasad, S, Galetta, SL (2010). Eye Movement Abnormalities in Multiple Sclerosis. *Neurologic Clinics* **28:** 641-655.

Prusky, GT, Alam, NM, Beekman, S, Douglas, RM (2004). Rapid Quantification of Adult and Developing Mouse Spatial Vision Using a Virtual Optomotor System. *Investigative Ophthalmology & Visual Science* **45:** 4611-4616.

Pryce, G, Ahmed, Z, Hankey, DJR, Jackson, SJ, Croxford, JL, Pocock, JM, Ledent, C, Petzold, A, Thompson, AJ, Giovannoni, G, Cuzner, ML, Baker, D (2003). Cannabinoids inhibit neurodegeneration in models of multiple sclerosis. *Brain* **126:** 2191-2202.

Pryce, G, O'Neill, JK, Croxford, JL, Amor, S, Hankey, DJ, East, E, Giovannoni, G, Baker, D (2005). Autoimmune tolerance eliminates relapses but fails to halt progression in a model of multiple sclerosis. *Journal of Neuroimmunology* **165:** 41-52.

Puk, O, Dalke, C, Hrabe de Angelis, M, Graw, J (2008). Variation of the response to the optokinetic drum among various strains of mice. *Frontiers in Bioscience* **13:** 6269-75.

Pulendran, B, Palucka, K, Banchereau, J (2001). Sensing Pathogens and Tuning Immune Responses. *Science* **293:** 253-256.

Pulicken, M, Gordon-Lipkin, E, Balcer, LJ, Frohman, E, Cutter, G, Calabresi, PA (2007). Optical coherence tomography and disease subtype in multiple sclerosis. *Neurology* **69:** 2085-2092.

Quarles, R, Everly, J, Brady, R (1973). Evidence for the close association of a glycoprotein with myelin in rat brain. *Journal of Neurochemistry* **21:** 1177-91.

Quigley, H, Nickells, R, Kerrigan, L, Pease, M, Thibault, D, Zack, D (1995). Retinal ganglion cell death in experimental glaucoma and after axotomy occurs by apoptosis. *Investigative Ophthalmology & Visual Science* **36:** 774-786.

Quigley, HA, Davis, EB, Anderson, DR (1977). Descending optic nerve degeneration in primates. *Investigative Ophthalmology & Visual Science* **16:** 841-849.

Racke, MK, Hu, W, Lovett-Racke, AE (2005). PTX cruiser: driving autoimmunity via TLR4. *Trends in Immunology* **26:** 289-291.

Ragonese, P, Aridon, P, Salemi, G, D'Amelio, M, Savettieri, G (2008). Mortality in multiple sclerosis: a review. *European Journal of Neurology* **15:** 123-127.

Ramagopalan, SV, Maugeri, NJ, Handunnetthi, L, Lincoln, MR, Orton, S-M, Dyment, DA, DeLuca, GC, Herrera, BM, Chao, MJ, Sadovnick, AD, Ebers, GC, Knight, JC (2009a). Expression of the Multiple Sclerosis-Associated MHC Class II Allele HLA-DRB1*1501 Is Regulated by Vitamin D. *PLoS Genet* **5:** e1000369.

Ramagopalan, V, Valdar, W, Dyment, D, DeLuca, G, Yeec, I, Giovannoni, G, Ebers, G, Sadovnick, D (2009b). Association of Infectious Mononucleosis with Multiple Sclerosis. *Neuroepidemiology* **32:** 257-262.

Ramsaransing, GSM, De Keyser, J (2006). Benign course in multiple sclerosis: a review. *Acta Neurologica Scandinavica* **113:** 359-369.

Ransohoff, RM (2006). EAE: pitfalls outweigh virtues of screening potential treatments for multiple sclerosis. *Trends in Immunology* **27:** 167-168.

Reddy, H, Narayanan, S, Arnoutelis, R, Jenkinson, M, Antel, J, Matthews, PM, Arnold, DL (2000). Evidence for adaptive functional changes in the cerebral cortex with axonal injury from multiple sclerosis. *Brain* **123:** 2314-2320.

Reddy, J, Waldner, H, Zhang, X, Illes, Z, Wucherpfennig, KW, Sobel, RA, Kuchroo, VK (2005). Cutting Edge: CD4+CD25+ Regulatory T Cells Contribute to Gender Differences in Susceptibility to Experimental Autoimmune Encephalomyelitis. *The Journal of Immunology* **175:** 5591-5595.

Reichel, M, Bainbridge, J, Baker, D, Thrasher, A, Bahattacharya, S, Ali, R (2001). An immune response after intraocular administration of an adenoviral vector containing a beta galactosidase reporter gene slows retinal degeneration in the rd mouse. *British Journal of Ophthalmology* **85:** 341-4.

Repine, J, Pfenninger, O, Talmage, D, Berger, E, Pettijohn, D (1981). Dimethyl sulfoxide prevents DNA nicking mediated by ionizing radiation or iron/hydrogen peroxide-generated hydroxyl radical. *Proceedings of the National Academy of Sciences United States America* **78:** 1001-1003.

Rice, C, Scolding, N (2007). Strategies for achieving and monitoring myelin repair. *Journal of Neurology* **254:** 275-283.

Ridder, WH, Nusinowitz, S (2006). The visual evoked potential in the mouse - Origins and response characteristics. *Vision Research* **46:** 902-913.

Rigby, WF, Waugh, M, Graziano, RF (1990). Regulation of human monocyte HLA-DR and CD4 antigen expression, and antigen presentation by 1,25-dihydroxyvitamin D3. *Blood* **76:** 189-197.

Riise, T (1997). Cluster studies in multiple sclerosis. *Neurology* **49:** S27-32.

Ringel, M, Schwindinger, W, Saji, M, Zeiger, M, Levine, M (1998). Determination of transgene copy number and expression level using denaturing gradient gel electrophoresis. *Biotechniques* **24:** 128-31.

Rivers, T, Schwentker, F (1935). Encephalomyelitis accompanied by myelin destruction experimentally produced in monkeys. *Journal of Experimental Medicine* **61:** 689-702.

Rivers, T, Sprunt, D, Berry, G (1933). Observations on attempts to produce acute disseminated encephalomyelitis in monkeys.Journal of Experimental Medicine**58:** 39-53.

Rizzo, JF, Andreoli, CM, Rabinov, JD (2002). Use of magnetic resonance imaging to differentiate optic neuritis and nonarteritic anterior ischemic optic neuropathy. *Ophthalmology* **109:** 1679-1684.

Rose, GH, Lindsley, DB (1968). Development of visually evoked potentials in kittens: specific and nonspecific responses. *Journal of Neurophysiology* **31:** 607-623.

Rudick, RA, Goodkin, DE, Jacobs, LD, Cookfair, DL, Herndon, RM, Richert, JR, Salazar, AM, Fischer, JS, Granger, CV, Simon, JH, Alam, JJ, Simonian, NA, Campion, MK, Bartoszak, DM, Bourdette, DN, Braiman, J, Brownscheidle, CM, Coats, ME, Cohan, SL, Dougherty, DS, Kinkel, RP, Mass, MK, Munschauer, FE, Priore, RL, Pullicino, PM, Scherokman, BJ, Weistock-Guttman, B, Whitham, RH, The Multiple Sclerosis Collaborative Research, G (1997). Impact of interferon beta-1a on neurologic disability in relapsing multiple sclerosis. *Neurology* **49:** 358-363.

Ruggeri, M, Wehbe, H, Jiao, S, Gregori, G, Jockovich, ME, Hackam, A, Duan, Y, Puliafito, CA (2007). In Vivo Three-Dimensional High-Resolution Imaging of Rodent Retina with Spectral-Domain Optical Coherence Tomography. *Investigative Ophthalmology & Visual Science* **48:** 1808-1814.

Runge, P, Hawes, N, Heckenlively, J, Lanegley, S, Roderick, T (1992). Autosomal dominant mouse cataract (Lop-10). Consistent differences of expression in heterozygotes. *Investigative Ophthalmology & Visual Science* **33:** 3202-8.

Ryan, M, McCarthy, L, Rappuoli, R, Mahon, BP, Mills, KH (1998). Pertussis toxin potentiates Th1 and Th2 responses to co-injected antigen: adjuvant action is associated with enhanced regulatory cytokine production and expression of the co-stimulatory molecules B7- 1, B7-2 and CD28. *International Immunology* **10:** 651-662.

Sadovnick, A, Armstrong, H, Rice, G, Bulman, D, Hashimoto, L, Paty, D, Hashimoto, S, Warren, S, Hader, W, Murray, T (1993). A population-based study of multiple sclerosis in twins: update. *Annals of Neurology* **33:** 281-5.

Sadovnick, AD, Dyment, DA, Ebers, GC, Risch, NJ, the Canadian Collaborative Study, G (1996). Evidence for genetic basis of multiple sclerosis. *The Lancet* **347:** 1728-1730.

Saito, T, Weiss, A, Miller, J, Norcross, M, Germain, R (1987). Predictable acquisition of a new MHC recognition specificity following expression of a transfected T-cell receptor β-chain gene. *Nature* **329:** 256-259.

Sakurai, M, Kanazawa, I (1999). Positive symptoms in multiple sclerosis: their treatment with sodium channel blockers, lidocaine and mexiletine. *Journal of the Neurological Sciences* **162:** 162-168.

Sawcer, S (2008). The complex genetics of multiple sclerosis: pitfalls and prospects. *Brain* **131:** 3118-3131.

Sawcer, S, Hellenthal, G, Matti, P, Spencer, CCA, Donnelly, P, Compston, A (2011). Genetic risk and a primary role for cell-mediated immune mechanisms in multiple sclerosis. *Nature* **476:** 214-219.

Schaefer, BC, Schaefer, ML, Kappler, JW, Marrack, P, Kedl, RM (2001). Observation of Antigen-Dependent CD8+ T-Cell/ Dendritic Cell Interactions in Vivo. *Cellular Immunology* **214:** 110-122.

Schauf, CL, Davis, FA, Marder, J (1974). Effects of carbamazepine on the ionic conductances of myxicola giant axons. *Journal of Pharmacology and Experimental Therapeutics* **189:** 538-543.

Schinkel, AH, Smit, JJM, van Tellingen, O, Beijnen, JH, Wagenaar, E, van Deemter, L, Mol, CAAM, van der Valk, MA, Robanus-Maandag, EC, te Riele, HPJ, Berns, AJM, Borst, P (1994). Disruption of the mouse mdr1a P-glycoprotein gene leads to a deficiency in the blood-brain barrier and to increased sensitivity to drugs. *Cell* **77:** 491-502.

Schmucker, C, Seeliger, M, Humphries, P, Biel, M, Schaeffel, F (2005). Grating Acuity at Different Luminances in Wild-Type Mice and in Mice Lacking Rod or Cone Function. *Investigative Ophthalmology & Visual Science* **46:** 398-407.

Schwid, SR, Trotter, JL (2000). Lessons from linomide: A failed trial, but not a failure. *Neurology* **54:** 1716-1717.

Scolding, NJ, Frith, S, Linington, C, Morgan, BP, Campbell, AK, Compston, DAS (1989). Myelin-oligodendrocyte glycoprotein (MOG) is a surface marker of oligodendrocyte maturation. *Journal of Neuroimmunology* **22:** 169-176.

Scwabe, S (1994). Oxcarbazepine: clinical development program. *Epilepsia* **35:** 51-3.

Sedgwick, JD, Mason, DW (1986). The mechanism of inhibition of experimental allergic encephalomyelitis in the rat by monoclonal antibody against CD4. *Journal of Neuroimmunology* **13:** 217-32.

Selhorst, JB, Chen, Y (2009). The Optic Nerve. *Seminars in Neurology* **29:** 029-035.

Serafini, B, Rosicarelli, B, Franciotta, D, Magliozzi, R, Reynolds, R, Cinque, P, Andreoni, L, Trivedi, P, Salvetti, M, Faggioni, A, Aloisi, F (2007). Dysregulated Epstein-Barr virus infection in the multiple sclerosis brain. *The Journal of Experimental Medicine* **204:** 2899-2912.

Sergott, RC, Frohman, E, Glanzman, R, Al-Sabbagh, A (2007). The role of optical coherence tomography in multiple sclerosis: Expert panel consensus. *Journal of the Neurological Sciences* **263:** 3-14.

Shams, P, Plant, G (2009). Optic neuritis: A review. *The International MS Journal* **16:** 82-89.

Shao, H, Huang, Z, Sun, SL, Kaplan, HJ, Sun, D (2004). Myelin/Oligodendrocyte Glycoprotein-Specific T-Cells Induce Severe Optic Neuritis in the C57Bl/6 Mouse. *Investigative Ophthalmology & Visual Science* **45:** 4060-4065.

Sherman, SM, V.A. Casagrande, RWGaSMS (2005). Thalamic relays and cortical functioning. *Progress in Brain Research* **149:** 107-126.

Shimohama, S, Tanino, H, Fujimoto, S (1999). Changes in Caspase Expression in Alzheimer's Disease: Comparison with Development and Aging. *Biochemical and Biophysical Research Communications* **256:** 381-384.

Shindler, KS, Guan, Y, Ventura, E, Bennett, J, Rostami, A (2006). Retinal ganglion cell loss induced by acute optic neuritis in a relapsing model of multiple sclerosis. *Multiple Sclerosis* **12:** 526-535.

Shindler, KS, Kenyon, LC, Dutt, M, Hingley, ST, Sarma, JD (2008). Experimental Optic Neuritis Induced by a Demyelinating Strain of Mouse Hepatitis Virus. *Journal of Virology* **82:** 8882-8886.

Shou, T, Liu, J, Wang, W, Zhou, Y, Zhao, K (2003). Differential Dendritic Shrinkage of Î± and Î² Retinal Ganglion Cells in Cats with Chronic Glaucoma. *Investigative Ophthalmology & Visual Science* **44:** 3005-3010.

Sincich, LC, Horton, JC (2005). The circuitry of V1 and V2: Integration of Color, Form, and Motion. *Annual Review of Neuroscience* **28:** 303-326.

Sinha, S, Kaler, LJ, Proctor, TM, Teuscher, C, Vandenbark, AA, Offner, H (2008). IL-13-Mediated Gender Difference in Susceptibility to Autoimmune Encephalomyelitis. *The Journal of Immunology* **180:** 2679-2685.

Smith, K, Kapoor, R, Hall, S, Davies, M (2001). Electrically active axons degenerate when exposed to nitric oxide. *Annals of Neurology* **49:** 470-6.

Smith, KJ, Lassmann, H (2002). The role of nitric oxide in multiple sclerosis. *The Lancet Neurology* **1:** 232-241.

Smith, T, Groom, A, Zhu, B, Turski, L (2000). Autoimmune encephalomyelitis ameliorated by AMPA antagonists. *Nature Medicine* **6:** 62-66.

Snellman, J, Kaur, T, Shen, Y, Nawy, S (2008). Regulation of ON bipolar cell activity. *Progress in Retinal and Eye Research* **27:** 450-463.

Söderström, M (2001). Optic neuritis and multiple sclerosis. *Acta Ophthalmologica Scandinavica* **79:** 223-227.

Solaro, C, Brichetto, G, Battaglia, MA, Messmer Uccelli, M, Mancardi, GL (2005). Antiepileptic medications in multiple sclerosis: adverse effects in a three-year follow-up study. *Neurological Sciences* **25:** 307-310.

Sospedra, M, Martin, R (2005). IMMUNOLOGY OF MULTIPLE SCLEROSIS*. *Annual Review of Immunology* **23:** 683.

Soto, A, Pérez-Samartín, AL, Etxebarria, E, Matute, C (2004). Excitotoxic insults to the optic nerve alter visual evoked potentials. *Neuroscience* **123:** 441-449.

Spiegel, S, Milstien, S (2003). Sphingosine-1-phosphate: an enigmatic signalling lipid. *Nature Reviews Molecular & Cell Biology* **4:** 397-407.

Steinman, L, Zamvil, SS (2005). Virtues and pitfalls of EAE for the development of therapies for multiple sclerosis. *Trends in Immunology* **26:** 565-571.

Sternberger, N, Quarles, R, Itoyama, Y, Webster, H (1979). Myelin-associated glycoprotein demonstrated immunocytochemically in myelin and myelin-forming cells of developing rat. *Proceedings of the National Academy of Sciences United States America* **76:** 1510-4.

Stout, A, Raphael, H, Kanterewicz, B, Klann, E, Reynolds, I (1998). Glutamate-induced neuron death requires mitochondrial calcium uptake. *Nature Neuroscience* **1:** 366-73.

Strain, GM, Tedford, BL (1993). Flash and pattern reversal visual evoked potentials in C57BL/6J and B6CBAF/J mice. *Brain Research Bulletin* **32:** 57-63.

Straus, S, Cohen, J, Tosato, G, Meier, J (1993). Epstein-Barr Virus Infections: Biology, Pathogenesis, and Management. *Annals of Internal Medicine* **118:** 45-58.

Stys, PK, Waxman, SG, Ransom, BR (1992). Ionic mechanisms of anoxic injury in mammalian CNS white matter: role of Na+ channels and Na(+)-Ca2+ exchanger. *Journal of Neuroscience* **12:** 430-439.

Su, K, Banker, G, Bourdette, D, Forte, M (2009). Axonal degeneration in multiple sclerosis: The mitochondrial hypothesis. *Current Neurology & Nerusocience Reports* **9:** 411-417.

Svingen, T, Spiller, CM, Kashimada, K, Harley, VR, Koopman, P (2009). Identification of suitable normalizing genes for quantitative real-time rt-pcr analysis of gene expression in fetal mouse gonads. *Sexual Development* **3:** 194-204.

Tarnawa, I, Bolcskei, H, Kocsis, P (2007). Blockers of voltage-gated sodium channels for the treatment of central nervous system diseases. *Recent Patents on CNS Drug Discovery* **2:** 57-58.

Tebano, M, Luzi, M, Palazzesi, S, Pomponi, M, Loizzo, A (1999). Effects of cholinergic drugs on neocortical EEG and flash-visual evoked potentials in the mouse. *Neuropsychobiology* **40:** 47-56.

Teh, H, Kisielow, P, Scott, B, Kishi, H, Uematsu, Y, Blüthmann, H, von Boehmer, H (1988). Thymic major histocompatibility complex antigens and the alpha beta T-cell receptor determine the CD4/CD8 phenotype of T cells. *Nature* **335:** 229-33.

Teuscher, C (1985). Experimental allergic orchitis in mice. II. Association of disease susceptibility with the locus controling Bordetella pertussis-induced sesnsitivity to histamine. *Immunogenetics* **22:** 417-25.

Thaung, C, Arnold, K, Jackson, IJ, Coffey, PJ (2002a). Presence of visual head tracking differentiates normal sighted from retinal degenerate mice. *Neuroscience Letters* **325:** 21-24.

Thaung, C, Arnolda, K, Jackson, I, Coffey, P (2002b). Presence of visual head tracking differentiates normal sighted from retinal degenerate mice. *Neuroscience Letters* **325:** 21-24.

The Optic Neuritis Study, G (2003). High- and low-risk profiles for the development of multiple sclerosis within 10 years after optic neuritis: experience of the optic neuritis treatment trial. *Archives in Ophthalmology* **121:** 944-9.

The Optic Neuritis Study, G (2008). Multiple Sclerosis Risk After Optic Neuritis: Final Optic Neuritis Treatment Trial Follow-up. *Archives in Neurology* **65:** 727-732.

Theiler, M (1937). Spontaneous encephalomyelitis of mice, a new virus disease. *Journal of Experimental Medicine* **65:** 705-19.

Thomas, BB, Seiler, MJ, Sadda, SR, Coffey, PJ, Aramant, RB (2004). Optokinetic test to evaluate visual acuity of each eye independently. *Journal of Neuroscience Methods* **138:** 7-13.

Thompson, C, Jacobsen, H, Pomeranz Krummel, D, Nagai, K, Cooke, A (2004). Non-depleting Anti-CD4 Antibody not only Prevents Onset but Resolves Sialadenitis in NOD Mice. *Autoimmunity* **37:** 549-554.

Thornberry, NA, Lazebnik, Y (1998). Caspases: Enemies Within. *Science* **281:** 1312-1316.

Thrower, BW (2009). Relapse Management in Multiple Sclerosis. *The Neurologist* **15:** 1-5

Tischner, D, Reichardt, HM (2007). Glucocorticoids in the control of neuroinflammation. *Molecular and Cellular Endocrinology* **275:** 62-70.

Tiwari, M, Lopez-Cruzan, M, Morgan, WW, Herman, B (2011). Loss of Caspase-2-dependent Apoptosis Induces Autophagy after Mitochondrial Oxidative Stress in Primary Cultures of Young Adult Cortical Neurons. *Journal of Biological Chemistry* **286:** 8493-8506.

Todd, L, King, J, Darlington, CL, Smith, CA, Paul, F (2001). Optokinetic reflex dysfunction in multiple sclerosis. *Neuroreport* **12:** 1399-1402.

Touil, T, Deloire-Grassin, MSA, Vital, C, Petry, KG, Brochet, B (2001). In vivo damage of CNS myelin and axons induced by peroxynitrite. *NeuroReport* **12:** 3637-3644.

Toussaint, D, Perier, O, Verstappen, A, Bervoets, S (1983). Clinicopathological study of the visual pathways, eyes and cerebral hemispheres in 32 cases of dissemianted sclerosis. *Journal of Clinical Neuroophthalmology* **3:** 211-20.

Tovey, M, Lallemand, C (2010). Adjuvant activity of cytokines. *Methods in Molecular Biology* **626:** 287-309.

Trapp, BD, Peterson, J, Ransohoff, RM, Rudick, R, Mork, S, Bo, L (1998). Axonal Transection in the Lesions of Multiple Sclerosis. *New England Journal of Medicine* **338:** 278-285.

Traugott, U, Reinherz, EL, Raine, CS (1983). Multiple sclerosis: distribution of T cell subsets within active chronic lesions. *Science* **219:** 308-10.

Treon, SP, Soumerai, JD, Hunter, ZR, Patterson, CJ, Ioakimidis, L, Kahl, B, Boxer, M (2011). Long-term follow-up of symptomatic patients with lymphoplasmacytic lymphoma/Waldenstrom macroglobulinemia treated with the anti-CD52 monoclonal antibody alemtuzumab. *Blood* **118:** 276-281.

Trip, SA, Schlottmann, P, Jones, S, Altmann, D, Garway-Heath, D, Thompson, A, Plant, G, Miller, D (2005). Retinal nerve fiber layer axonal loss and visual dysfunction in optic neuritis. *Annals of Neurology* **58:** 383-391.

Tsuji, S, Matsumoto, M, Takeuchi, O, Akira, S, Azuma, I, Hayashi, A, Toyoshima, K, Seya, T (2000). Maturation of Human Dendritic Cells by Cell Wall Skeleton of Mycobacterium bovis Bacillus Calmette-Guerin: Involvement of Toll-Like Receptors. *Infection & Immunity* **68:** 6883-6890.

Twyman, C, Berger, J (2010). A giant MS plaque mimicking PML during natalizumab treatment. *Journal of Neurological Sciences* **291:** 110-3.

Uematsu, Y, Ryser, S, Dembic, Z, Borgulya, P, Krimpenfort, P, Berns, A, von Boehmer, H, Steinmetz, M (1988). In transgenic mice the introduced functional T cell receptor [beta] gene prevents expression of endogenous [beta] genes. *Cell* **52:** 831-841.

Urano, T, Matsuura, T, Yukawa, E, Arai, M, Hara, Y, Yamakawa, R (2011). Retinal nerve fiber layer thickness changes following optic neuritis caused by multiple sclerosis. *Japanese Journal of Ophthalmology* **55:** 45-48.

van der Stelt, M, Veldhuis, WB, BÃ¤r, PR, Veldink, GA, Vliegenthart, JFG, Nicolay, K (2001). Neuroprotection by delta 9-Tetrahydrocannabinol, the Main Active Compound in Marijuana, against Ouabain-Induced In Vivo Excitotoxicity. *The Journal of Neuroscience* **21:** 6475-6479.

van der Veen, RC, R. Hinton, D, Incardonna, F, Hofman, FM (1997). Extensive peroxynitrite activity during progressive stages of central nervous system inflammation. *Journal of Neuroimmunology* **77:** 1-7.

Vidal, M, Morris, R, Grosveld, F, Spanopoulou, E (1990). Tissue-specific control elements of the Thy-1 gene. *The EMBO Journal* **9:** 833-840.

Visscher, B, Detels, R, Coulson, A, Malmgren, R, Dudley, J (1977). Latitude, migration, and the prevalence of multiple sclerosis. *American Journal of Epidemiology* **106:** 470-5.

Waldner, H, Whitters, MJ, Sobel, RA, Collins, M, Kuchroo, VK (2000). Fulminant spontaneous autoimmunity of the central nervous system in mice transgenic for the myelin proteolipid protein-specific T cell receptor. *Proceedings of the National Academy of Science United States America* **97:** 3412-3417.

Wang, J-Y, Wu, J-N, Cherng, T-L, Hoffer, BJ, Chen, H-H, Borlongan, CV, Wang, Y (2001). Vitamin D3 attenuates 6-hydroxydopamine-induced neurotoxicity in rats. *Brain Research* **904:** 67-75.

Wang, L, Miura, M, Bergeron, L, Zhu, H, Yuan, J (1994). Ich-1, an Ice/ced-3-related gene, encodes both positive and negative regulators of programmed cell death. *Cell* **78:** 739-750.

Warner, HB, Carp, RI (1981). Multiple sclerosis and epstein-barr virus. *The Lancet* **318:** 1290-1290.

Waxman, SG (1977). Conduction in Myelinated, Unmyelinated, and Demyelinated Fibers. *Archives of Neurology* **34:** 585-589.

Waxman, SG (1998). Demyelinating Diseases -- New Pathological Insights, New Therapeutic Targets. *New England Journal of Medicine***338:** 323-325.

Waxman, SG (2006). Ions, energy and axonal injury: towards a molecular neurology of multiple sclerosis. *Trends in Molecular Medicine* **12:** 192-195.

Waxman, SG (2008). Mechanisms of Disease: sodium channels and neuroprotection in multiple sclerosis[mdash]current status. *Nature Clinical Practice Neurology* **4:** 159-169.

Weaver, VM, Carson, CE, Walker, PR, Chaly, N, Lach, B, Raymond, Y, Brown, DL, Sikorska, M (1996). Degradation of nuclear matrix and DNA cleavage in apoptotic thymocytes. *Journal of Cell Science* **109:** 45-56.

Webb, R, Hughes, G, Pomerantzeff, O (1980). Flying spot TV ophthalmascope. *Applied Ophthalmology* **19:** 2991-2997.

Weetman, A (2009). Immune reconstitution syndrome and the thyroid. *Best Practice & Research Clinical Endocrinology & Metabolism* **23:** 693-702.

Weiner, HL (2004). Multiple Sclerosis Is an Inflammatory T-Cell-Mediated Autoimmune Disease. *Archives of Neurology* **61:** 1613-1615.

Weinreb, RN (1993). Laser scanning tomography to diagnose and monitor glaucoma. *Current Opinion in Ophthalmology* **4:** 3-6.

Whitaker, JN (1994). Rationale for immunotherapy in multiple sclerosis. *Annals of Neurology* **36:** S103-7.

Willis, SN, Stadelmann, C, Rodig, SJ, Caron, T, Gattenloehner, S, Mallozzi, SS, Roughan, JE, Almendinger, SE, Blewett, MM, Bruck, W, Hafler, DA, O'Connor, KC (2009). Epstein-Barr virus infection is not a characteristic feature of multiple sclerosis brain. *Brain* **132:** 3318-3328.

Willow, M, Catterall, WA (1982). Inhibition of binding of [3H]batrachotoxinin A 20-alpha-benzoate to sodium channels by the anticonvulsant drugs diphenylhydantoin and carbamazepine. *Molecular Pharmacology* **22:** 627-635.

Wojtkowski, M, Srinivasan, V, Fujimoto, JG, Ko, T, Schuman, JS, Kowalczyk, A, Duker, JS (2005). Three-dimensional Retinal Imaging with High-Speed Ultrahigh-Resolution Optical Coherence Tomography. *Ophthalmology* **112:** 1734-1746.

Wolf-Schnurrbusch, UEK, Ceklic, L, Brinkmann, CK, Iliev, ME, Frey, M, Rothenbuehler, SP, Enzmann, V, Wolf, S (2009). Macular Thickness Measurements in Healthy Eyes Using Six Different Optical Coherence Tomography Instruments. *Investigative Ophthalmology & Visual Science* **50:** 3432-3437.

Wolf, A, Kabat, E, Bezer, A (1947). The pathology of acute disseminated encephalomyelitis produced experimentally in the rhesus monkey and its resemblance to human demyelinating disease. *Jorunal of Neuropathology & Experimental Neurology* **6:** 333-57.

Wu, J, Seregard, S, Spangberg, B, Oskarsson, M, Chen, E (1999). Blue light induced apoptosis in rat retina. *Eye* **13:** 577-83.

Wujek, JR, Bjartmar, C, Richer, E, Ransohoff, RM, Yu, MIN, Tuohy, VK, Trapp, BD (2002). Axon Loss in the Spinal Cord Determines Permanent Neurological Disability in an Animal Model of Multiple Sclerosis. *Journal of Neuropathology & Experimental Neurology* **61:** 23-32.

Xiao, BG, Linington, C, Link, H (1991). Antibodies to myelin-oligodendrocyte glycoprotein in cerebrospinal fluid from patients with multiple sclerosis and controls. *Journal of Neuroimmunology* **31:** 91-96.

Xu, H, Manivannan, A, Goatman, KA, Liversidge, J, Sharp, PF, Forrester, JV, Crane, IJ (2002). Improved Leukocyte Tracking in Mouse Retinal and Choroidal Circulation. *Experimental Eye Research* **74:** 403-410.

Yanagi, Y, Yoshikai, Y, Leggett, K, Clark, SP, Aleksander, I, Mak, TW (1984). A human T cell-specific cDNA clone encodes a protein having extensive homology to immunoglobulin chains. *Nature* **308:** 145-9.

Yang, T, P, S, Green, G, Kitts, P, Chen, Y, Lybarger, L, Chervenak, R, Patterson, G, Piston, D, Kain, S (1998). Improved fluorescence and dual color detection with enhanced blue and green variants of the green fluorescent protein. *Journal of Biological Chemistry* **273:** 8212-6.

Yao, D, Liu, X, Hudson, L, Webster, H (1996). Insulin-like growth factor-I given subcutaneously reduces clinical deficits, decreases lesion severity and upregulates synthesis of myelin proteins in experimental autoimmune encephalomyelitis. *Life Sciences* **58:** 1301-1306.

Yednock, TA, Cannon, C, Fritz, LC, Sanchez-Madrid, F, Steinman, L, Karin, N (1992). Prevention of experimental auotimmune encephalomyelitis by antibodies against alpha 4 beta 1 integrin. *Nature* **5:** 63-6.

Yin, X, Crawford, TO, Griffin, JW, Tu, P-h, Lee, VMY, Li, C, Roder, J, Trapp, BD (1998). Myelin-Associated Glycoprotein Is a Myelin Signal that Modulates the Caliber of Myelinated Axons. *Journal of Neuroscience* **18:** 1953-1962.

Youl, BD, Turano, G, Miller, DH, Towell, AD, Macmanus, DG, Moore, SG, Jones, SJ, Barrett, G, Kendall, BE, Moseley, IF, Tofts, PS, Halliday, AM, McDonald, WI (1991). The pathophysiology of acute optic neuritis: an association of gadolinium leakage with clinical and electrophysiological deficits. *Brain* **114:** 2437-2450.

Yu, M, Narayanan, SP, Wang, F, Morse, E, Macklin, WB, Peachey, NS (2011). Visual abnormalities associated with enhanced optic nerve myelination. *Brain Research* **1374:** 36-42.

Ziskin, JL, Nishiyama, A, Rubio, M, Fukaya, M, Bergles, DE (2007). Vesicular release of glutamate from unmyelinated axons in white matter. *Nature Neuroscience* **10:** 321-330.